

An Exploration of Alkali Metal Ferrate Chemistry: Synthesis and Exploitation for N-Heterocyclic Carbene and Fluoroarene Functionalisation



Lewis Caradoc Huw Maddock

Department of Pure and Applied Chemistry

University of Strathclyde

A thesis submitted to the Department of Pure and Applied Chemistry, University of Strathclyde, in part fulfilment of the requirements for the degree of Doctor of Philosophy.

September 2016

Declaration

This thesis is the result of the author's original research. It has been composed by the author and has not been previously submitted for examination which has led to the award of a degree.

The copyright of this thesis belongs to the author under the terms of the United Kingdom Copyright Acts as qualified by the University of Strathclyde Regulation 3.50. Due acknowledgement must always be made of the use of any material contained in, or derived from, this thesis

Lewis Caradoc Huw Maddock

September 2016

Dedicated to the memory of my late grandfather Dr Alfred Gavin Maddock. A distinguished and brilliant chemist whose work and life has inspired me greatly.

Acknowledgements

There are a large number of people I have to thank and acknowledge for their help, motivation, friendship and for a whole host of other things over an incredibly enjoyable and life-changing period of nearly four years; five if I include my Master's year.

First and foremost I must give enormous thanks my primary academic supervisor Professor Eva Hevia for all her exceptional support, encouragement, motivation, guidance, knowledge, innovation and approachability that has made my project a success and Strathclyde a great place to be. I feel privileged to have been part of her group during a period when she has gained a number of awards and recognitions for her achievements, a large number of very high-quality publications and obtained her professorship at a very young age.

I am also very thankful to my second academic supervisor Professor Robert Mulvey with whom I completed my Master's project with, which stimulated my interest in research and organometallic chemistry. Rab has been a vast fountain of knowledge and insight and I have valued not only his approachability but also his list of recommended Glasgow restaurants.

Additionally, I would like to thank Dr Charles O'Hara and Dr Stuart Robertson, both of whom have served as tough but fair internal examiners. Stuart has been a great help, particularly with matters of X-ray crystallography and possess some silky football skills of which I have been witness to. Charlie's door has always been open and he has always been more than happy to go above and beyond to help myself and others.

I would like to thank Dr Jan Klett, Dr Thomas Cadenbach and Dr Tracy Nixon. Jan, an exceptionally talented and intelligent practical chemist, gave me my first introduction to air-sensitive chemistry during my Master's project and I have endeavoured to emulate his meticulous approach. Though only working together for the initial three months of my PhD, Thomas taught me a great deal about iron and ferrate chemistry, perhaps most importantly the secrets of the successful synthesis of $\text{Fe}(\text{HMDS})_2$. Tracy was invaluable during the direct ferration project, working tirelessly on the challenging organic syntheses, purifications and characterisations.

I was lucky to start my PhD at the same time as two others in the Hevia group, Marco and Marina, both of whom I have become great friends with as we have helped and supported each other through good and bad times in our PhDs together. Starting in the Hevia group the following year were Andy and Laia. Thank you to Laia for your friendship and for

introducing me to yoga. Andy, you're not so bad when you're not grumpy, even with some of your questionable music taste.

I'd like to thank the current post-docs in the Hevia group Alberto and Ross and past-member Tobi for all their generous help and advice over the years as-well as post-docs from other groups, Antonio and Markus who have helped me, particularly with crystallography.

Thank you to the rest of PhD students (past and present) for friendship, help and support and all the fun times inside and outside of the lab. Sam, Etienne, Silvia, Ana, Donna, Jenny, Sarah, Ben, Elaine, Emma and new-starts Vicky and Michael. A special mention to those whom I have worked alongside in the β -Lab (Sam, Marco, Andy, Silvia, Donna, Tobi, Tracy, Javi) for all the camaraderie, helping each other out and putting up with some (read: lots of) foul language and loss of temper on my part over minor practical problems which were all of my own doing.

I am grateful to the hard-working and enthusiastic Master's project students I mentored, Jamie McIntyre and Stuart Dargo. Both worked very hard on challenging ferrate chemistry projects and came away with good results and successes. Particular thanks to Jamie for the results he attained with DPA and the sodium ferrate system which are detailed in Chapter 1.

I am indebted to Dr Alan Kennedy, an X-ray crystallography guru, who has checked all my crystal structures and made them as good as they can possibly be as well as helping me learn much about X-ray crystallography. I'm sorry I left the liquid N₂ running unattended in the lab that time! I must also thank Professor Bill Clegg, Dr Mike Probert and Dr Paul Waddell at Newcastle University who collected data for two important crystal structures at the Diamond Light Source in Oxfordshire.

I am thankful to our collaborators in Barcelona, Dr Guillem Aromí and Ivana Borilovic, who have acquired magnetic data on a number of my compounds and produced comprehensive reports on each.

I have enjoyed working with Dr Chris Dodds in the 2nd and 3rd year teaching labs demonstrating to undergraduate students, something which I think has helped my development as a chemist and kept me on my toes with the basics. Chris has always been a source of great advice in post-graduate chemistry life and is always interested to hear about my research.

Craig Irving, amongst being one of the top people you want to know in the department at Strathclyde, has helped me numerous times with acquiring good NMR spectra on tricky paramagnetic compounds. I am also thankful to Alexander Clunie for the difficult job of running my elemental analysis samples and making the time to do so and Patricia Keating for help with GC-MS.

I must thank Janie-Anne Pickrell who works tirelessly to keep the inorganic labs organised and running smoothly for all of the students, post-docs and academics. I am very grateful also to Isabel Scott who has sorted many administration issues for me outwith the lab.

I would like to thank all my friends outside the lab (most who'll never read this) for taking an interest in my research, often putting up with (sometimes) dull chemistry chat but mostly making life very enjoyable over the past 4 years. Thank you Iain for being my flatmate for the majority of the time, for all the awesome parties we've hosted at 95 Morrison Street. A very special thank you to Rachel who has supported me massively and kept me sane during this final year. A big thank you to friends in Glasgow, Amir, Kirsty, Alanna, Lewis, Laura and new recruit Joanne for all the great times in the city and the rest scattered elsewhere, Eamon, Matt, Sean, Lawrie, Scott, Tai, Rob and a host of others.

I am forever grateful to my parents Robert and Jenny for their enduring love, support and encouragement throughout my whole university career; I would not have gone to university or completed a PhD without them. I also thank an amazing woman, Margaret Maddock, my grandmother for all her love and support and incredible stories. Thank you to my sister, Rosie, whom I was lucky to be born ahead of otherwise I would have been outshone and who I am sure will go on to become an excellent scientist. Thank you to my great-aunt Kate and her best friend Natasha for always being a welcoming home in Glasgow and stories of my great-uncle Phil.

Finally, I give thanks to the late Dr Alfred Maddock. Alfred was an eminent and exceptional chemist whom I credit for sparking a keen interest in chemistry and science from a young age and remains someone I continue to look up to and am inspired by.

Abstract

Building on previous developments on cooperative heterobimetallic reagents, this thesis aims to advance the understanding of the preparation and synthetic exploitation of alkali metal ferrates of Fe(II).

Using bis(amide) $\text{Fe}\{\text{N}(\text{SiMe}_3)_2\}_2$ as a precursor, here we report the syntheses and structures of a variety of sodium ferrates that have been prepared via direct co-complexation, where the single metal components $\text{NaN}(\text{SiMe}_3)_2$ and $\text{Fe}\{\text{N}(\text{SiMe}_3)_2\}_2$ self-assemble in the presence of a range of Lewis donors with different electronic properties and denticities. Furthermore, in some cases the presence of these donors is not required and the isolation and structural elucidation of two novel unsolvated sodium ferrates has been accomplished which display unique polymeric arrangements in the solid state.

The ability of sodium ferrates to functionalise NHC ligands has also been assessed, finding that when unsaturated NHC IPr (IPr = 1,3-bis(diisopropylphenyl)-imidazol-2-ylidene) is treated sequentially with $\text{NaCH}_2\text{SiMe}_3$ and $\text{Fe}\{\text{N}(\text{SiMe}_3)_2\}_2$, sodium ferrate $(\text{THF})_3\cdot\text{Na}[\text{C}\{\{\text{N}(2,6\text{-}^i\text{Pr}_2\text{C}_6\text{H}_3)\}_2\text{CHCFe}(\text{HMDS})_2\}]$ (**15**) is formed, containing an anionic NHC which binds to Fe via its C4 position and to Na through its C2 site. Interestingly, this complex was found to be an excellent precursor for Fe-*abnormal* NHC complexes and when treated with MeOTf afforded $[\text{CH}_3\text{C}\{\{\text{N}(2,6\text{-}^i\text{Pr}_2\text{C}_6\text{H}_3)\}_2\text{CHCFe}(\text{HMDS})_2\}]$ (**16**).

1,4-dioxane solvate $[\text{dioxane}\cdot\text{NaFe}(\text{HMDS})_3]$ (**17a**) has been found to be an efficient chemoselective base to promote the direct ferration at room temperature of a wide range of fluoroaromatic molecules. Structural elucidation of key organometallic intermediates has revealed the synergic bonding of the metals with Fe occupying the position previously filled by an H atom forming a strong Fe-C sigma bond, whereas the Na atom forms a dative bond with the F atom. These studies have revealed an important alkali metal effect, thus when the Na atom in **17a** is replaced by Li or K, the ferration processes are inhibited. Remarkably, by using two molar equivalents of **17a**, it is possible to di-ferrate tri- and tetrafluoro-substituted aromatics. These reactions take place at ambient temperature with excellent yields.

Reaction of 1,3,5-trifluorobenzene with three molar equivalents of **17a**, led to the isolation of $[\text{1,3-bis}(\text{FeHMDS})\text{-2,4,6-tris}(\text{HMDS})\text{-C}_6\text{H}]$ (**38**) resulting from the unprecedented two-fold C-H metallation/three-fold C-F activation of the substrate. Mechanistic studies suggest the

reaction is partly driven by the formation of NaF. Magnetic studies using have revealed that this new compound displays single-molecule magnet behaviour.

Publication and Conference Presentations

Publication in a Peer Reviewed Journal

Sodium Ferrate Complexes Containing Neutral and Anionic N-Heterocyclic Carbene Ligands: Structural, Synthetic, and Magnetic Insights, Maddock, L. C. H.; Cadenbach, T.; Kennedy, A. R.; Borilovic, I.; Aromí, G.; Hevia, E. *Inorg. Chem.* **2015**, *54*, 9201. DOI: 10.1021/acs.inorgchem.5b01638.

Chapter 2 is adapted from the publication above.

Conference Presentations (Oral)

New Expeditions in Alkali metal Ferrate Chemistry: Stoichiometric and Catalytic Applications, University of Strathclyde Inorganic Section West Brewery Talks, 11th June 2014, West Brewery, Glasgow

Novel Structural and Synthetic Insights in Alkali metal Ferrate Chemistry, 248th American Chemical Society National Meeting, 10th-14th August 2014, San Francisco, CA, USA

Conference Presentations (Poster)

Novel Structural and Synthetic Insights in Alkali metal Ferrate Chemistry, Universities of Scotland Inorganic Conference, 25th-26th July 2013, University of Edinburgh

Introducing N-Heterocyclic Carbenes into Ferrate Chemistry, Universities of Scotland Inorganic Conference, 4th-5th September 2014, University of Glasgow

Unexpected Sodium Ferrate-Mediated and Temperature Controlled C-H and C-F Activations of 1,3,5-trifluorobenzene, Universities of Scotland Inorganic Conference, 2nd-3rd July 2015, Heriot-Watt University, Edinburgh

Unexpected Sodium Ferrate-Mediated and Temperature Controlled C-H and C-F Activations of 1,3,5-trifluorobenzene, Royal Society of Chemistry Main Group Interest Group Annual Meeting, 11th September 2015, Burlington House, London

Nomenclature and Common Abbreviations

$^{\circ}$ – Degrees

η – Eta (denoting hapticity)

∞ – Infinity (denoting a long polymeric chain)

σ – Sigma (denoting a sigma bond)

θ – Theta (denoting angle)

^1H – Hydrogen-1

12-crown-4 – 1,4,7,10-tetraoxacyclododecane

$^{13}\text{C}\{^1\text{H}\}$ – Carbon-13 proton decoupled

18-crown-6 – 1,4,7,10,13,16-hexaoxacyclooctadecane

$^{19}\text{F}\{^1\text{H}\}$ – Fluorine-19 proton decoupled

2,2,2-crypt – 4,7,13,16,21,24-Hexaoxa-1,10-diazabicyclo[8.8.8]hexacosane

$^{31}\text{P}\{^1\text{H}\}$ – Phosphorous-31 proton decoupled

Å – Ångstroms

AC – Alternating Current

acac – Acetylacetonate

AlEt_3 – Triethyl Aluminium

AM – Alkali Metal

AMMM – Alkali-Metal-Mediated Metallation

*a*NHC – ‘Abnormal’ N-Heterocyclic Carbene

Ap^{TMS} – 4-methyl-2-[(trimethylsilyl)amino]pyridyl

Ar^{Pr^i} – $\text{C}_6\text{H}_3\text{-2,6}(\text{C}_6\text{H}_3\text{-2,6-}^i\text{pr}_2)_2$

$^{\text{Bu}}\text{ArOH}$ – 2,6-(di-*tert*-butyl)-4-(methyl)-phenol

^{Me}ArOH – 2,4,6-(trimethyl)phenol

ATP – Adenosine Triphosphate

BC – Before Christ

BEt₃ – Triethylborane

BTA – Benzotriazolyl

ⁿBu – *normal*-butyl

ⁿBuLi – *n*-butyllithium

^sBuLi – *sec*-butyllithium

^tBu – *tert*-butyl

C₆D₆ – Deuterated Benzene

C₆H₅F – Fluorobenzene

ca. – Circa

CaCl₂ – Calcium Chloride

CaH₂ – Calcium Hydride

CCDC – Cambridge Crystallographic Data Centre

cf. – Compare with

CFCs – Chlorofluorocarbons

CIP – Contacted Ion-Pair

COE – *cis*-cyclooctene

COT – 1,3,5,7-*cyclo*-octatetraene

Cp – Cyclopentadienyl

Cp* - Pentamethylcyclopentadienyl

D₂O – Deuterated Water

d₅-pyr – Deuterated Pyridine

d₈-tol – Deuterated Toluene

d₈-THF – Deuterated Tetrahydrofuran

DA – Diisopropylamide

DA(H) – Diisopropylamine

DC – Direct Current

DFT – Density Functional Theory

DG – Directing Group

Dipp – 2,6-diisopropylphenyl

DoM – Directed *ortho*-Metallation

DMEDA – *N,N'*-dimethylethylenediamine

DPA – 2,2'-dipyridylamide

DPA(H) – 2,2'-dipyridylamine

DSIP – Donor-Separated Ion-Pair

DTEDA – *N,N'*-di-*tert*-butylethylenediamine

E – Energy

EPR – Electron Paramagnetic Resonance Spectroscopy

eq. – Equivalents

ESI – Electrospray Ionisation

ESR – Electron Spin Resonance Spectroscopy

Et – Ethyl

Et₂O – Diethyl ether

g – *g* factor, a dimensionless magnetic moment quantity characterising the magnetic moment and gyromagnetic ratio of a particle or nucleus

GUI – Graphical User Interface

i – *Ips*

Fe(acac)₃ – Iron(III) Acetylacetonate

FeBr₂ – Iron(II) Bromide

FeCl₂ – Iron(II) Chloride

FeCl₃ – Iron(III) Chloride

Fe(HMDS)₂ – Iron bis[bis(trimethylsilyl)amide]

FG – Functional Group

GC-MS – Gas Chromatography-Mass Spectrometry

H₂ – Dihydrogen

H₂NDipp – 2,6-diisopropylaniline

HCl·NEt₃ – Triethylamine Hydrochloride

HFCs – Hydrofluorocarbons

H₃PO₄ – Phosphoric Acid

HMDS – 1,1,1,3,3,3-hexamethyldisilazide/bis(trimethylsilyl)amide, N(SiMe₃)₂

HMDS(H) – 1,1,1,3,3,3-hexamethyldisilazane/bis(trimethylsilyl)amine

HR-MS – High Resolution-Mass Spectrometry

ICE – Inverse Crown Ether

IMes – 1,3-bis(2,4,6-trimethylphenyl)imidazol-2-ylidene

in situ – In the reaction mixture

in vacuo – Under Vacuum

IPr – 1,3-bis-(2,6-diisopropylphenyl)imidazol-2-ylidene

κ – Kappa (denoting denticity)

K – Kelvin (or Potassium)

KC₈ – Potassium Graphite

KHMDS – Potassium Bis(trimethylsilyl)amide

L – Orbital Angular Momentum

LiBr – Lithium Bromide

LiCl – Lithium Chloride

LDA – Lithium Diisopropylamide

LiHMDS – Lithium Bis(trimethylsilyl)amide

LiTMP – Lithium 2,2,6,6-tetramethylpiperidide

Me – Methyl

Me₆TREN – Tris[2-(dimethylamino)ethyl]amine

MeLi – Methyllithium

MeOTf – Methyl Triflate

Mes – Mesityl, 1,3,5-trimethylbenzene

m- – *Meta*

N₂ – Dinitrogen

Na₂S₂O₃ – Sodium Thiosulfate

NaHMDS – Sodium Bis(trimethylsilyl)amide

NOESY – Nuclear Overhauser Effect Spectroscopy

NHC – N-Heterocyclic Carbene

NMR – Nuclear Magnetic Resonance

OTf – Triflate, Trifluoromethanesulfonate

P₂O₅ – Phosphorus Pentoxide

p- – *Para*

PCy₃ – Tricyclohexylphosphine

Ph – Phenyl

PhB(MesIm)₃ – Phenyltris(1-mesitylimidazol-2-ylidene)borate

PhLi – Phenyllithium

Ph₂SiCl₂ – Dichlorodiphenylsilane

PMDETA – *N,N,N',N',N''*-pentamethyldiethylenetriamine

PMe₃ – Trimethylphosphine

PPh₃ – Triphenylphosphine

ppm – Parts Per Million

PTFE – Polytetrafluoroethylene

o- – *Ortho*

ox – Oxalate

r.d.s – Rate Determining Step

RT (or rt/r.t.) – Room (ambient) Temperature, *ca.* 20°C

S₈ – Sulfur flowers, α -Sulfur, cyclo-S₈

S=PMe₃ – Trimethylphosphine Sulfide

S=PPh₃ – Triphenylphosphine Sulfide

S_EAr – Electrophilic Aromatic Substitution

SET – Single Electron Transfer

SMM – Single-Molecule Magnet

SQUID – Superconducting Quantum Interference Device

SSIP – Solvent Separated Ion-Pair

Σ – Sum of

T – Tesla

T – Temperature

TEMPO – (2,2,6,6-tetramethylpiperidin-1-yl)oxyl

THF – Tetrahydrofuran

THP – Tetrahydropyran

thym – thymine²⁻

TIP – Temperature Independent Paramagnetism

TMEDA – *N,N,N',N'*-tetramethylethylenediamine

TMP – 2,2,6,6-tetramethylpiperidine

TMP(H) – 2,2,6,6-tetramethylpiperidine

TMS – Trimethylsilyl

tz – 1,2,3-triazolyl

μ – Mu (denoting bridging ligand)

μ_B – Bohr Magnetons

μ_{eff} – Effective Magnetic Moment

vide infra – See below

vide supra – See above

w/w – weight/weight, mass fraction

χ_M – Magnetic Susceptibility

XRD – Single-crystal X-ray Diffraction

ZFS – Zero-Field Splitting

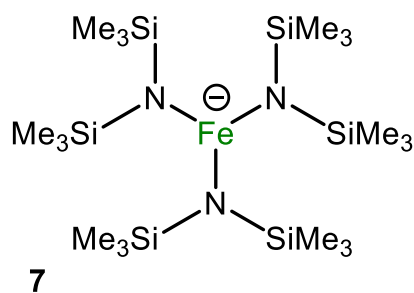
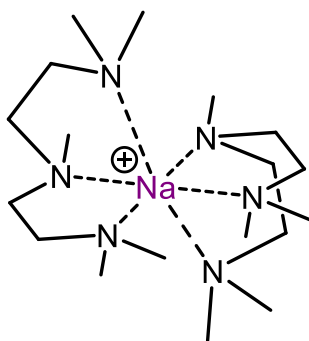
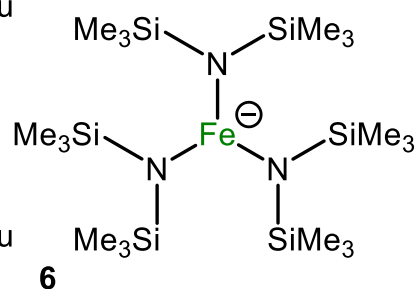
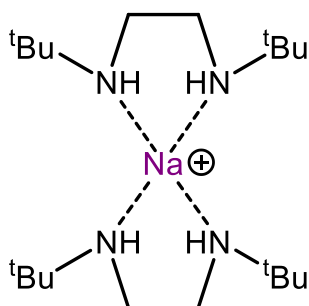
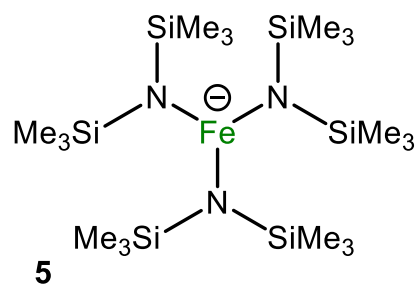
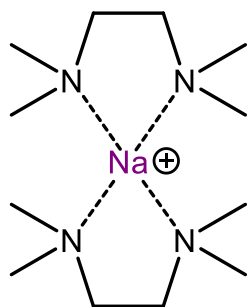
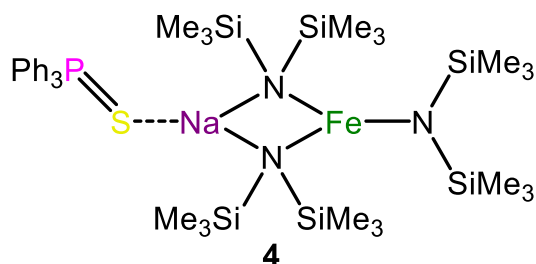
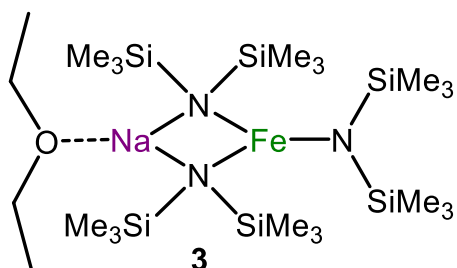
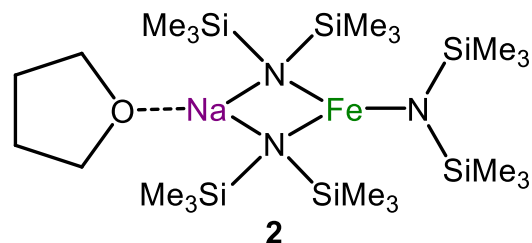
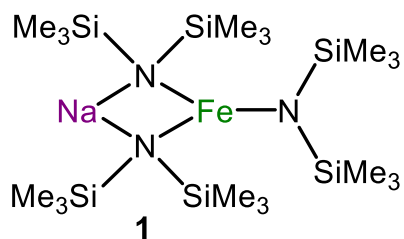
List of Numbered Compounds

- 1 $[\{\text{NaFe}(\text{HMDS})_3\}_\infty]$
- 2 $[\text{THF} \cdot \text{NaFe}(\text{HMDS})_3]$
- 3 $[\text{Et}_2\text{O} \cdot \text{NaFe}(\text{HMDS})_3]$
- 4 $[\text{PPh}_3=\text{S} \cdot \text{NaFe}(\text{HMDS})_3]$
- 5 $[\text{Na}(\text{TMEDA})_2]^+[\text{Fe}(\text{HMDS})_3]^-$
- 6 $[\text{Na}(\text{DTEDA})_2]^+[\text{Fe}(\text{HMDS})_3]^-$
- 7 $[\text{Na}(\text{PMDETA})_2]^+[\text{Fe}(\text{HMDS})_3]^-$
- 8 $[\text{Me}_6\text{TREN} \cdot \text{Na}]^+[\text{Fe}(\text{HMDS})_3]^-$
- 9 $[\{\text{Fe}(\text{HMDS})(\text{DPA})\}_2]$
- 10 $[(\text{THF})_2 \cdot \text{NaFe}(\text{DPA})(\text{HMDS})_2]$
- 11 $[\{\text{THF} \cdot \text{NaFe}(\text{DPA})_3\}_\infty]$
- 12 $[\{\text{NaFe}(\text{HMDS})_2(\text{CH}_2\text{SiMe}_3)\}_\infty]$
- 13 $[\text{Na}(\text{IPr})_2]^+[\text{Fe}(\text{HMDS})_3]^-$
- 14 $[(\text{THF})_3 \cdot \text{NaIPr}]^+[\text{Fe}(\text{HMDS})_2(\text{CH}_2\text{SiMe}_3)]^-$
- 15 $(\text{THF})_3 \cdot \text{Na}[\text{C}\{\text{N}(2,6\text{-}^i\text{Pr}_2\text{C}_6\text{H}_3)_2\text{CHCFe}(\text{HMDS})_2\}]$
- 16 $[\text{CH}_3\text{C}\{\text{N}(2,6\text{-}^i\text{Pr}_2\text{C}_6\text{H}_3)_2\text{CHCFe}(\text{HMDS})_2\}]$
- 17 $[\text{dioxane} \cdot \{\text{NaFe}(\text{HMDS})_3\}_2]$
- 17a $[\text{dioxane} \cdot \text{NaFe}(\text{HMDS})_3]$
- 18 $[\{\text{dioxane} \cdot \text{NaFe}(\text{C}_6\text{H}_4\text{F})(\text{HMDS})_2\}_\infty]$
- 19 $[\{\text{dioxane} \cdot \text{NaFe}(1,3\text{-C}_6\text{H}_3\text{F}_2)(\text{HMDS})_2\}_\infty]$
- 20 $[\{(\text{dioxane})_2 \cdot \text{Na}_2\text{Fe}(1,3\text{-C}_6\text{H}_3\text{F}_2)(\text{HMDS})_2\}^+\{\text{Fe}(\text{HMDS})_3\}^-]_\infty$
- 21 $[\text{dioxane} \cdot \{\text{NaFe}(1,4\text{-C}_6\text{H}_3\text{F}_2)(\text{HMDS})_2\}_2]_\infty$
- 22 $[\text{dioxane} \cdot \{\text{NaFe}(1,2,4\text{-C}_6\text{H}_2\text{F}_3)(\text{HMDS})_2\}_2]_\infty$
- 23 $[\{\text{dioxane} \cdot \text{NaFe}(\text{HMDS})_2\}_2(1,2,4,5\text{-C}_6\text{F}_4)]_\infty$
- 24 $[\text{dioxane} \cdot \{\text{NaFe}(\text{C}_6\text{F}_5)(\text{HMDS})_2\}_2]_\infty$
- 25 $[\{\text{dioxane} \cdot \text{NaFe}(1\text{-C}_{10}\text{H}_6\text{F})(\text{HMDS})_2\}_\infty]$
- 26 $[\text{dioxane} \cdot \{\text{dioxane} \cdot \text{NaFe}(1\text{-Br-}3,5\text{-C}_6\text{H}_2\text{F}_2)(\text{HMDS})_2\}_2]$

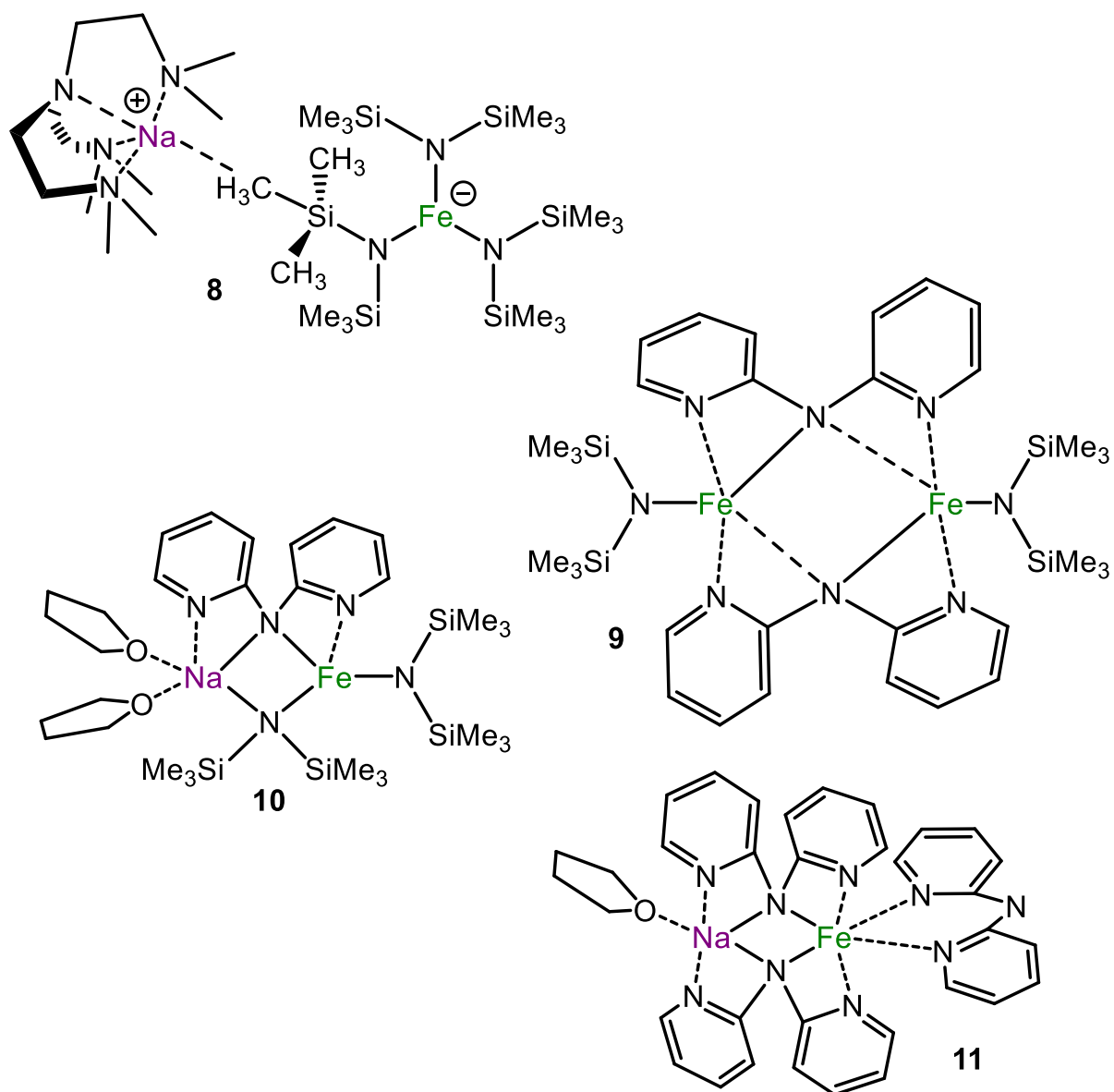
- 27 $[\{(dioxane)_2 \cdot Na_2Fe(3-C_6H_3FOMe)(HMDS)_2\}^+ \{Fe(HMDS)_3\}^-]_\infty$
- 28 $[dioxane \cdot \{Na(PhOMe)_3\}_2]^{2+} [\{Fe(HMDS)_3\}_2]^{2-}$
- 29 $[dioxane \cdot \{NaFe(3,5-C_6H_2F_2OMe)(HMDS)_2\}_2]_\infty$
- 30 $[Na_2Fe_2(HMDS)_4(O)]$
- 31 $[\{dioxane \cdot (NaHMDS)_2\}_\infty]$
- 32 $[dioxane \cdot LiFe(HMDS)_3]$
- 33 $[\{dioxane \cdot KFe(HMDS)_3\}_\infty]$
- 34 $[\{KFe(HMDS)_3\}_\infty]$
- 35 $[dioxane \cdot \{NaFe(HMDS)_2(CH_2SiMe_3)\}_2]$
- 36 $[\{(dioxane)_{1.5} \cdot NaFe(1,3,5-C_6H_2F_3)(HMDS)_2\}_2]$
- 37 $[\{dioxane \cdot NaFe(HMDS)_2\}_2(1,3,5-C_6HF_3)]_\infty$
- 38 $[1,3-bis(FeHMDS)-2,4,6-tris(HMDS)-C_6H]$
- 39 $[1,3-bis(FeHMDS)-2,4,6-tris(HMDS)-C_6F]$
- 40 $[1,3-bis(FeHMDS)-2,4,6-tris(HMDS)-C_6Br]$
- 41 $[1,3-diiodo-2,4,6-tris(HMDS)-C_6H]$
- 42 $[1,3,5-tris(HMDS)-C_6H]$
- 43 $[dioxane \cdot LiFe(HMDS)_2(1,3,5-C_6H_2F_3)]$

Compounds Prepared Within This Thesis

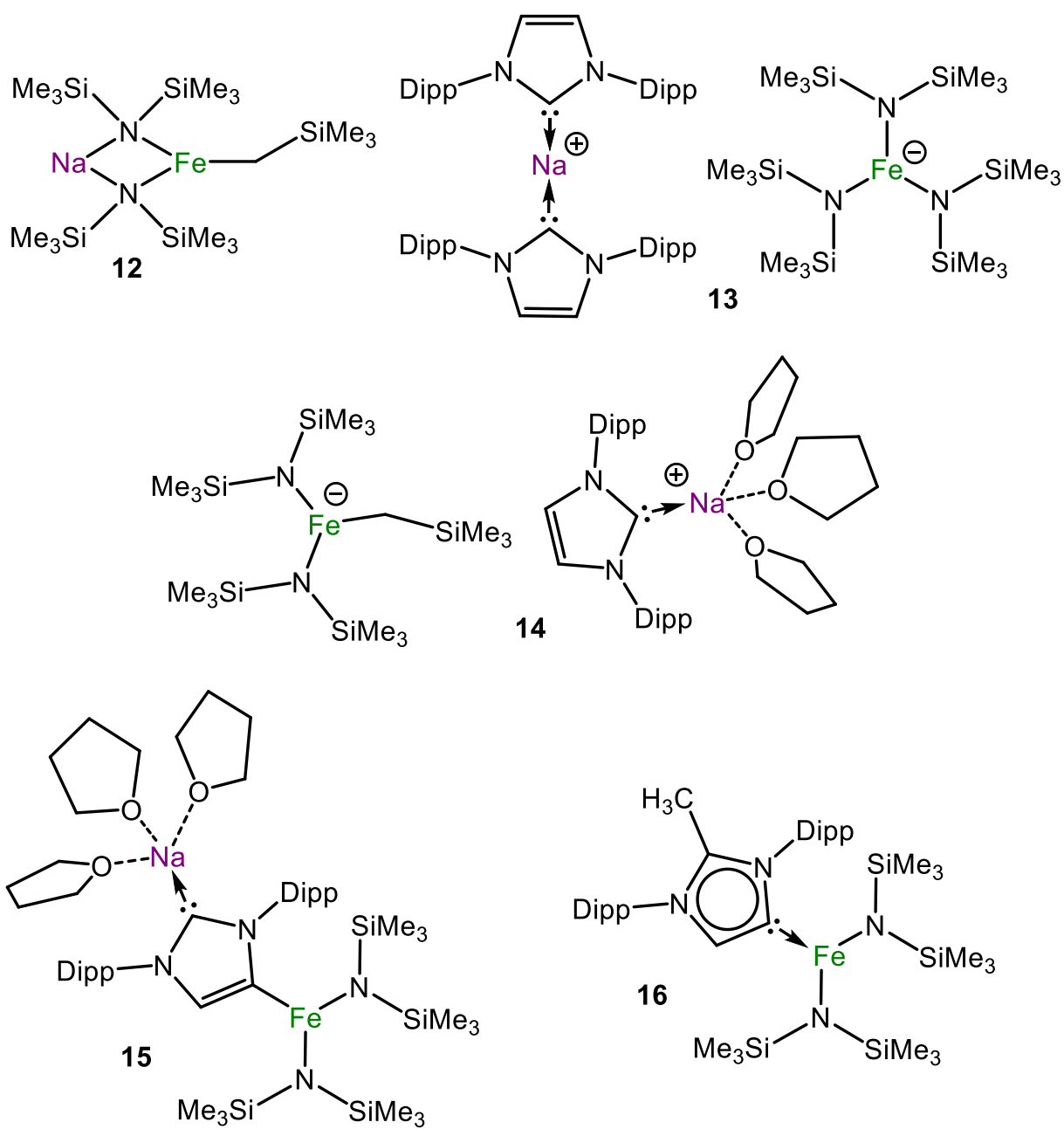
Chapter 1



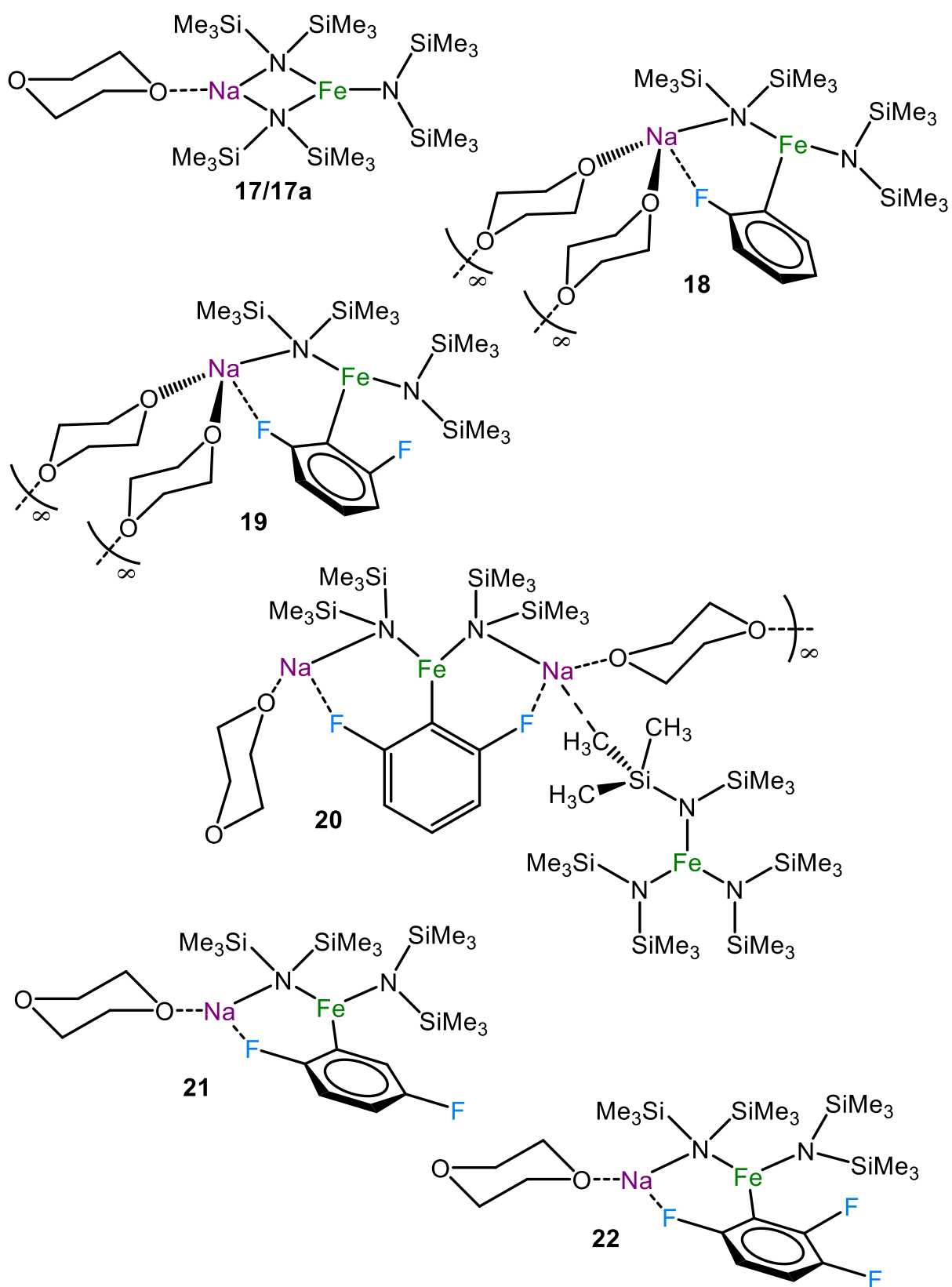
Chapter 1



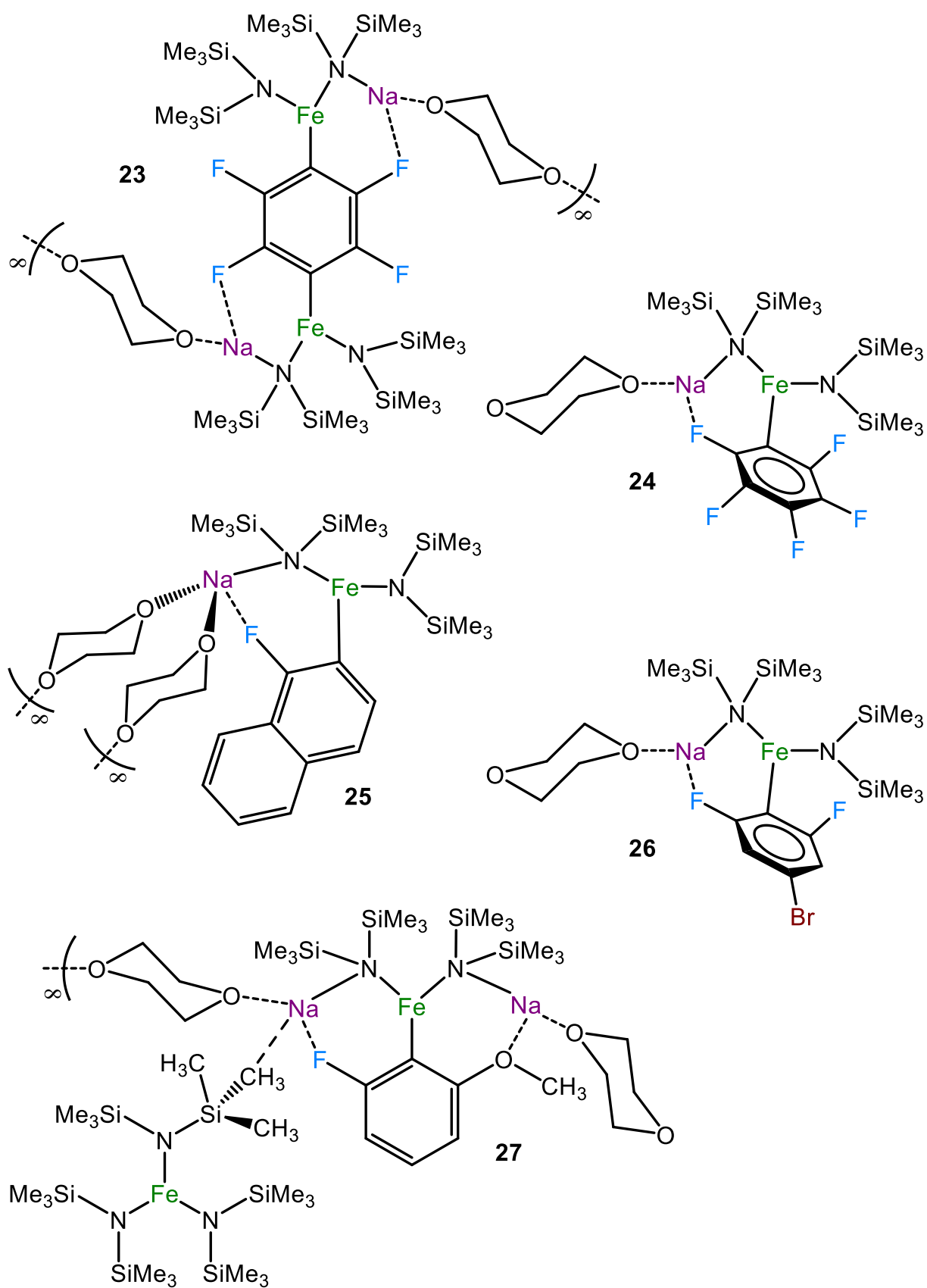
Chapter 2



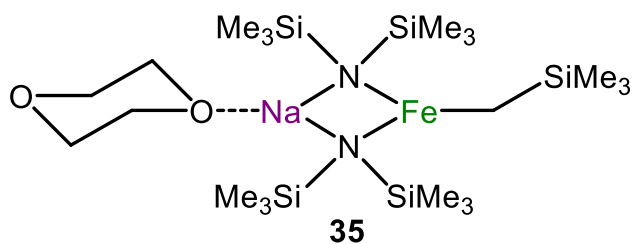
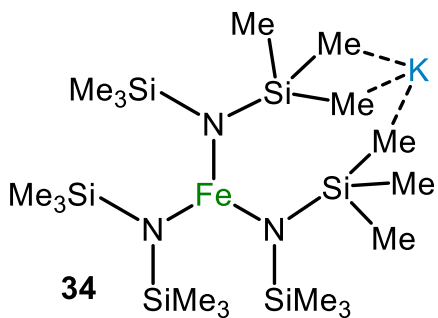
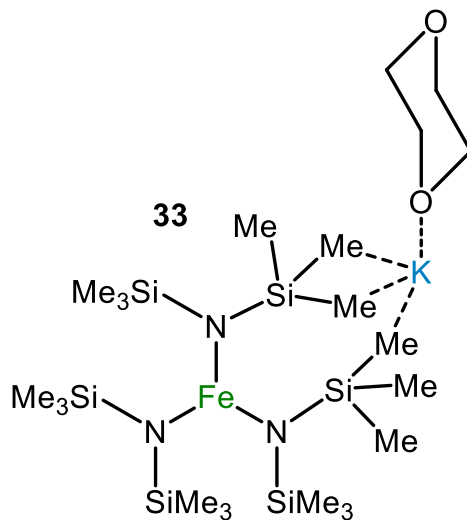
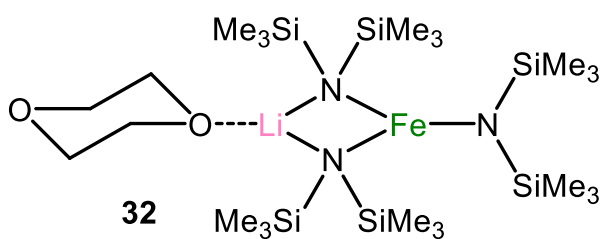
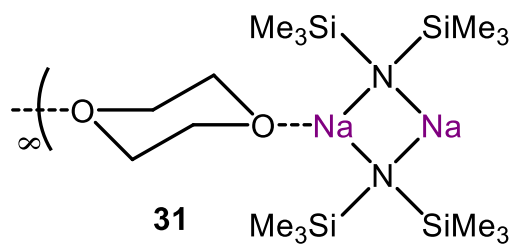
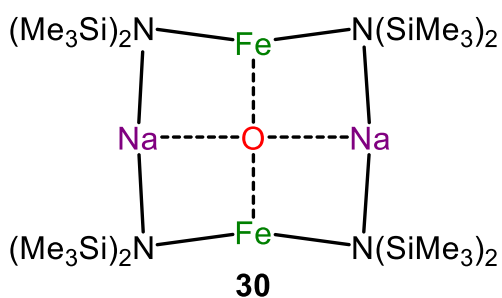
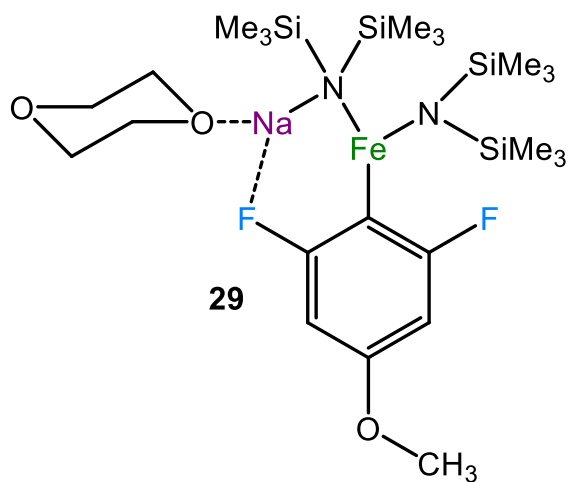
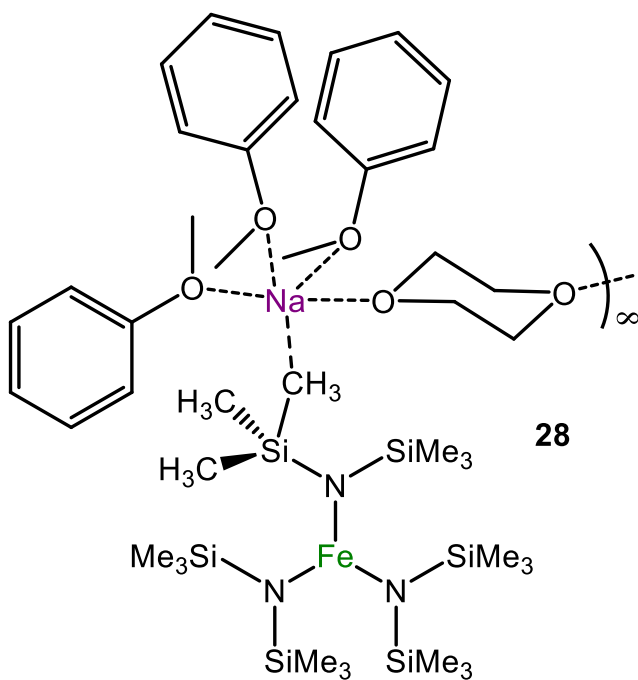
Chapter 3



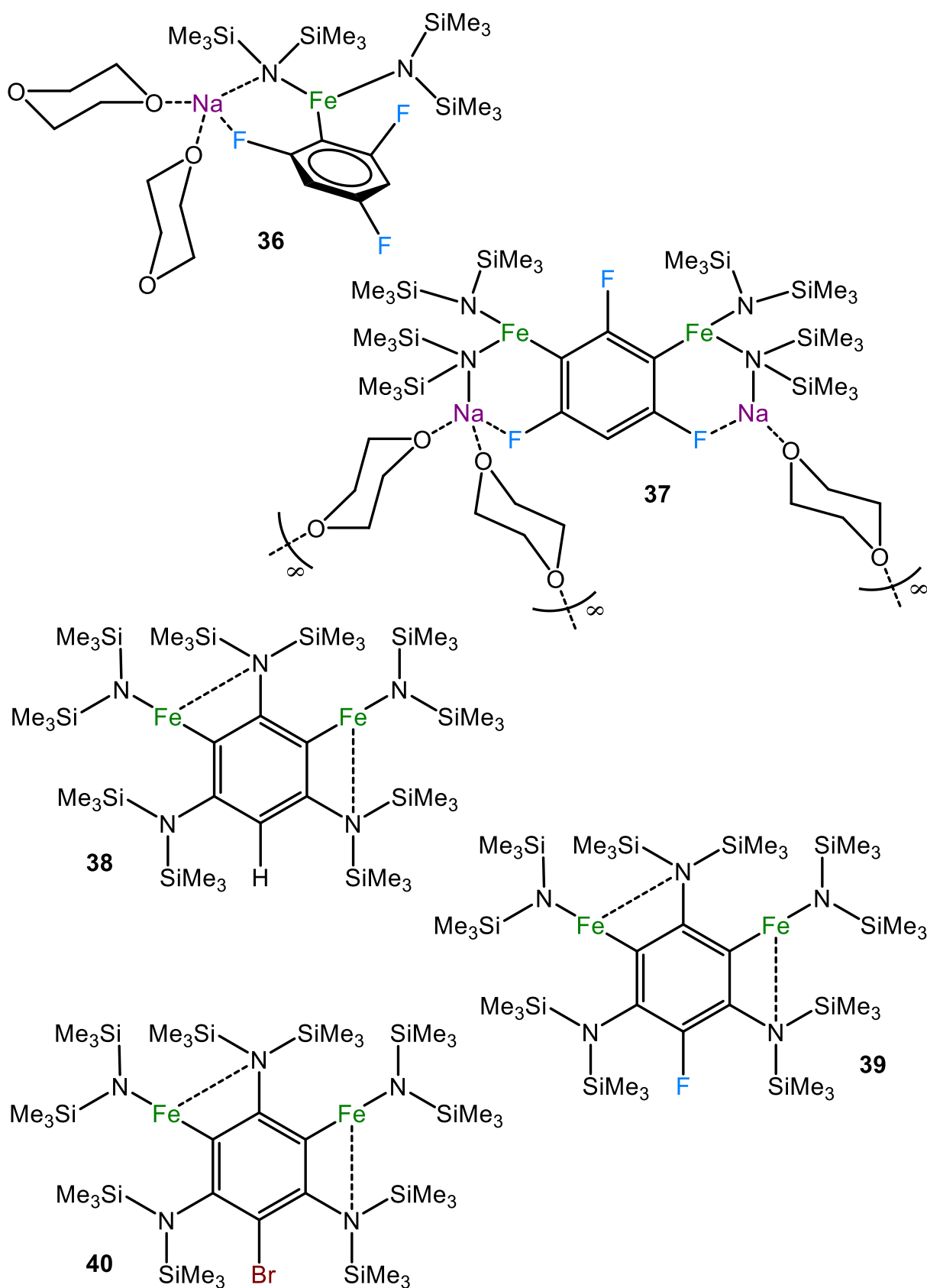
Chapter 3



Chapter 3



Chapter 4



Chapter 4

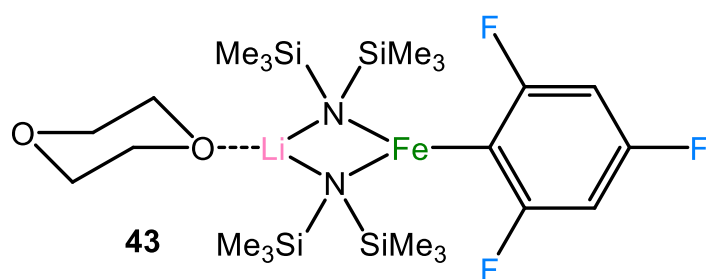
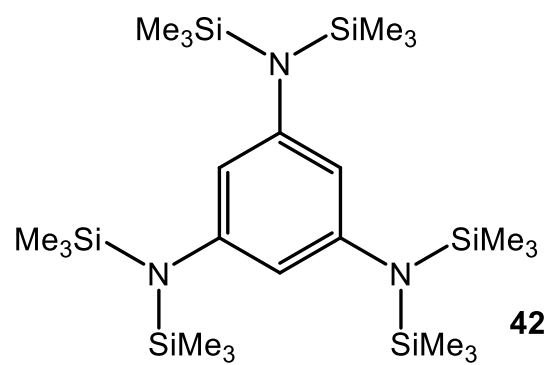
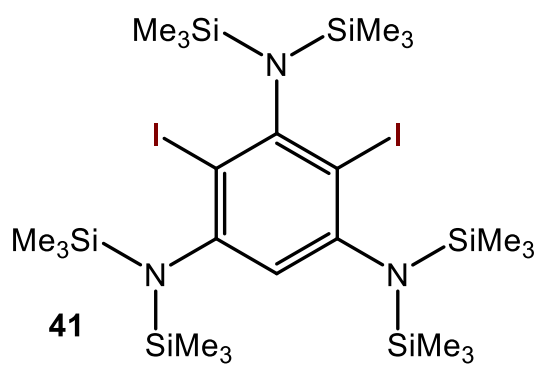


Table of Contents

Declaration	i
Dedication	ii
Acknowledgments	iii
Abstract	vi
Publication and Conference Presentations	viii
Nomenclature and Common Abbreviations	x
List of Numbered Compounds	xvii
Compounds Prepared Within This Thesis	xix
Table of Contents	xxvii

I Introduction

I.I	Cooperative Bimetallic Complexes	1
I.II	Iron Chemistry	6
I.III	Ferrate Chemistry	12
I.IV	Gap in the Knowledge	15
I.V	Aims	16

Chapter 1 Structural Variations of Sodium Ferrates with Lewis Donors

1.1	Results and Discussion	19
1.1.1	Assessing Co-complexation Reactions: Synthesis of Solvent-Free $[\{\text{NaFe}(\text{HMDS})_3\}_\infty]$	19
1.1.2	Introduction to NMR Spectroscopy of Paramagnetic Species	22
1.1.3	Assessing Donor Effects in Sodium Ferrate Chemistry: $[\{\text{NaFe}(\text{HMDS})_3\}_\infty]$ and Lewis Donors	27
1.1.3.1	Monodentate Lewis Donors: THF, Et ₂ O and S=PPh ₃	28
1.1.3.2	Bidentate Lewis Donors: TMEDA and DTEDA	35
1.1.3.3	Polydentate Lewis Donors: PMDETA and Me ₆ TREN	38

1.1.4	Transamination Reactions with 2,2'-Dipyridylamine	41
1.1.4.1	Magnetometry Studies of Fe and Ferrate DPA Complexes	50
1.2	Conclusions	55

Chapter 2 N-Heterocyclic Carbene Stabilised Sodium Ferrates: Structural, Synthetic and Magnetic Studies

2.1	Introduction to N-Heterocyclic Carbenes: Normal, Abnormal and Anionic	56
2.2	Iron N-Heterocyclic Carbene Complexes	58
2.3	Results and Discussion	61
2.3.1	[{NaFe(HMDS)₂(CH₂SiMe₃)}]: A Mixed Amido/Alkyl Sodium Ferrate	61
2.3.2	Reactivity Studies with IPr	63
2.3.3	Anionic to Abnormal: An Abnormal NHC-Fe Complex via Electrophilic Interception	70
2.3.4	Magnetometry Studies of Sodium Ferrate NHC Complexes	73
2.4	Conclusions	78

Chapter 3 Direct Ferration of Fluoroaromatic Substrates

3.1	C-H Activation of Fluorinated Aromatic Molecules	79
3.1.1	Deprotonative Metallation of Fluoroaromatics	80
3.2	Results and Discussion	86
3.2.1	Synthesis of an Efficient Sodium Ferrate Base for the Metallation of Fluorinated Aryl Substrates	86
3.2.2	Direct <i>ortho</i>-Ferration of Fluorobenzene	88
3.2.3	Exploration of Substrate Scope	93
3.2.3.1	Methodology for Ferration and Electrophilic Iodination of Fluorinated Aryl Substrates	94
3.2.4	Synthesis, Isolation and Structural Characterisation of Ferrated Intermediates	97

3.2.4.1	Structural and Spectroscopic Studies on Metallated Intermediates of Direct Ferration Reactions: (a) Polyfluoroarenes	100
3.2.4.2	Structural and Spectroscopic Studies on Metallated Intermediates of Direct Ferration Reactions: (b) Other Substituted Fluoroarenes	108
3.2.5	Structural Summary	114
3.2.6	Magnetometry Studies of Ferrated Fluoroaromatic Complexes	117
3.2.7	Negative Results	121
3.2.8	Other Structures Obtained from C-H Activation Studies	123
3.2.8.1	Importance of Air and Moisture in Ferration Processes	123
3.2.8.2	A Polymeric NaHMDS 1,4-Dioxane Solvate	129
3.2.8.3	Exploring the Alkali Metal Effect	131
3.2.8.4	Synthesis of a Heteroleptic Sodium Ferrate Dioxane Base	135
3.3	Conclusions	136

Chapter 4 C-H and C-F Activation of 1,3,5-Trifluorobenzenes

4.1	Introduction to C-F Bond Activation	138
4.2	Results and Discussion	143
4.2.1	Mono- and Di-Ferration	143
4.2.2	Di-Ferration and Three-Fold C-F Activation	148
4.2.3	Mechanistic Investigations	158
4.2.3.1	Assessing the Reaction of 1,3,5-Trifluorobenzene with Single-Metal Components of 17a	159
4.2.3.2	Dynamic Nature of the Reaction	160
4.2.3.3	Extension to 1,3,5-Trifluorobenzene Derivatives	162
4.2.3.4	Thermal Stabilities of Complexes 36 and 37	166
4.2.3.5	From Di-metallation to C-F Activation	167
4.2.3.6	Mechanistic Proposal: Cascade Reaction	169
4.2.4	Electrophilic Quenching	171
4.2.5	Magnetometry Studies	173
4.2.5.1	Static Magnetic Properties of Complexes 38 and 39	173
4.2.5.2	Dynamic Magnetic Properties of Complexes 38 and 39	175
4.2.5.3	Static Magnetic Properties of Complexes 36 and 37	183
4.2.6	Other Associated Reactions	187

4.3	Conclusions	191
II	Conclusions and Further Work	
<hr/>		
II.I	Conclusions	193
II.II	Further work	195
III	Experimental	
<hr/>		
III.I	General Experimental Techniques	198
III.I.I	Schlenk Techniques	198
III.I.II	Glove Box	199
III.I.III	Solvent Drying and Purification	200
III.I.IV	Commercial Reagents	200
III.I.V	Preparation of Starting Materials	200
III.I.VI	NMR Spectroscopy	201
III.I.VII	Magnetometry Studies	202
III.I.VIII	Organic Work-Up	202
III.I.IX	Gas Chromatography-Mass Spectrometry	203
III.I.X	Elemental Analysis	203
III.II	Synthesis and Characterisation of Numbered Inorganic Compounds	203
III.II.I	Chapter 1	203
III.II.II	Chapter 2	209
III.II.III	Chapter 3	212
III.II.IV	Chapter 4	221
III.III	Synthesis and Characterisation of Numbered Organic Compounds	225
III.III.I	Chapter 3	225
III.III.II	Chapter 4	230

III.IV	X-Ray Crystallography	232
III.IV.I	Chapter 1 Crystal Structures	232
III.IV.II	Chapter 2 Crystal Structures	236
III.IV.III	Chapter 3 Crystal Structures	239
III.IV.IV	Chapter 4 Crystal Structures	246
III.V	Supplementary Magnetic Data	248
References		250

I – Introduction

I.I Cooperative Bimetallic Complexes

Bimetallic compounds which combine two different metals of markedly different polarities are currently attracting widespread interest amongst the vast community of synthetic chemists.¹ Switching on cooperative effects, these mixed-metal compounds have emerged as a new family of versatile and effective organometallic reagents which can participate in numerous key organic transformations such as deprotonative metallation, metal/halogen exchange or nucleophilic addition reactions to name a few.² Generally known as ‘ate’ compounds, these systems combine a strongly polar metal (e.g. a Group 1 alkali metal) with a lower polarity metal (such as Mg, Zn, Al) in a discrete molecular framework supported by an array of anionic basic ligands and often neutral Lewis donors (Figure I-1).

Outperforming traditional single-metal reagents, these bimetallic species exhibit unique synergic reactivity profiles, offering in many cases, enhanced selectivities and functional group tolerances.³ Thus, unlike traditional polar organometallic reagents such as organolithiums that usually require the use of extremely low temperature (-78°C), bimetallic reagents such as alkali metal magnesiates, zincates or aluminates can be efficiently used at ambient temperatures without observing undesired side reactions.

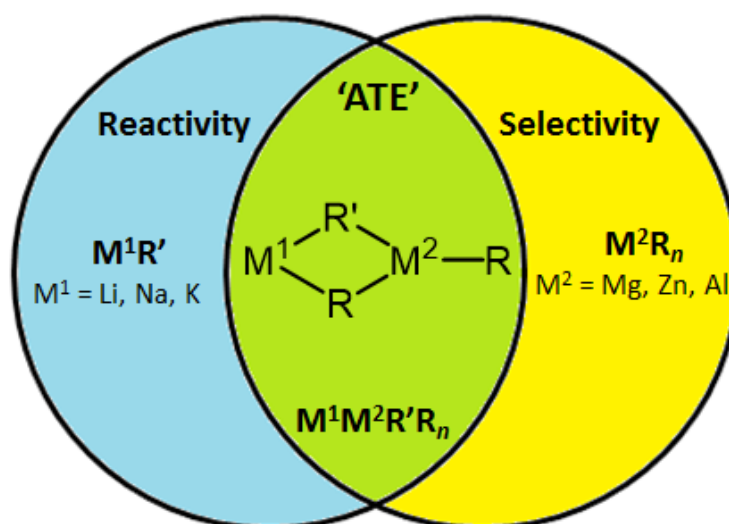
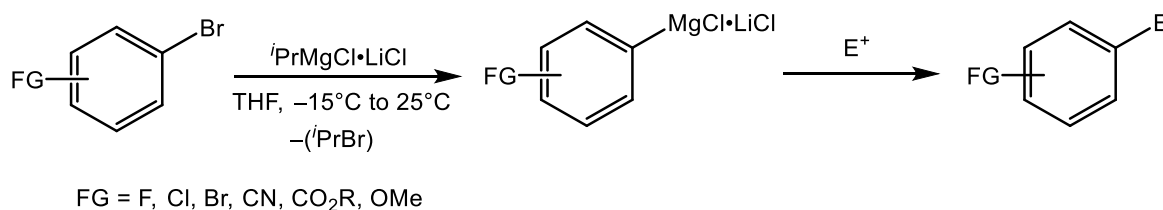


Figure I-1 - Representative example of a mixed-metal ate complex.

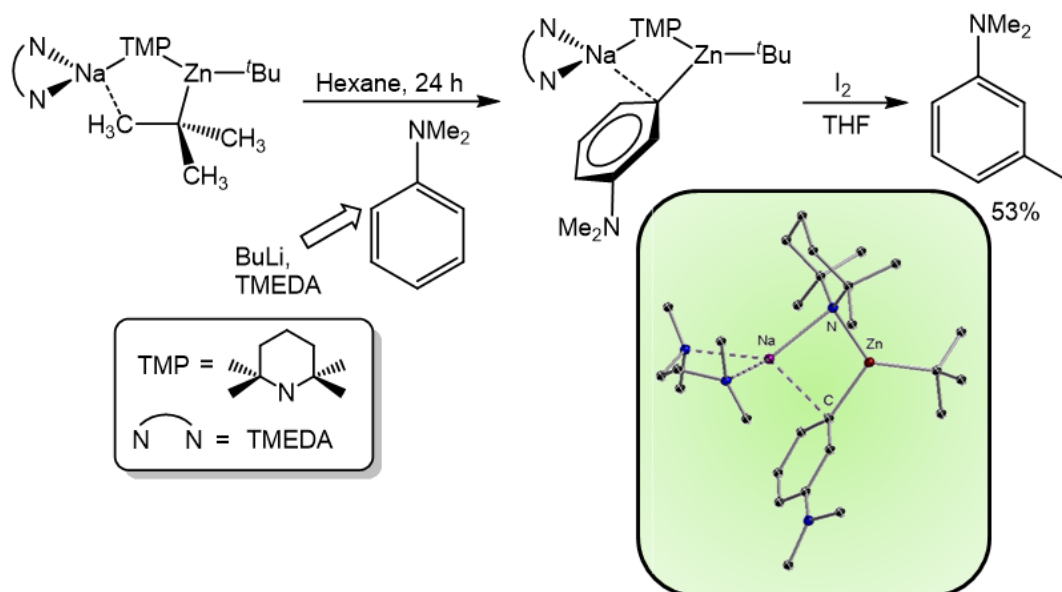
An important landmark in this evolving area of research is the development of “turbo-Grignard” reagents (of the formula $\text{RMgCl}\cdot\text{LiCl}$, R = alkyl group) by the Knochel research

group⁴, where the addition of stoichiometric amounts of LiCl to Grignard reagents can greatly enhance the nucleophilicity of the latter⁵, allowing access to highly functionalised organomagnesium reagents via direct Mg-halogen exchange (Scheme I-1). Related systems where the alkyl group is replaced by the amido TMP (2,2,6,6-tetramethylpiperidide), also known as “turbo-Hauser” bases,⁶ have found widespread applications for the metallation (via metal-hydrogen exchange) of a variety of substituted aromatic and heteroaromatic molecules.⁷



Scheme I-1 - Direct Mg-halogen exchange by the “turbo-Grignard” reagent *i*PrMgCl·LiCl on a variety of substituted aryl substrates.

Another milestone in the field is the use of heterobimetallic amide reagents, reported by Mulvey, for alkali metal-mediated metallation (AMMM)^{1,8} processes, facilitating in certain cases the regioselective deprotonation of organic substrates in remote positions, not available using conventional monometallic bases. Thus for example, when *N,N*-dimethylaniline is reacted with mixed sodium-zinc complex [(TMEDA)NaZn(TMP)(*t*Bu)₂] (TMEDA = *N,N,N',N'*-tetramethylethylenediamine) it is possible to directly replace one of its meta-hydrogens with a zinc centre (Scheme I-2).^{9,10}



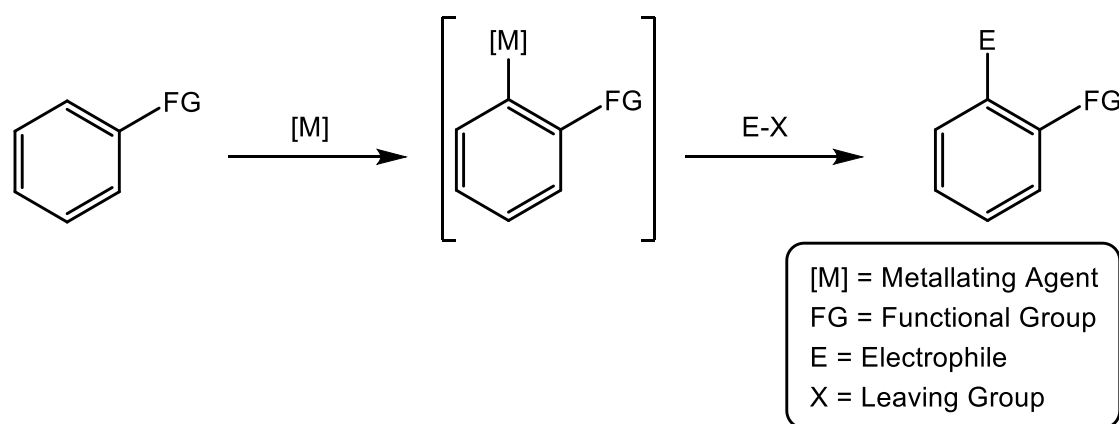
Scheme I-2 - Unusual meta-metallation of *N,N*-dimethylaniline with a sodium-zincate base and the crystal structure of the intermediate metallated complex. Hydrogen atoms omitted for clarity.

From an organic perspective, the regioselectivity of this reaction is truly surprising as conventional single-metal reagents deprotonate this molecule exclusively at the *ortho* position (which is activated by the presence of the NMe_2 group).¹¹ This synergic deprotonation constituted the first example of direct-*meta*-metallation where the cooperative effect of both metals, Na and Zn, overrides the activating and acidifying effect of the NMe_2 group.¹² By isolating and structurally defining the organometallic intermediate, the authors demonstrate that the reaction is in fact an example of direct zincation, where the Zn centre forms a strong sigma bond to the *meta*-carbon that has experienced the metallation whereas the alkali metal adopts a perpendicular disposition, π -engaging with the metallated ring (see Scheme I-2). Computational studies on this reaction using DFT calculations show that these unique and distinct bonding modes between the metals has a major role in the stabilisation of this intermediate.

Another innovative in the field of heterobimetallic chemistry has been the development of the “LiC-KOR” superbases, pioneered by Schlosser and Lochmann.^{13–15} These superbasic reagents are formed *in situ* by the combination of an alkyl lithium reagent (LiC) with a potassium alkoxide (KOR) in solution and typically exhibit dramatically enhanced reactivity and selectivity for metal/hydrogen exchange when compared to their monometallic components;^{15,16} a benchmark of their strength being their ability to metallate benzene and toluene.¹⁷ Expansion to other alkali metal alkoxides has led to the establishment of many

useful superbase systems which have enjoyed widespread application within synthetic chemistry.¹⁸⁻²⁰

Countless key organic transformations for synthesis are carried out via metallation reactions.⁸ By selectively replacing a non-polar C-H bond by a much more polar and therefore reactive M-C bond, deprotonative metallation of a target molecule opens the door to a world of synthetic possibilities (Scheme I-3). Traditionally these types of reactions have been the domain of Group 1 polar organometallics such as organolithiums or lithium amide reagents; the main reason for this being the high reactivity of their Li-C or Li-N bonds, as well as their ready availability.²¹ Nevertheless, these hard, polar bases suffer from a number of drawbacks. Due to their hyper-reactivity, sub-ambient temperatures are routinely required (typically -78°C) to prevent unwanted side reactions, especially with substituents bearing sensitive functional groups (poor tolerance) and a lack of selectivity is also a common feature.²² Whilst the use of softer metals such as aluminium or magnesium presents an alternative option, they are generally found to be much less reactive being considered weak bases.



Scheme I-3 - Generalised scheme of deprotonative metallation followed by quenching with an electrophile.

Within the context of heterobimetallic reagents and their applications in deprotonative metallation chemistry, structural and theoretical studies have demonstrated that the lower polarity metal in these systems actually carries out the deprotonation, occupying the position vacated by the departing H. As opposed to their homometallic relatives many of these specially designed multi-component bases do not require extreme temperatures, generally possess a higher thermodynamic stability and, remarkably, in many cases allow for the

trapping of metallated intermediate species, providing crucial insight into their reactivity and mechanisms.^{1,3,7,11}

Reagents featuring magnesium, zinc or aluminium in combination with an alkali metal have been rapidly developed and thoroughly studied, attracting widespread interest over the last two decades.^{1,12,24} Additionally many more examples exist with metals such as cadmium²⁵ and gallium.²⁶ In the closing remarks of a review in this evolving area of research, Mulvey details considerations for “special mixed-metal-induced regioselective magnesiations or zincations” based on the evidence seen up to that date.²⁷ They included the following:

- i) Intimate contact of the alkali metal and secondary metal through an amido or alkyl bridge. DFT calculations showed that on many occasions the generation of a mixed-metal structure is thermodynamically driven, energetically preferred over two homometallic components.
- ii) The aromatic substrate to be deprotonated enters the coordination sphere of the alkali metal (ergo AMMM) and is held by some type of π -interaction of the arene or a dative bond with one of the substituents on the ring.
- iii) Pre-binding of the substrate lowers the entropy, in turn raising the basicity of the secondary metal.

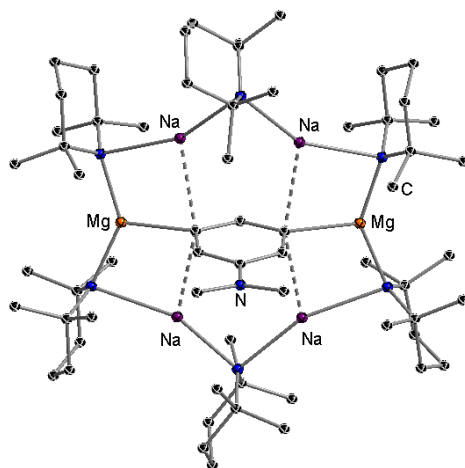


Figure I-2 – Crystal structure of *meta-meta'* deprotonated *N,N*-dimethylaniline within a Na/Mg inverse crown. Hydrogen atoms omitted for clarity.

A recent report in *Science* has revealed supramolecular Na/Mg template bases, capable of unprecedented *ortho-meta'* and *meta-meta'* deprotonations of aryl substrates, where the ring structure of the mixed-metal base controls the regioselectivity of the deprotonation process.²⁸

Thus, an *in situ* prepared disodium-monomagnesium alkyl-amide mixture can doubly-deprotonate substrates such as *N,N*-dimethylaniline (Figure I-2) giving rise to an ‘inverse crown’ solid state architecture. Along with the prevalent central core rhombic motif frameworks (e.g. $\{M^1XM^2X\}$ where $X = N$ or C , as exemplified in Figure I-1 and Scheme I-2), ‘inverse crowns’ are another commonly displayed structural scaffold found for many bimetallic ate complexes.^{1,8,27} They are termed as such as there is a specific role reversal (compared to traditional crown ethers)²⁹, whereby the surrounding rings are now Lewis acidic, due to metal atoms occupying sites where ether oxygen atoms would habitually sit, and the central “guest” positions which are now Lewis basic (Figure I-3). Many are also formed from bimetallic amide complexes by the inadvertent or controlled exposure to air or water, consequently inserting an oxide anion into the centre of the molecule; this subset are referred to as ‘inverse crown ethers’ (ICE).³⁰

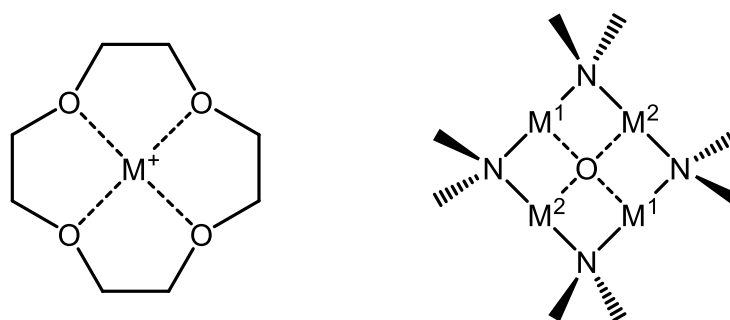


Figure I-3 - Structural representations of a traditional crown ether and an inverse crown ether complex.

I.II Iron Chemistry

Iron is the 26th atomic element and by mass, the most common present on Earth, forming a substantial quantity of its inner and outer core.³¹ It is believed the first uses of iron may extend as far back to such historic civilizations as the ancient Egyptians (*circa* 3000 BC) and the Babylonians (*circa* 1900 BC).³² The pre-historic era featuring the prevailing use of iron, universally known as the ‘Iron Age’, when iron superseded bronze as the material of choice for primitive weapons and tools used by our ancestors, can be furthest traced back to around 1200 BC, although starting dates and time periods varied geographically.

In the present day iron has become one of the most important raw materials present on Earth. The iron mining industry’s global worth extends into the trillions of dollars and is arguably

the World's most significant industry after the petroleum industry. A phenomenal amount of iron ore is mined each year, worldwide production of iron ore in 2015 was an estimated 3.3 billion metric tons.³³ The majority of iron ore (up to 98%) is fed directly into the steel industry,³⁴ which since the industrial revolution has helped accelerate the rapid growth of cities all over the world with steel providing essential construction materials for technical infrastructure, buildings, machinery, automobiles and tools.

Biologically, iron is abundant and features among the twelve most important chemical elements essential for life for both animals and plants. It is benign and essentially non-toxic therefore it comes as no surprise that iron is found in all living life-forms, with the human body containing around 4-5 g of iron.³⁵ Iron is found at the active sites of a number biological catalysts, owing to its duality as an electron donor and acceptor, it is key for the transport and metabolism of small molecules. Perhaps most identifiable in humans is iron as the metal ion cofactor of the metalloprotein haemoglobin (Figure I-4) which, water aside, is the majority constituent of red blood cells.³⁶ Bound within a heterocyclic porphyrin ring, the iron(II) centre plays an essential role binding and releasing dioxygen (and carbon dioxide) and is the foremost oxygen transporter within the body.³⁷

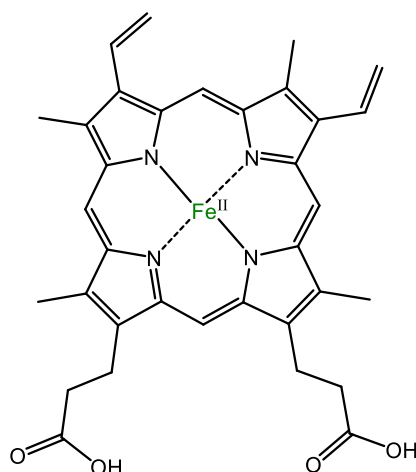


Figure I-4 - Structure of Heme B with its iron(II) centre, a cofactor of haemoglobin.

Also in the human body iron active sites are found in cytochromes which are accountable for the synthesis of ATP and as part of iron-sulfur clusters which carry out mitochondrial electron transport via oxidation-reduction reactions.³⁸

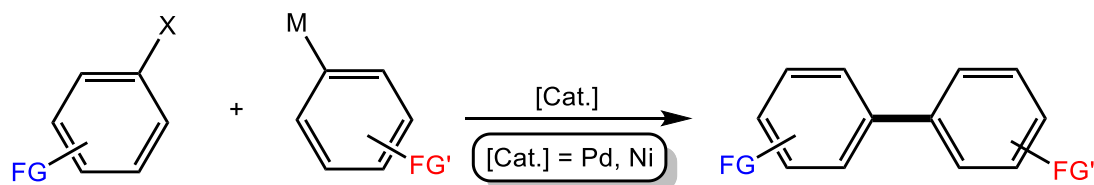
Elsewhere in nature, certain bacteria and microorganisms possess enzymes that can fix atmospheric N_2 , nitrogenases³⁹, which all contain iron-sulfur clusters and iron is also present in the three classes of hydrogenase enzymes⁴⁰ ([Fe], [FeFe] and [FeNi] hydrogenases), whose function is to reversibly oxidise H_2 .

As with many instances in nature, there is a great desire within the scientific community to replicate and mimic such seamlessly efficient biocatalytic functions and to apply them to synthetically useful processes in areas of pharmaceuticals, fine chemicals, materials and more. Indeed the challenging area of biomimetic (or bio-inspired) chemistry has attracted the attention of many inorganic chemists who have managed to create a number of analogues.⁴¹ These biological examples convey the prodigious importance of iron and also highlight some of its beneficial and unique capabilities in addition to its environmentally and biologically benign character.

The revolutionary synthesis, discovery and structural elucidation of ferrocene ($Fe\{C_5H_5\}_2$) in the 1950's (along with its many analogues and derivatives)⁴² is often credited with the acceleration and growth of organometallic chemistry in the latter half of the 20th century. Organoiron compounds have found significant application in organic synthesis such as iron pentacarbonyl ($Fe(CO)_5$) for CO substitution and disodium tetracarbonylferrate for the synthesis of aldehydes.⁴³

Moreover, iron features as a popular choice of catalyst for what are arguably two of the most important synthetic chemical processes today; the Haber-Bosch Process⁴⁴ for the conversion of atmospheric N_2 and H_2 to ammonia and the Fischer-Tropsch Process⁴⁵ for the conversion of CO and H_2 (syngas) into liquid hydrocarbons.

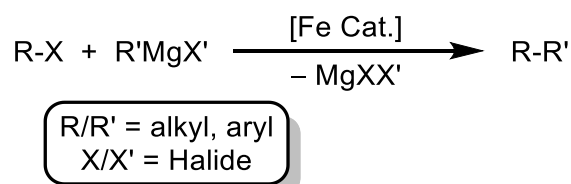
Contrary to these successes, amongst many fields of synthetic chemistry, iron has been superseded by noble metals.⁴⁶ A clear example of this is in the catalysis of one of the most essential transformations in organic chemistry as a vehicle to generate new C-C bonds: cross-coupling reactions. This widely used synthetic methodology features heavily within pharmaceutical and medicinal chemistry and other areas of chemical industry. Traditionally such reactions are carried out between an organic electrophile possessing a leaving group and an organometallic nucleophile in the presence of a transition metal catalyst (Scheme I-4).



Scheme I-4 - Typical aryl-aryl cross-coupling reaction.

Copper, cobalt and iron have all been found to be effective catalysts but the two most superior metals for permitting these reactions are palladium⁴⁷ and nickel.^{48,49} Both offer a number of distinct advantages including a high functional group tolerance and excellent performance with a wide scope of reagents.^{50,51} Contrariwise, Pd is extremely expensive (Pd £12210/kg 15th June 2016⁵² vs Iron Ore (fine) £0.04/kg 31st March 2016)⁵³ whilst many Ni compounds are highly toxic and both require costly and sensitive ligands present to be operational.⁵⁴⁻⁵⁶ Extended reaction times at elevated temperatures are also a common feature when using these metal catalysts. Thus, there is a requirement for the development of catalysts boasting superior economic and ecological features.

Iron's role as a catalyst for the construction of new carbon-carbon bonds has been somewhat neglected in the literature due, to a large extent, to the immense devotion of effort into the research of these precious transition metal catalysts. Despite this, it is known that cheap and environmentally benign iron salts (e.g. FeCl₂, FeCl₃, Fe(acac)₃, etc., acac = acetylacetonate) are capable of acting as catalysts (or pre-catalysts), not only for cross-coupling reactions but also for a host of other valuable organic reactions (such as polymerisations, oxidations, hydrogenations, cycloadditions, etc.), many of which are summarised in an excellent review article by Bolm and co-workers.⁵⁷ Unfortunately only until quite recently, many of the known catalytic reactions have been limited in scope or do not allow for practical applications.⁵⁸



Scheme I-5 – A representative scheme for traditional Fe-Cat. cross-coupling between a Grignard and an organohalide.

Iron-catalysed cross-coupling reactions have routinely been between a Grignard reagent (RMgX) and an organohalide (R-X), catalysed by a small quantity of an iron salt (Scheme I-5). Contrasting with the well-established mechanistic proposals on Pd-catalysis,⁵⁹ there is no general mechanism in Fe-catalysis. The issue of catalytic mechanisms of iron-catalysed cross-couplings and the identity of the catalytically-active intermediate species have been contentious to say the least. Iron catalysis is somewhat of a black box, which involves the formation of tremendously sensitive and short-lived catalytic species generated *in situ*, currently lacking in structural definition. Moreover, speculation on the oxidation state of iron in the active species has varied through its numerous available valent forms,⁶⁰ giving rise to proposals of multiple (sometimes interconnected) reaction pathways,⁶¹ including radical pathways⁶¹ or even the formation of Fe nanoparticles.⁶²

Interesting of late has been the hypotheses surrounding the involvement of bimetallic ferrate species as potential active species in Fe-catalysed cross-couplings.^{63–67} Encouragingly a number of low-valent ferrate species have been structurally characterised, featuring Fe in combination with either Mg^{68–70} or Li.⁶¹

Fürstner has demonstrated a number of well-defined, structurally characterised, heterobimetallic ferrate complexes that are capable of acting as (pre-)catalysts in Fe-catalysed cross-coupling processes; a selection of which are presented in Figure I-5.⁶⁶ The remarkable Fe^{II} “super-ate” complex [(Me₄Fe)(MeLi)][{Li(Et₂O)}₂] (Figure I-5, top left), synthesised from excess MeLi and FeCl₃ in diethyl ether, can replicate the reactivity of MeMgBr and catalytic quantities of Fe(acac)₃ in THF towards a range of electrophiles.^{61,71} Fe⁰ complex [Li(TMEDA)]⁺[Fe(C₂H₄)₂(Cp)]⁻ (Cp = cyclopentadienyl) (Figure I-5, top right) and [Li(TMEDA)₂]⁺[Fe(C₂H₄)₄]⁻ (Figure I-5, bottom),⁷² thoroughly unusual in that Fe resides in a formal –2 oxidation state, are able to catalyse cross-coupling reactions between alkyl halides and aryl Grignards.^{61,73}

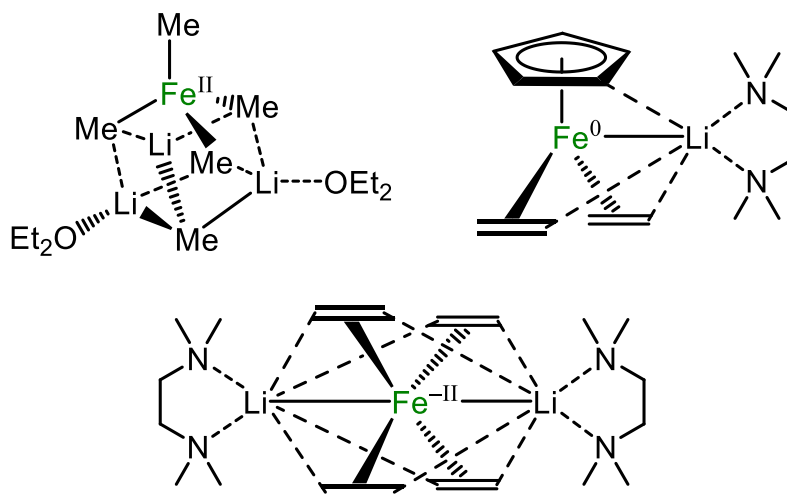
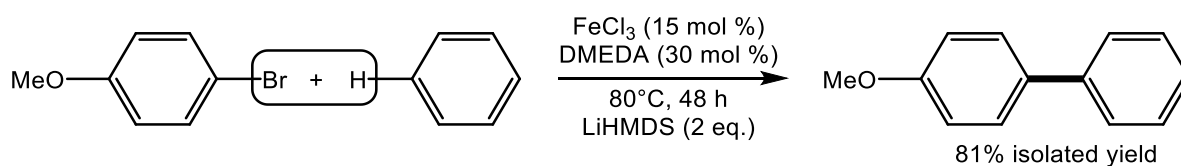


Figure I-5 – A selection of structurally well-defined low-valent lithium ferrate pre-catalyst complexes. Fe^{II} “super-ate” complex [(Me₄Fe)(MeLi)][{Li(Et₂O)}₂] (top left), Fe⁰ complex [Li(TMEDA)]⁺[Fe(C₂H₄)₂(Cp)]⁻ (top right) and unusual Fe^{-II} complex [Li(TMEDA)₂]⁺[Fe(C₂H₄)₄]⁻ (bottom).

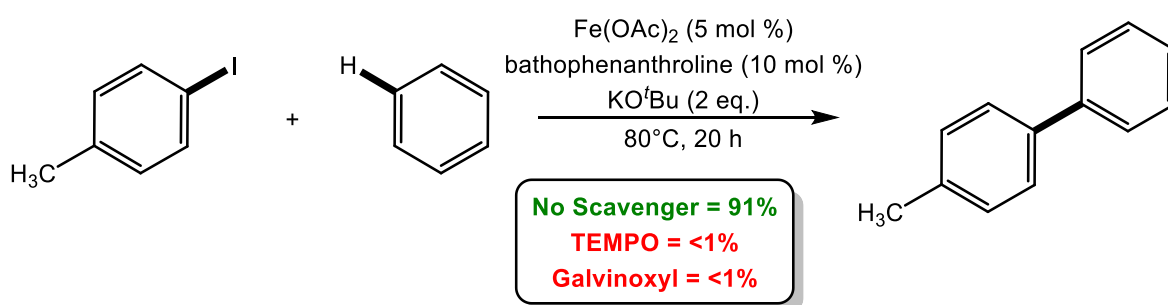
Furthermore, a number of recently published articles have shown iron catalysts capable of direct C-H transformations⁷⁴ on unactivated substrates; in some cases negating the use of an organohalide⁷⁵ or remarkably without the use of a Grignard reagent when the Fe complex is present in a stoichiometric quantity.⁷⁶

A great contemporary example of this is work by Lei and co-workers demonstrating aryl-aryl coupling featuring the first examples of direct arylation of unactivated arenes catalysed by iron.⁷⁷ Their best result was achieved with a combination of FeCl₃ (15 mol%), the bidentate donor ligand DMEDA (*N,N'*-dimethylethylenediamine, 30 mol%) and LiHMDS in excess (2 or 3 eq., HMDS = 1,1,1,3,3,3-hexamethyldisilazide), shown in Scheme I-6. Although the authors do not propose a plausible mechanism for this transformation, initial studies suggest the involvement of radicals; however, the formation of a lithium ferrate species cannot be ruled out. In this regard, unpublished work within our own group has shown that Fe(II) complex [Li(DMEDA)₂]⁺[Fe(HMDS)₃]⁻ can achieve comparable yields for the coupling of bromoanisole and benzene than when using FeCl₃, DMEDA and LiHMDS.⁷⁸



Scheme I-6 - Cross-coupling of 4-bromoanisole with unactivated benzene via Fe-catalysis.

Independently, though within the same year, Charette and colleagues reported Fe-catalysed aryl-aryl coupling reactions via a direct C-H transformation.⁷⁹ In this case, the authors found that with the addition of the free radical scavenger species TEMPO or Galvinoxyl,⁸⁰ the reaction was shut down (Scheme I-7). This spurred them to propose a plausible Single Electron Transfer (SET) mechanistic pathway, analogous to a metal-catalysed living radical polymerisation reaction.

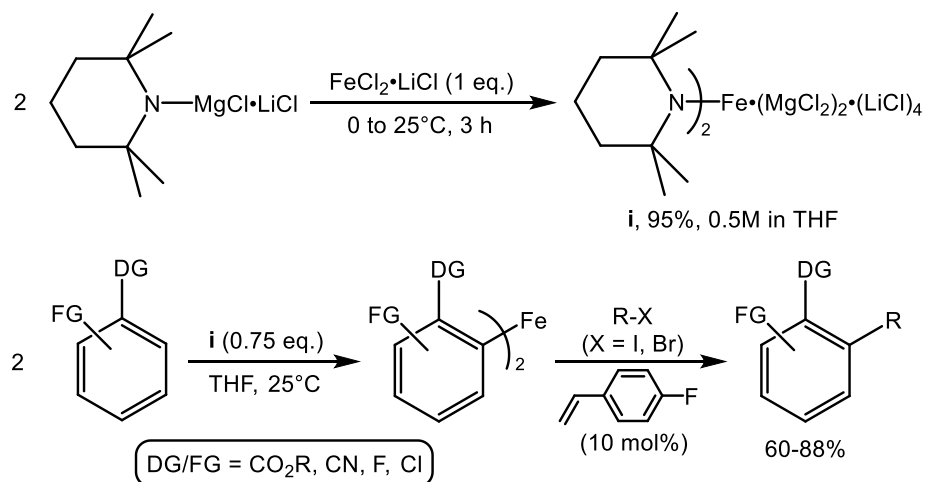


Scheme I-7 - Iron-catalysed cross-coupling inhibited in the presence of radical scavengers.

I.III Ferrate Chemistry

Assessing other instances of alkali metal ferrates in the literature there is a relative scarcity, particularly for structurally defined examples.

Mongin has reported lithium ferrate complex $[\text{LiFe}(\text{TMP})_3]$ can facilitate the metallation of 2-methoxypyridine (and a number of other aromatic/heteroaromatic substrates) at ambient temperature in THF, which can be subsequently quenched by a range of electrophiles such as I_2 , pivalaldehyde, benzoyl chloride and 3,4,5-trimethoxybenzaldehyde.⁸¹ Knochel has demonstrated the synthesis of the Fe(II) complex $[(\text{TMP})_2\text{Fe} \cdot (\text{MgCl}_2)_2 \cdot (\text{LiCl})_4]$ (**i**), capable of mediating cross-coupling of functionalised arenes with alkylhalides (Scheme I-8).



Scheme I-8 – Preparation of magnesium ferrate complex **i** and subsequent ferration and cross-coupling of functionalised arenes. DG = directing group, FG = Functional Group.

Two equivalents of turbo-Hauser reagent [$\text{TMPMgCl} \cdot \text{LiCl}$] are combined with an equivalent of $\text{FeCl}_2 \cdot \text{LiCl}$ to generate mixed Mg/Fe amido complex **i**. In turn, complex **i** is used to ferrate a broad range of functionalised arene substrates prior to undergoing cross-coupling with alkyl iodides or bromides. Notwithstanding, amongst Mongin and Knochel's elegant examples of ferrate complexes no structural or spectroscopic characterisation is provided, thus their ferrates are solely putative and their reports lack a characterised metallated intermediate to fully complete the picture.

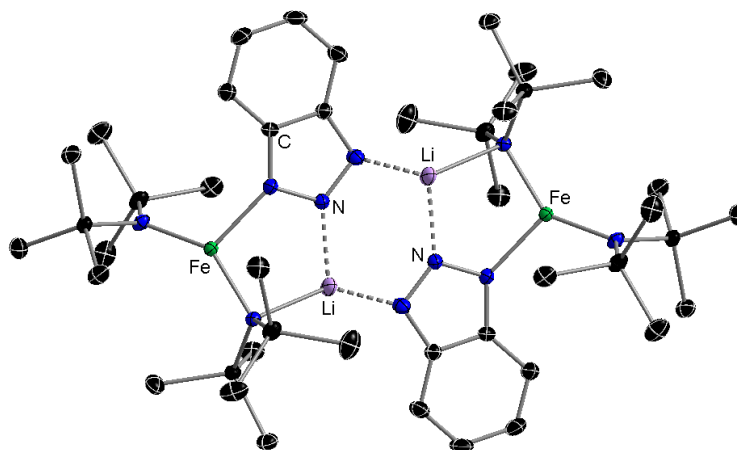
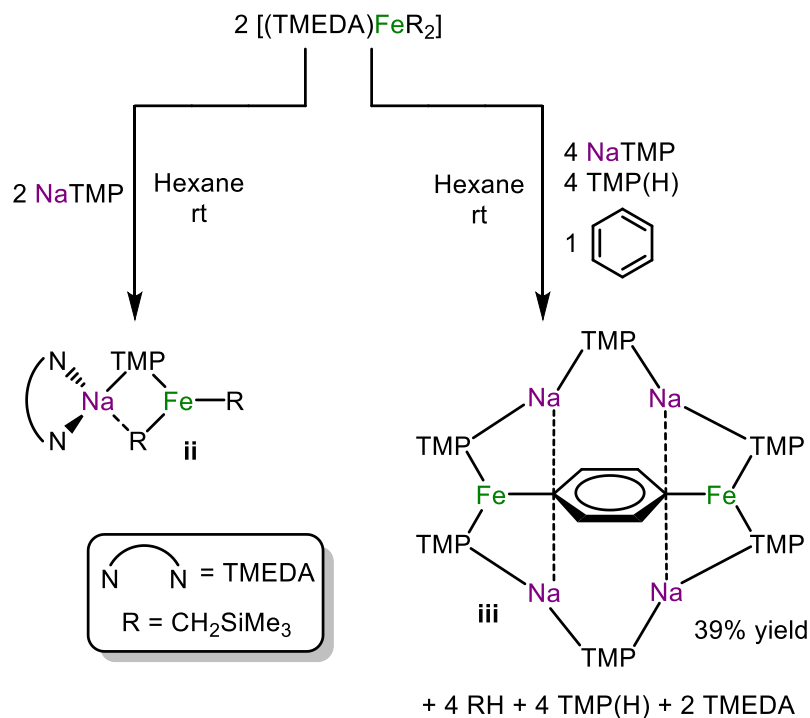


Figure I-6 – Crystal structure of $[\text{LiFe}(\text{BTA})(\text{HMDS})_2]_2$. Hydrogen atoms omitted for clarity. Thermal ellipsoids displayed at 50% probability level.

Identifying $[\text{Fe}(\text{HMDS})_2]_2$ may allow for a route to Fe(II) cage complexes, in 2011 Layfield presented the synthesis and structural characterisation of dimeric lithium ferrate $[\text{LiFe}(\text{BTA})(\text{HMDS})_2]_2$ (BTA = benzotriazolyl) (Figure I-6) along with a monometallic

trinuclear Fe cage complex. In the conclusions he notes the mixed-metal complex contains two potential reactive HMDS ligands, which may allow for the synthesis of Fe cage complexes of higher nuclearity.



Scheme I-9 – Synthesis of sodium ferrate complexes **ii** and **iii**.

A relevant contribution concerning structurally defined ferrate complexes and their applications in metallation comes from Klett, Mulvey and co-workers.⁸² In their 2009 publication they reveal the synthesis and solid-state structure of alkyl sodium ferrate [(TMEDA)NaFe(TMP)(CH₂SiMe₃)₂] (**ii**) (Scheme I-9, left). Addition of benzene to a solution of **ii** in hexane yielded no solid product, however, addition of NaTMP (4 eq.), TMP(H) (4 eq.) and benzene (1 eq.) to two equivalents of precursor [(TMEDA)Fe(CH₂SiMe₃)₂] resulted in the extraordinary di-deprotonation of benzene (Scheme I-9, right). [Na₄Fe₂(TMP)₆(C₆H₄)] (**iii**) is an inverse crown structure comprising of a 12-atom ring hosting a benzene ring deprotonated at the 1 and 4 positions, supported by Fe-C σ -bonds and Na---C electrostatic contacts to the π -system (Figure I-7); the isostructural Mg congener has also been reported.⁸³ Undoubtedly this is a fascinating demonstration of the potential of alkali metal ferrate systems.

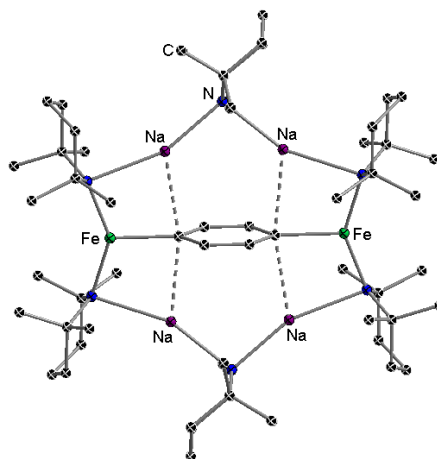


Figure I-7 – Crystal structure of $[\text{Na}_4\text{Fe}_2(\text{TMP})_6(\text{C}_4\text{H}_4)]$ (iii). Hydrogen atoms omitted for clarity.

I.IV Gap in the Knowledge

Building upon previous studies on alkali metal magnesiate and zincate chemistry, one of the interests of our group is to expand cooperative effects to transition metal systems. Base metal iron is the ideal candidate; hugely abundant and thus a cheap raw material with the highly desirable benefits of being ecologically and biologically benign.

Recent studies in Fe-catalysed C-C bond formation processes have postulated the possible involvement of active bimetallic species, which combine iron with a more polar metal such as lithium or magnesium, as key reactive intermediates in these important transformations,^{64,84,85} however it should be noted that the number of alkali metal ferrates structurally defined is scarce and no systematic studies on their synthesis and isolation have been reported. Exploration in this area through a conscious effort to structurally define reactive species and intermediates could offer great insight into catalytic mechanisms and uncovering the ‘active catalytic species’ of iron and its oxidation states whose true identities still remain hidden.⁸⁴ The potential of novel alkali metal ferrate systems has been explored and demonstrated to a minor extent,^{81,82,86} but there remains a wealth of valuable mixed-metal species containing iron to be discovered, structurally characterised and undergo reactivity studies.

I.V Aims

The overarching aim of this project is to rationally design novel alkali metal ferrates and to exploit their cooperative behaviour in synthesis, advancing the understanding of their reactivities.

Fe(II) has been chosen for this study due to the structural similarities of some of organometallic compounds of this metal, in this oxidation state, with magnesium. Key analytical methods for the characterisation of the new compounds have been single-crystal X-ray crystallography and paramagnetic NMR spectroscopy as well as magnetometry studies primarily with SQUID measurements.

Aiming to understand the effect of Lewis donors in the synthesis and structure of sodium ferrates, Chapter 1 presents a systematic study on co-complexation reactions of Na and Fe HMDS-based amides with commodity donors such as TMEDA, PMDETA and Et₂O to name just a few.

Chapter 2 assesses the ability of sodium ferrates to functionalise N-heterocyclic carbenes (NHCs) and their possible application for the synthesis of *abnormal* NHC-Fe complexes.

Expanding the synthetic potential of these cooperative bimetallics, Chapter 3 presents our findings on sodium-mediated ferration reactions, which allow for direct Fe-H exchange with a wide range of F-substituted aromatics.

The unprecedented ability of these compounds to facilitate C-F bond activation processes is the primary focus of Chapter 4.

Chapter 1 – Structural Variations of Sodium Ferrates with Lewis Donors

Given the relative paucity of structurally defined alkali metal ferrate species, this chapter systematically investigates the synthesis of mixed alkali metal/iron complexes by co-complexation of single metal reagents in the presence of an assortment of Lewis donors with different denticities and donor abilities.

Along with DA and TMP (diisopropylamide and 2,2,6,6-tetramethylpiperidide, respectively), HMDS (1,1,1,3,3,3-hexamethyldisilazide) is one of the most frequently utilised amide ligands in inorganic synthesis (Figure 1.1).⁸⁷ Lacking β -hydrogens and having a considerable steric bulk, we chose this amido group for the synthesis of a family of homoleptic alkali metal ferrates.

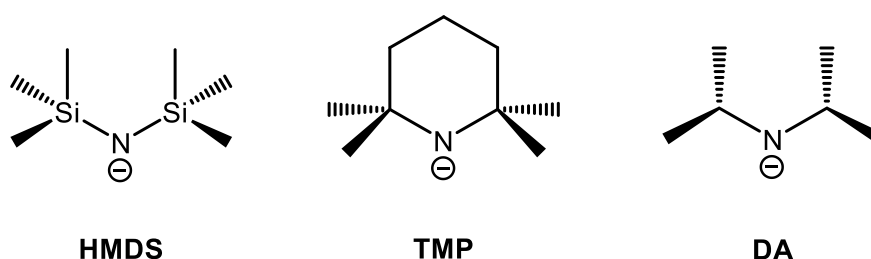


Figure 1.1 - Structures of three key utility amides in mixed-metal chemistry.

Focussing primarily on mixed sodium-iron species, it should be noted that both homoleptic reagents, NaHMDS and $\text{Fe}(\text{HMDS})_2$, are known and their structures have been elucidated by X-ray crystallography. The solid-state structure of NaHMDS has been reported as a linear polymeric chain⁸⁸ and a polymorphic form adopting a cyclic trimeric structure; a structure retained in non-polar solvents (Figure 1.2, left).^{89,90} Contrastingly $\text{Fe}(\text{HMDS})_2$ displays a dimeric structure (Figure 1.2, right), though when dissolved in a non-polar solvent exists as a monomer at ambient temperatures.^{91,92} $\text{Fe}(\text{HMDS})_2$ is prepared via a salt-metathesis method combining FeBr_2 with two equivalents of LiHMDS.⁹¹ LiBr is removed by filtration and the product is purified by an innovative distillation method (see Section III.I.V) to afford an extremely air-sensitive emerald green liquid which is subsequently stored at -35°C within a glove box for convenient handling as a solid. Great care and caution must be taken when handling $\text{Fe}(\text{HMDS})_2$ in the absence of a solvent as it can rapidly decompose at ambient temperature, even under a moderate stream of ‘dry’ argon.

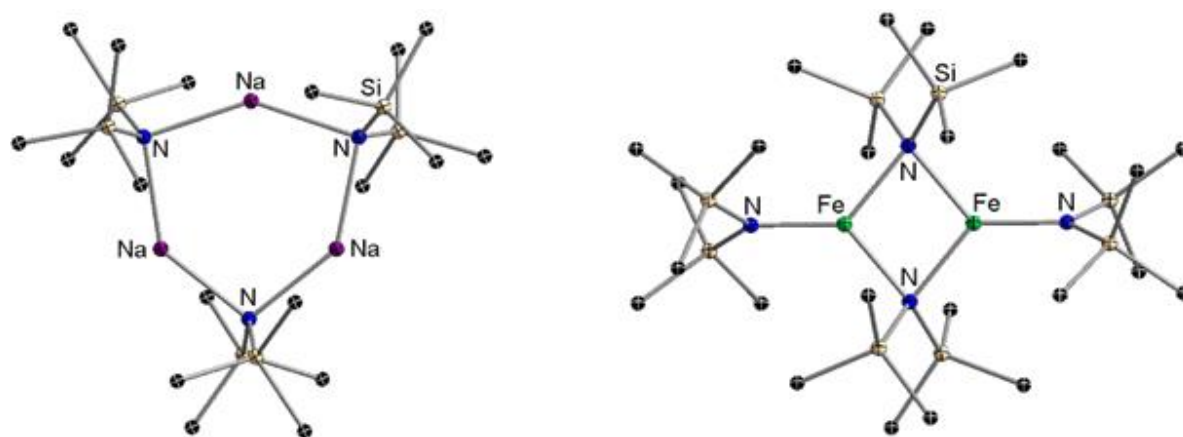


Figure 1.2 - Crystal structures of Na- and Fe-bis(trimethylsilyl)amides. Hydrogen atoms omitted for clarity.

Some of the studies included in this chapter employ DPA (2,2'-dipyridylamide) which offers a variety of coordination modes. DPA can potentially ligate through three N sites; one central amido N and two neutral pyridyl N atoms at the 2 and 2' ring positions (with respect to N_{amido}).⁹³ Rotation around the two $N_{\text{amido}}\text{-C}$ bonds allows for DPA adopt three different conformations; namely *syn/syn*, *syn/anti* and *anti/anti* (Figure 1.3).⁹⁴

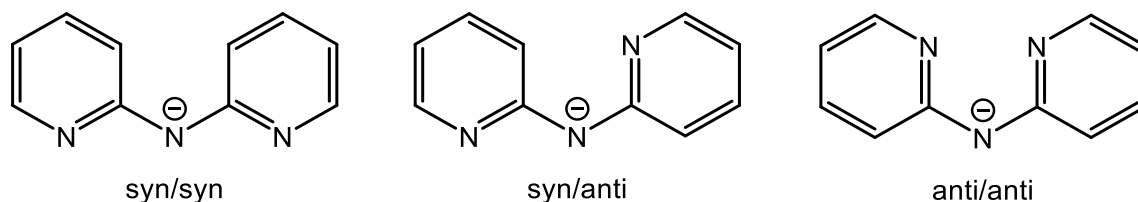


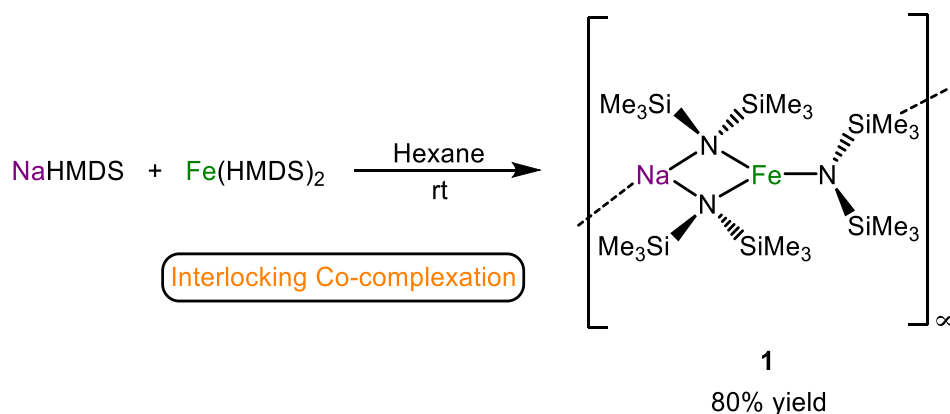
Figure 1.3 - The three conformational arrangements of 2,2'-dipyridylamide.

Here we present our findings on the synthesis, structural elucidation and characterisation of a new family of sodium ferrate complexes which can be used as precursors to access novel sodium ferrates bearing DPA fragments.

1.1 Results and Discussion

1.1.1 Assessing Co-complexation Reactions: Synthesis of Solvent-Free $[\{\text{NaFe}(\text{HMDS})_3\}_\infty]$

We began our studies by mixing equimolar quantities of NaHMDS and $\text{Fe}(\text{HMDS})_2$ in non-coordinating hexane solvent (Scheme 1.1).



Scheme 1.1 - Synthesis of **1** via a mixed-metal amide co-complexation approach.

The reaction mixture was allowed to stir for one hour and afforded a dark green solution after gentle heating. Considering that NaHMDS is sparingly soluble in hexane, the formation of this solution suggested that the co-complexation reaction had taken place as it has been documented in the literature that mixed-metal (ate) reagents tend to be more soluble than their single-metal components.⁹⁵ Upon concentration, this solution afforded green needle-like crystals of the homoleptic sodium ferrate $[\{\text{NaFe}(\text{HMDS})_3\}_\infty]$ (**1**) in an 80% isolated yield. These were analysed by single-crystal X-ray crystallography to determine the structure of **1** (Figure 1.4 and Figure 1.5).

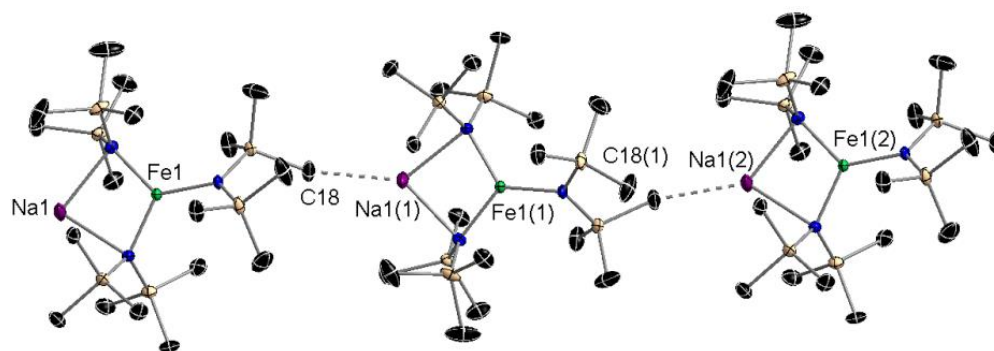


Figure 1.4 – Section of polymeric chain in **1** showing propagation and selected atom labelling, Na1(1)---C18 2.838(4) Å. Hydrogen atoms omitted for clarity. Thermal ellipsoids displayed at 50% probability level.

Sodium ferrate **1** exhibits a polymeric structure composed of $\{\text{Na}(\mu\text{-HMDS})_2\text{Fe}(\text{HMDS})\}$ units (Figure 1.4). In the asymmetric unit of **1** two of the amide groups act as bridges between Na and Fe to form a planar four-membered $\{\text{NaNFeN}\}$ ring in a contacted ion-pair (CIP) motif. The remaining HMDS group coordinates terminally to the iron centre but interacts via one of its methyl groups (C18) of the SiMe_3 substituents with a Na (2.838(4) Å) from a neighbouring $\{\text{Na}(\mu\text{-HMDS})_2\text{Fe}(\text{HMDS})\}$ unit, giving rise to a one-dimensional polymeric chain structure, allowing each Na to attain further coordinative stabilisation.

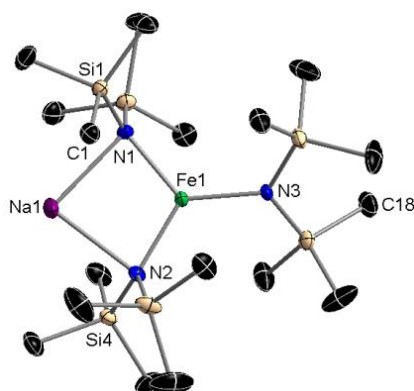


Figure 1.5 – Asymmetric unit of $[\{\text{NaFe}(\text{HMDS})_3\}]_\infty$ (**1**). Hydrogen atoms omitted for clarity. Thermal ellipsoids displayed at 50% probability level. Selected bond distances (Å) and angles (°): Fe1-N1 2.036(2), Fe1-N2 2.032(2), Fe1-N3 1.964(2), Fe1---Na1 3.0131(13), Na1-N1 2.502(3), Na1-N2 2.492(3); N1-Fe1-N2 110.48(10), N1-Fe1-N3 124.93(10), N2-Fe1-N3 124.56(10), Na1-N1-Fe1 82.51(8), Na1-N2-Fe1 82.86(8), Na1--Fe1-N3 176.00(9), N1-Na1-N2 84.03(9).

The iron centre resides in a distorted trigonal planar geometry (sum of angles around Fe = 359.97° , ranging from $110.48(10)^\circ$ to $124.93(10)^\circ$). The Fe-N distances of the bridging amido ligands are almost identical at 2.036(2) and 2.032(2) Å, only slightly shorter than those described for the dimeric precursor $\text{Fe}(\text{HMDS})_2$ (average Fe-N_{bridging} distance = 2.085 Å).⁹²

Contrastingly the terminal Fe-N bond distance in **1** is significantly shorter (1.964(2) Å) which is consistent with the lower coordination number of the N atom. Conversely, the Na atom binds to two amido groups forming Na-N bonds whose values (Na-N1 2.503(2) Å and Na-N2 2.492(3) Å) are significantly elongated in comparison to those found in trimeric [$\{\text{NaHMDS}\}_3$] (average Na-N distance = 2.381 Å).⁸⁹

The polymeric structure of **1** contrasts with that recently reported for the lithium analogue, [$\text{LiFe}(\text{HMDS})_3$], which exhibits a monomeric motif.⁹⁶ Formally two-coordinate bonded to bridging amido N atoms at distances of 2.027(6) and 2.056(6) Å, Li attains further stabilisation via short contacts to HMDS methyl groups (at distances of 2.317(1) and 2.348(2) Å). In comparison to sodium, the smaller lithium cation resides considerably closer to the Fe centre (Li---Fe 2.596(1) Å, *cf.* Na1---Fe1 3.0131(13) Å) and is thus ‘sunken’ further into the sphere of steric bulk of the bridging HMDS ligands, favouring intramolecular Li-Me interactions. The Fe-N bond lengths are similar to those in **1** (Fe-N_{bridging} 2.038(3) and 2.058(2) Å; Fe-N_{terminal} 1.940(3) Å), though the angles around Fe differ somewhat with a narrower internal N-Fe-N angle of 99.9(1)° (*cf.* N1-Fe1-N2 110.48(10)° for **1**).

The different bonding modes of Na and Fe in **1** represent an example of *ancillary* and *anchoring* bonding, prevalent throughout hetero-bimetallic chemistry.^{83,97,98} The foundations for this molecular architecture are provided by the stronger, more covalent Fe-N σ -bonds; these are termed *anchoring* bonds.⁸³ In the case of **1** the three available HMDS groups will preferentially bind to more Lewis acidic Fe(II) to prioritise a (distorted) trigonal planar geometry. The more ionic interactions of the alkali metal, seeking to achieve coordinative saturation by any available means, are designated *ancillary* bonds.⁸³ In the instances of CIPs, the alkali metal inserts itself into the framework forming weaker M-N bonds with additional longer M---CH₃ electrostatic interactions in order to contribute to the overall stability of the ate complex. The concept of *ancillary* and *anchoring* bonding is demonstrated in the CIP structures detailed *vide infra*, in some cases with Lewis basic donor molecules providing *ancillary* bonding opportunities.

1.1.2 Introduction to NMR Spectroscopy of Paramagnetic Species

The characterization of paramagnetic species, those containing nuclei that possess unpaired electrons, by NMR spectroscopy presents a host of problems which much be taken into account.⁹⁹ Notwithstanding, by careful manipulation of the acquisition parameters and correct sample preparation, good quality and informative spectra can be obtained in many cases.

Chemical shifts can vary wildly from those observed in diamagnetic molecules. The large magnetic moment of the unpaired electrons is responsible for dramatic chemical shifts of resonating nuclei, this is thought to be the result of two interactions. Firstly, a *through-bond* Fermi contact interaction, where the unpaired spin interacts with the nuclei via delocalisation. Secondly, a *through-space* dipolar interaction of the magnetic moments of the unpaired electron(s) and the nucleus when the metal centre displays substantial magnetic anisotropy.⁹⁹ Thus it is not uncommon to find extremely large upfield (shielded) or downfield (deshielded) resonances, in the case of ¹H NMR spectroscopy sometimes >100 ppm or <-100 ppm, well outside of the typical 16 to -5 ppm range. Multiple paramagnetic centres only complicate matters further. Noteworthy also is that these chemical shifts are not dependant on the orientation of the molecules with respect to the magnetic field and so are termed “isotropically shifted” resonances.¹⁰⁰

In addition to extremely large chemical shifts the large magnetic moment of the unpaired electron can also drastically affect nuclear relaxation processes, typically causing fast relaxation. Both the T_1 (spin-lattice relaxation time) and T_2 (spin-spin relaxation time) terms are affected manifesting itself in the loss of signal intensity and the significant broadening of resonances, respectively.^{99,101}

These effects have made the characterisation of high-spin Fe(II) compounds contained in this thesis particularly challenging. Nevertheless, to counter these effects clean crystalline samples have been used where possible with large spectral windows, shorter radio frequency pulse times and a number of post-measurement corrections have been applied to generate informative NMR spectra.

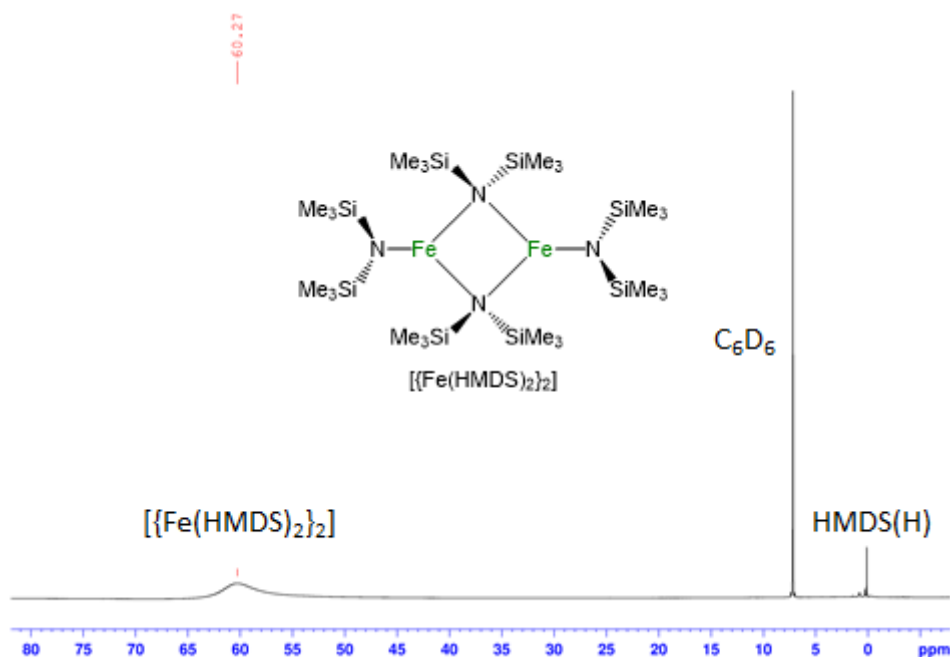


Figure 1.6 – ^1H NMR spectrum of $[\{\text{Fe}(\text{HMDS})_2\}_2]$ in C_6D_6 .

The ^1H NMR spectrum of $\text{Fe}(\text{HMDS})_2$ in C_6D_6 displays a very broad singlet at 60.27 ppm (Figure 1.6). This chemical shift is comparable to that described by Power *et al.* for the same species in the also arene solvent d_8 -toluene, ~ 63 ppm at 30°C .⁹² When a ^1H NMR spectrum of polymeric **1** was recorded in C_6D_6 , the signal for the HMDS groups is dramatically shifted upfield to -4.72 ppm (Figure 1.7). For reference, the ^1H NMR spectrum of NaHMDS in C_6D_6 displays a sharp singlet at 0.11 ppm. Remarkably, in the $^{13}\text{C}\{^1\text{H}\}$ NMR spectrum a weak and broad signal is observed in the far downfield region at 333.41 ppm for the HMDS methyl carbons. The observed resonances for HMDS in the ^1H and $^{13}\text{C}\{^1\text{H}\}$ NMR spectra for **1** are characteristic of many of the sodium ferrate complexes described *vide infra*, which show resonances at similar ppm ranges (approximate ranges of -1 to -6 ppm for ^1H NMR spectroscopy and 320 to 360 ppm for $^{13}\text{C}\{^1\text{H}\}$ NMR spectroscopy).

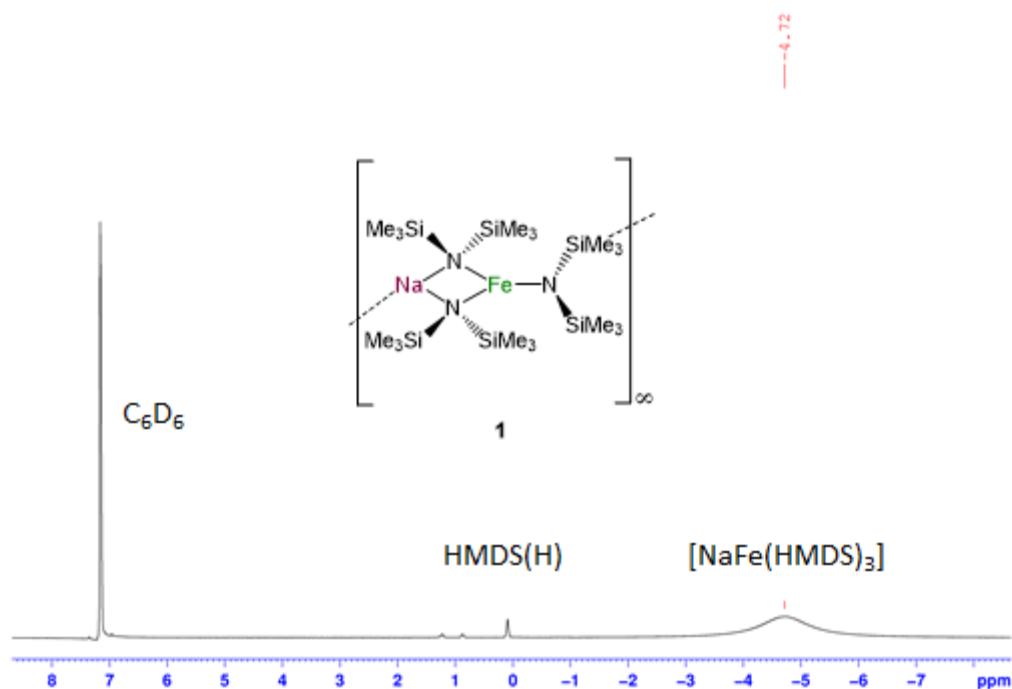


Figure 1.7 – ^1H NMR spectrum of $[\{\text{NaFe}(\text{HMDS})_3\}_\infty]$ (**1**) in C_6D_6 .

The solution magnetic susceptibility of **1** was measured in d_8 -tol via the Evans method^{102,103} affording a solution magnetic moment value of $4.72 \mu_{\text{B}}$, close to the spin-only value $4.90 \mu_{\text{B}}$ expected for a high-spin Fe(II) complex ($S = 2$).¹⁰⁴ The high-spin nature of the Fe(II) centre in **1** (and the majority of the subsequent compounds presented herein) can be rationalised by Fe being surrounded by weak field amido ligands (HMDS) and the possession of an alkali metal cation to stabilise the anionic charge.¹⁰⁵

Holland and co-workers have investigated in detail a number of planar three-coordinate high-spin Fe(II) systems featuring the bidentate β -diketaminato ligand, with results allowing them to draw a number of conclusions about their electronic and spectroscopic properties.^{106–110} From ^1H NMR spectra obtained, in most cases all or nearly all H atoms can be accounted for. A logical trend is observed whereby H atoms in closer proximity to the paramagnetic metal centre show the most broadened and least resolved resonances, and often are furthest shifted up and downfield. H atoms residing further away from the paramagnetic metal centre (both *through-bond* and *through-space*) show far sharper and well resolved signals.

Holland's isolated Fe(II)- β -diketaminato complexes possess a high-spin ($S = 2$) electronic configuration. Using computational methods the authors propose an orbital splitting diagram

for their distorted trigonal planar structures (Figure 1.8); symmetry is lowered from D_{3h} (for a perfectly trigonal planar structure) to C_{2v} , involving the removal of degeneracies.^{106,107}

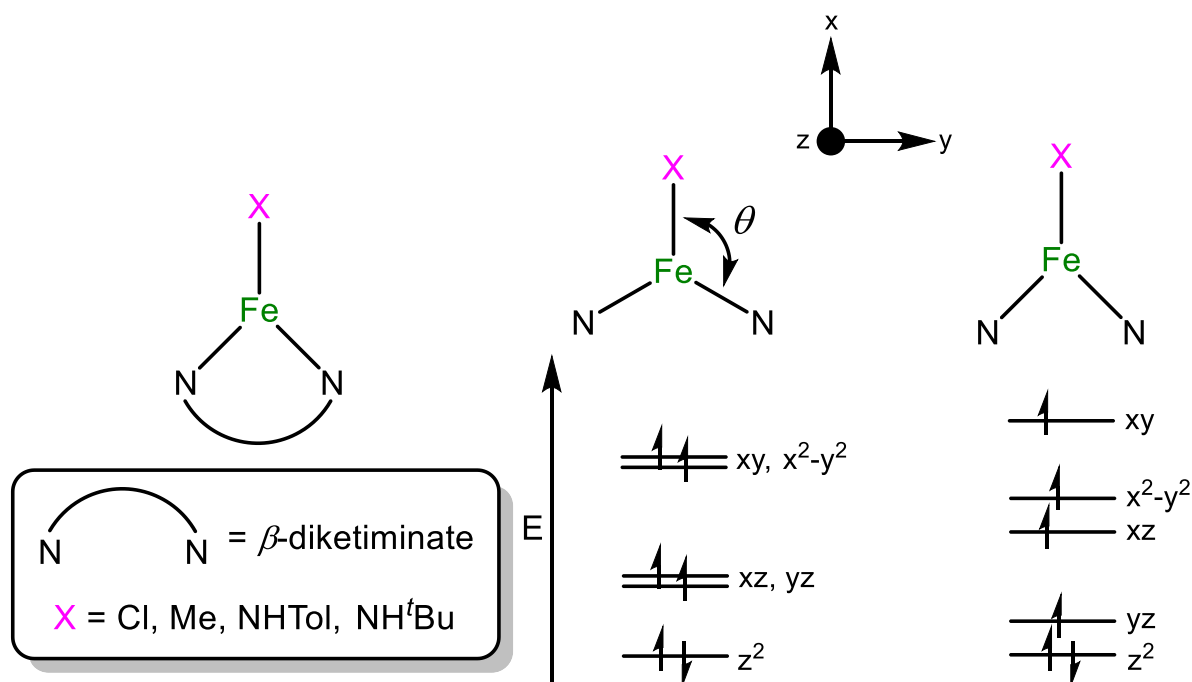
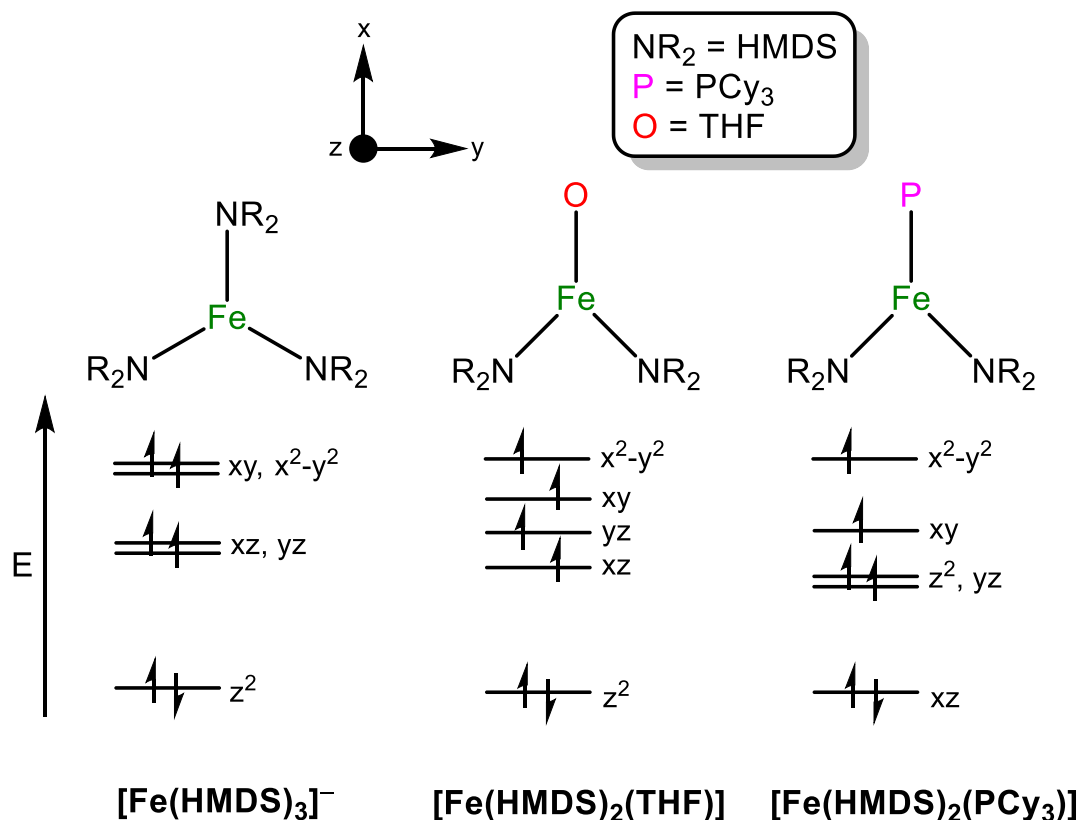


Figure 1.8 – Trigonal planar geometry of a 3-coordinate Fe(II) centre with D_{3h} symmetry (left) where $\theta = 120^\circ$ and distorted trigonal geometry with C_{2v} symmetry (right) with associated 3-d orbital levels. [Figure adapted from papers by Holland *et al.*]^{106,110}

Similarly, Eichhöfer *et al.* used DFT calculations to calculate the electronic structures of three trigonal planar Fe(II) complexes (Figure 1.9).¹¹¹ For homoleptic solvent separated ion-pair (SSIP) complex $[\text{Li}(15\text{-crown-5})]^+[\text{Fe}(\text{HMDS})_3]^-$ (Figure 1.9, left) the Fe anion (which will be encountered in Section 1.1.3.2) is perfectly trigonal planar (D_{3h}) thus the calculated electronic splitting pattern is identical to that shown on the left in Figure 1.8 with degenerate xz/yz and xy/x^2-y^2 orbitals. In the heteroleptic systems degeneracy is removed; for $[\text{Fe}(\text{HMDS})_2(\text{THF})]$ the ordering is similar to the D_{3h} case, however, replacing THF with PCy_3 induces more separation between the orbitals (except for z^2 and yz which become degenerate) and alters the ordering.

Figure 1.9 – Electronic structures for *d*-orbitals in three iron(II) complexes.¹¹¹

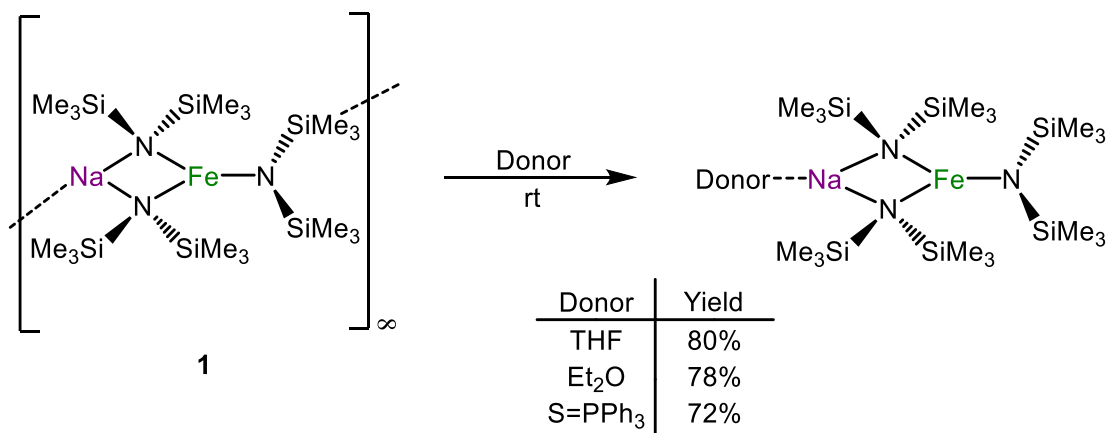
Considering both Holland's and Eichhöfer's investigations, the best approximation for the electronic structure of **1** (and other tris(HMDS)-Fe(II) complexes detailed *vide infra*) would be that calculated for an ideal trigonal planar geometry (D_{3h}). The geometry in **1** is pseudo-trigonal planar around Fe, distorted to a degree (N-Fe-N angles = $110.48(10)^\circ$, $124.93(10)^\circ$ and $124.56(10)^\circ$, $\Sigma_{\text{angles}} = 359.97^\circ$) but not as much as Holland's β -diketaminate complexes with a bite angle of around 95° . It is likely the minor distortions in the angles will result in a small loss of degeneracy as we move closer to C_{2v} symmetry (akin to Figure 1.8, right). For heteroleptic $\{Fe(HMDS)_2X\}$ systems (where X = NHC or aryl group) that will be encountered in later chapters, the electronic structures are likely to be significantly altered dependant on the nature of the ligand and the type of bonding they establish (σ and π interactions).

1.1.3 Assessing Donor Effects in Sodium Ferrate Chemistry: $[\{\text{NaFe}(\text{HMDS})_3\}_\infty]$ and Lewis Donors

The degree of aggregation of polar organometallic reagents plays a pivotal role in controlling their reactivity.⁸⁷ This is perhaps best illustrated by comparing the reactivity of $n\text{BuLi}$ towards benzene. Using a non-polar solvent such as hexane, $n\text{BuLi}$ adopts a hexameric structure and is unable to deprotonate benzene, however on the addition of the bidentate Lewis base TMEDA, the aggregation of $n\text{BuLi}$ changes to a dimer,¹¹² $[\{\text{TMEDA}\cdot\text{Li}n\text{Bu}\}_2]$ and this smaller oligomer is now sufficiently reactive enough to deprotonate benzene to form $[\{\text{PhLi}(\text{TMEDA})\}_2]$.¹¹³ Similar effects have been described in bimetallic chemistry. Thus for example the lithium zincate $[\text{LiZn}(\text{TMP})(t\text{Bu})_2]$ fails to metallate *N,N*-diisopropylbenzamide, forming instead the coordination adduct $[\{(i\text{Pr})_2\text{NC}(\text{Ph})(=\text{O})\}\text{Li}(\text{TMP})(t\text{Bu})\text{Zn}(t\text{Bu})]$,¹¹⁴ whereas when using the TMEDA complex, $[(\text{TMEDA})\text{LiZn}(\text{TMP})(t\text{Bu})_2]$, efficient *ortho*-deprotonation of this substrate takes place at ambient temperature.¹¹⁵

In order to assess the role donor molecules may play in the constitution and reactivity of sodium ferrate $[\{\text{NaFe}(\text{HMDS})_3\}_\infty]$, polymeric solvent-free **1** was reacted with a range of donors of different denticities and donor abilities. This study includes monodentate THF, diethyl ether and triphenylphosphine sulfide (summarised in Scheme 1.2) and the following polydentate N-donors: bidentate TMEDA and DTEDA; tridentate PMDETA and tetradentate $\text{Me}_6\text{-TREN}$.

1.1.3.1 Monodentate Lewis Donors: THF, Et₂O and S=PPh₃



Scheme 1.2 - Overview of reactions of **1** with monodentate Lewis donors.

Compound **1** was formed *in situ* as previously described. One equivalent of the relevant monodentate ligand (THF, Et₂O, S=PPh₃) was introduced affording complexes **2**, **3** and **4**, respectively, with respective yields of 80, 78 and 72%. The donors have effectively broken the polymeric structure of **1** to give monomeric structures where now the heteroatom (O or S) is bonded to sodium. A comparison of the main geometrical parameters of these structures is shown in Table 1.1.

Upon the addition of one equivalent of THF to an *in situ* solution of **1** in hexane, immediate precipitation occurred. Dissolution was achieved by gentle heating and slow cooling to -30°C induced crystallisation, forming green plate-like crystals of [THF·NaFe(HMDS)₃] (**2**) (Figure 1.10).

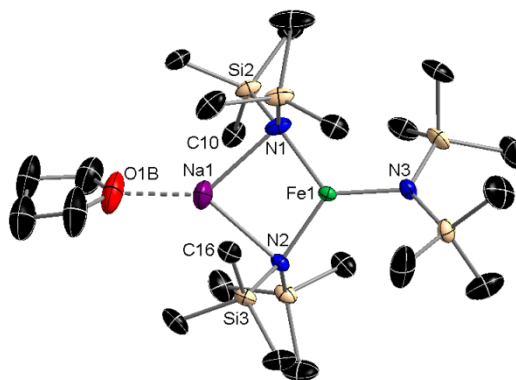
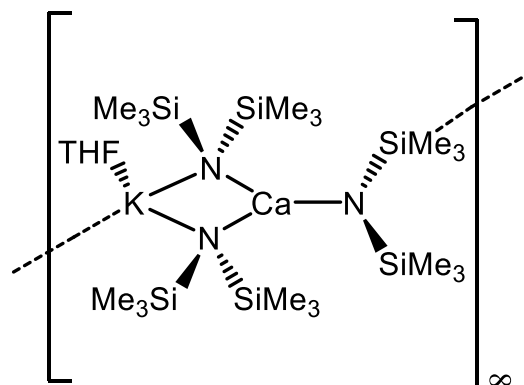


Figure 1.10 – Molecular structure of compound **2**. Hydrogen atoms, THF bipoositional disorder and TMS rotational disorder (Si2 and Si3) omitted for clarity. Thermal ellipsoids displayed at 50% probability level. Selected bond distances (Å) and angles (°): Fe1-N1 2.0372(16), Fe1-N2 2.0348(15), Fe1-N3 1.9621(16), Fe1---Na1 3.0092(10), Na1-N1 2.485(2), Na1-N2 2.4916(19), Na1-O1B 2.243(10); N1-Fe1-N2 110.20(7), N1-Fe1-N3 122.98(7), N2-Fe1-N3 126.76(7), Na1-N1-Fe 82.79(6), Na1-N2-Fe 82.67(6), Na1---Fe1-N3 175.75(5), N1-Na1-N2 84.26(6), N1-Na1-O1B 136.9(5), N2-Na1-O1B 136.4(5).

The structure of a polymorph of **2** has recently been reported by Lerner and co-workers.¹¹⁶ In this case $[\text{THF}\cdot\text{NaFe}(\text{HMDS})_3]$ is obtained by reduction of $\text{Fe}(\text{HMDS})_3$ by the sodium silanide $[(\text{THF})_2\cdot\text{Na}(\text{Si}^i\text{Bu}_3)]$ in a mixture of benzene and THF. The crystals they obtain were solved in the orthorhombic $C222_1$ space group and contain units of free benzene solvent, whereas crystals of **2** were solved in the triclinic $P-1$ space group, containing no free solvent molecules and possessing different unit cell dimensions. The corresponding lithium adduct, $[\text{THF}\cdot\text{LiFe}(\text{HMDS})_3]$, has been reported recently by Layfield and is isostructural with **2**, showing almost identical Fe-N bond lengths, thus further reinforcing the idea of the *anchoring* Fe-N bonds within the ferrate.⁹⁶

Drawing a parallel with Group 2 bimetallic compounds, the structure of **2** bears a strong resemblance with that described by Mulvey and Henderson in the potassium calciate $[\{\text{THF}\cdot\text{KCa}(\text{HMDS})_3\}_\infty]$ although in this case K attains higher coordination by forming long distance electrostatic interactions with methyl groups on the terminal HMDS group attached to Ca to display a polymeric structure (Figure 1.11).¹¹⁷

Figure 1.11 – Structural representation of $[\{\text{THF}\cdot\text{KCa}(\text{HMDS})_3\}_\infty]$.

Additionally monomeric complexes have been described featuring Li in combination with a variable secondary metal and an equivalent of THF to give the compounds $[\text{THF}\cdot\text{LiMn}(\text{HMDS})_3]^{118}$, $[\text{THF}\cdot\text{LiCa}(\text{HMDS})_3]^{119}$ and $[\text{THF}\cdot\text{LiMg}(\text{HMDS})_3]^{120}$.

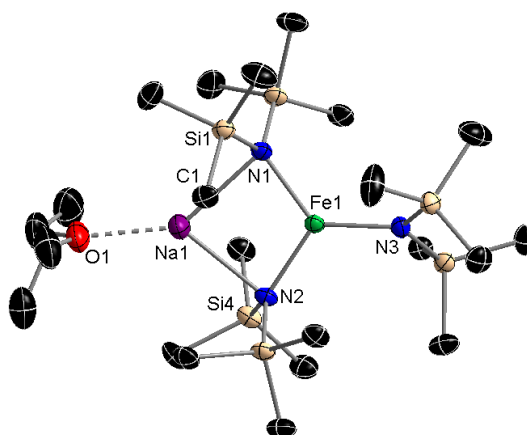


Figure 1.12 – Molecular structure of complex **3**. Hydrogen atoms and co-crystallised hexane solvent omitted for clarity. Thermal ellipsoids displayed at 50% probability level. Selected bond distances (Å) and angles (°): Fe1-N1 2.038(2), Fe1-N2 2.031(2), Fe1-N3 1.963(2), Fe1---Na1 3.0764(12), Na1-N1 2.570(2), Na1-N2 2.524(3), Na1-O1 2.312(3), Na1-C1 3.104(3); N1-Fe1-N2 110.67(9), N1-Fe1-N3 127.05(9), N2-Fe1-N3 122.28(9), Na1-N1-Fe1 82.91(8), Na1-N2-Fe1 84.23(8), Na1---Fe1-N3 176.51(7), N1-Na1-N2 82.15(8), O1-Na1---Fe1 168.85(10).

The crystal of diethyl ether solvate $[\text{Et}_2\text{O}\cdot\text{NaFe}(\text{HMDS})_3]$ (**3**) is shown in Figure 1.12. Complex **3** exhibits a similar contacted ion-pair structural motif described for **2** with Na now solvated by a molecule of Et_2O .

When $\text{S}=\text{PPh}_3$ was added to a solution of **1** in hexane before cooling slowly to -30°C , a green solution deposited crystals of $[\text{Ph}_3\text{P}=\text{S}\cdot\text{NaFe}(\text{HMDS})_3]$ (**4**) (Figure 1.13).

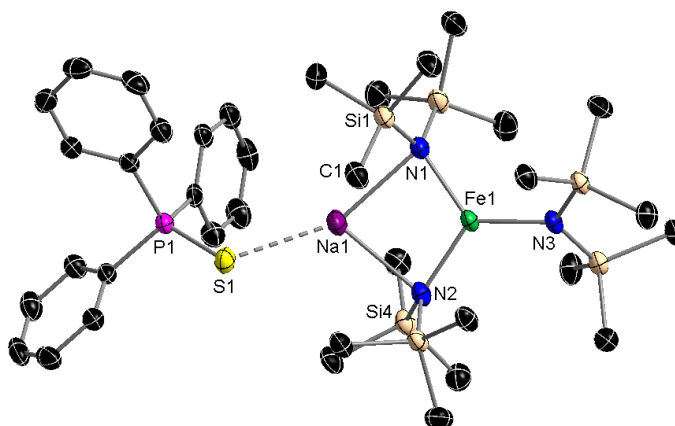


Figure 1.13 – Molecular structure of complex **4**. Hydrogen atoms omitted for clarity. Thermal ellipsoids displayed at 50% probability level. Selected bond distances (Å) and angles (°): Fe1-N1 2.030(2), Fe1-N2 2.023(3), Fe1-N3 1.968(2), Fe1---Na1 3.0662(14), Na1-N1 2.569(3), Na1-N2 2.533(3), Na1---C1 3.022(4), Na1-S1 2.8302(16), S1-P1 1.9699(10); N1-Fe1-N2 111.35(10), N1-Fe1-N3 125.38(10), N2-Fe1-N3 123.26(10), Na1-N1-Fe1 82.73(9), Na1-N2-Fe1 83.79(9), Na1---Fe1-N3 175.75(5), N1-Na1-N2 81.99(9), Na1-S1-P1 109.25(5).

It should be noted that there are only few examples of complexes in the literature containing $S=PPh_3$ as a donor ligand[†] and as far as we can ascertain this is only the second example of a phosphine sulphide coordinated to Na to be structurally characterised after the sodium dimer $[\{(THF)_2 \cdot Na\{4,5-(P=SPh_2)_2tz\}\}_2]$ ($tz = 1,2,3$ -triazolyl) shown in Figure 1.14, possessing a Na-S bond distance of 3.038(1), noticeably longer than the Na1-S1 bond distance (2.8302(16) Å) in **4**.¹²¹

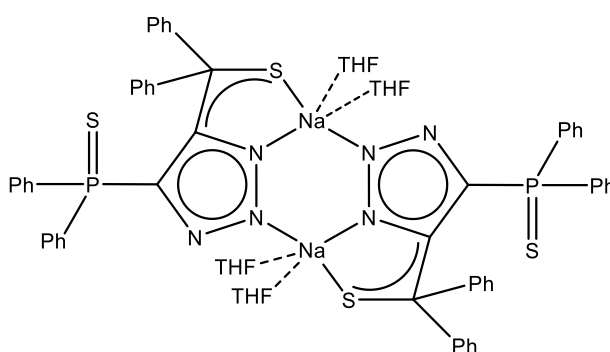


Figure 1.14 – Structure of $[\{(THF)_2 \cdot Na\{4,5-(P=SPh_2)_2tz\}\}_2]$.

Holland has reported the synthesis of alkali metal iron(I) sulfide complexes (Na and K) which reveal S bridging between two Fe centres supported by β -diketaminato ligands (Figure

[†] A search of the Cambridge Crystallographic Data Centre (CCDC) found only 12 crystallographically characterised structures featuring $S=PPh_3$ as a ligand to a metal, predominately transition metals plus one Al and one Sn example. Cambridge Crystallographic Database search, “ $Ph_3P=S$ - - - AM”; any metal, any bond”, March 2016.

1.15).¹²² Two alkali metal cations are sandwiched between the aryl groups of the β -diketaminato ligand, residing directly above and below S to give an overall structural motif akin to an inverse crown.

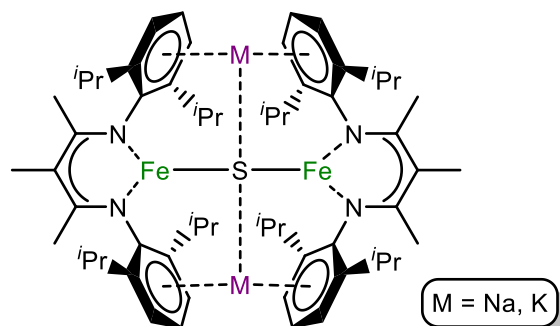


Figure 1.15 – Structure of Holland's alkali metal iron(I) sulfide complex.¹²²

In the case of **4**, reasoning neutral PPh_3 could be suitably labile and be able to release S to facilitate the formation a sodium iron sulfide complex, **4** was refluxed in hexane for 12 hours. However, no products other than **4** were found, surmising that **4** is very thermally stable.

A comparison of the main geometrical parameters of **1**, $[\text{THF} \cdot \text{NaFe}(\text{HMDS})_3]^{116}$ (rather than **2**, as the authors report no structural disorder), **3** and **4** is shown in Table 1.1 below.

Table 1.1 - Selected geometrical parameters of compounds **1**, $[\text{THF} \cdot \text{NaFe}(\text{HMDS})_3]$, **3** and **4**. Bond distances are given in Ångstroms and bond angles given in degrees ($^\circ$).

Bond/Angle	1	$[\text{THF} \cdot \text{NaFe}(\text{HMDS})_3]^{116}$	3	4
Fe-N1	2.036(2)	2.0427(11)	2.038(2)	2.030(2)
Fe-N2	2.032(2)	2.0428(11)	2.031(2)	2.023(3)
Fe-N3	1.964(2)	1.9599(14)	1.963(2)	1.968(2)
Mean Fe-N	2.011	2.015	2.011	2.007
Fe---Na	3.0131(13)	2.9630(9)	3.0764	3.0662(14)
Na-N1	2.503(2)	2.4453(13)	2.570(2)	2.569(3)
Na-N2	2.492(3)	2.4453(13)	2.524(3)	2.533(3)
Mean Na-N	2.498	2.4453	2.547	2.551

N1-Fe-N2	110.48(10)	109.66(6)	110.67(9)	111.35(10)
N1-Fe-N3	124.93(10)	125.17(3)	127.05(9)	125.38(10)
N2-Fe-N3	124.56(10)	125.17(3)	122.28(9)	123.26(10)
Σ(N-Fe-N) angles	359.97	360	360	359.99
Fe deviation from N1-N2-N3 plane	0.0186(1)	0	0.0022(1)	0.0125(1)
N1-Na-N2	84.03(9)	86.133(35)	82.15(8)	81.99(9)

Overall the CIP structures show a very marginal variation in the lengths of the *anchoring* Fe-N bonds (both bridging and terminal) and the N-Fe-N bond angles, favouring a distorted trigonal planar geometry with the amido HMDS ligands. In all cases, the terminal Fe-N3 bonds are shorter compared to the bridging Fe-N1/N2 bonds and the sum of the N-Fe-N bond angles are (practically) equal to 360°. With sodium achieving coordinative stabilisation through *ancillary* bonding in the molecular frameworks, the Na-N and Fe---Na distances and the N1-Na1-N2 angles vary to a larger degree, though not tremendously.

In **4**, Na completes its coordination sphere this time by bonding to the S atom of the phosphine sulphide (Na1-S1 2.8302(16) Å). The S-P bond distance in **4** (1.9699(10) Å) is slightly elongated from that in free S=PPh₃ (average 1.950 Å).¹²³ The more electronegative S atom (compared to O) could be expected to be a stronger donor, able to pull Na away from the Fe centre and bridging N atoms to a larger degree. Indeed compound **4** possesses the longest mean Na-N bond length (2.551 Å) and the most acute N1-Na-N2 angle (81.99(9)°), though it has the second largest Fe---Na separation (3.0662(14) Å) after compound **3**. It may be reasonable to assume large steric bulk of S=PPh₃ (considerably more than that of either THF or Et₂O) may have an influence on how well it can bond to Na in the HMDS sodium ferrate framework.

Table 1.2 – ^1H and $^{13}\text{C}\{^1\text{H}\}$ NMR spectroscopic chemical shift values (in ppm) for the HMDS groups in $[\{\text{Fe}(\text{HMDS})_2\}_2]$ and complexes **1-4** in C_6D_6 .

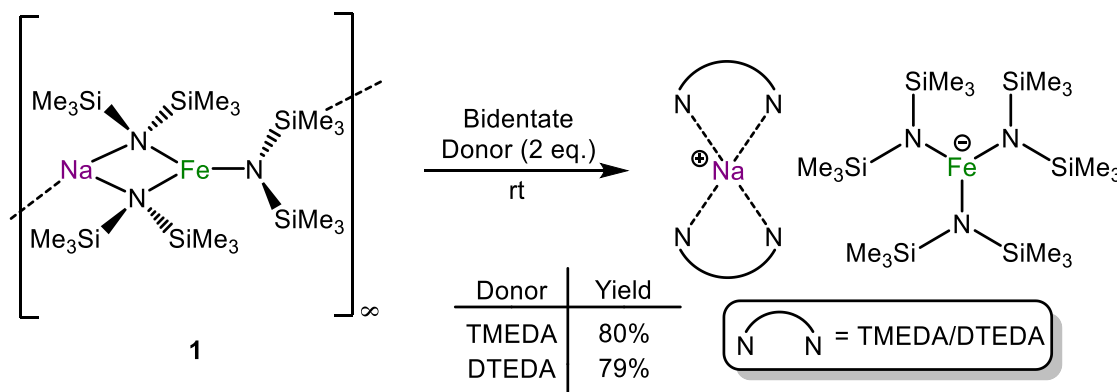
Complex	HMDS Resonance in C_6D_6	
	^1H δ/ppm	$^{13}\text{C}\{^1\text{H}\}$ δ/ppm
$[\{\text{Fe}(\text{HMDS})_2\}_2]$	60.27	-
1	-4.72	333.41
2	-4.74	330.32
3	-4.81	327.22
4	-4.70	327.62

The ^1H and $^{13}\text{C}\{^1\text{H}\}$ NMR spectra of **2**, **3** and **4** all appear very similar to those for **1** concerning the HMDS methyl groups. Table 1.2 shows a comparison of the chemical shifts for the HMDS group H atoms and carbons for $[\{\text{Fe}(\text{HMDS})_2\}_2]$ and complexes **1-4**. For CIP complexes **1-4** a very broad upfield singlet, centred between -4.70 and -4.81 ppm, is apparent for the HMDS H atoms in the ^1H NMR spectra. In the $^{13}\text{C}\{^1\text{H}\}$ NMR spectra, a weak and broad resonance is seen *circa* 330 ppm for the HMDS carbon atoms.

The ^1H NMR spectrum of **2**, shows signals for THF (10.86 and 6.35 ppm) which have shifted and broadened considerably (from free THF at 3.57 and 1.40 ppm),¹²⁴ indicating that in C_6D_6 solution, THF remains coordinated to Na. Similarly for **3**, signals for Et_2O at 10.18 (CH_2) and 4.52 (CH_3) ppm are shifted considerably from those of free Et_2O in C_6D_6 (3.26 and 1.11 ppm, respectively)¹²⁴, allowing for the same conclusion to be drawn.

The ^1H NMR spectrum of **4** shows two signals in the aromatic region at 7.90 and 7.45 ppm (*meta* and *para* H atoms, respectively) and a further broad signal at 10.22 ppm (*ortho* H atoms) accounting for the phenyl H atoms. In the $^{13}\text{C}\{^1\text{H}\}$ NMR spectrum three weak resonances are seen in the aromatic region at 136.54, 133.32 and 130.62 ppm (*ipso*, *para* and *ortho* C atoms, respectively); it is likely the resonance for the *meta* carbons is obscured by the large solvent peaks. Curiously and despite several attempts, no visible resonances could be found in the $^{31}\text{P}\{^1\text{H}\}$ NMR spectrum (spectral window 300 to -300 ppm), perhaps due to extreme shifting or broadening of the resonance due to the presence of paramagnetic Fe(II). Comparing with the NMR spectra of pure $\text{S}=\text{PPh}_3$ (see Section III.I.V), it is likely **4** retains its structure in C_6D_6 at ambient temperature, as evidenced by the shifting and loss of resolution (multiplets to singlets for aromatic H's) of signals and the lack of observed resonance in the $^{31}\text{P}\{^1\text{H}\}$ NMR spectrum of **4**.

1.1.3.2 Bidentate Lewis Donors: TMEDA and DTEDA

Scheme 1.3 - Synthesis of complexes **5** and **6**.

Moving to bidentate amino donors, the addition of either 2 equivalents of TMEDA (*N,N,N',N'*-tetramethylethylenediamine) or 2 equivalents DTEDA (*N,N'*-di-*tert*-butylethylenediamine) to **1** (Scheme 1.3) yielded solvent separated ion-pairs $[\text{Na}(\text{TMEDA})_2]^+[\text{Fe}(\text{HMDS})_3]^-$ (**5**) (Figure 1.16) and $[\text{Na}(\text{DTEDA})_2]^+[\text{Fe}(\text{HMDS})_3]^-$ (**6**) (Figure 1.17), in yields of 80 and 79%, respectively.

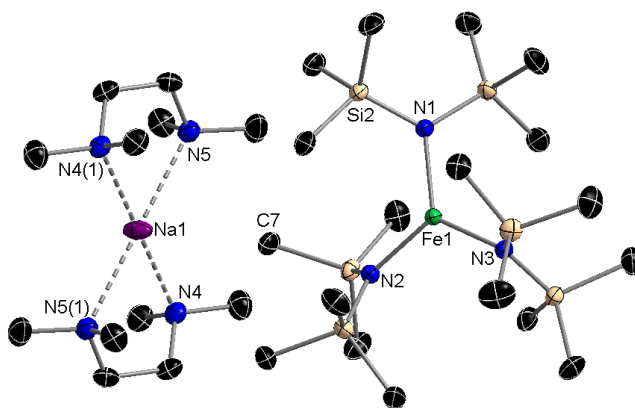


Figure 1.16 – X-ray crystal structure of complex **5** (both TMEDA groups symmetrically equivalent). Hydrogen atoms and second unit of $[\text{Na}(\text{TMEDA})_2]^+$ in asymmetric unit featuring disorder in the TMEDA groups omitted for clarity. Thermal ellipsoids displayed at 50% probability level. Selected bond distances (Å) and angles (°): Fe1-N1 1.9839(16), Fe1-N2 1.9899(15), Fe1-N3 1.9937(16), Na1-N4 2.4605(17), Na1-N5 2.5859(17); N1-Fe1-N2 119.19(7), N1-Fe1-N3 121.18(6), N2-Fe1-N3 119.63(7), N4-Na1-N5 73.65(6), N4-Na1-N4(1) 180, N4-Na1-N5(1) 106.35(6), N5-Na1-N4(1) 106.35(6), N5-Na1-N5(1) 180.

Looking upon the structure of **5**, sodium is centrally coordinated by four donating nitrogen atoms of two molecules of TMEDA in a distorted square planar geometry (sum of angles around Na = 360°). The Na-N bond distances are slightly uneven with a Na-N4 distance of

2.4604(17) Å and Na-N5 distance of 2.5859(17) Å. The structure of **5** displays a near perfectly trigonal planar Fe^{II} centre (sum of N-Fe-N angles 360°, ranging from 119.19(7)° to 121.18(6)°) which is bound to three terminal HMDS ligands. This is in part evidenced by the average Fe-N bond lengths; 1.993(3) Å for compound **5** versus 1.917(4) Å for Fe^{III}(HMDS)₃ which is also trigonal planar in the solid state.¹²⁵

In the case of DTEDA, X-ray crystallographic analysis suggests that the formation of [Na(DTEDA)₂]⁺[Fe(HMDS)₃]⁻ (**6**) (Figure 1.17) has taken place. However, this structural determination is severely affected by disorder (within the ^tBu and SiMe₃ groups) which greatly compromises the accuracy of the structure.

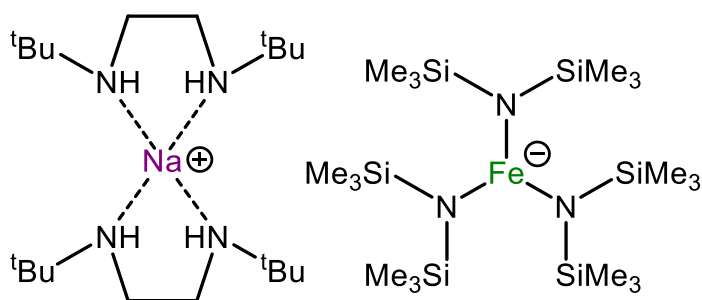


Figure 1.17 – Proposed structure of complex **6**.

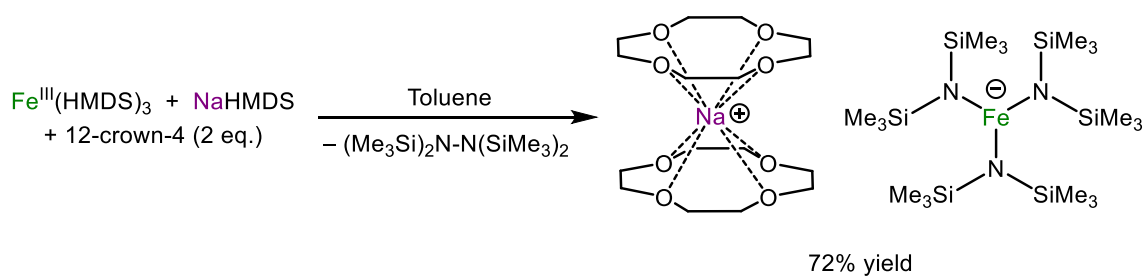
Supporting the formation of **6**, it should be mentioned that when the closely related reaction of LiHMDS and Fe(HMDS)₂ was carried out in the presence of DTEDA, parent lithium analogue [Li(DTEDA)₂]⁺[Fe(HMDS)₃]⁻ was structurally defined.⁷⁸ Furthermore, ¹H and ¹³C{¹H} NMR spectroscopic analysis of **6** in d₈-THF supports the formation of theSSIP structure depicted in Figure 1.17. Moreover, quantitative CHN elemental microanalysis data obtained for **6** (see Section III.II.I) closely matches calculated values for [Na(DTEDA)₂]⁺[Fe(HMDS)₃]⁻.

Interestingly even when a molar equivalent of these bidentate donors is employed compounds **5** and **6** are obtained, although in reduced yields (42 and 37%, respectively, with a maximum possible yield of 50%).

In contrast to contacted ion-pair species **1-4**, SSIP complexes **5** and **6** presented poor solubility in C₆D₆ and deuterated toluene arene solvents for NMR spectroscopic analysis, thus more polar d₈-THF was used. Resonances in the ¹H NMR spectra corresponding to HMDS groups surrounding the Fe centre (-2.37 ppm for **5** and **6**) are shifted minorly downfield as compared to those observed for contacted ion-pair complexes **1-4** (circa -4.7 ppm). This

downfield shifting trend is also observed in the $^{13}\text{C}\{^1\text{H}\}$ spectra for the HMDS carbons to a somewhat larger degree (resonances at 347.81 ppm). The chemical shifts for the Lewis donors however appear well resolved and differ only marginally than those of the free Lewis donors in d_8 -THF,^{126,127} which is consistent with TMEDA and DTEDA being displaced in solution by donor solvent d_8 -THF.

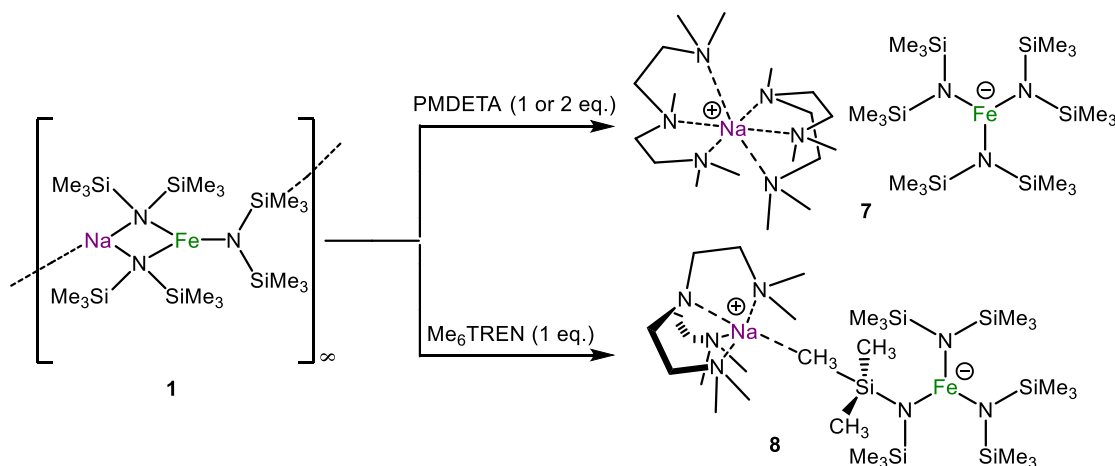
Structurally related to both **5** and **6**, an example of a SSIP sodium ferrate with the formula $[\text{Na}(\text{12-crown-4})_2]^+[\text{Fe}(\text{HMDS})_3]^-$ was reported by Dehnicke and co-workers in 1996 which features an $\text{Fe}^{\text{II}}(\text{HMDS})_3$ anionic moiety.¹²⁸ Upon reacting $\text{Fe}^{\text{III}}(\text{HMDS})_3$ with NaHMDS and 2 equivalents of 12-crown-4 the Fe^{II} sodium ferrate is obtained along with half an equivalent of the hydrazine adduct $(\text{Me}_3\text{Si})_2\text{N}-\text{N}(\text{SiMe}_3)_2$ (Scheme 1.4). The average Fe-N bond length of 1.981 Å and sum of N-Fe-N angles, 360° , compare favourably with **5** and **6**.



Scheme 1.4 - Synthesis of $[\text{Na}(\text{12-crown-4})_2]^+[\text{Fe}(\text{HMDS})_3]^-$.¹²⁸

1.1.3.3 Polydentate Lewis Donors: PMDETA and Me₆TREN

To further explore the structural variations of this family of sodium ferrates, we then studied the reaction of **1** with the polydentate N-ligands PMDETA and Me₆TREN (Scheme 1.5).



Scheme 1.5 – Reactions of **1** with polydentate donors PMDETA and Me₆TREN.

Sodium ferrate **1** was reacted with one equivalent of tridentate donor PMDETA, the formation of the SSIP $[\text{Na}(\text{PMDETA})_2]^+[\text{Fe}(\text{HMDS})_3]^-$ (**9**) (Figure 1.18) was observed in a 41% yield (note that under these conditions the maximum achievable yield is 50%), in a similar fashion to **5** and **6**. When the reaction was performed with a rational two molar equivalents of PMDETA, **7** was obtained in an increased 81% yield. X-ray crystallographic studies revealed that **7** exhibits a SSIP ion-pair structure, with Fe bonded to the three terminal HMDS groups and Na chelated by two molecules of PMDETA. Interestingly, it should be noted that for each of these tridentate ligands, Na forms shorter (stronger) bonds with two of the three available N atoms. Equatorial nitrogens N2, N3, N5 and N6 adopt a pseudo square planar geometry around Na, akin to TMEDA in **5**. These shorter Na-N bond distances in **7** (average 2.5468 Å) are comparable with those described for TMEDA-solvate **5** (average Na-N bond length 2.5232 Å). Na exhibits longer distance contacts with axial N1 and N4 atoms (Na1-N1 3.014(3) Å, Na1-N4 2.883(3) Å) which cap above and below the plane. Thus overall, Na exhibits a distorted octahedral geometry with the PMDETA ligands acting almost as TMEDA-mimics (*cf.* complex **5**).

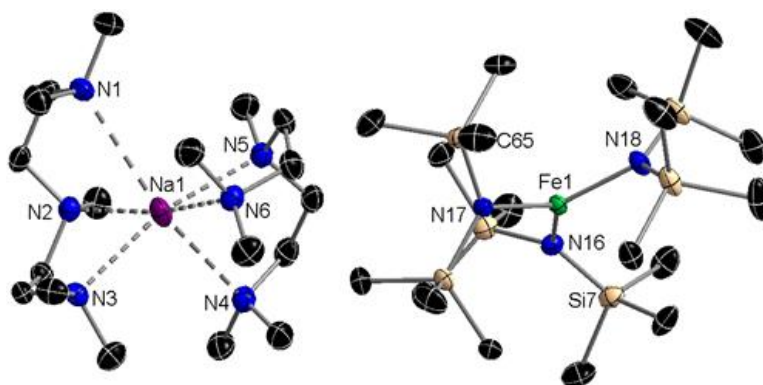


Figure 1.18 –Molecular structure of compound **7**. Hydrogen atoms and second equivalent of $[\text{Na}(\text{PMDETA})_2]^+[\text{Fe}(\text{HMDS})_3]^-$ in the asymmetric unit, with disorder in the PMDETA groups, omitted for clarity. Thermal ellipsoids displayed at 50% probability level. Selected bond distances (Å) and angles (°): Fe1-N16 1.984(2), Fe1-N17 1.985(2), Fe1-N18 1.979(2), Na1-N1 3.014(3), Na1-N2 2.516(2), Na1-N3 2.576(2), Na1-N4 2.883(3), Na1-N5 2.496(2), Na1-N6 2.599(3); N16-Fe1-N17 120.62(9), N16-Fe1-N18 119.25(9), N17-Fe1-N18 120.12(9), N1-Na1-N2 66.89(8), N1-Na1-N3 99.87(8), N1-Na1-N4 150.55(8), N1-Na1-N5 94.09(8), N1-Na1-N6 99.87(8), N2-Na1-N3 74.18(8), N2-Na1-N4 97.27(8), N2-Na1-N5 115.30(8), N2-Na1-N6 164.02(9), N3-Na1-N4 99.16(8), N3-Na1-N5 165.54(9), N3-Na1-N6 100.58(8), N4-Na1-N5 69.59(8), N4-Na1-N6 98.48(8), N5-Na1-N6 73.11(8).

The cation $[\text{Na}(\text{PMDETA})_2]^+$ has also been found in the related sodium magnesiate $[\text{Na}(\text{PMDETA})_2]^+[\text{Mg}(\text{TMP})_3]^-$.¹²⁹ The cationic unit for this SSIP ion-pair structure is essentially the same as that displayed in **7**, with PMDETA using primarily two of its three available nitrogens to coordinate to Na. The mean short and long Na-N bond distances (2.530 Å and 2.933 Å, respectively) are almost equivalent with **7**. Regarding the anionic component of **7**, the $[\text{Fe}(\text{HMDS})_3]^-$ unit is analogous with the previously described SSIP ion-pair **5** and thus warrants no further discussion.

On the other hand, when the denticity of the N-donor ligand was increased, using tetradentate Me_6TREN (1 eq.) as a Lewis base, the reaction with **1** led to the isolation of $[\text{Me}_6\text{TREN}\cdot\text{Na}]^+[\text{Fe}(\text{HMDS})_3]^-$ (**8**) (Figure 1.19) in an 84% yield.

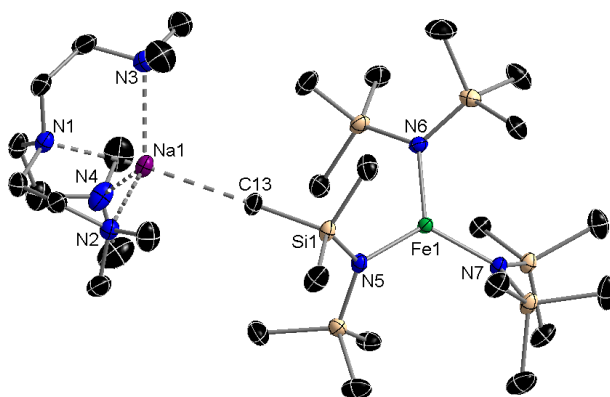


Figure 1.19 –X-ray crystal structure of complex **8**. Hydrogen atoms omitted for clarity. Thermal ellipsoids displayed at 50% probability level. Selected bond distances (Å) and angles (°): Fe1-N5 1.9931(16), Fe1-N6 1.9861(16), Fe1-N7 1.9927(15), Na1---C13 2.727(2), Na1-N1 2.4272(18), Na1-N2 2.4846(19), Na1-N3 2.4954(19), Na1-N4 2.459(2); N5-Fe1-N6 119.25(6), N5-Fe1-N7 121.93(6), N6-Fe1-N7 118.83(7), N1-Na1-N2 75.57(6), N1-Na1-N3 75.83(6), N1-Na1-N4 75.40(6), N1-Na1---C13 167.18(8), N2-Na1-N3 117.97(6), N2-Na1-N4 108.59(7), N2-Na1---C13 92.13(7), N3-Na1-N4 115.47(7), N3-Na1---C13 107.73(7), N4-Na1---C13 112.66(8), Na1---C13-Si1 173.36(13).

Contrasting with the structures of **5**, **6** and **7**, which contain two equivalents of the relevant N-donor ligand, in **8** Na binds to just one molecule of Me₆TREN. Exhibiting a κ^4 coordination, this ligand caps the Na centre on the rear face (at an average Na-N bond distance of 2.4666 Å), with Na positioned slightly above the N2-N3-N4 plane (0.6164(1) Å deviation) in a distorted trigonal bipyramidal geometry. The exposed face of the sodium forms a long distance electrostatic contact with the C13 methyl carbon of an HMDS group attached to iron (Na---C13 2.727(2) Å). The trigonal planar [Fe(HMDS)₃]⁻ anion has bond lengths and angles comparable to the SSIP **5** and **7** (*vide supra*). Compound **8** can be envisaged as an intermediate between a contacted ion-pair and a solvent separated structure. The formation of this electrostatic Na---C contact does not affect the Fe-N bond distance of the relevant HMDS ligand (Fe-N5 1.9931(16) Å) which is of the same range as the remaining Fe-N bonds in **8** (Fe-N6 1.9861(16) Å, Fe-N7 1.9927(15) Å).

Tripodal tetraamino Me₆TREN has been most frequently reported as a supporting ligand for d-block metals,¹³⁰ less so for Group 1 metals. There are only a handful of examples where this ligand is coordinated to Na.^{131–136} In most of these examples Na is also attached to an anionic ligand, with Me₆TREN facilitating the formation of low aggregates. Related to **8**, O'Hara has recently reported the structures of [$\{\text{Na}_5(\mu\text{-HMDS})_5(\mu_5\text{-X})\}\{\text{Na}(\text{Me}_6\text{TREN})\}$] (where X = Cl or Br) where Na binds to one molecule of Me₆TREN as well as forming a long distance Na---C electrostatic interaction with a Me group of a SiMe₃ fragment (Figure

1.20).¹³⁶ Their Na---C distances are found to be longer at 2.955(3) and 2.955(4) Å (Cl and Br, respectively) than 2.727(2) Å for **8**, though they exhibit shorter mean Na-N bond lengths with Me₆TREN (2.4363 and 2.4365 Å, Cl and Br, respectively) than those in **8** (mean Na-N distance 2.4666 Å).

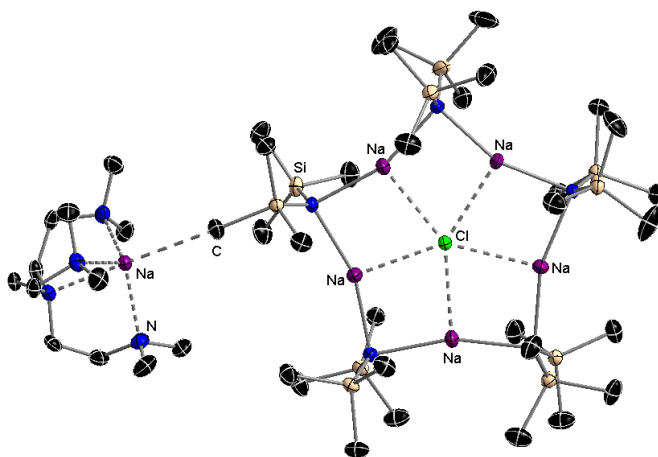
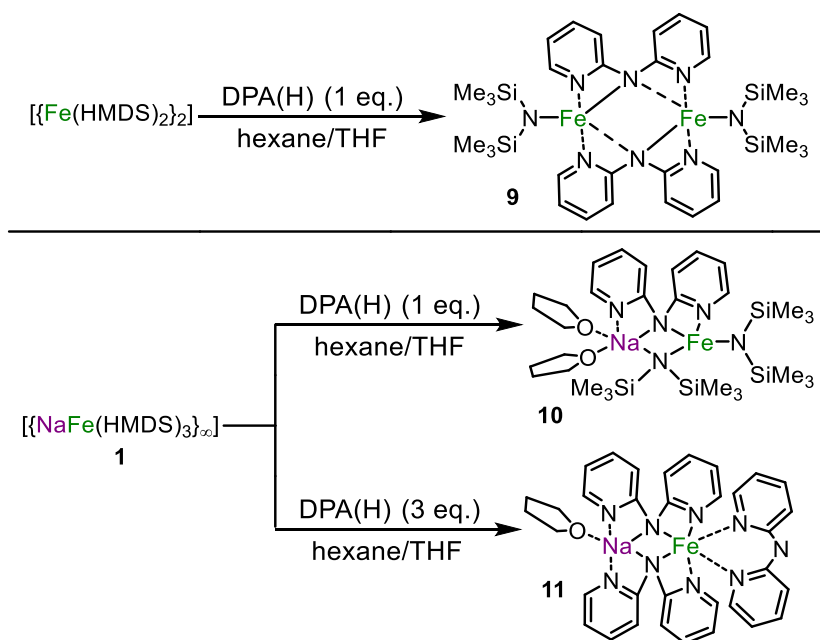


Figure 1.20 – Crystal structure of $[\{Na_5(\mu\text{-HMDS})_5(\mu_5\text{-Cl})\}\{Na(\text{Me}_6\text{TREN})\}]$. Hydrogen atoms omitted for clarity. Thermal ellipsoids displayed at 50% probability level.

As discussed for **5** and **6**, SSIP species **7** and **8** showed poor solubility in C₆D₆. ¹H and ¹³C{¹H} NMR spectroscopic characterisation of these compounds in d₈-THF reveal that under these conditions the N donors coordinated to Na are displaced by the deuterated solvent. Broad signals at -2.42 and -2.46 ppm were observed for **7** and **8**, respectively that are assigned to the anionic [Fe(HMDS)₃]⁻ fragment.

1.1.4 Transamination Reactions with 2,2'-Dipyridylamine

After exploration of the structural variances of homoleptic sodium ferrate **1**, we were curious to explore its reactivity towards amines (transamination reactions) as a vehicle to access novel sodium ferrates. As an initial venture, heterocyclic 2,2'-dipyridylamide (DPA) was chosen as a suitable candidate for a transamination with HMDS (Scheme 1.6). Though less prevalent throughout organometallic chemistry than HMDS, DPA has been utilised in a number of varied branches of chemistry including materials science,¹³⁷ catalysis,¹³⁸ supramolecular chemistry¹³⁹ and even in mixed-metal chemistry.¹⁴⁰



Scheme 1.6 – Reactions carried out with DPA(H).

We began by introducing one equivalent of DPA(H) (2,2'-dipyridylamine) to a solution of our homometallic precursor $\text{Fe}(\text{HMDS})_2$ in hexane (Scheme 1.6, top) which turned the green solution brown with an off-white precipitate. Addition of THF solubilised the precipitate and cooling to -30°C furnished a crop of orange plate-like crystals. From X-ray diffraction studies the structure was determined to be heteroleptic bis(amide) $[\{\text{Fe}(\text{HMDS})(\text{DPA})\}_2]$ (**9**), isolated in a 38% yield (Figure 1.21).

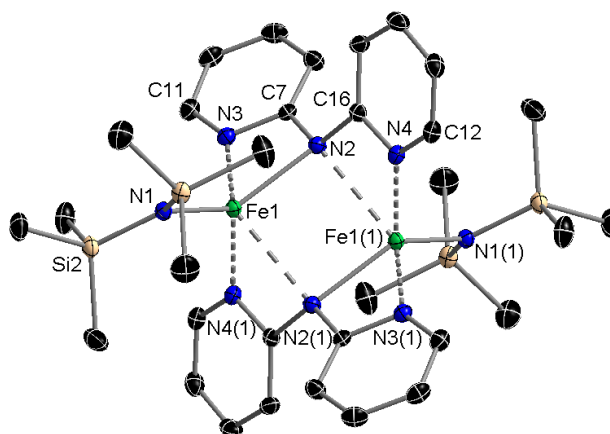


Figure 1.21 –X-ray crystal structure of complex **9**. Hydrogen atoms omitted for clarity. Thermal ellipsoids displayed at 50% probability level. Selected bond distances (Å) and angles ($^\circ$): Fe1-N1 1.9583(14), Fe1-N2 2.1642(14), Fe1-N3 2.2112(15), Fe1-N(4) 2.1044(14), Fe1---N2(1) 2.546(1), Fe1---Fe1(1) 3.3609(1); N1-Fe1-N2 134.76(6), N1-Fe1-N3 119.34(6), N1-Fe1-N4(1) 111.04(6), N2-Fe1-N3 61.70(5), N2-Fe1-N4(1) 113.54(5), N3-Fe1-N4(1) 97.63(5), N1-Fe1---Fe1(1) 134.078(1).

[{Fe(HMDS)(DPA)}₂] (**9**) exhibits a dimeric arrangement with a novel eight-membered {FeNCNFeNCN} core. Each Fe atom binds to a terminal HMDS group and to two bridging DPA ligands which provide supplementary coordination to the Fe centres through their neutral ring nitrogens with the pyridyl rings in a syn/syn conformation (a linear array of the N atoms), the pyridyl N atoms ‘pointing’ in the same direction as the amido N thus maximising interaction with the Fe centres. Fe is formally five-coordinate considering the long contact to the opposing central amido nitrogen (Fe1---N2(1) 2.546(1)) though much shorter bond distances are observed to amido nitrogens N1 and N2 (1.9583(14) and 2.1642(14) Å, respectively) and to pyridyl nitrogens N3 and N4(1) (2.2112(15) and 2.1044(14) Å, respectively). Discounting N2(1), a distorted tetrahedral geometry around Fe is present (average N-Fe-N angle = 106.36°, range 61.70(5) to 134.76(6)°, excluding N2(1)).

The ¹H NMR spectrum for **9** (recorded in C₆D₆) is nicely resolved with resonances that account for all H atoms present in **9**. The signal for the HMDS H atoms appears at 17.01 ppm as a broad singlet, though much less broad than for [{Fe(HMDS)₂}₂] (*cf.* 60.27 ppm). Four more resonances are visible (each integrating correctly to 2 hydrogens) for the aryl ring H atoms between 47.15 and -14.31 ppm, though it would be ambiguous to attempt to further assign these due to the large isotropic shifts.

Whilst there are structural examples of iron and DPA/DPA(H) together, DPA/DPA(H) coordinating to Fe solely via the pyridyl N atoms, only two examples exhibit an Fe-N_{amido} bond. [Fe₄(O)(DPA)₆] was reported in 2000 by Cotton *et al.*, prepared from DPA(H), MeLi and FeCl₂.¹⁴¹ Though all equivalents of DPA(H) have been deprotonated and (through loss of LiCl) exist in the DPA amido form, only the 3 equivalents on the ‘bottom face’ of the {Fe₄(O)} core bond through their amido N atoms whilst the 3 equivalents on the ‘top face’ act only as bidentate ligands through their pyridyl N atoms (Figure 1.22).

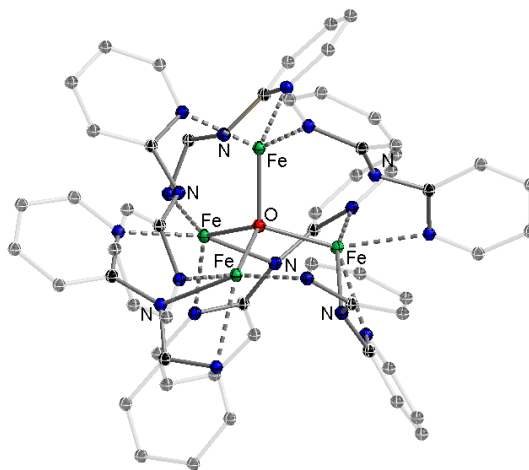


Figure 1.22 – Central core of $[\text{Fe}_4(\text{O})(\text{DPA})_6]$.¹⁴¹ Amido N's labelled with solid line bonds and pyridyl N bonds shown dashed. Hydrogen atoms omitted and outer ring carbons transparent for clarity.

A very recent publication by McKenzie and co-workers explores the reaction between $[\{\text{Fe}(\text{Mes})_2\}_2]$ and $\text{DPA}(\text{H})$.¹⁴² The authors state that for divalent transition metals the common structural motifs are of the form $[\{\text{M}(\text{DPA})_2\}_2]$ or $[\text{M}_3(\text{DPA})_4\text{X}_2]$ (all published examples with Fe supported solely by pyridyl N atoms and X, X = OTf or halogen), commonly known as ‘extended metal atom chains’.^{143–146} The result of their reaction however is $[\{\text{Fe}(\text{Mes})(\text{DPA})\}_2]$ (Figure 1.23), closely related to **9**.

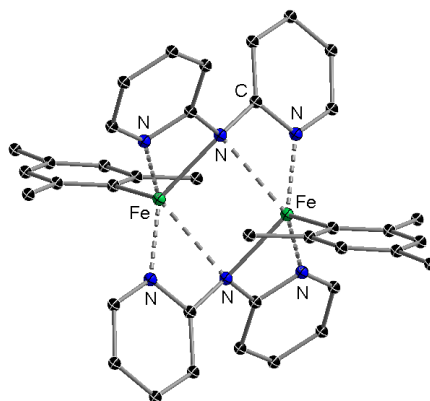
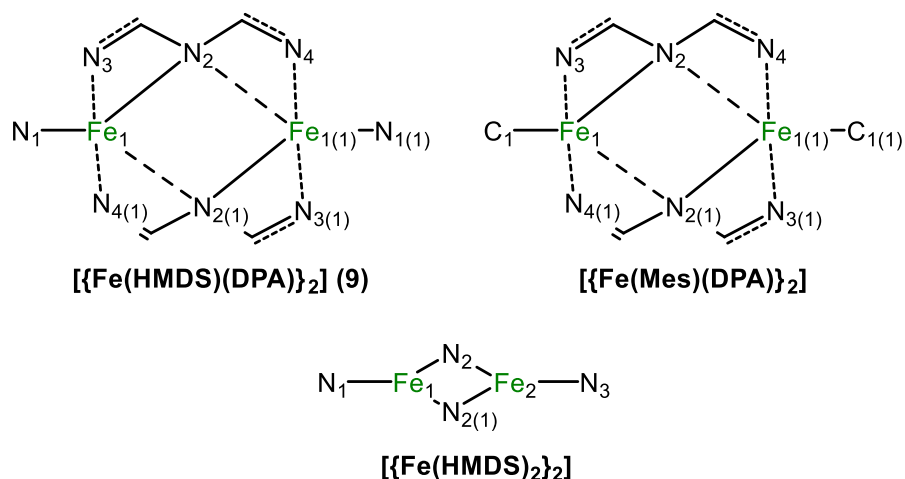


Figure 1.23 – Crystal structure of $[\{\text{Fe}(\text{Mes})(\text{DPA})\}_2]$. Hydrogen atoms omitted for clarity.

From the same reaction they also obtain the product $[\text{Fe}_4(\text{O})(\text{DPA})_6][\text{Fe}_2\text{Cl}(\text{DPA})_3] \cdot (\text{toluene})_3$; tetranuclear and dinuclear structures that co-crystallise together as a result of $\text{H}_2\text{O}/\text{O}_2$ and Cl contaminations, respectively. The tetranuclear motif is identical to $[\text{Fe}_4(\text{O})(\text{DPA})_6]$ that had earlier been crystallographically characterised by Cotton co-workers.¹⁴¹

Figure 1.24 - Central iron-nitrogen cores of **9**, [Fe(Mes)(DPA)]₂ and [Fe(HMDS)₂]₂.

A comparison of selected geometrical parameters between **9**, [Fe(Mes)(DPA)]₂ and [Fe(HMDS)₂]₂ is presented in Table 1.3 with core structures denoted in Figure 1.24.

Table 1.3 - Selected geometrical parameters of compounds **9**, [Fe(Mes)(DPA)]₂ and [Fe(HMDS)₂]₂. Bond distances are given in Ångstroms and bond angles given in degrees (°).

Bond/Angle		9	[Fe(Mes)(DPA)] ₂ ¹⁴²	[Fe(HMDS) ₂] ₂ ⁹²
Terminal	Fe1-N1/C1	1.9583(14)	1.973(3)	1.927(2) ^a
Bridging	Fe1-N2	2.1642(14)	2.147(3)	2.086(2) ^a
Amido	Fe1-N2(1)	2.546(1)	2.470(3)	2.086(2) ^a
Pyridyl	Fe1---N3	2.2112(15)	2.248(3)	-
	Fe1---N4(1)	2.1044(14)	2.130(3)	-
Angles	Fe1---Fe1(1)/Fe2	3.3609(1)	3.043(1)	2.663(2) ^a
	N1/C1-Fe1-N2	134.76(6)	116.85(11)	129.7(1) ^a
	N1/C1-Fe1-N2(1)	108.652(1)	110.73(8)	129.7(1) ^a
	N2-Fe1-N2(1)	89.320(1)	97.89(9)	100.5(1) ^a
	Σ(N-Fe-N) angles	332.732	325.47	359.9 ^a
	N1/C1-Fe1---Fe(1)	134.078(1)	127.29(7)	180.00(1) ^a
	Fe1-N2-Fe1(1)/Fe2	90.680(1)	82.10(7)	79.4(1) ^a

^a[Fe(HMDS)₂]₂ does not contain a central inversion centre but instead a 2-fold axis along the Fe1---Fe2 vector thus there are some very marginal differences in Fe-N bond lengths and angles. For simplicity the longest bond distances and most obtuse angles which occur around Fe1 are given in the table above.

Moving from $[\{\text{Fe}(\text{HMDS})_2\}_2]$ to **9**, Fe increases its coordination number from three to five, consequently **9** displays a marginally lengthened Fe1-N1 bond (1.927(2) vs 1.9583(14) Å, respectively) and a considerably lengthened Fe---Fe separation (2.663(2) vs 3.3609(1) Å, respectively). In comparison to the corresponding Fe-N_{amido} bonds in $[\{\text{Fe}(\text{Mes})(\text{DPA})\}_2]$, **9** exhibits longer bond distances as well as a larger separation between Fe centres (3.043(1) Å for $[\{\text{Fe}(\text{Mes})(\text{DPA})\}_2]$). Conversely, in comparison to $[\{\text{Fe}(\text{Mes})(\text{DPA})\}_2]$, **9** exhibits marginally shorter Fe-N_{pyridyl} bond lengths (Fe1-N3 2.248(3) vs 2.2112(15) Å and Fe-N4(1) 2.130(3) vs 2.1044(14) Å for $[\{\text{Fe}(\text{Mes})(\text{DPA})\}_2]$ vs **9**, respectively).

We next investigated the incorporation of DPA groups in sodium ferrate complexes by treating **1** with variable quantities of DPA(H) (Scheme 1.6). Addition of one molar equivalent of DPA(H) to a solution of **1** in hexane immediately afforded a brown suspension which could be solubilised with a small quantity of THF (Scheme 1.6, middle). Orange crystals were obtained at -30°C of $[(\text{THF})_2\cdot\text{NaFe}(\text{DPA})(\text{HMDS})_2]$ (**10**) (Figure 1.25) in a 60% yield.

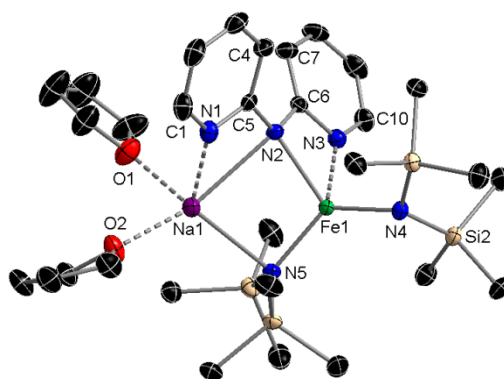


Figure 1.25 – Molecular structure of complex **10**. Hydrogen atoms and disorder present in the two THF molecules and one SiMe₃ unit omitted for clarity. Thermal ellipsoids displayed at 50% probability level. Selected bond distances (Å) and angles (°): Fe1-N2 2.1723(13), Fe1-N3 2.1844(14), Fe1-N4 1.9769(14), Fe1-N5 2.0171(14), Fe1---Na1 3.2253(7), Na1-N1 2.3822(17), Na1-N2 2.6710(15), Na1-N5 2.5464(15), Na1-O1 2.3479(15), Na1-O2 2.3425(14); N2-Fe1-N3 61.71(5), N2-Fe1-N4 118.24(6), N2-Fe1-N5 105.93(5), N3-Fe1-N4 103.30(6), N3-Fe1-N5 121.04(6), N4-Fe1-N5 128.42(6), Na1-N2-Fe1 82.82(5), Na1-N5-Fe1 89.16(5), Na1---Fe1-N4 145.19(4), N1-Na1-N2 53.62(5), N1-Na1-N5 119.96(5), N1-Na1-O1 91.84(6), N1-Na1-O2 98.80(6), N2-Na1-N5 79.73(5), N2-Na1-O1 94.22(5), N2-Na1-O2 152.28(5), N5-Na1-O1 131.07(6), N5-Na1-O2 118.20(5), O1-Na1-O2 88.84(5).

X-ray crystallographic studies confirmed the incorporation of one DPA ligand in the ferrate structure which acts as a bridge between Na and Fe to generate a monomeric contacted ion-pair structure. DPA's central amido nitrogen N2 bridges between Fe and Na at distances of

2.1723(13) and 2.6710(15) Å, respectively, whilst neutral pyridyl nitrogens N1 and N3 provide additional coordination to Na and Fe, respectively. Complex **10** is most comparable with homoleptic sodium ferrate **2**, albeit with an extra molecule of coordinating solvent THF. The iron(II) centre resides in what is effectively a trigonal planar geometry (between amido nitrogens N2, N4 and N5) that is distorted to a much larger degree than for the previously described sodium ferrate structures (sum of angles = 352.59°, range 105.93(5)° to 128.42(6)°, *cf.* 359.94° for **2**). Coordination by pyridyl nitrogen N3 to Fe (2.1844(14) Å) causes a pyramidalisation effect resulting in Fe lying above the N2-N4-N5 plane by 0.3204(1) Å (*cf.* 0.0289(1) Å in **2**). Comparing respective Fe-N_{amido} distances between **10** and homoleptic HMDS CIP complexes **1-4**, terminal Fe1-N4 at 1.9769(14) Å is lengthened slightly when comparing to the average Fe-N_{terminal} distance of 1.963 Å though bridging Fe1-N5 (2.0171(14) Å) is shorter than the mean Fe-N_{bridging} distance of 2.0344 Å, conceivably because penta-coordinate Na requires less electron donation for stabilisation than tri-coordinate Na in complexes **1-4**. It is clear to see that in **10** when considering the Fe-N bond lengths the stronger interactions (by way of shorter bond distances) are to the amido N atoms, even though they (N2 and N5) bridge to coordinate to Na and pyridyl N3 solely coordinates to Fe. Sodium's coordination sphere is occupied by bridging amido nitrogens N2 and N5 at an average Na-N_{amido} distance of 2.6087 Å, considerably longer for the respective average Na-N_{amido} distance of 2.4883 Å for **2**. This is rational, however, because Na is more closely bonded to pyridyl N1 (Na1-N1 2.3822(17) Å) and two equivalents of THF complete Na's coordination sphere ensuring a monomeric product. With increased *ancillary* bonding opportunities penta-coordinate Na resides 3.2253(7) Å from the Fe centre, an appreciably longer distance than three-coordinate Na in **2** (Na1---Fe1 3.0092(10) Å).

The ¹H NMR spectrum of **10** in C₆D₆ reveals one very broad signal at 6.39 ppm and two sharper (but still quite broadened) signals at 4.97 and 2.12 ppm. Due to the extremely broad nature of signal at 6.39 ppm there is considerable overlapping with the residual solvent signal and the signal at 4.97 ppm, thus a meaningful integration and assignment for these resonances is not achievable for **10**. By comparing this spectrum with those collected for compounds **1-9**, it could be reasoned that the two sharper signals (at 4.97 and 2.12 ppm) are THF; these molecules reside far from the paramagnetic Fe centre in the solid state. The extremely broadened signal at 6.39 ppm would then likely be a coalescence of HMDS and DPA resonances, plausible considering the delocalised ring systems.

Via a similar method to **10**, three equivalents of DPA(H) were introduced to a solution of **1** (Scheme 1.6, bottom). Yellow crystals grown from a solution of toluene/THF at -30°C were of polymeric [$\{\text{THF}\cdot\text{NaFe}(\text{DPA})_3\}_n$] (**11**) (Figure 1.26), recovered in a low 18% yield.

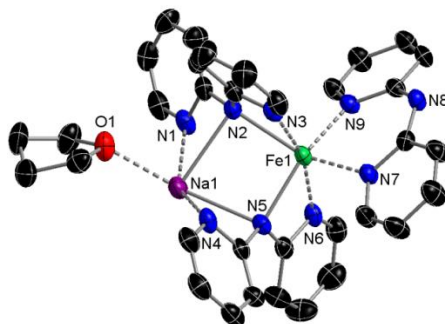


Figure 1.26 – Monomeric unit of complex **11**. Hydrogen atoms and co-crystallised disordered toluene omitted for clarity. Thermal ellipsoids displayed at 50% probability level. Selected bond distances (\AA) and angles ($^{\circ}$): Fe1-N2 2.286(4), Fe1-N3 2.177(4), Fe1-N5 2.159(3), Fe1-N6 2.262(4), Fe1-N7 2.127(3), Fe1-N9 2.101(3), Fe1--Na1 3.4879(17), Na1-N1 2.512(4), Na1-N2 2.571(4), Na1-N4 2.602(4), Na1-N5 2.512(4), Na1-O1 2.362(4), Na1-N8(1) 2.480(4); N2-Fe1-N3 60.34(13), N2-Fe1-N5 92.97(13), N2-Fe1-N6 112.41(13), N2-Fe1-N7 152.05(14), N2-Fe1-N9 93.73(14), N3-Fe1-N5 103.05(14), N3-Fe1-N6 162.71(12), N3-Fe1-N7 92.74(14), N3-Fe1-N9 102.07(14), N5-Fe1-N6 60.46(13), N5-Fe1-N7 101.03(14), N5-Fe1-N9 154.03(14), N6-Fe1-N7 95.53(14), N6-Fe1-N9 93.87(13), N7-Fe1-N9 84.21(14), Na1-N2-Fe1 91.61(13), Na1-N5-Fe1 96.31(14), N1-Na1-N2 53.13(12), N1-Na1-N4 147.38(13), N1-Na1-N5 110.86(13), N1-Na1-O1 87.01(14), N1-Na1-N8(1) 103.22(13), N2-Na1-N4 94.31(12), N2-Na1-N5 78.73(12), N2-Na1-O1 94.62(13), N2-Na1-N8(1) 153.95(15), N4-Na1-N5 52.85(12), N4-Na1-O1 98.97(14), N4-Na1-N8(1) 108.15(14), N5-Na1-O1 149.71(14), N5-Na1-N8(1) 104.14(13), O1-Na1-N8(1) 94.72(13).

Complex **1** has undergone a three-fold transamination to release three equivalents of HMDS(H), incorporating three DPA ligands to furnish a new homoleptic sodium ferrate [$\{\text{THF}\cdot\text{NaFe}(\text{DPA})_3\}_n$] (**11**). The bridging DPA ligands effectively mirror one another by significant twisting of the pyridyl rings from the $\{\text{Na1-N2-Fe1-N5}\}$ core plane in order to accommodate the steric bulk and simultaneously allow for N_{pyridyl} coordination to the two metal centres (Figure 1.27).

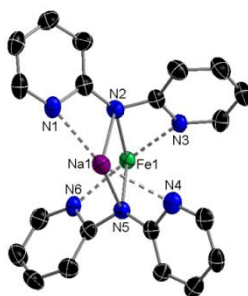


Figure 1.27 – Alternate view of the Na/Fe core and two bridging DPA ligands of **11**. Hydrogen atoms omitted for clarity. Thermal ellipsoids displayed at 50% probability level.

Interestingly, Fe is hexacoordinated residing between three DPA moieties. Fe bonds to amido nitrogens (N2 and N5) and pyridyl nitrogens (N3 and N6) of the bridging DPA groups, similar to **10**. Surprisingly however, the terminal DPA ligand adopts an anti/anti conformation, thus Fe is supported by the two pyridyl nitrogens (N7 and N9) whilst bridgehead N8 points away to sodium on a second monomer unit (at a distance of 2.480(4) Å) to give a 1D polymeric chain (Figure 1.28). Incorporating two bridging DPA groups in syn/syn conformation it is understandable that **11** contains the largest Na---Fe separation of any of the previously described CIP sodium ferrates at 3.4879(17) Å. Na is also hexacoordinated, featuring *ancillary* bonding to the two bridging amido nitrogens N2 and N5 (at distances of 2.571(4) and 2.512(4) Å, respectively), pyridyl nitrogens N1 and N4 (at distances of 2.512(4) and 2.602(4) Å, respectively), though is most closely bonded to amido N8(1) at 2.480(4) Å, completing its coordination sphere with a molecule of THF.

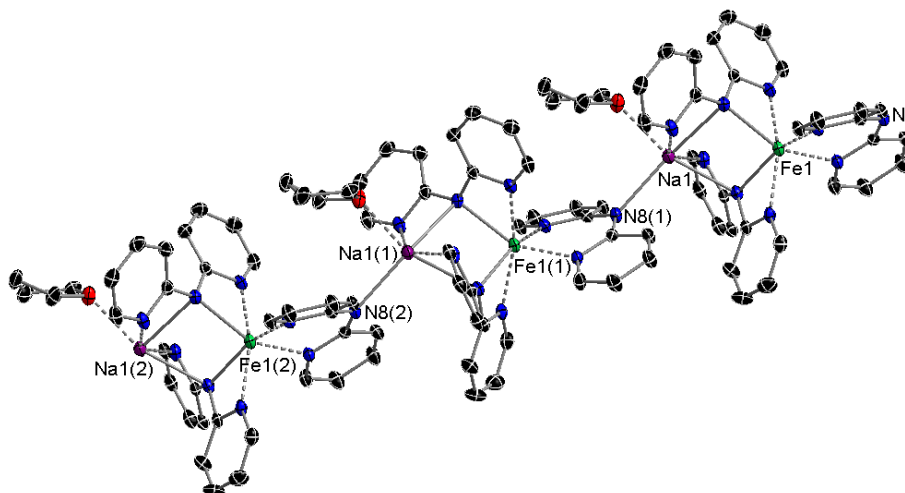


Figure 1.28 - Section of polymeric chain in **11** showing propagation and selected atom labelling, Na1-N8(1) 2.480(4) Å. Hydrogen atoms omitted for clarity. Thermal ellipsoids displayed at 30% probability level.

The ^1H NMR spectrum of **11** in C_6D_6 showed number of poorly resolved broad and overlapping signals (between 0 and 30 ppm) which precluded the meaningful assignment of the resonances.

Except for loosely related K/Co/Fe oxalate complex $[\text{K}(18\text{-crown-6})]^+[\text{Co}(\text{DPA})\text{Fe}(\text{ox})_3]^-$ (ox = oxalate),¹⁴⁷ where there is no coordination between Fe and DPA, as far as can be ascertained, **10** and **11** represent the first examples of DPA ferrate complexes. An interesting precedence of DPA in mixed-metal chemistry are the sodium zincates $[(\text{TMEDA})_2\text{Na}_2(\mu\text{-DPA})_2\text{Zn}(\text{tBu})_2]$ and $[\text{Na}(\text{THF})_6]^+[\text{Zn}(\text{tBu})_2(\text{DPA})\text{Zn}(\text{tBu})_2]^-$ described by Mulvey *et al.*¹⁴⁰ In

the former structure one DPA bridges syn/syn between the two Na atoms and another anti/anti with N_{amido} bridging the Na atoms and the pyridyl N atoms coordinating to Zn (Figure 1.29, left). In the latter SSIP, a single unit of DPA is inserted between two Zn centres in an anti/anti conformation (Figure 1.29, right).

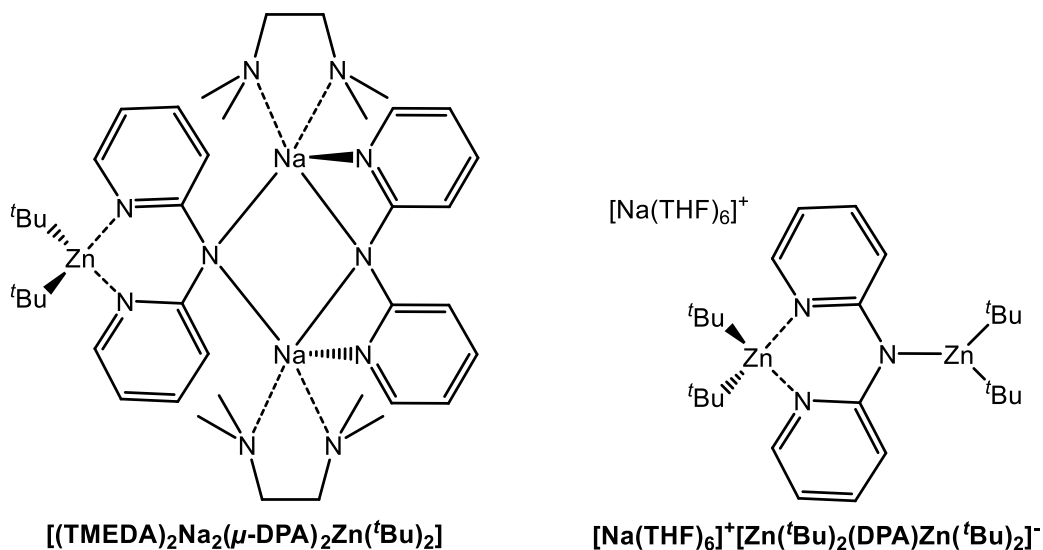


Figure 1.29 – Structures of DPA sodium zincates.¹⁴⁰

1.1.4.1 Magnetometry Studies of Fe and Ferrate DPA Complexes

The electronic structures of the Fe(II) centres in complexes **9** and **11** were studied through bulk magnetisation measurements (SQUID) and EPR spectroscopy (**9** only). Thus, molar paramagnetic susceptibility (χ_M) data was collected on microcrystalline samples in the warming mode from 2 to 300 K, under a constant magnetic field of 0.5 T. Additionally, this study was complemented with magnetisation measurements at 2 K under variable magnetic field (0 to 5 T). Resulting $\chi_M T$ vs T and $M/N\mu_B$ vs H curves and their best fits are represented in Figure 1.30 and Figure 1.32. Variable temperature X-Band EPR spectra (9.418 GHz) of a powder sample of complex **9** were recorded in the temperature range between 4 K and 50 K and the obtained results are shown in Figure 1.31.

A magnetic study of **9** reveals the existence of ferromagnetic interactions between two Fe(II) centres in the structure (Figure 1.30).

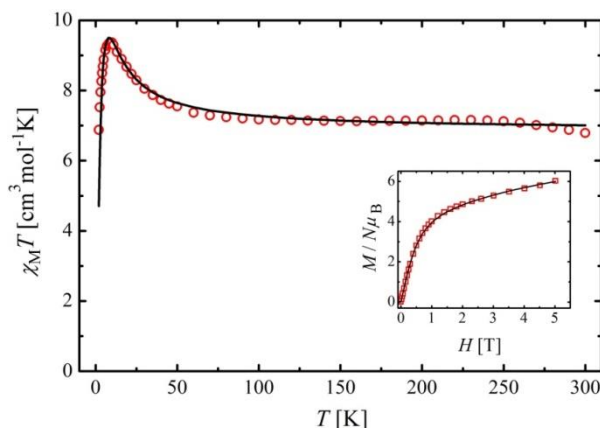


Figure 1.30 – $\chi_M T$ vs T and $M/N\mu_B$ vs H (inset) curves of compound **9**. Measurement setup: warming mode (2→300 K), $B = 0.5$ T; $T_{\text{mag}} = 2$ K. Solid line represents the result of the best fit.

At ambient temperature (300 K), the value of $\chi_M T$ product of $6.79 \text{ cm}^3 \text{ K mol}^{-1}$ is higher than expected for two non-interacting high-spin ($S = 2$) iron(II) centres (expected value is $6.00 \text{ cm}^3 \text{ K mol}^{-1}$ taking into account $g = 2.0$). The estimated g factor for the ambient temperature data of 2.13 (Curie Law) reveals the existence of unquenched angular momentum coupled to the electronic spin. Upon lowering the temperature from 300 K to 250 K, a steady increase of $\chi_M T$ takes place (from 6.79 at 300 K to $7.12 \text{ cm}^3 \text{ K mol}^{-1}$ at 250 K), which is attributed to a small decomposition of the sample upon warming. Below 250 K, the $\chi_M T$ product is slowly increasing until 50 K (slightly negative linear slope up to $7.55 \text{ cm}^3 \text{ K mol}^{-1}$) followed by a sharp increase with a $\chi_M T$ maximum at 9 K ($9.37 \text{ cm}^3 \text{ K mol}^{-1}$). An abrupt decrease is observed in the lowest temperature range ending at $\chi_M T$ value of $6.88 \text{ cm}^3 \text{ K mol}^{-1}$ at 2 K. The latter can be attributed to the effects of the zero-field splitting (ZFS). Moreover, the ZFS effects are clearly visible from the $M/N\mu_B$ vs H curve which fails to reach saturation even at the highest magnetic field (measured $6.02 \mu_B$ at 5 T; expected $8 \mu_B$ for $g = 2.0$ and $S = 4$ or two $S = 2$).

Simultaneous fit of the experimental data ($\chi_M T$ vs T and $M/N\mu_B$ vs H) was completed using the program PHI¹⁴⁸ by matrix diagonalisation of the (perturbative) anisotropic spin Hamiltonian defined in Equation (1.1):

$$\hat{H} = D \sum_i (\hat{S}_{iz}^2 - \frac{1}{3} \hat{S}_i^2) + E \sum_i (\hat{S}_{ix}^2 - \hat{S}_{iy}^2) + g\mu_B B \sum_i \hat{S}_i - 2J(\hat{S}_1 \hat{S}_2) \quad (1.1)$$

where J is the exchange constant, \hat{S}_i ($i = 1, 2$) is the total spin operator of the individual Fe(II) ions (\hat{S}_{ij} ($j = x, y, z$) are the operators of its components), B is the magnetic induction, μ_B is the Bohr magneton while D and E stand for axial and rhombic ZFS parameters, respectively. In order to avoid the overparameterisation of the spin Hamiltonian, the isotropic g factor was fixed at 2.14. The best set of parameters for two high-spin ($S = 2$) Fe(II) ions includes the exchange constant $J = 1.01 \text{ cm}^{-1}$, ZFS components $D = 7.31 \text{ cm}^{-1}$ and $|E| = 1.36 \text{ cm}^{-1}$ as well as the small intermolecular interaction $zJ = 0.02 \text{ cm}^{-1}$. Taking into account the reported negative values of ZFS parameter D for other trigonal-pyramidal iron(II) molecular magnets,^{149,150} a second set of parameters was obtained with $J = 0.93 \text{ cm}^{-1}$ and ZFS components $D = -5.59 \text{ cm}^{-1}$ and $|E| = 1.45 \text{ cm}^{-1}$ which presented slightly higher deviations from the experimental data at low temperature. In both cases, large values of the rhombic ZFS parameter E reflect directly significant distortions of the basal FeN_3 plane from the ideal three-fold symmetry. Furthermore, the possible change in sign of D can be rationalised with the position of apical $-N$ donor atom. In the structure of **9**, the axial pyridine ligand completely breaks the symmetry of the coordination environment around Fe(II), differing significantly from the regular trigonal-pyramidal systems reported by Long *et al.* where all N–Fe–N angles between the apical and equatorial bonds are almost identical.^{149,150} Consequently, the asymmetric ligand field in **9** breaks the degeneracy of d_{xz} and d_{yz} levels and affects the orbital angular momentum of the system, hence its anisotropy.

The short intramolecular Fe(II) distance (3.3611(6) Å) justifies the existence of the magnetic exchange between two spin carriers while the bridging geometry of two dipyridylamine ligands supports its ferromagnetic nature. The most appropriate pathway for the exchange involves the spin polarization mechanism, by which the electronic cloud of species linking paramagnetic centres (N–C–N bridges of DPA ligands) is polarised by the spin of the latter (Fe(II) centres). In addition, this conclusion is supported by the small value of J (1.01 cm^{-1}). The unusual ligating motif from the structure of **9** was also reported for the compound $[\{\text{Fe}(\text{Mes})(\text{DPA})\}_2]$.¹⁴² Although no magnetic studies were undertaken, the DFT calculations confirmed the high-spin configurations and the local spin densities of 3.62 at the iron(II) centres ($S = 4$ ground state).¹⁴²

Variable temperature EPR spectra (Figure 1.31) mirror remarkably well the magnetic behaviour of **9** observed from SQUID measurements and confirms the oxidation state of +2 for the iron centres. The latter is obvious from the fact that the sample is EPR silent above 40 K. Upon further cooling down to 4 K, one resonance starts to appear in the low-field region

(g value of 12.93) with increasing intensity. The observed spectral feature is related with $S = 4$ state of the Fe(II) dimer where a forbidden transition occurs between levels $M_S = 4$ and $M_S = -4$ ($\Delta M_S = 8$) which are split in zero magnetic field by $\sim E^2/D$.¹⁵¹

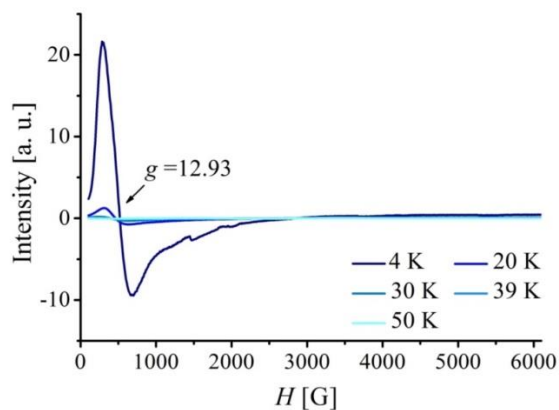


Figure 1.31 – Variable temperature (4-50 K) X-band EPR spectra ($f = 9.418$ GHz) of a powdered sample of complex **9**.

Compound **11** displays the typical magnetic behaviour expected for an isolated high-spin ($S = 2$) iron(II) centre by following the Curie Law in the high temperature region and by exhibiting some anisotropy which governs the low temperature behaviour (Figure 1.32).

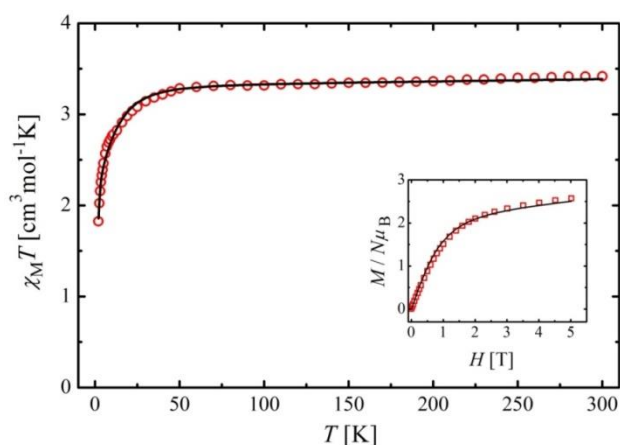


Figure 1.32 – $\chi_M T$ vs T and $M/N\mu_B$ vs H (inset) curves of compound **11**. Measurement setup: warming mode ($2 \rightarrow 300$ K), $B = 0.5$ T; $T_{\text{mag}} = 2$ K. Solid line represents the result of the fit.

At ambient temperature (300 K), the value of $\chi_M T$ product is $3.417 \text{ cm}^3 \text{ K mol}^{-1}$ which is higher than expected for an isolated high-spin ($S = 2$) iron(II) centre (expected value is $3.00 \text{ cm}^3 \text{ K mol}^{-1}$ taking into account $g = 2.0$). The estimated g factor from the Curie Law is $g = 2.13$ suggesting the presence of unquenched angular momentum coupled to the electronic

spin. Upon lowering the temperature, the $\chi_M T$ product is slowly decreasing between 300 K ($3.417 \text{ cm}^3 \text{ K mol}^{-1}$) and 45 K ($3.251 \text{ cm}^3 \text{ K mol}^{-1}$). The positive slope of the curve is a manifestation of temperature independent paramagnetism (TIP) with an estimated value of $250 \times 10^{-6} \text{ cm}^3 \text{ mol}^{-1}$. Below 45 K, the $\chi_M T$ product starts to decline abruptly ending at $1.825 \text{ cm}^3 \text{ K mol}^{-1}$ at 2 K. The low-temperature behaviour displayed could be ascribed to the effects of the zero-field splitting, weak antiferromagnetic interactions between the molecules or combination of both. However, the variable field magnetisation measurements at 2 K confirm undoubtedly the largest contribution of the ZFS effects since the $M/N\mu_B$ vs H curve stays far from saturation even at the highest magnetic field (measured $2.57 \mu_B$ at 5 T; expected $4 \mu_B$ for $g = 2$ and $S = 2$). The experimental data were fit using the program PHI¹⁴⁸ by matrix diagonalisation of the (perturbative) anisotropic spin Hamiltonian defined in Equation (1.2):

$$\hat{H} = D \left(\hat{S}_z^2 - \frac{1}{3} \hat{S}^2 \right) + E \left(\hat{S}_x^2 - \hat{S}_y^2 \right) + \mu_B \hat{S} g B \quad (1.2)$$

In this equation, D and E stand for axial and rhombic ZFS parameters, respectively, \hat{S} is the total spin operator of the Fe(II) ion and \hat{S}_i ($i = x, y, z$) are the operators of its components. B is the magnetic induction and μ_B is the Bohr magneton. The best fit of the experimental data was with a fixed isotropic g factor at 2.10 and with correction for TIP of $250 \times 10^{-6} \text{ cm}^3 \text{ mol}^{-1}$ yielded the ZFS parameters $D = -10.48 \text{ cm}^{-1}$ and $E = -0.79 \text{ cm}^{-1}$ as well as weak intermolecular interaction $zJ = 0.01 \text{ cm}^{-1}$ (Figure 1.32). A survey of fits employing positive D values could not reproduce the low-temperature behaviour well without forcing the excessively high E/D ratios (0.47-0.50).

The obtained results demonstrate that the iron(II) centre stays trapped in the high-spin state and does not exhibit thermally induced spin-crossover behaviour, thus confirming the findings from the crystal structure (Fe–N bond lengths at 123 K $> 2.1 \text{ \AA}$). Although the $-N_6$ coordination environment around the metal centre is appropriate for appearance of switching phenomena, large distortions from ideal octahedral geometry, imposed by the restricted bite angles of chelating ligands, generate a high barrier for the possible transition to the singlet state.¹⁵² Evaluation of the local distortion around the octahedral Fe(II) ion in the structure of **11** through the parameters Σ and Θ gave the respective values of $142.4(5)^\circ$ and $503.7(10)^\circ$ which fall into the reported ranges for predominately high-spin states.^{153–156} These findings are also consistent with the reported magnetic data for other compounds with identical coordination geometry.^{157,158}

1.2 Conclusions

An exploration into the structural variations of HMDS-based sodium ferrates has been undertaken uncovering a family of contacted ion-pair and solvent separated ion-pair structures utilising mono-, di- and polydentate Lewis basic donors. Furthermore, heterocyclic amide 2,2'-dipyridylamine has successfully been introduced into monometallic (Fe) HMDS and sodium ferrate scaffolds. In the majority of cases, Fe shows a preference to attain a trigonal planar geometry with the HMDS amido ligands; these strong Fe-N σ -sigma bonds *anchoring* the structure and showing little difference in bond lengths between structures. Na achieves coordinative stabilisation via *ancillary* bonding. With no donor or monodentate Lewis donors present, contacted ion-pair structures were obtained whilst when Lewis donor molecules of higher denticity were present, solvent separated ion-pair structures were found. Within CIP structures **1-4**, **10** and **11**, Na engages with two amido groups, forming additional bonds with either monodentate Lewis donors, supplementary amino N atoms (e.g. pyridyl N's), HMDS methyl groups, or a combination thereof. In SSIP complexes **5-8**, Na is abstracted from the Fe centre and coordinatively satisfied by the neutral N atoms.

The combination of trigonal planar geometry and weak field amido ligands preserve the high spin ($S = 2$) state of Fe(II) from its [$\{\text{Fe}(\text{HMDS})_2\}_2$] precursor. Further characterisation by NMR spectroscopy has enabled the acquisition of good quality ^1H (and in some cases $^{13}\text{C}\{^1\text{H}\}$) NMR spectra), which are lacking in the current literature, concerning ferrate species. This has allowed us to identify certain spectroscopic features exhibited by the described complexes upon where certain signals appear, beneficial for interpreting spectra of further (and more complicated) ferrate species.

With good fundamental grounding on the constitution of these heterobimetallic sodium ferrate reagents, we look towards further exploring their reactivity through metallation chemistry and as candidates for selective bases like their successful Na/Mg and Na/Zn congeners before them. Especially encouraging is that in currently unpublished research⁷⁸ within the group it has been found that related and structurally characterised HMDS-based lithium ferrates can catalytically facilitate the cross coupling of unactivated arenes with aryl halides.⁷⁷ Studies included in this chapter provide new insights into the possible identity of the active species involved in this type of iron-catalysed cross-coupling process.

Chapter 2 – N-Heterocyclic Carbene Stabilised Sodium Ferrates: Structural, Synthetic and Magnetic Studies

2.1 Introduction to N-Heterocyclic Carbenes: Normal, Abnormal and Anionic

Since Arduengo's seminal report on the isolation of the first stable N-heterocyclic carbene (NHC),¹⁵⁹ an enormous amount of research activity has been devoted to advancing the chemistry of these seminal ligands, leading to important breakthroughs in synthesis and catalysis. The remarkable stability of NHCs as well as the fine control of their steric and electronic properties, by modifying their substituents on the imidazole backbone and/or on the N atoms,¹⁶⁰ have been key in many of these advances,^{161,162} focusing primarily on the synthesis of transition metal complexes and their applications as catalysts.^{163–165}

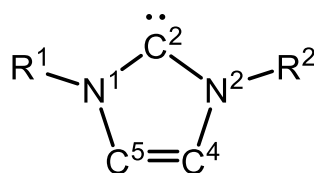


Figure 2.1 – Typical molecular framework of an unsaturated NHC. The above notation shall be used throughout this chapter where C2 constitutes the ‘normal’ position and C4 constitutes the ‘abnormal’ position (essentially interchangeable with C5).

Typically, the carbenic functionality on an NHC is located at its C2 position (Figure 2.1), being stabilised by the combination of π -donation of the adjacent N lone pairs into the empty p_{π} orbital of the carbene, along with steric stabilisation from the commonly bulky substituents on the N atoms.¹⁶⁶ Notwithstanding, in some special cases the carbenic carbon can be located at the *abnormal* C4 position (Figure 2.2, centre), being then only stabilised by only one N atom. This special family of NHCs are termed ‘*abnormal*’ (*a*NHCs) or mesoionic NHCs.^{167–169} Although these ligands are much more unstable than their ‘*normal*’ analogues, with the only examples of free *a*NHCs being isolated by blocking their C2 and C5 positions in the imidazole ring,¹⁷⁰ several studies have shown these type of NHCs tend to bind more strongly to metallic fragments as evidenced by the shorter M-C bond distances.^{171–174} Although in some cases it can be difficult to distinguish between steric and electronic effects, this has been

attributed to a combination of the relief in the steric congestion around the metal centre as well as an increase in the σ -donor ability of the carbene ligand.^{175,176}

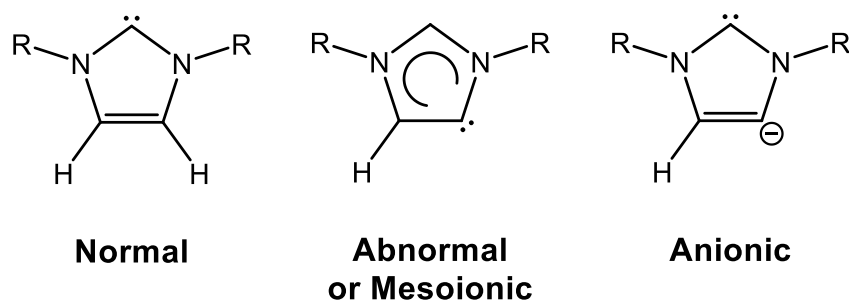
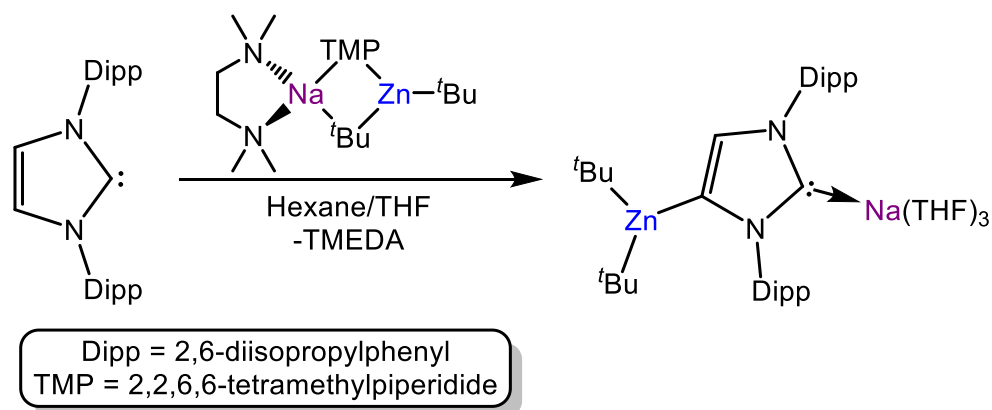


Figure 2.2 - Types of N-heterocyclic carbenes: *normal*, *abnormal* or mesoionic and anionic.

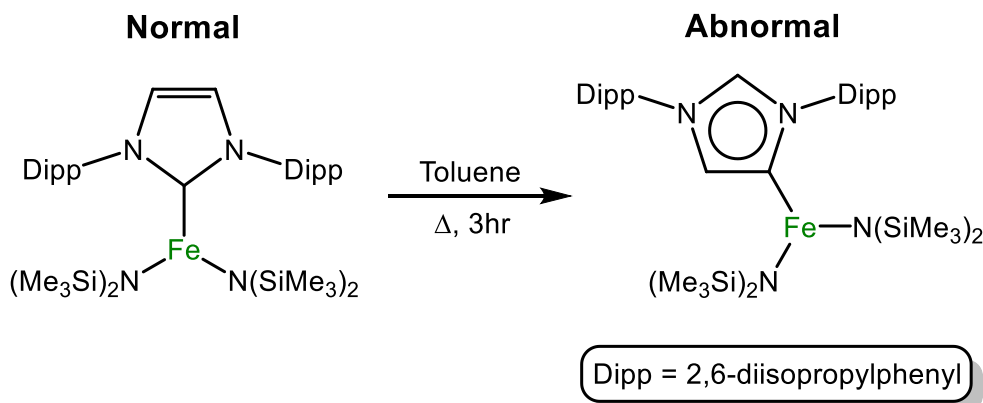
Most of the synthetic protocols granting access to *abnormal* carbene complexes involve the use of chelating NHC ligands with their C2 position blocked by an aryl group.^{177–179} Recent studies on three-coordinate iron and cobalt NHC complexes have revealed that it is possible to thermally induce the rearrangement of the relevant *normal* NHC complexes into their *abnormal* isomers.^{180,181} These findings suggest that the *abnormal* bonding in these complexes may be thermodynamically controlled.

Within main-group chemistry, Robinson has shown an elegant approach to access *abnormal* boron-NHC complexes, where firstly the unsaturated carbene IPr (1,3-bis-(2,6-diisopropylphenyl)imidazol-2-ylidene) is deprotonated at its C4 position by ⁿBuLi, followed by addition of BEt₃, forming an anionic NHC complex (Figure 2.2, right), where Li is attached to the *normal* C2 position of the carbene whereas B binds to the C4 position of the imidazole ring.¹⁸² Protonation of this compound using HCl·NEt₃ led to formation of the relevant *a*NHC-BEt₃ adduct, with subsequent elimination of LiCl.¹⁸³ This synthetic route employing an anionic carbene as a precursor for an *abnormal* main-group-NHC complex has also been demonstrated for lithium zincate reagents.¹⁸⁴ Related to these findings, our group has shown that using cooperative bimetallic systems,^{1,8,27} in particular sodium zincates, it is possible to prepare anionic NHC ligands via direct Zn-H exchange reactions (Scheme 2.1) which can subsequently undergo transmetalation to transition metal complexes such as [ClAu(PPh₃)] disclosing a new route to prepare transition metal complexes containing these anionic ligands.¹⁸⁵

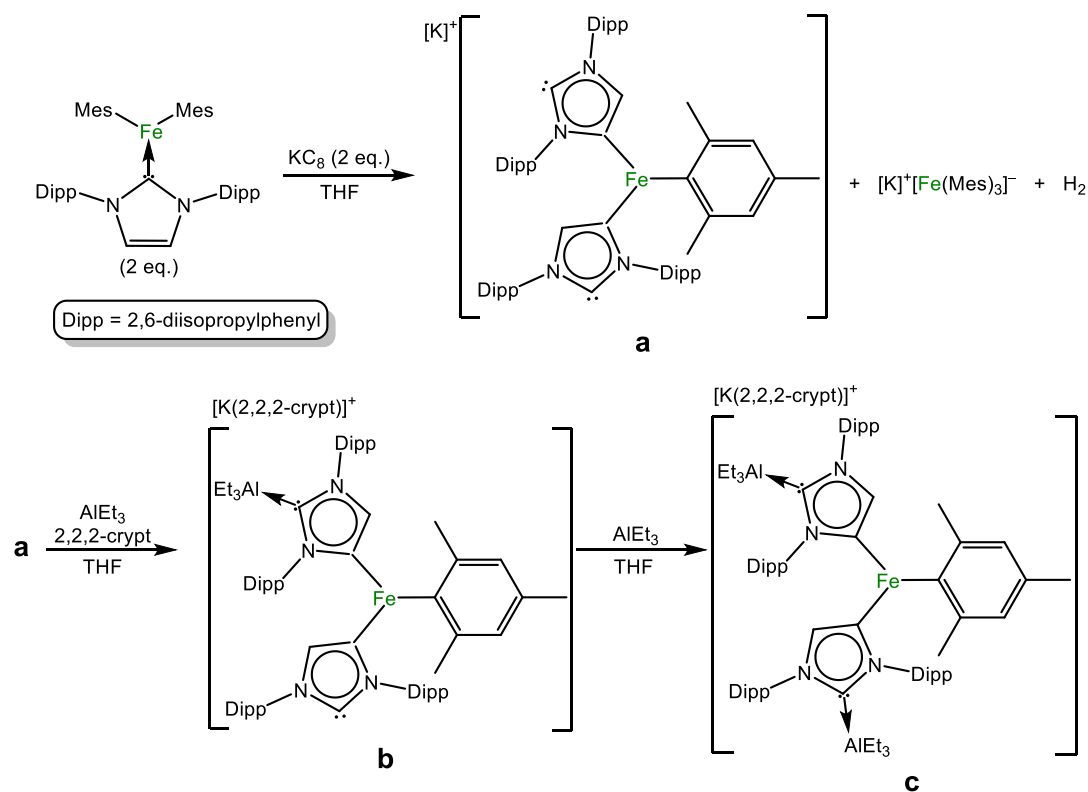
Scheme 2.1 – Direct zincation of IPr by a bimetallic sodium zincate generating an anionic NHC.¹⁸⁵

2.2 Iron N-Heterocyclic Carbene Complexes

Iron NHC complexes have garnered considerable interest lately with examples of tris-, bis- and mono-dentate complexes; some finding applications in homogeneous catalysis and bio-mimetic chemistry.^{186,187} Monodentate three-coordinate Fe-NHCs are currently rare. Deng *et al.* produced the first example in 2011, [(ⁱPrMe₂)Fe(Mes)₂],¹⁸⁸ closely followed by the synthesis [(IPr)Fe(HMDS)₂]¹⁸⁹ from Layfield and co-workers. Further to this, Layfield recently reported on the thermal isomerisation of this complex to the *abnormal* carbene isomer [(*a*IPr)Fe(HMDS)₂] upon refluxing in toluene for 3 hours (Scheme 2.2).¹⁸⁰ With this discovery of thermal isomerisation from the *normal* to *abnormal* NHC complex it is within the realm of possibility that Fe-NHC catalysts^{186,187} could isomerise, with the *abnormal* isomer as the active species in high temperature reactions, especially when one considers homogeneous catalytic reactions involving *in situ* carbene generation where structural evidence is not provided.¹⁶⁷

Scheme 2.2 - Normal to abnormal Fe-NHC thermal isomerisation.¹⁸⁰

Goicoechea *et al.* have synthesised and characterised the potassium salt of an Fe(II) anionic carbene complex (where the Fe centre is bound to the *abnormal* C4 positions of IPr), $[\text{K}]^+[(\text{IPr})_2\text{FeMes}]^-$ (**a**); the product of a disproportionation reaction between $[(\text{IPr})\text{Fe}(\text{Mes})_2]$ and two equivalents of potassium graphite which also yields $[\text{K}]^+[\text{Fe}(\text{Mes})_3]^-$ and H_2 (Scheme 2.3, top). Compound **a** undergoes further coordination with Lewis acidic AlEt_3 at the NHCs' C2 positions (**b** and **c**, Scheme 2.3, bottom).¹⁹⁰ Currently, to the best of our knowledge, only two other publications detail structures of Fe-*a*NHCs. Danopoulos *et al.* in 2004 used the pincer ligand 2,6-bis(imidazolylidene)pyridine to coordinate an Fe centre where they found one of the four chelating NHCs was bound abnormally from the C4 position.¹⁹¹ Grubbs *et al.* have disclosed the preparation of the diiron species $[(a\text{NHC})\text{Fe}_2(\text{COT})_2]$ (*a*NHC = 1,3-bis(2,6-diisopropylphenyl)-2,5-diphenyl-imidazol-4-ylidene, COT = 1,3,5,7-cyclo-octatetraene).¹⁹²

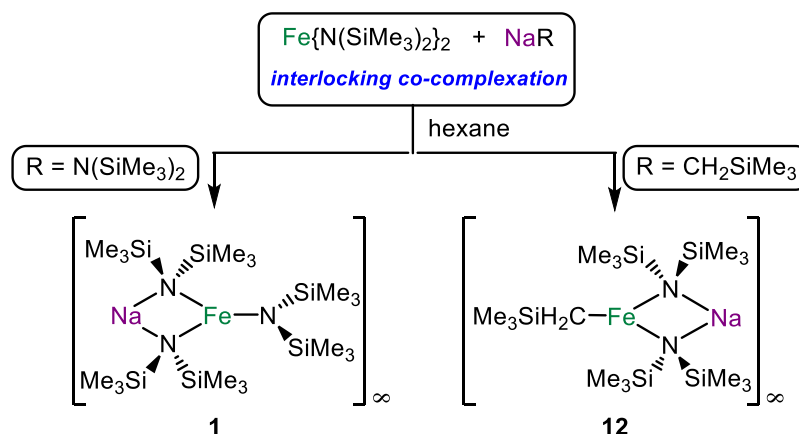


Scheme 2.3 - Synthesis of anionic NHC-Fe complex **a** and subsequent additions of triethyl aluminium to yield products **b** and **c**.

Inspired by these recent breakthroughs in iron NHC chemistry, which include novel coordination chemistry and catalytic applications,^{186,187} here we detail our findings on the synthesis of sodium ferrate complexes containing N-heterocyclic carbenes, using IPr as a case study, as well as assessing the potential of these complexes to act as precursors of *a*NHC-Fe complexes.

2.3 Results and Discussion¹⁹³

2.3.1 $[\{\text{NaFe}(\text{HMDS})_2(\text{CH}_2\text{SiMe}_3)\}_\infty]$: A Mixed Amido/Alkyl Sodium Ferrate



Scheme 2.4 - Synthesis of donor-solvent-free sodium ferrates **1** and **12**.

Following the same strategy used for the synthesis of $[\{\text{NaFe}(\text{HMDS})_3\}_\infty]$ (**1**), by assessing the co-complexation of sodium alkyl $\text{NaCH}_2\text{SiMe}_3$ and $\text{Fe}(\text{HMDS})_2$ in hexane at 0°C we attempted the synthesis of a heteroleptic sodium alkyl-bis(amido) ferrate (Scheme 2.4, right).

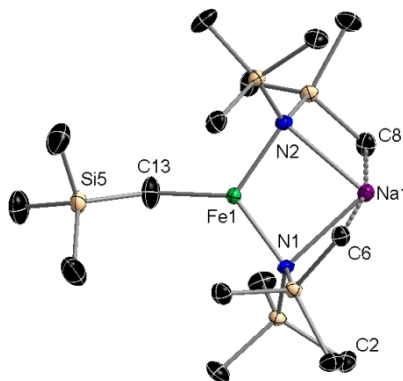


Figure 2.3 - Asymmetric unit of $[\{\text{NaFe}(\text{HMDS})_2(\text{CH}_2\text{SiMe}_3)\}_\infty]$ (**12**). Hydrogen atoms omitted for clarity.

Thermal ellipsoids displayed at 50% probability level. Selected bond distances (Å) and angles ($^\circ$): Fe1-N1 2.0308(17), Fe1-N2 2.0306(17), Fe1-C13 2.051(2), Fe1---Na1 3.0401(9), Na-N1 2.4804(19), Na-N2 2.4702(19), Na1-C6 2.7013(21), Na1-C8 2.7275(21); N1-Fe1-N2 107.96(7), N1-Fe1-C13 129.08(10), N2-Fe1-C13 121.83(10), Na-N1-Fe1 84.11, Na1-N2-Fe1 84.38, Na1---Fe1-C13 165.55(7), N1-Na1-N2 83.14(6).

Pleasingly $[\{\text{NaFe}(\text{HMDS})_2(\text{CH}_2\text{SiMe}_3)\}_\infty]$ (**12**) was isolated as blue/green block-like crystals in a 73% yield and its structure established by X-ray crystallography (Figure 2.3). Sharing some structural features with **1**, complex **12** contains a planar four-membered $\{\text{NaNFeN}\}$

central core where both metals are connected by two HMDS bridges. Coordinatively unsaturated within the asymmetric unit, solvent and donor-free Na attains a higher coordination number by forming intermolecular interactions with the HMDS groups of adjacent molecular units (via Na---Me long distance electrostatic contacts, Na1(1)---C2 2.838(4) Å; Na1(1)---C12(2) 3.041(2) Å), which affords a 1D ‘zigzag’ polymeric chain structure (Figure 2.4); a head-to-head arrangement contrasting with **1**’s head-to-tail polymeric arrangement. Additionally, the sodium cation also exhibits electrostatic contacts to HMDS methyl groups within the monomeric unit (Na1-C6 2.7013(21) Å; Na1-C8 2.7275(21) Å). The alkyl groups reside in terminal positions, running along opposite edges of the polymeric chain in a staggered fashion, with a Fe1-C13 bond length of 2.051(2) Å. The main geometrical parameters within the dinuclear {NaNFeN} ring show little variation to those discussed for **1**, the internal N1-Fe1-N2 angle is slightly contracted to 107.96(10)° (*cf.* 110.48(10)° for **1**) and sum of angles around Fe are 358.87° (range 107.96(10)° to 129.08(10)°).

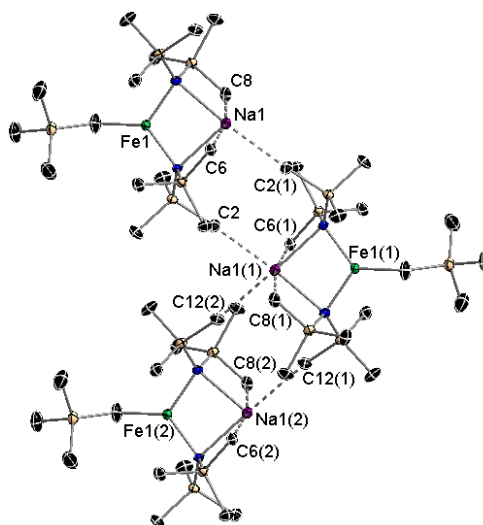


Figure 2.4 - Section of polymeric chain showing intermolecular and intramolecular Na---Me contacts: Na1(1)---C2 2.838(4) Å, Na1(1)---C12(2) 3.041(2) Å.

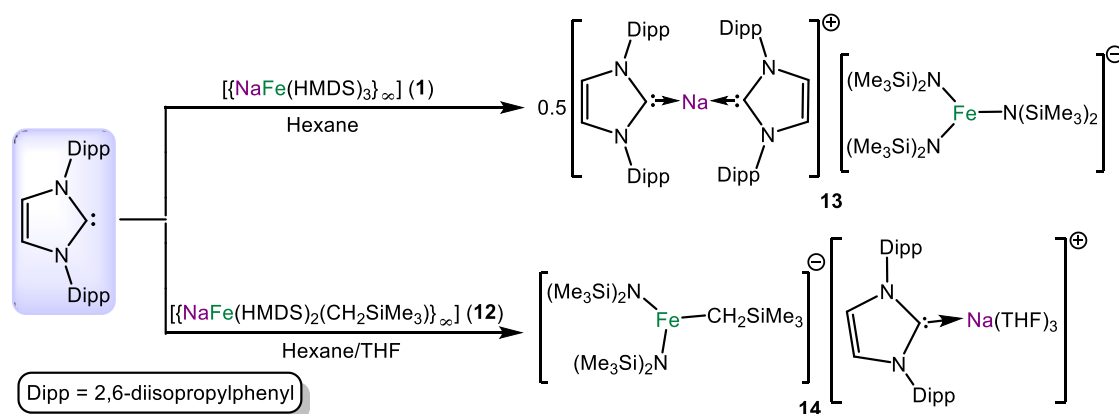
Illustrating the structural similarities of Mn(II) and Fe(II) in heterobimetallic chemistry, this motif is almost identical to that described by Mulvey and Klett for $[\{\text{NaMn}(\text{HMDS})_2(\text{CH}_2\text{SiMe}_3)\}_\infty]$.¹⁹⁴ The propagation mode in **12**, exclusively involving Na---Me bonds, however contrasts with that found in the related magnesiate $[\{\text{NaMg}(\text{HMDS})_2(^n\text{Bu})\}_\infty]$, which polymerises via the anionic C of the butyl group giving rise to a linear chain.¹⁹⁵

Like **1**, complex **12** displays good solubility in C_6D_6 , suggesting that its polymeric structure observed in the solid state is not retained in solution. The 1H NMR spectrum for **12** shows a very broad upfield resonance for the HMDS H atoms at -8.57 ppm (*cf.* -4.72 ppm for **1**) whilst the broad resonance for monosilyl group methyl H atoms appears downfield at 13.51 ppm. No resonance is observed for the CH_2 H atoms of the C directly attached to the paramagnetic Fe(II) centre, conceivably it may be hidden beneath one of the two signals or broadened to a degree that it is lost within the baseline.

2.3.2 Reactivity Studies with IPr

The reactivity of novel donor-free and solvent-free sodium ferrates **1** and **12** towards N-heterocyclic carbene IPr was investigated. The unsaturated N-heterocyclic carbene IPr was first synthesised by Arduengo and co-workers and has become ubiquitous in modern NHC chemistry thus it was chosen as a model substrate.¹⁹⁶

Treating hexane solutions of both bimetallic compounds with equimolar quantities of IPr led to significant colour changes (from green to light brown) and the formation of insoluble products. Addition of fluorobenzene in the case of **1** and THF for **12** afforded crystals of the NHC-stabilised sodium ferrates $[Na(IPr)_2]^+[Fe(HMDS)_3]^-$ (**13**) and $[(THF)_3 \cdot NaIPr]^+[Fe(HMDS)_2(CH_2SiMe_3)]^-$ (**14**) in 35 and 70% yields, respectively (note that the yield of **13** can rise to 73% with two equivalents of IPr according to its rational stoichiometry) (Scheme 2.5).



Scheme 2.5 - Synthesis of NHC-stabilised sodium ferrates **13** and **14**.

X-ray crystallographic studies established the molecular structures of **13** and **14**. In both cases the infinite polymeric arrangements of sodium ferrates **1** or **12** have deaggregated to form discrete monomeric donor-separated ion-pair structures where the NHC ligands act as neutral lone-pair donors stabilising the alkali metal (Figure 2.5 and Figure 2.6). The molecular structure of **13** comprises a cationic moiety where the Na centre is solvated by two neutral IPr ligands in a near-linear disposition ($C1-Na1-C29$ $168.95(17)^\circ$) and the same anionic ferrate moiety, featuring a strictly planar tri-coordinate Fe(II) centre (sum of N-Fe-N angles = 360°), that was observed for complexes **5**, **7** and **8**. Interestingly, the structure of **13** bears a strong resemblance to the sodium magnesiate $[Na(IPr)_2]^+[Mg(HMDS)_3]^-$ reported by Hill,¹⁹⁷ which contains the same cationic moiety, with the Na and Mg centres exhibiting almost identical coordination environments to those described above for Na and Fe, respectively in **13**.

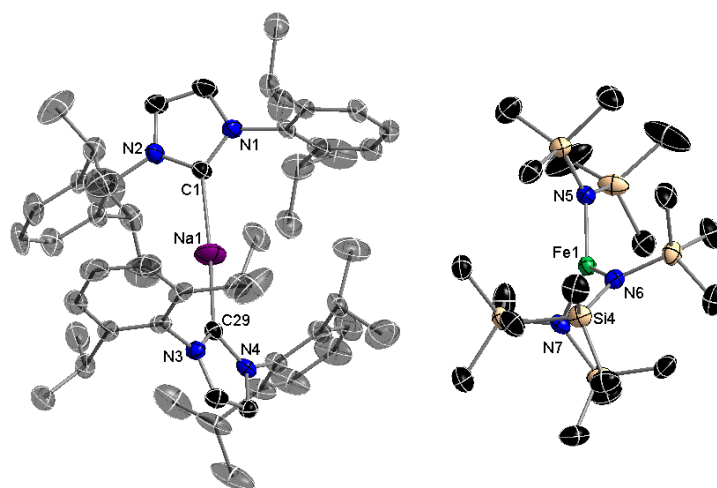


Figure 2.5 - X-ray crystal structure of compound **13**. Hydrogen atoms and disorder components in isopropyl groups omitted for clarity. Thermal ellipsoids displayed at 50% probability level. Selected bond distances (Å) and angles ($^\circ$): Fe1-N5 1.996(3), Fe1-N6 1.993(3), Fe1-N7 1.990(3), Na1-C1 2.445(4), Na1-C29 2.460(4), C1-N1 1.360(5), C1-N2 1.362(5), C29-N3 1.363(5), C29-N4 1.362(5); N5-Fe1-N6 121.15(13), N5-Fe1-N7 119.66(13), N6-Fe1-N7 119.20(13), C1-Na1-C29 168.95(17), Na1-C1-N1 137.4(3), Na1-C1-N2 120.2(3), N1-C1-N2 102.3(3), Na1-C29-N3 142.9(3), Na1-C29-N4 114.7(3), N3-C29-N4 102.3(3).

Diverging from **13**, the Na centre in **14** binds to only one IPr ligand but completes a distorted tetrahedral geometry by coordinating three molecules of the donor solvent THF (average angle around Na, 108.7° , values ranging from $89.5(6)$ to $126.5(6)^\circ$). Although the structure of this cation is not known the coordination around Na is almost identical to that described in the sodium zincate $[(THF)_3Na][C\{[N(2,6-*i*Pr_2C_6H_3)]_2CHCZn(*t*Bu_2)\}]$, which contains an anionic version of the NHC ligand IPr¹⁸⁵ coordinating to a $\{Na(THF)_3\}$ cation via its C2 position

forming a Na-C bond of 2.501(3) Å, of similar strength to that found in **14** (Na1-C2, 2.551(3) Å). The structure of **14** is completed by the heteroleptic ferrate anion [Fe(HMDS)₂(CH₂SiMe₃)][−], which as a consequence of its lack of interaction with the Na centre, exhibits a significantly wider N3-Fe1-N4 bond angle (123.40(10)°) and slightly shorter Fe-N bond distances (average 1.9855 Å) than those observed in the contacted ion-pair precursor **12** (107.96(7)° and 2.0307 Å).

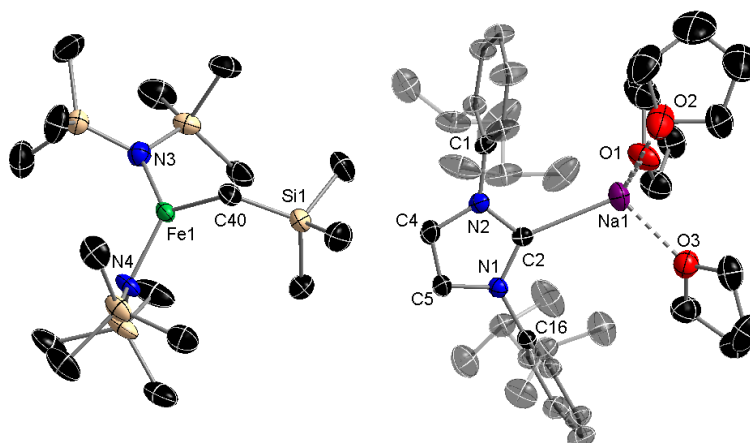


Figure 2.6 - Molecular structure of [THF₃·NaIPr]⁺[Fe(HMDS)₂(CH₂SiMe₃)][−] (**14**). Hydrogen atoms and disorder components in isopropyl, THF and SiMe₃ groups omitted for clarity. Thermal ellipsoids displayed at 50% probability level. Selected bond distances (Å) and angles (°): Fe1-N3 1.982(2), Fe1-N4 1.989(2), Fe1-C40 2.065(3), C40-Si1 1.831(3), Na1-C2 2.551(3), Na1-O1 2.348(2), Na1-O2 2.32(3), Na1-O3 2.307(2), C2-N1 1.365(3), C2-N2 1.363(3); N3-Fe1-N4 123.40(10), N3-Fe1-C40 119.56(11), N4-Fe1-C40 116.84(11), Na1-C2-N1 121.30(16), Na1-C2-N2 121.30(16), N1-C2-N2 101.9(2), C2-Na1-O1 122.69(9), C2-Na1-O2 126.5(6), C2-Na1-O3 110.69(9), O1-Na1-O2 89.5(6), O1-Na1-O3 101.60(9), O2-Na1-O3 101.3(5).

The ¹H NMR spectra of **13** and **14** in d₈-THF show a well resolved set of resonances assignable to the IPr ligands, appearing at almost the same chemical shifts as those found for the free carbene, suggesting that in this ethereal solvent the sodium centre is solvated by d₈-THF molecules rather than by the neutral sterically imposing NHC. In addition for **13**, a broad low frequency resonance is observed at −2.39 ppm, which can be assigned to the HMDS groups bound to the paramagnetic Fe(II) centre. In the case of **14** the SiMe₃ resonances appear at −3.77 and 7.80 ppm for the HMDS and monosilyl groups, respectively. The solution phase magnetic moments of **13** and **14** (4.90 and 4.40 μ_B, respectively), determined using the Evans method,^{102,103} are consistent with a high spin (*S* = 2) configuration for iron.

The formation of coordination products **13** and **14** in the reactions of sodium ferrates **1** and **12** with IPr contrasts with our previous findings using a related family of amido-based bimetallic reagents, in particular sodium zincates, which can promote the deprotonation of several unsaturated NHCs at the ‘*abnormal*’ C4 position of the imidazole ring under mild reaction conditions via a direct zincation process.¹⁸⁵ Even under harsher reaction conditions, by heating the reaction mixtures at 70°C for 12 hours, only adducts **13** and **14** were obtained.

Since using a preformed sodium ferrate does not promote the metallation of IPr, we next attempted an indirect approach, by treating the previously reported three-coordinate NHC complex [(IPr)Fe(HMDS)₂]¹⁸⁹ with either sodium reagents NaHMDS or NaCH₂SiMe₃. Interestingly these reactions also yielded only complexes **13** and **14**, respectively, revealing that under these conditions, not only do the polar sodium reagents fail to metallate IPr but also maintain the preference of the iron (II) bis(amido) fragment to coordinate to another anionic ligand (either HMDS or CH₂SiMe₃) rather than to the neutral NHC. It should be noted that similar reactivity has been found for alkylzinc and alkylgallium NHC complexes that when treated with organolithium reagents form the relevant co-complexation lithium ate species, with the NHC ligand coordinated to Li (Figure 2.7).^{185,198}

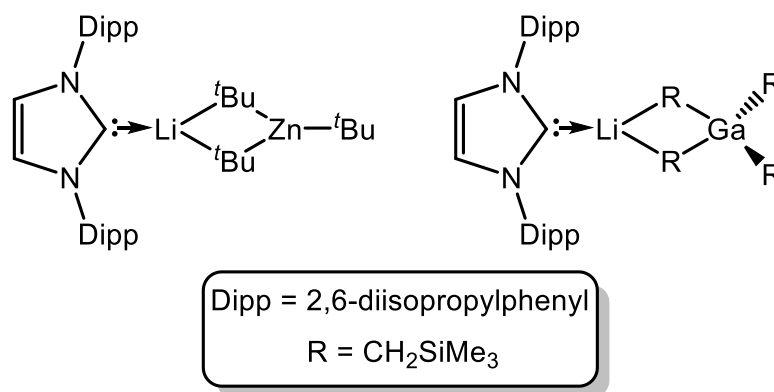
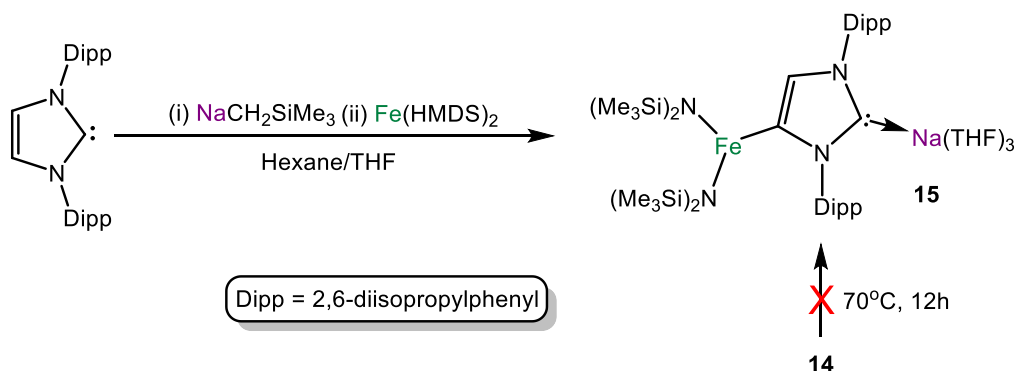


Figure 2.7 – NHC-Li alkylzinc¹⁸⁵ and alkylgallium¹⁹⁸ products.

On the other hand, contrasting with these studies, Robinson has demonstrated that when the free IPr is treated with ⁿBuLi the straightforward selective lithiation of the NHC occurs at the C4 position of the imidazole ring, affording a novel anionic carbene lithium complex.¹⁸²

Inspired by these lithiation studies, we first treated IPr in hexane with an equimolar amount of the sodium alkyl $\text{NaCH}_2\text{SiMe}_3$, leading almost instantaneously to a white solid which was subsequently reacted with one equivalent of $\text{Fe}(\text{HMDS})_2$. Introduction of THF afforded a green/brown solution which upon cooling to -30°C deposited green crystals of heteroleptic ferrate $(\text{THF})_3\cdot\text{Na}[:\text{C}\{\text{[N}(2,6\text{-}i\text{-Pr}_2\text{C}_6\text{H}_3)]_2\text{CHCFe}(\text{HMDS})_2\}]$ (**15**) in a 60% yield (Scheme 2.6).



Scheme 2.6 - Synthesis of NHC-stabilised sodium ferrate **15** via an indirect ferration approach.

X-ray crystallographic studies established the contacted ion-pair structure (shown in Figure 2.8) where the carbene has now been incorporated into the ferrate scaffold acting as an anionic ligand, coordinating through its *normal* C2 position to Na (Na1-C2 2.510(4) Å), whilst Fe occupies the position previously filled by a H atom, bonding to the C4 position (Fe1-C4 2.085(4) Å). Understandably this distance is shorter than that reported for the neutral *abnormal* complex $[(a\text{IPr})\text{Fe}(\text{HMDS})_2]^{180}$ which also displays a tri-coordinate Fe atom connected to HMDS groups at the C4 position of a neutral NHC ligand.

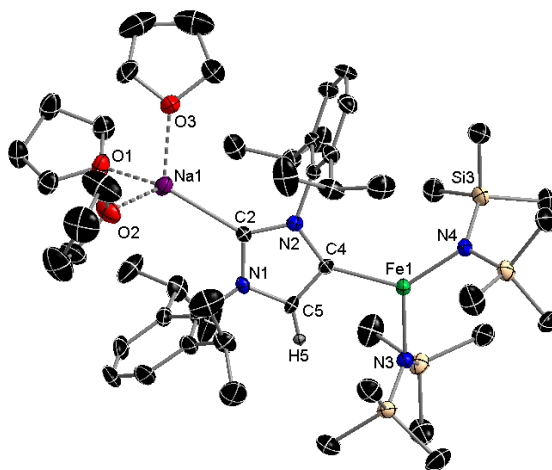
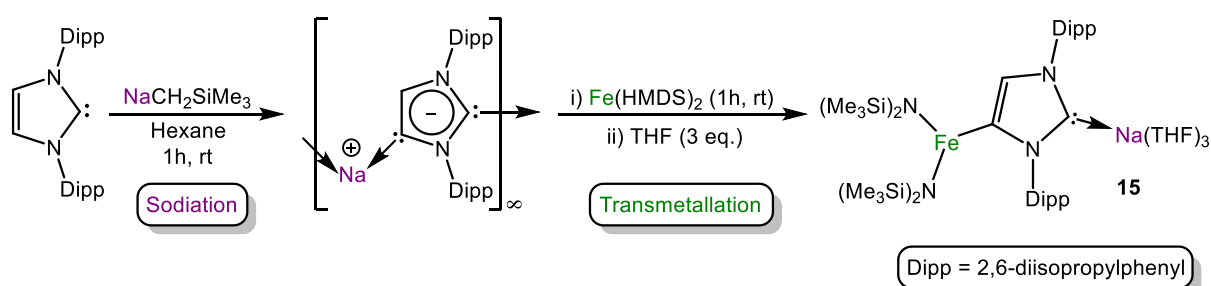


Figure 2.8 - Molecular structure of complex **15**. Hydrogen atoms (except H5) omitted for clarity. Thermal ellipsoids displayed at 50% probability level. Selected bond distances (Å) and angles (°): Fe1-C4 2.085(4), Fe1-N3 1.998(3), Fe1-N4 1.973(3), Na1-C2 2.510(4), Na1-O1 2.336(3), Na1-O2 2.313(3), Na1-O3 2.286(3), C2-N1 1.357(4), C2-N2 1.371(4); C4-Fe1-N3 105.15(14), C4-Fe1-N4 131.45(14), N3-Fe1-N4 123.39(13), Fe1-C4-N2 139.3(3), Na1-C2-N1 121.3(2), Na1-C2-N2 136.9(3), N1-C2-N2 101.7(3), C2-Na1-O1 122.76(12), C2-Na1-O2 123.23(12), C2-Na1-O3 119.00(12), O1-Na1-O2 96.46(12), O1-Na1-O3 95.16(12), O2-Na1-O3 93.05(12).

In agreement with its anionic ate constitution, its Fe-N distances (Fe1-N3 1.998(3) Å, Fe1-N4 1.973(3) Å) are similar to those found for homoleptic **13** (average Fe-N bond length 1.993 Å) and slightly elongated compared to those reported for [(*a*IPr)Fe(HMDS)₂]¹⁸⁰ (average Fe-N bond length 1.962 Å). Likening the molecular structures of **14** and **15**, it could be tempting to describe **14** as a pre-metallation complex of **15**, however it should be noted that **14** is a stable species that does not evolve to **15** even under forcing reaction conditions (70°C, 12 hours, Scheme 2.6) which makes this assumption very unlikely. This highlights the importance of the synthetic methods employed and the remarkable differences that can be realised in bimetallic chemistry by having the two metals operate either in a stepwise or synchronous manner.^{12,199}

The ¹H NMR spectrum of **15** in C₆D₆ exhibits a series of broad resonances in the range 10.59 to -6.94 ppm, including a signal at -4.21 ppm, which integrating for 36 H can be assigned to the HMDS hydrogen atoms. In addition, another broad low frequency resonance is observed at -26.37 ppm, which has been attributed to the CH fragment of the imidazolyl ring. The complexity and broadness of this NMR spectrum contrast with the well resolved and relative simplicity of the spectra recorded for **13** and **14**, where neutral IPr is not attached to a paramagnetic Fe(II) centre.

The formation of **15** can be rationalised in terms of a stepwise indirect ferration process. Initially IPr is deprotonated at its backbone C4 position by the polar organosodium reagent to form $[\text{Na}]^+[\text{IPr}]^-$, which in turn undergoes transmetalation with the more electronegative iron bis(amide). Although the white powder obtained by reacting IPr with $\text{NaCH}_2\text{SiMe}_3$ cannot be characterised spectroscopically due to its complete lack of solubility in organic solvents such as THF or toluene, the isolation of **15** provides compelling proof that the metallation of the NHC has occurred. Indeed, the sodiation of IPr has been reported when reacted with the template base $[\text{Na}_2\text{Mg}_2(\text{TMP})_6(\text{tBu})_2]$; NaTMP being identified as the likely culprit.²⁰⁰ On its own, $\text{Fe}(\text{HMDS})_2$ cannot metallate IPr but instead forms the adduct $[(\text{IPr})\text{Fe}(\text{HMDS})_2]$.¹⁸⁹



Scheme 2.7 – Stepwise mechanism for the indirect ferration of IPr; sodiation and subsequent transmetalation.

C4-deprotonation of unsaturated NHCs constitutes one of the main synthetic routes to access anionic (or ditopic) NHCs.^{172,201} To date, only four efficient metallating reagents have proved capable of selectively abstracting a H from the imidazole ring of IPr; monometallic organolithium reagents tBuLi ^{182,202} and $\text{LiCH}_2\text{SiMe}_3$ ¹⁹⁸, NaTMP ²⁰⁰ and mixed-metal system $[(\text{TMEDA})\text{NaZn}(\text{TMP})(\text{tBu})_2]$.¹⁸⁵ Additionally, Arnold *et al.* have described the isolation of a bimetallic potassium/yttrium anionic N-heterocyclic dicarbene complex resulting from the reduction of an yttrium NHC complex with potassium naphthalenide, which is formally a deprotonation product.²⁰³ Our studies show that sodium alkyl $\text{NaCH}_2\text{SiMe}_3$ can also promote the selective metallation (Na-H exchange) reaction of the imidazole ring at its C4 position.

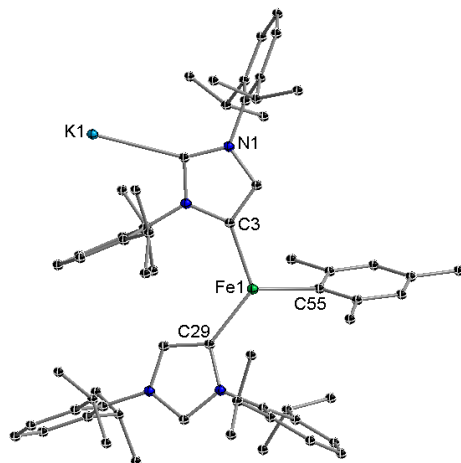
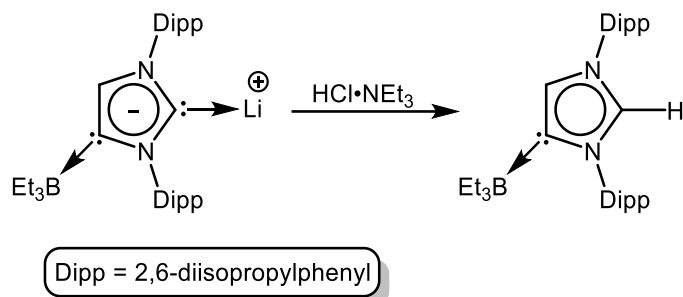


Figure 2.9 - Structure of $\text{K}[\{\text{:C}[\text{N}(2,6\text{-}i\text{Pr}_2\text{C}_6\text{H}_3)]_2(\text{CH})\text{C}\}_2\text{Fe}(\text{Mes})]$.¹⁹⁰ Hydrogen atoms omitted for clarity.

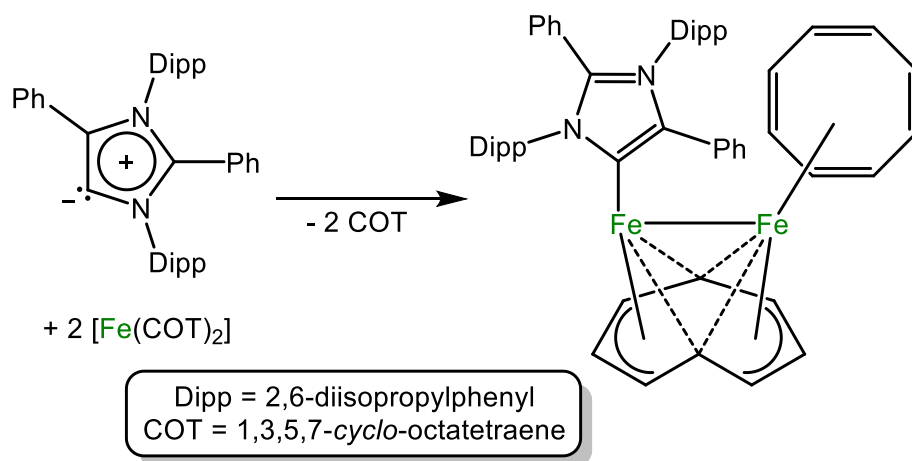
Related to the synthesis of **15**, it should be noted that Goicoechea has recently demonstrated the reduction of $[(\text{IPr})\text{Fe}(\text{Mes})_2]$ (Mes = mesityl) with potassium graphite which allows for the isolation of the iron complex $\text{K}[\{\text{:C}[\text{N}(2,6\text{-}i\text{Pr}_2\text{C}_6\text{H}_3)]_2(\text{CH})\text{C}\}_2\text{Fe}(\text{Mes})]$ (Figure 2.9).¹⁹⁰ Two anionic carbenes bind through their C4 positions to Fe at distances of 2.071(2) and 2.064(2) Å (Fe1-C3 and Fe1-C29 , respectively). These bond lengths are noticeably shorter than the Fe1-C4 bond distance of 2.085(4) Å in **15**; likely a result of sterics as the planar mesityl group is able to rotate perpendicular to the planes of the heterocyclic NHC rings whereas this cannot be achieved by the two bulky HMDS groups in complex **15**.

2.3.3 Anionic to Abnormal: An Abnormal NHC-Fe Complex via Electrophilic Interception

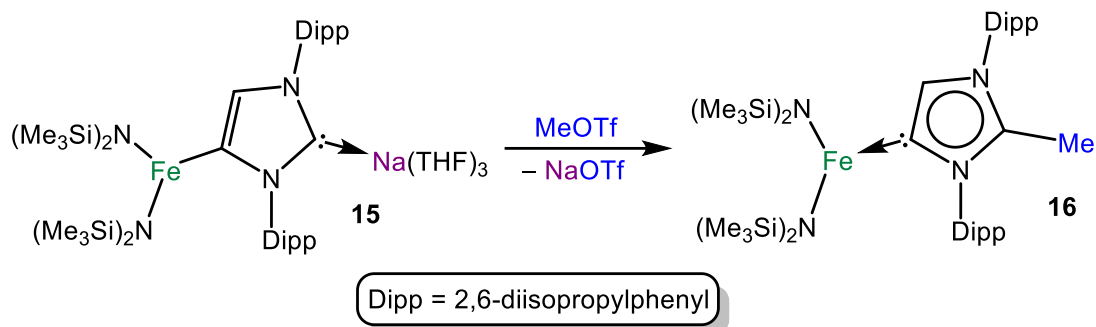
Recent studies in main-group chemistry have shown that certain anionic NHC complexes (B and Zn based) when treated with a suitable electrophile such as $\text{HCl}\cdot\text{NEt}_3$ or MeOTf can be transformed into their neutral *abnormal* adducts, where the imidazole ring of the NHC binds to the metal/main-group atom through its backbone using its C4 position (Scheme 2.8).^{183,184}

Scheme 2.8 – Electrophilic quenching of Li/B anionic NHC to furnish a boron *abnormal* NHC.¹⁸³

Although within transition metals, *abnormal* carbene complexes are more abundant than with *s*- and *p*-block elements,^{167,169,175} the number of Fe complexes containing these ligands is still limited to just a few recent examples.^{111,180,191,192} Some of these studies employ pincer ligands,¹⁹¹ whereas Grubbs has used Bertrand's isolable *abnormal* carbene (*a*NHC = 1,3-bis(2,6-diisopropylphenyl)-2,5-diphenyl-imidazol-4-ylidene)¹⁷⁰ to trap and stabilise a unique intermediate di-iron COT complex (Scheme 2.9).¹⁹² More recently, Layfield has reported a thermally induced rearrangement of [(IPr)Fe(HMDS)₂] which after 3 hours in refluxing toluene solution evolves to its *abnormal* isomer [(*a*IPr)Fe(HMDS)₂] (Scheme 2.2, *vide supra*).¹⁸⁰

Scheme 2.9 – Synthesis of a di-iron COT *a*NHC complex.¹⁹²

Intrigued by these precedents, we next pondered whether electrophilic interception of anionic NHC complex **15** could also allow access to a neutral *abnormal* Fe complex. Thus, **15** was treated with 0.9 equivalents of MeOTf at -78°C in toluene (Scheme 2.10).

Scheme 2.10 - Electrophilic interception of anionic NHC complex **15** with MeOTf.

The reaction took place with the formation of a white precipitate (presumably NaOTf) affording neutral *abnormal* Fe NHC complex $[\text{CH}_3\text{C}\{\text{N}(2,6\text{-}i\text{Pr}_2\text{C}_6\text{H}_3)\}_2\text{CHCFe}(\text{HMDS})_2\}$ (**16**) as a yellow crystalline solid in a 28% isolated yield. Compound **16** is obtained as the result of the selective methylation of the C2 position of the anionic NHC ligand present in **15**, leaving its Fe-C4 bond and more importantly the Fe-N bonds intact. This is particularly noteworthy as recent studies have shown that the amido groups in the related complex $[(\text{IPr})\text{Fe}(\text{HMDS})_2]$ can display basic lability metallating substrates such as PhSeH with the subsequent formation of HMDS(H).²⁰⁴

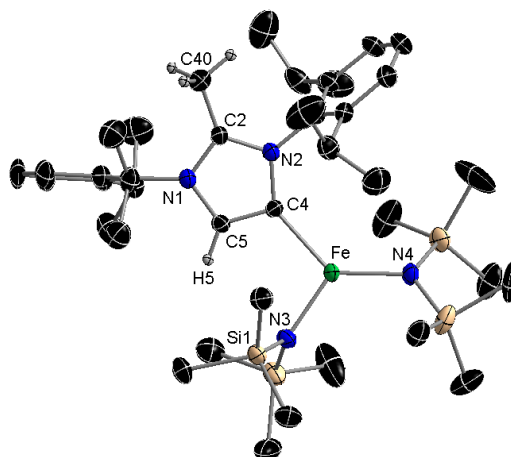


Figure 2.10 - Molecular structure of complex **16**. Hydrogen atoms (except H5 and C40 hydrogens) and disorder components in SiMe_3 group omitted for clarity. Thermal ellipsoids displayed at 50% probability level. Selected bond distances (Å) and angles (°): Fe1-C4 2.113(2), Fe1-N3 1.9732(19), Fe1-N4 1.9459(19), C2-N1 1.330(4), C2-N2 1.341(3), C2-C40 1.491(3); C4-Fe1-N3 104.02(8), C4-Fe1-N4 132.84(8), N3-Fe1-N4 123.14(8), Fe1-C4-N2 140.30(16), C40-C2-N1 125.3(2), C40-C2-N2 126.9(2), N1-C2-N2 107.46(19).

The molecular structure of **16** was established by X-ray crystallographic studies (Figure 2.10). The bond length of 1.491(3) Å for C2-C40 is consistent with a single bond while the Fe1-C4

bond length (2.113(2) Å) is only slightly elongated with respect to that in the anionic complex **15** (2.085(4) Å) and almost identical to that reported for [(*a*IPr)Fe(HMDS)₂] (2.117(2) Å).¹⁸⁰ Supporting previous studies that have described *abnormal* NHC ligands as stronger σ -donors than their *normal* isomers,¹⁷⁰ the Fe1-C4 distance in **16** is shorter than in the related complex containing a *normal* NHC ligand [(IPr)Fe(HMDS)₂] (2.182(2) Å) which also features a tri-coordinate Fe centre.¹⁸⁹

The ¹H NMR spectrum of paramagnetic **16** in d₈-toluene features a series of broad resonances in the range of 29.37 to –33.29 ppm. A distinctive very broad resonance for the hydrogen atom located at the C5 position on the imidazole ring can be seen at –33.29 ppm, which is just slightly upfield to that observed for the same H atom in ferrate **15** (at –26.37 ppm), whilst the resonances for the CH₃ group attached to the C2 atoms of the carbene and the HMDS groups appear downfield at 29.36 and –5.05 ppm, respectively. Resonances for the aromatic H atoms are observed at 10.78, 9.64 and 8.58 ppm whilst the lack of symmetry in the imidazole ring is evidenced by the presence of two distinct sets of signals for the isopropyl substitutes (δ = 1.32 and 1.21 ppm for CH's and δ = 4.53, 0.98, –3.40 and –6.96 ppm for the Me groups). The solution effective magnetic moment was measured by the Evans method and found to be 4.78 μ_B , consistent with an $S = 2$ ground state.

2.3.4 Magnetometry Studies of Sodium Ferrate NHC Complexes

The electronic structures of the Fe(II) centres in complexes **1** and **12-16** was studied through bulk magnetisation measurements (SQUID). Molar paramagnetic susceptibility (χ_M) data was collected on microcrystalline samples in the 2 to 300 K temperature range, under a constant magnetic field of 0.5 T (0.1 T in the case of **13**), in the warming mode. The results are represented below in Figure 2.11 in the form of $\chi_M T$ vs T curves.

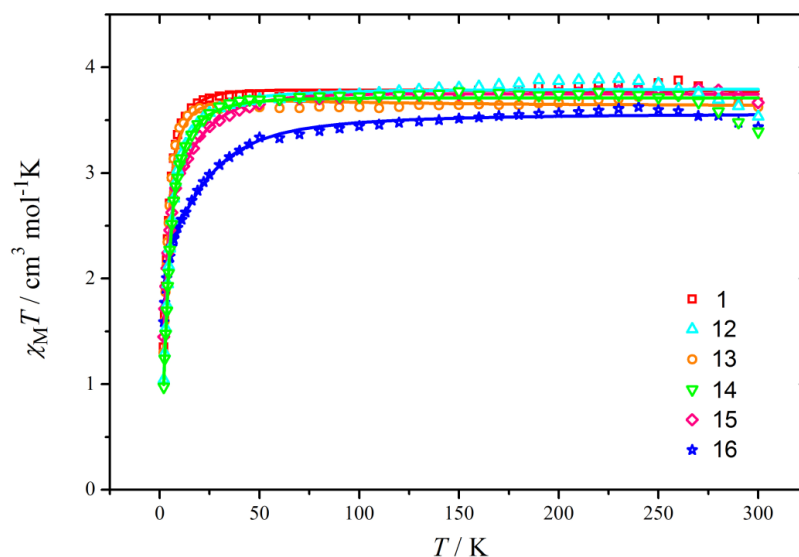


Figure 2.11 - $\chi_M T$ vs T curves of compounds **1** and **12-16** (measurement setup: 2→300 K). Solid lines represent the results of the fits.

In all cases, the $\chi_M T$ product at 300 K is slightly higher than the expected value ($3.00 \text{ cm}^3 \text{ K mol}^{-1}$ for $g = 2.0$) for one uncoupled high-spin ($S = 2$) iron(II) centre ($3.67, 3.53, 3.62, 3.39, 3.67$ and $3.44 \text{ cm}^3 \text{ K mol}^{-1}$ for **1** and **12-16**, respectively) indicating that the ligand field is insufficient to force a violation of Hund's rule. The estimated g values using the Curie Law for the ambient temperature data are $g = 2.21, 2.17, 2.20, 2.13, 2.21$ and 2.14 , respectively, which suggests the presence of unquenched angular momenta, which in turn is coupled to the electronic spin, thus leading to susceptibility values larger than the calculated for "spin-only" systems. Inspection of the curves reveals that in lowering the temperature from 300 K, a slight increase of $\chi_M T$ takes place for all the compounds, which is attributed to a slight decomposition of the sample occurred upon warming (almost certainly involving the oxidation to Fe^{III}).

Upon analysing the $\chi_M T$ product below the almost imperceptible maximum (near 260 K) a very slightly positive slope is barely appreciable, most likely explained by the influence of a weak temperature-independent contribution to paramagnetism. Sharp decreases are observed for all the products at the lowest temperatures, leading to $\chi_M T$ values of $1.35, 1.04, 1.30, 0.97, 1.45$ and $1.59 \text{ cm}^3 \text{ K mol}^{-1}$ (for **1** and **12-16**, respectively) at 2 K. This very apparent decline is explained by the effect of zero-field splitting which is another consequence of the presence of spin-orbit coupling. The latter is explained by the nature of the electronic states of Fe(II) in this coordination environment, which in their ground state are expected to lack any orbital angular momentum ($L = 0$), that is however altered by mixing of electronic excited states with

non-zero L . The effects of this mixing can be modelled using the perturbation theory. Thus, the experimental data were fit using the program PHI¹⁴⁸ by matrix diagonalisation of the (perturbative) anisotropic spin Hamiltonian defined in Equation (2.1):

$$\hat{H} = D \left(\hat{S}_z^2 - \frac{1}{3} \hat{S}^2 \right) + E \left(\hat{S}_x^2 - \hat{S}_y^2 \right) + \mu_B \cdot (\hat{S}_x g_x B_x + \hat{S}_y g_y B_y + \hat{S}_z g_z B_z) \quad (2.1)$$

In this equation, D and E stand for axial and rhombic ZFS parameters, respectively, \hat{S} is the total spin operator and \hat{S}_i ($i = x, y, z$) are the operators of its components. B_i ($i = x, y, z$) are the components of the magnetic induction and μ_B is the Bohr magneton. The anisotropy of the g factor was considered by setting $g_x = g_y \neq g_z$, which takes into account the trigonal planar coordination environment around Fe(II). No intermolecular interactions were considered, given the large distance between paramagnetic centres.

Table 2.1 – Fitting Parameters for compounds **1** and **12-16**.

Compound	$\chi_M T^a$ at r.t. (g)	μ_{eff}^b at r.t	$\chi_M T^a$ at 2 K	$g_x = g_y$	g_z	D (cm ⁻¹)	E (cm ⁻¹)
1	3.67 (2.21)	5.42	1.35	2.30	2.12	7.5	0.0
12	3.53 (2.17)	5.32	1.04	2.23	2.28	9.6	0.0
13	3.62 (2.20)	5.38	1.30	2.30	1.97	8.3	0.0
14	3.39 (2.13)	5.21	0.97	2.26	2.15	10.2	±0.1
15	3.67 (2.21)	5.42	1.45	2.17	2.35	-15.5	±4.2
16	3.44 (2.14)	5.25	1.59	2.21	2.12	-17.7	±0.7

^aIn units of cm³ K mol⁻¹ ^bIn units of Bohr magnetons.

The results from the fitting are presented above in Table 2.1. For compounds **1** and **13**, the best fits reveal the presence of axial zero-field splitting (D values of +7.5 and +8.3 cm⁻¹, respectively, and $E = 0$) with anisotropic g values where $g_x = g_y > g_z$. These parameters are in accordance with the consistency criterion derived from perturbation theory defined as $D = 0.5 \lambda(g_z - g_x)$,²⁰⁵ taking a value of the spin-orbit coupling parameter λ for Fe(II) close to the that of the free ion (-102 cm⁻¹).²⁰⁶ Quite similar values were previously reported for the related compound [Li(15-crown-5)]⁺[Fe(HMDS)₃]⁻, which exhibits a higher degree of axiality.¹¹¹ Heteroleptic compounds **12** and **14** follow an almost identical pattern of behaviour as the above systems (D values of +9.6 and +10.2 cm⁻¹, respectively, and $E = 0$). These values of D suggest that replacing one [N(SiMe₃)₂]⁻ ligand with [CH₂SiMe₃]⁻ does not significantly modify the crystal field around the Fe(II) ion, as can be expected bearing in mind the

structural and electronic similarity of those ligands. The slightly differing effect on the magnetic properties can however be interpreted in terms of the different donor character of the ligands.

In contrast to this, the fits for compounds **15** and **16** led to negative D values (-15.5 and -17.7 cm^{-1} , respectively) with the appearance of a rhombic zero-field splitting parameter, E (± 4.2 and ± 0.7 cm^{-1}). The latter is the natural consequence of the deviation from the idealised trigonal environment around the metal ion resulting from the presence of NHC ligands, which introduce a new interaction with the metal d orbitals due to π -donating character of the heterocycles. In fact, this not only generates rhombicity but changes the sign of the anisotropy, turning to axial instead of easy plane. A drastic change in anisotropy of $3d$ metals as a result of changes to the π -donor properties of ligands as observed here, has been previously predicted theoretically.²⁰⁷ The anisotropy to the g factor (Table 2.1) is featured in these fits by components not differing significantly but leading to two qualitatively distinct behaviours; for of **16**, $g_x = g_y > g_z$ while for **15** $g_z > g_x = g_y$. This means that **16** does not comply with the above mentioned criteria, which could be explained by the presence of strong spin-orbit coupling interactions. The latter weakens the accuracy of the perturbative model assumed with the spin Hamiltonian of Equation (2.1).

In any case, the observations are perfectly in line with the behaviour revealed by other complexes of the type $[\text{Fe}(\text{HMDS})_2\text{L}]$ (where L = neutral ligand such as PCy_3 , THF or IPr) previously reported, all exhibiting negative D parameters and moderate E values that can be fine-tuned by changing the substituents on the ligands employed (see Table 2.2).^{96,111,189,208} On the other hand, the important effect to the anisotropy caused by the π bonding character of the NHC donors present in **15** and **16** is very significant and, to the best of our knowledge, it is revealed here for the first time. The gradation of D is also reflected in the values of χ_{MT} at low temperatures, which follow the order $\{\text{Fe}(\text{HMDS})_2(\text{CH}_2\text{SiMe}_3)\}^- \approx [\{\text{NaFe}(\text{HMDS})_2(\text{CH}_2\text{SiMe}_3)\}_\infty] < \{\text{Fe}(\text{HMDS})_3\}^- \approx [\{\text{NaFe}(\text{HMDS})_3\}_\infty] < (\text{THF})_3 \cdot \text{Na}[:\text{C}\{\text{N}(2,6\text{-}^i\text{Pr}_2\text{C}_6\text{H}_3)_2\}\text{CHCFe}(\text{HMDS})_2\}] < [\text{CH}_3\text{C}\{\text{N}(2,6\text{-}^i\text{Pr}_2\text{C}_6\text{H}_3)_2\}\text{CHCFe}(\text{HMDS})_2\}]$. The negative D parameter values for **15** and **16** are consistent with this (which imply population of states with higher angular momenta at lower temperatures). For the other complexes, this is a consequence of the stronger σ -donor character of the carbanion over the amido ligand, which, for a positive D parameter, implies a larger population of the diamagnetic ground state at lower temperatures.

Table 2.2 - Fitting parameters for compounds **1** and **12-16** and related Fe(II) compounds in the literature.

Compound	$\chi_M T^a$ at r.t. (g)	$g_x = g_y$	g_z	D (cm ⁻¹)	E (cm ⁻¹)
1	3.67 (2.21)	2.30	2.12	7.5	0.0
12	3.53 (2.17)	2.23	2.28	9.6	0.0
13	3.62 (2.20)	2.30	1.97	8.3	0.0
14	3.39 (2.13)	2.26	2.15	10.2	±0.1
15	3.67 (2.21)	2.17	2.35	-15.5	±4.2
16	3.44 (2.14)	2.21	2.12	-17.7	±0.7
[Fe{N(SiMe ₃) ₂ } ₂ (THF)] ¹¹¹	3.66 (2.21)	2.07	2.28	-20	±4.0
[Fe{N(SiMe ₃) ₂ } ₂ (PCy ₃)] ^{111,208}	4.07 (2.33)	2.14	2.61	-33	±3.4
[Li(15-crown-5)] ⁺ [Fe{N(SiMe ₃) ₂ } ₃] ⁻¹¹¹	3.50 (2.16)	2.18	1.91	9.9	±0.0
[LiFe{N(SiMe ₃) ₂ } ₃] ⁹⁶	3.00 (2.00)	-	-	-	-
[THF·LiFe{N(SiMe ₃) ₂ } ₃] ⁹⁶	3.31 (2.10)	-	-	-	-
[(IPr)Fe{N(SiMe ₃) ₂ } ₂] ¹⁸⁹	3.85 (2.27)	$g = 2.27$		-18.2	
[(IMes)Fe{N(SiMe ₃) ₂ } ₂] ¹⁸⁹	3.75 (2.24)	$g = 2.24$		-23.3	
[{Li(BTA)Fe{N(SiMe ₃) ₂ } ₃ } ₂] ⁸⁵	7.2 (2.19)	$g = 2.2$		-10.5	

^aIn units of cm³ K mol⁻¹; IPr = 1,3-bis(diisopropylphenyl)-imidazol-2-ylidene; IMes = 1,3-bis(2,4,6-trimethylphenyl)-imidazole-2-ylidene; BTA = benzotriazolyl.

2.4 Conclusions

Building on the synthesis of homoleptic solvent-free sodium ferrate **1**, heteroleptic **12** has been synthesized straightforwardly by co-complexation of $\text{Fe}(\text{HMDS})_2$ with the sodium alkyl reagent $\text{NaCH}_2\text{SiMe}_3$. The complicated polymeric arrangements of **1** and **12** can be broken down by introducing unsaturated carbene IPr to form the discrete NHC-separated ion-pair ferrate **13** and partially NHC-separated (THF is also needed) ion-pair **14**, respectively. In these complexes the IPr neutral donor coordinates preferentially to the Na atom, while more Lewis acidic Fe is coordinated exclusively to anionic ligand sets. Interestingly, **13** and **14** were also obtained when the NHC complex $[(\text{IPr})\text{Fe}(\text{HMDS})_2]$ was treated with NaHMDS and $\text{NaCH}_2\text{SiMe}_3$, respectively. Contrastingly, sequentially reacting IPr with $\text{NaCH}_2\text{SiMe}_3$ then $\text{Fe}(\text{HMDS})_2$ allows for the isolation of heteroleptic ferrate **15** where both metals are connected by an anionic NHC. Compound **15** can be envisaged as a product of an indirect ferration process, where IPr is first metallated (sodiated) by the polar sodium reagent which in turn undergoes fast transmetallation with $\text{Fe}(\text{HMDS})_2$. Collectively these findings illustrate the significantly different outcomes that are possible in mixed-metal chemistry, when the synergy created by two metals operates simultaneously in the one molecule or in a stepwise manner in two molecules. Unveiling a new approach in transition metal chemistry, treatment of **15** with 0.9 eq. of MeOTf led to the isolation of the tri-coordinate neutral iron *abnormal* NHC complex **16** together with NaOTf. Studies probing the magnetic susceptibility properties of **1** and **12-16** have revealed an important change to their anisotropy by replacing a pure σ -donor from an idealised trigonal coordination environment (**1** and **12-14**) by an NHC that can offer π donating character (**15** and **16**).

Chapter 3 – Direct Ferration of Fluoroaromatic Substrates

3.1 C-H Activation of Fluorinated Aromatic Molecules

The desire to perform C-H activation processes on unactivated and moderately activated small organic molecules efficiently, without the use of toxic heavy metals, is strong within the chemistry community.²⁰⁹ The exchange of a proton for a metal centre, replacing a non-polar C-H σ -bond to create a more polar (and thus more reactive) metal-carbon bond is especially useful for the purpose of functionalisation of small organic molecules, which can subsequently be employed for electrophilic quenching, cross-coupling processes, nucleophilic additions or other synthetic methods.

Highly desirable for functionalisation are organofluorine molecules, a hugely important class of compound that continues to grow in significance in numerous fields of chemistry such as agrochemicals, biochemistry, materials science and most prominently, pharmaceuticals.²¹⁰⁻²¹² Veritably, despite being all but absent within natural products,²¹³ fluorine is present in an estimated 20-25% of drug molecules.²¹²⁻²¹⁵ The inclusion of fluorine within drug molecules is multi-beneficial as fluorine's size, electronegativity and propensity for electrostatic interactions allows for modulation of a molecule's pK_a , conformation, lipophilicity, pharmacokinetics and metabolic stability.^{213,215}

Fluoroaromatics are an especially important sub-class of compound, of which there are no known naturally occurring aryl fluorides,²¹² but importantly, 10% of new pharmaceuticals produced in industry contain a fluoroarene.²¹⁶ Fluoroaryl moieties are present in some of the world's leading pharmaceutical drugs (Figure 3.1) including former market-leading statin Lipitor, used for the prevention of cardiovascular disease.²¹⁴

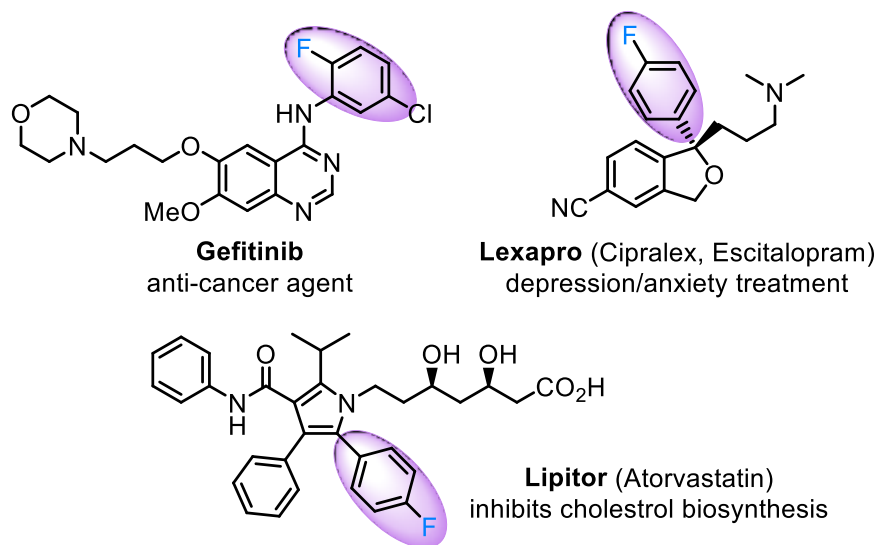
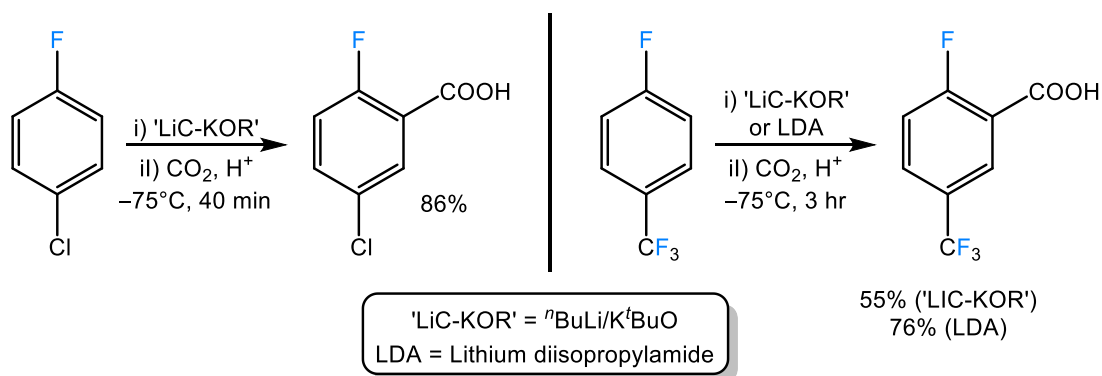


Figure 3.1 – Selection of important aryl fluoride containing drug molecules.

Taking all these aspects into consideration, the C-H activation of fluorinated aromatic molecules is adventitious and necessary in order to access important and useful aryl fluoride-containing molecular architectures. Utilising inexpensive base metals such as iron over expensive noble metals (Rh, Ru, Pt, Pd, etc.) to promote such processes is exceedingly beneficial in not only reducing costs to access high-value fluoroaromatic complexes but when considering medicinal uses, traces of residual Fe from synthesis in such complexes is orders of magnitude safer than noble metals which exhibit a far greater toxicity.²¹⁷

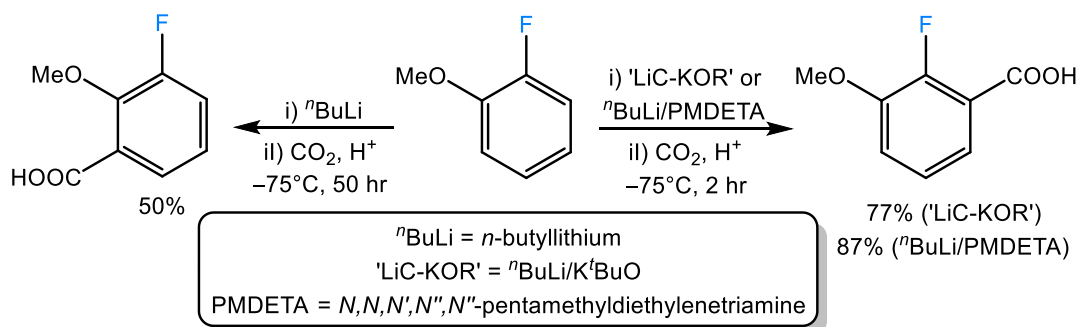
3.1.1 Deprotonative Metallation of Fluoroaromatics

Fluorine is the most electronegative element in the periodic table, scoring highest on the Pauling scale of electronegativity.²¹⁸ Accordingly, F has a significant inductive effect on the aromatic ring (via the withdrawal of electron density),^{19,219} thus increasing the acidity of the surrounding hydrogen atoms,²²⁰ most pertinently at positions *ortho* to F.^{221,222} Hence, within the context of directed metallation, F is activating and *ortho*-directing.^{219,223,224} *Intramolecularly*, F has been shown to have a stronger effect than the other halogens^{223,225} and the CF₃ group,^{223,224,226} as exemplified in Scheme 3.1. *Intermolecularly*, fluorobenzene was found to be eight times more reactive towards ^sBuLi (THF, -100°C) and twenty times more reactive towards LiTMP (THF, -75°C) in comparison to chlorobenzene, demonstrating superior *ortho*-directing power through intermolecular kinetic competition experiments.²²³



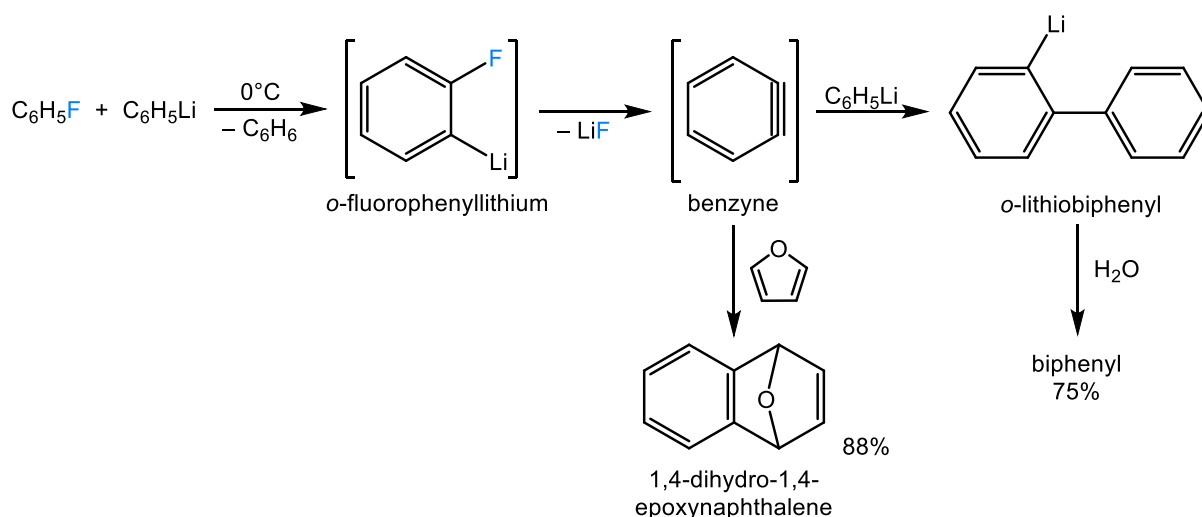
Scheme 3.1 – Preferential directed metallation at the *ortho*-position with respect to fluorine. Fluorine establishes a stronger inductive *ortho*-directing effect over Cl ²²⁵ and CF_3 ^{224,226} groups.

For substituted fluoroarenes (other than those containing halogens and CF_3 groups), it is of utmost importance to also consider coordinative effects, whereby substituents can offer stabilisation via lone pair donation to the deprotonating metal reagent thus directing metallation *ortho* to that group, a phenomenon competing with inductive effects.²²¹ By way of example, the methoxy group (OCH_3) holds weaker inductive effects than fluorine¹⁹ but offers superior coordinative ability.²¹⁹ With judicious choice of base (and donor ligand), metallation can be achieved at positions *ortho* to F or *ortho* to the superior coordinative substituent, this is known as ‘optional site selectivity’.²²¹ Theoretical and experimental observations dictate poorly solvated (thus highly aggregated) organolithium compounds (e.g. $n\text{BuLi}$) seek to achieve coordinative stabilisation thus will deprotonate (almost) exclusively at the adjacent site to the substituent that can offer greatest coordination whilst fully complexed and more polar bases (e.g. $n\text{BuLi}/\text{PMDETA}$, LiTMP , superbasic mixtures) favour attack at the most inductively activated aromatic position, i.e. *ortho* to the most electronegative atom (Scheme 3.2).^{221,223}



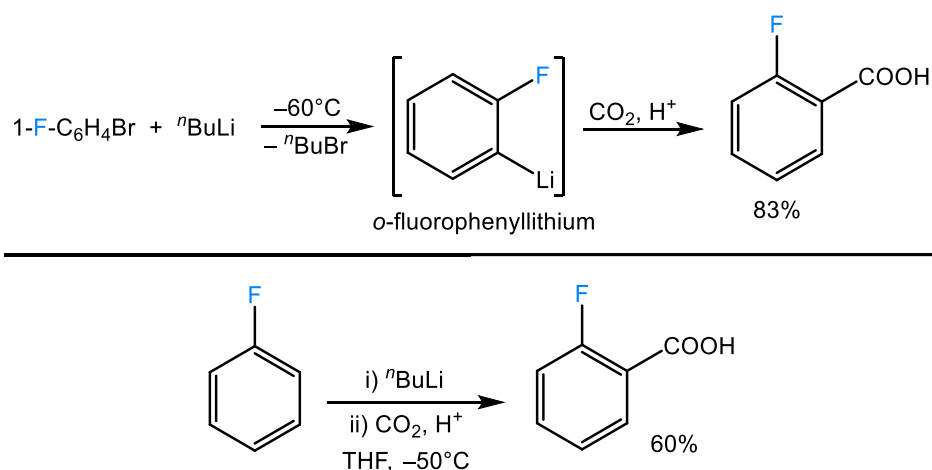
Scheme 3.2 – Optional site selectivity with 2-fluoroanisole.²²⁷ Reactions are 100% regioselective.

Seminal work undertaken by the groups of Wittig and Gilman in the 1940's and 50's reported the metallation of fluorobenzene with strong alkali metal bases and explanations of the complex chemistry that entailed. Wittig first disclosed the metallation of C_6H_5F with phenyllithium (PhLi) at $0^\circ C$ in THF in 1940.²²⁸ Unlike other haloarenes that preferentially undergo lithium-halogen exchange, the authors proposed that biphenyl obtained in a 75% yield was the result of an *ortho*-lithiation process. Shortly after it was established that the reactive *o*-fluorophenyllithium intermediate is initially formed followed by rapid LiF salt elimination to generate benzyne to which PhLi can add to form *o*-lithiobiphenyl and thus biphenyl upon subsequent organic work-up (Scheme 3.3).²²⁹ Whilst Roberts provided the first experimental proof of benzyne formation with ^{14}C -labelled chlorobenzene,²³⁰ Wittig used furan to trap benzyne by way of a [4+2] cycloaddition to yield the *endo*-oxide Diels-Alder product (1,4-dihydro-1,4-epoxynaphthalene).^{231,232}



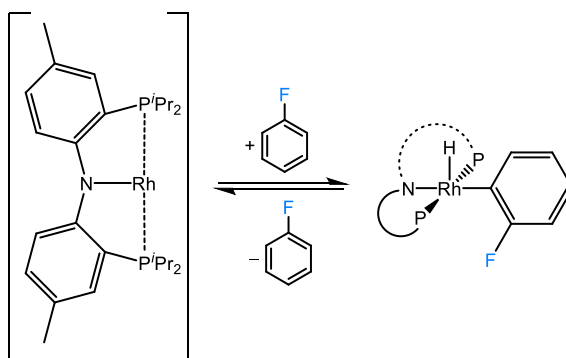
Scheme 3.3 – Summary of Wittig's *o*-lithiation of fluorobenzene, subsequent salt elimination with benzyne formation and addition of phenyllithium^{228,229,232} or trapping with furan.^{231,232}

Gilman *et al.* detailed their success in forming *o*-fluorophenyllithium (from a mixture of 2-fluorobromobenzene and nBuLi) at temperatures below $-60^\circ C$, successfully inhibiting benzyne formation, allowing them to quench with CO_2 and upon acidic work-up generating the corresponding *o*-fluorobenzoic acid (Scheme 3.4, top); they also detected the formation of benzyne derived products upon allowing *o*-fluorophenyllithium to warm to ambient temperature.²³³ Then in the following year, Gilman and Soddy reported the successful *ortho*-lithiation and subsequent carbonation of fluorobenzene in THF at $-50^\circ C$ (Scheme 3.4, bottom).²³⁴



Scheme 3.4 – Gilman’s work avoiding benzyne formation to quench *o*-fluorophenyllithium²³³ and direct lithiation and quenching of fluorobenzene at -50°C .²³⁴

Assessing the published literature to date, comparatively little can be found for structurally authenticated examples of direct *ortho*-metallations of fluorobenzene. The few examples that have been reported have utilised precious transition metals rhodium^{235,236} (Scheme 3.5), platinum,²³⁷ tungsten,²³⁸ titanium²³⁹ and iridium.²⁴⁰ In all cases bar one (where deprotonation is accompanied by loss of H from the organometallic to form and release H₂),²³⁶ metallation is achieved via oxidative addition of fluorobenzene.

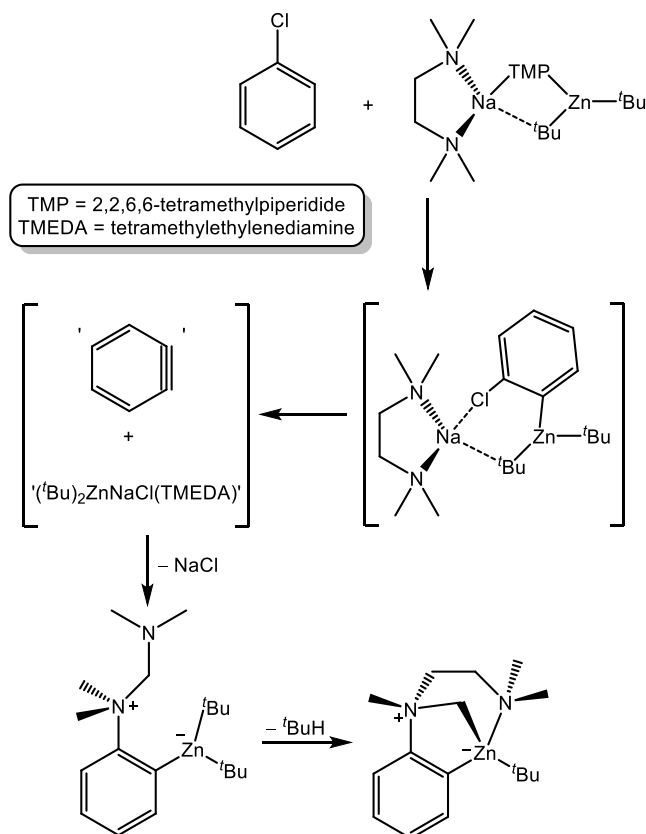


Scheme 3.5 – Reversible oxidative addition of fluorobenzene to a rhodium complex.²³⁵

Within cooperative bimetallic chemistry, it has been established that fluorobenzene can be *ortho*-metallated by the LiC-KOR superbases at temperatures below -75°C .^{226,241}

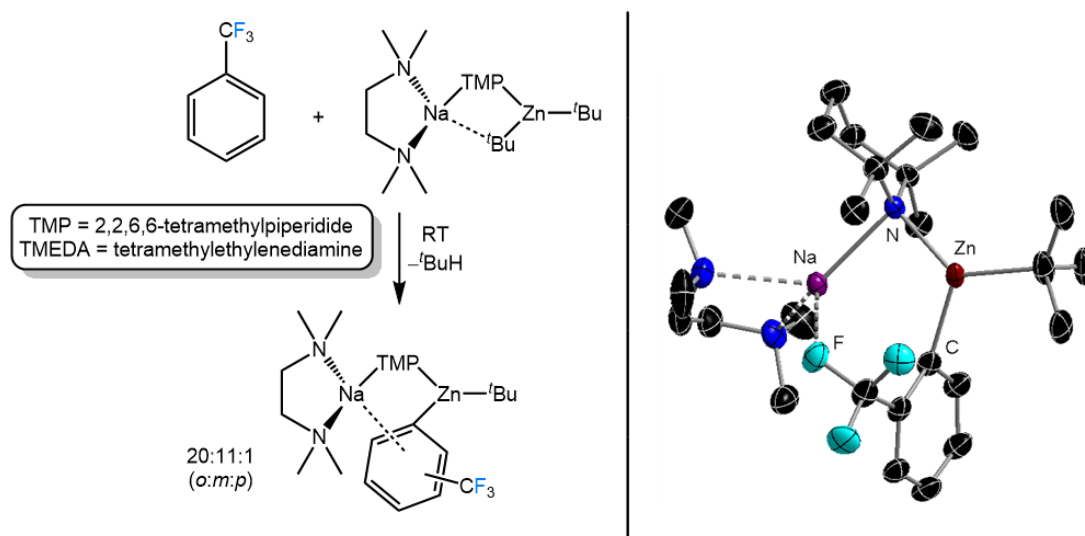
Relatedly, within zincate chemistry Mulvey has reported on the *ortho*-zincation of chlorobenzene where the mixed Na/Zn base [(TMEDA)NaZn(TMP)(^tBu)₂] led to the postulated formation of a benzyne (through NaCl salt elimination), a pathway rationalised by

the isolation of zwitterionic organozinc products (Scheme 3.6).²⁴² Despite the lower polarity of Zn-C bonds (*vs* Li-C bonds), the Na---Cl interaction is strong enough that benzyne formation takes place.



Scheme 3.6 – Proposed mechanistic pathway of zincation of chlorobenzene followed by benzyne formation and isolation of α -zincated N ylides.²⁴²

The reactivity of $[(\text{TMEDA})\text{NaZn}(\text{TMP})(\text{tBu})_2]$ with α,α,α -trifluorotoluene is also of note, where at 0°C SSIP complex $[\text{Na}(\text{TMEDA})_2]^+[\text{Zn}(\text{C}_6\text{H}_4\text{CF}_3)(\text{tBu})_2]^-$ (kinetic product, not pictured) is formed in a small quantity along with the major product, CIP complex $[(\text{TMEDA})\text{NaZn}(\text{C}_6\text{H}_4\text{CF}_3)(\text{TMP})(\text{tBu})]$, as *ortho*, *meta* and *para* regioisomers isolated in a 20:11:1 ratio (Scheme 3.7, left).²⁴³ The *ortho* regioisomer (thermodynamic product) shows a clear electrostatic contact between Na and one F at a distance of 2.435 Å (Scheme 3.7, right). Contrasting with chlorobenzene, salt elimination is not observed with α,α,α -trifluorotoluene.



Scheme 3.7 – Reaction of α,α,α -trifluorotoluene with sodium zincate $[(\text{TMEDA})\text{NaZn}(\text{TMP})(t\text{Bu})_2]$ and structure of *ortho* regioisomer of $[(\text{TMEDA})\text{NaZn}(\text{C}_6\text{H}_4\text{CF}_3)(\text{TMP})(t\text{Bu})]$.²⁴³ Hydrogen atoms are omitted for clarity. Thermal ellipsoids displayed at 30% probability level.

Structures of metallated intermediates of α,α,α -trifluorotoluene have also been disclosed with monometallic reagent $t\text{BuNa}$ supported by either TMEDA or PMDETA (Figure 3.2).²⁴⁴ $[\{\text{TMEDA}\cdot\text{Na}(\text{C}_6\text{H}_4\text{CF}_3)\}_2]$ and $[\{\text{PMDETA}\cdot\text{Na}(\text{C}_6\text{H}_4\text{CF}_3)\}_2]$ each display a Na-F dative interaction at distances of 2.6415(7) and 2.6750(9) Å, respectively.

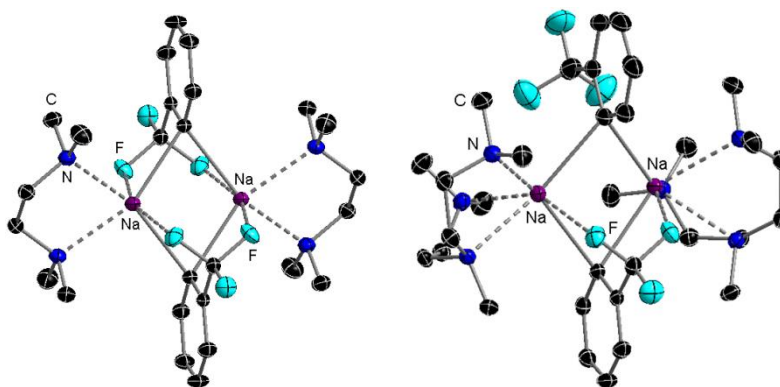


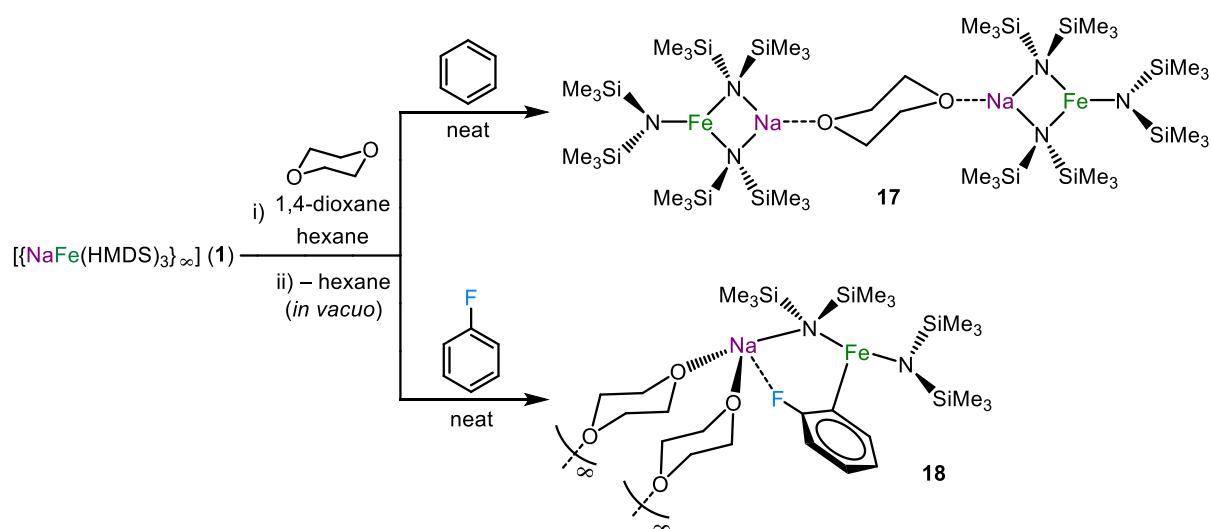
Figure 3.2 – Dimeric structures of sodiated α,α,α -trifluorotoluene supported by TMEDA (left) and PMDETA (right).²⁴⁴

Presented in this chapter are successes in direct C-H activation of fluorinated aromatic molecules with a Na/Fe cooperative bimetallic base. Described herein are results with a range of fluoro-substituted aromatics that allowed for the development of a methodology for chemoselective direct *ortho*-ferration. Isolation and structural elucidation of key ferrated intermediates is also included.

3.2 Results and Discussion

3.2.1 Synthesis of an Efficient Sodium Ferrate Base for the Metallation of Fluorinated Aryl Substrates

Parallel to the investigations of sodium ferrate complex **1** with neutral Lewis basic donors as detailed in Chapter 1, the reaction of **1** with 1,4-dioxane was explored. Despite possessing two oxygen atoms, 1,4-dioxane is generally precluded from chelating to a single metal centre due to the positioning of the O atoms in the six-membered ring, though it well-known to facilitate aggregation of metal complexes by bridging between metal centres.^{95,98,245,246}



Scheme 3.8 – Reactions of **1** with 1,4-dioxane and products obtained from neat benzene (**17**) or fluorobenzene (**18**) solvents.

Thus, the addition of molar equivalents of 1,4-dioxane to two separate solutions of **1** in hexane was carried out with the immediate precipitation of a white solid (Scheme 3.8). Volatiles were removed *in vacuo* and the green/white solid was solubilised by two separate solvents; one with the addition of 5 mL of benzene and the other by the addition of 5 mL of fluorobenzene.

Gentle heating and slow cooling to ambient temperature of the green benzene solution yielded large green crystals of $[\text{dioxane} \cdot \{\text{NaFe}(\text{HMDS})_3\}_2]$ (**17**) (Figure 3.3) in a 63% yield; whose solid-state structure was established by X-ray crystallography.

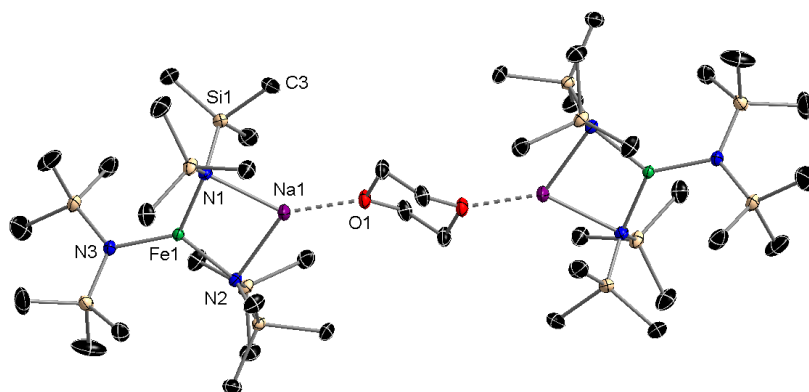
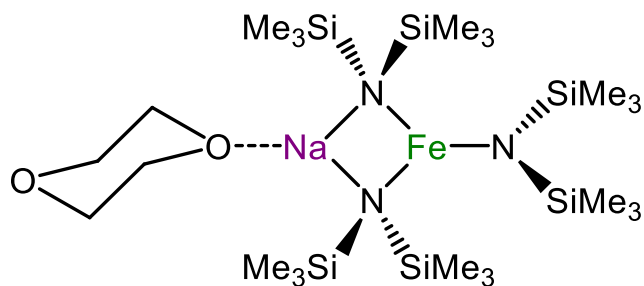


Figure 3.3 – Crystal structure of complex **17**. Hydrogen atoms and a molecule of co-crystallised benzene solvent omitted for clarity. Thermal ellipsoids displayed at 50% probability level. Selected bond distances (Å) and angles (°): Fe1-N1 2.0378(12), Fe1-N2 2.0625(11), Fe1-N3 1.9443(12), Fe1---Na1 2.9995(6), Na1-N1 2.4395(13), Na1-N2 2.4894(13), Na1-O1 2.2828(12); N1-Fe1-N2 109.17(5), N1-Fe1-N3 125.93(5), N2-Fe1-N3 124.91(5), Na1-N1-Fe1 83.61(4), Na1-N2-Fe1 81.86(4), Na1---Fe1-N3 179.22(4), N1-Na1-N2 85.36(4), O1-Na1-N1 139.03(5), O1-Na1-N2 135.49(4).

Complex **17** displays a dimeric structure where two symmetrically equivalent, monomeric $\{\text{NaFe}(\text{HMDS})_3\}$ units are bridged by 1,4,-dioxane, Na1 bonding to O1 at a distance of 2.2828(12) Å. The primary bond lengths and angles around the metal centres are comparable with homoleptic CIP structures **1-4** (see Table 1.1, *vide supra*) with no value deviating significantly. Fe retains its distorted trigonal planar geometry (sum of angles around Fe = 360.01°, range 109.17(5) to 125.93(5)°), whilst Na remains contacted via bridging HMDS nitrogens (Na1-N1 2.4395(13) Å, Na1-N2 2.4894(13) Å).

The ^1H and $^{13}\text{C}\{^1\text{H}\}$ NMR spectra of **17** was recorded in d_8 -toluene. The HMDS hydrogen and carbon signals are found at -4.72 and 338.57, respectively (in a similar range to those reported for CIP structures **1-4** recorded in C_6D_6 , see Table 1.2, *vide supra*). A broad signal is observed in the ^1H NMR spectrum for the 1,4-dioxane H atoms at 6.17 ppm, whilst in the $^{13}\text{C}\{^1\text{H}\}$ NMR spectrum a resonance at 76.32 ppm corresponds to the CH_2 groups.

It must be noted that whilst the combination of equimolar equivalents of **1** and 1,4-dioxane crystallises as hemisolvate **17** (i.e. 0.5 equivalents of 1,4-dioxane per $\{\text{NaFe}(\text{HMDS})_3\}$), it is found that the full equivalent of 1,4-dioxane is retained in the green/white amorphous solid when the solution is subject to vacuum. Thus herein, **17a** shall refer to the stoichiometrically correct sodium ferrate base $[\text{dioxane}\cdot\text{NaFe}(\text{HMDS})_3]$ as depicted in Figure 3.4.

Figure 3.4 – ChemDraw depiction of [dioxane·NaFe(HMDS)₃] (**17a**).

3.2.2 Direct *ortho*-Ferration of Fluorobenzene

Compound **17a** was allowed to stir overnight dissolved in fluorobenzene (Scheme 3.8, bottom). A distinct solution colour change from green to light brown was observed, before cooling to -30°C whereupon a small number of colourless crystals became apparent. Upon X-ray crystallographic analysis of the crystals a different unit cell to that of **17** was found. Fascinatingly, the structure was revealed as [$\{\text{dioxane}\cdot\text{NaFe}(\text{C}_6\text{H}_4\text{F})(\text{HMDS})_2\}_\infty$] (**18**), where a molecule of fluorobenzene has been *ortho*-ferrated and replaced one of the HMDS groups initially present in **17** (Figure 3.5).

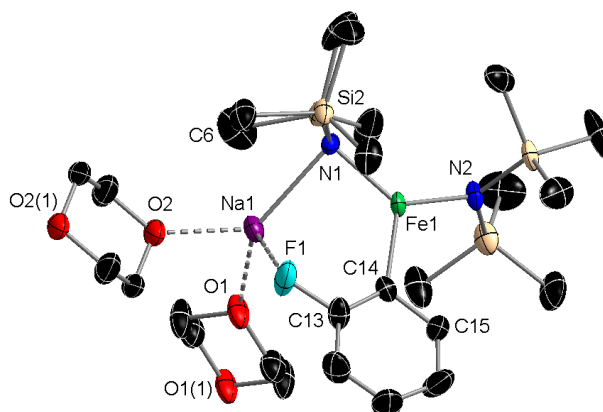


Figure 3.5 – Molecular structure of complex **18** with extra equivalent of 1,4-dioxane shown in the asymmetric unit. Hydrogen atoms, disordered co-crystallised fluorobenzene and disorder in two TMS groups omitted for clarity. Thermal ellipsoids displayed at 50% probability level. Selected bond distances (Å) and angles ($^{\circ}$): Fe1-C14 2.102(4), Fe1-N1 1.995(3), Fe1-N2 1.941(3), Fe1---Na1 3.2081(16), Na1-F1 2.206(3), Na1-N1 2.513(4), Na1-O1 2.333(4), Na1-O2 2.339(3); C14-Fe1-N1 117.52(16), C14-Fe1-N2 114.63(17), N1-Fe1-N2 127.82(15), Na1-N1-Fe1 89.98(13), Na1-Fe1-N2 149.35(11), Na1-F1-C13 119.2(3), N1-Na1-F1 95.54(13), N1-Na1-O1 135.90(14), N1-Na1-O2 128.65(14), O1-Na1-F1 99.19(16), O1-Na1-O2 93.11(13), O2-Na1-F1 88.91(13).

With the concomitant loss of HMDS(H) a new Fe-C σ -bond (Fe1-C14 2.102(4) Å) has been formed closing a six-membered {NaNFeCCF} ring. Fe retains its distorted trigonal planar geometry (sum of angles around Fe = 359.97°, range 114.63(17) to 127.82(15)°), along with the aryl ring aligning with the N1-Fe1-N2 plane (dihedral angles N1-Fe1-C14-C13 0.038(525)° and N2-Fe1-C14-C13 178.308(431)°). Interestingly, the sodium atom interacts with the metallated arene by forming a strong dative bond with its F atom (2.206(3) Å). This interaction can be understood considering their opposite positioning either side of the periodic table, corresponding to a large difference in electronegativity between the two elements; C-F--M⁺ interactions are undeniably strongest with hard cations such as upper Group 1 alkali metals.²¹⁰ As well as bonding to a bridging HMDS group, Na satisfies its coordination environment bonding to two bridging molecules of 1,4-dioxane that bind to neighbouring {NaFe(C₆H₄F)(HMDS)₂} units, giving rise to a one-dimensional ‘zigzag’ polymeric chain structure (Figure 3.6).

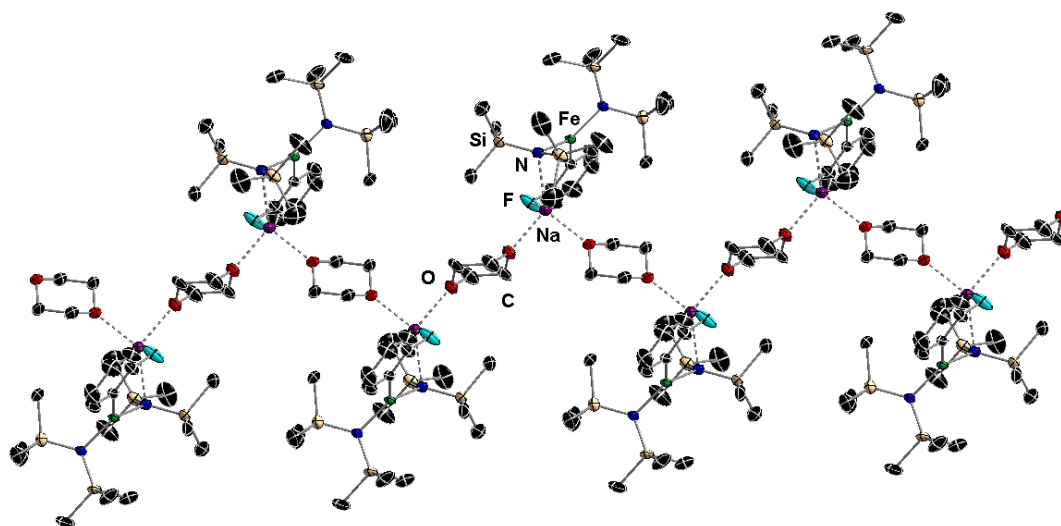


Figure 3.6 – Section of the 1-D polymeric chain of compound **18**. Hydrogen atoms omitted for clarity. Thermal ellipsoids displayed at 50% probability level.

The ¹H NMR spectrum of complex **18** was recorded in C₆D₆ (Figure 3.7). The characteristic very broad resonance for the HMDS H atoms is seen at –2.88 ppm, a small downfield shift from those observed for CIP complexes **1-4** and **17** (circa –4.7 ppm). A broad signal integrated to eight H atoms at 3.35 ppm is assigned to 1,4-dioxane. By means of widening the spectral window, all four signals for the aromatic ring H atoms can be viewed; strikingly, the most downfield resonance appears at 181.84 ppm whilst the furthest upfield resonance

appears at -56.11 ppm. Due to these extremely large isotropic shifts, further assignment of the aryl hydrogen resonances (i.e. to which carbon atoms) is not possible in this instance.

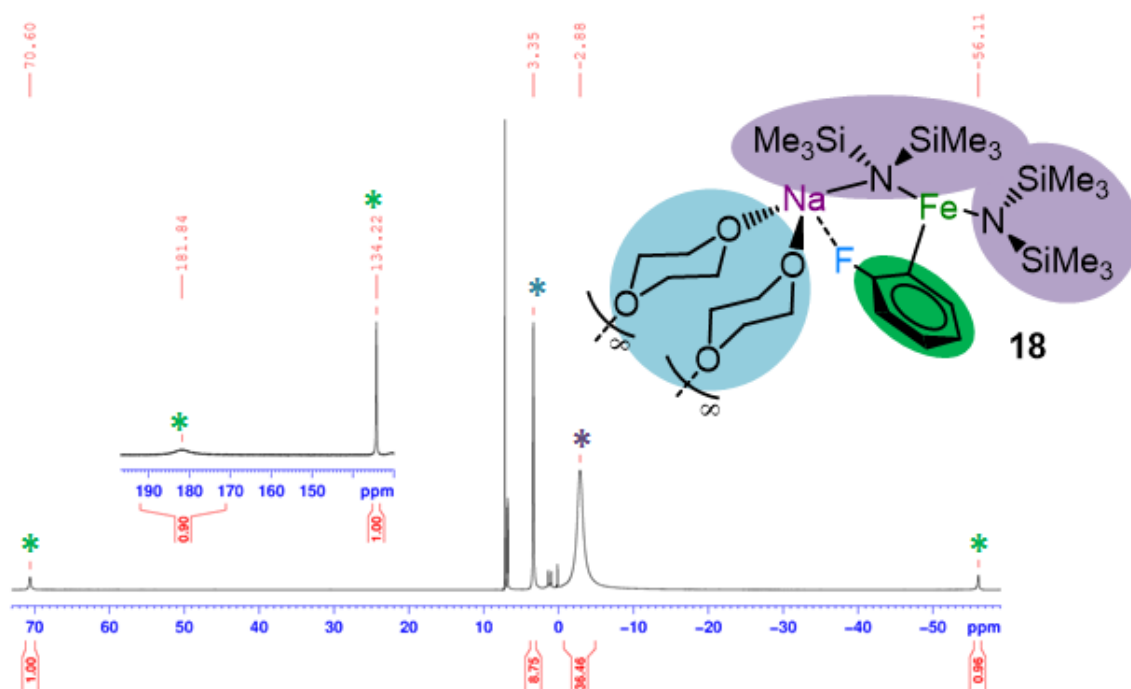
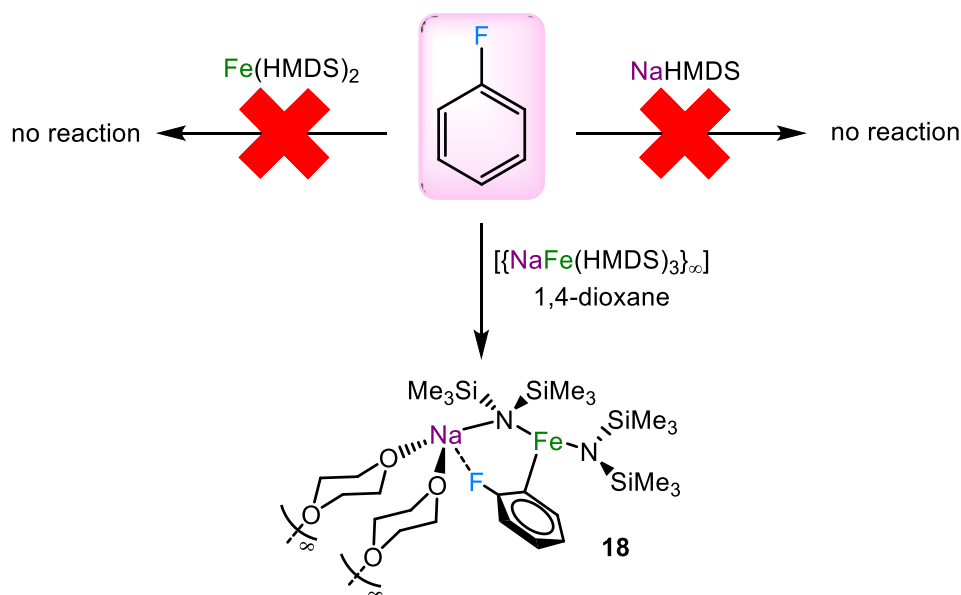


Figure 3.7 – Annotated ^1H NMR spectrum of complex **18** in C_6D_6 .

It should be noted that under the conditions of stirring at ambient temperature overnight (with crystallisation at -30°C) the crystalline yield obtained was 47%. When stirred at 50°C overnight (and conducted on a 10 mmol scale) an 82% yield was achieved. Investigating whether it would be possible to metallate a stoichiometric quantity of fluorobenzene, a molar equivalent was added to a mixture of **1** and 1,4-dioxane (1 eq.) synthesised first in hexane before removal under vacuum and redissolving in benzene and stirring overnight at 50°C . A number of crystals were analysed by X-ray crystallography but in all cases their unit cells matched that for **17**. A crude ^1H NMR spectrum of the solid recovered from the reaction matched that of **17** also, showing the faintest small resonances ($<1\%$) in the positions seen in the spectrum of **18**.

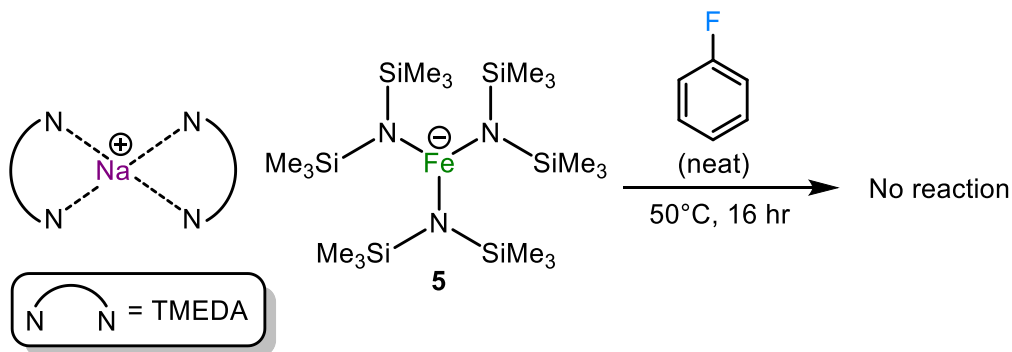


Scheme 3.9 – Direct *ortho*-ferration of fluorobenzene via mixed metal synergy: Monometallic components *versus* the mixed-metal complex.

Demonstrating the synergic reactivity of **17a** towards fluorobenzene, when its independent components NaHMDS and $\text{Fe}(\text{HMDS})_2$ were reacted separately with fluorobenzene (Scheme 3.9), no reaction was observed, as demonstrated by X-ray crystallography and ^1H , $^{13}\text{C}\{^1\text{H}\}$ and $^{19}\text{F}\{^1\text{H}\}$ NMR spectroscopy which showed only the recovery of starting material, demonstrating that the formation of **18** an example of cooperative metallation, which can be described as sodium-mediated ferration.

Considering the isolation of reactive intermediate **18**, this C-H activation, as far as we can ascertain, is unprecedented within iron chemistry. Indeed, there are scarce structural examples of selective metallation of fluorobenzene in the scientific literature (as discussed in Section 3.1.1). Fluorobenzene is a relatively inert arene compound ($\text{p}K_{\text{a}} = 36.8$ at the *ortho* position; 42.3 and 43.7 for *meta* and *para* positions, respectively)²⁴⁷ and can be used as a solvent for highly polar species, which makes the result all the more surprising.^{248,249} Furthermore, it should be pointed out that $\text{C}_6\text{H}_5\text{F}$ was used as a neat solvent for the growth of crystals of SSIP complexes **5-8** and **13**, none of which showed any evidence of metallation of the solvent. Moreover, no reaction was overserved when more forcing conditions were employed. When $[\text{Na}(\text{TMEDA})_2]^+[\text{Fe}(\text{HMDS})_3]^-$ (**5**) was dissolved and heated in neat fluorobenzene overnight at 50°C only crystals of **5** were recovered (Scheme 3.10), with no evidence of metallation of $\text{C}_6\text{H}_5\text{F}$ was observed by ^1H NMR spectroscopic analysis of the

solution. Thus, these findings suggest that CIP sodium ferrate complexes may possess stronger ferrating abilities than their SSIP counterparts, necessitating a close proximity of the alkali and transition metal centres for reactivity.



Scheme 3.10 – SSIP complex **5** is unreactive towards fluorobenzene.

The synthesis of **18** can be compared and contrasted to the reactions of sodium zincate [(TMEDA)NaZn(TMP)(^tBu)₂] with chlorobenzene and α,α,α -trifluorotoluene (see Section 3.1.1). Despite possessing a strong alkali metal–halogen interaction, reactive intermediate **18** can be isolated and does not succumb to salt elimination/benzyne formation as chlorobenzene does. The Na-F bond distance in **18** is noticeably shorter (2.206(3) Å) than for the *ortho* metallated α,α,α -trifluorotoluene complex [(TMEDA)NaZn(C₆H₄CF₃)(TMP)(^tBu)] which is reported as 2.435 Å.

Akin to postulated mechanisms for Directed *ortho*-Metallation (DoM), it can be hypothesised that fluorobenzene is brought into proximity of the sodium ferrate by the electrostatic attraction between electropositive Na and highly electronegative F, further increasing the acidity of the *ortho* hydrogens thus priming fluorobenzene for deprotonation by Fe and basic HMDS. Contrasting with important early work from Witting and Gilman (see Section 3.1.1), metallated intermediate **18** is formed at ambient temperature or 50°C and is stable at ambient temperature, showing no evidence of salt elimination (NaF) or benzyne formation, though of course there is substantial difference in bond polarity when comparing and highly polarised Li-C bond to far less polarised Fe-C bond.

3.2.3 Exploration of Substrate Scope

Encouraged by the synthesis and characterisation of **18**, the direct ferration of 1,3-difluorobenzene was attempted next. Disappointingly, reactions of neat 1,3-difluorobenzene yielded crystals at -30°C that redissolved at ambient temperature. The reaction was attempted using a stoichiometric quantity of 1,3,-difluorobenzene which is substantially more activated than fluorobenzene (in $\text{p}K_{\text{a}}$ terms = 28.7 vs 36.8, respectively).²⁴⁷ Thus, a 1:1 mixture of base to substrate in benzene stirred at 50°C overnight (though the reaction also works at ambient temperature) gave large green crystals. Uncovered by X-ray crystallography the crystals were found to be $[\{\text{dioxane}\cdot\text{NaFe}(1,3\text{-C}_6\text{H}_3\text{F}_2)(\text{HMDS})_2\}_{\infty}]$ (**19**), synthesised in a 60% yield (Figure 3.8).

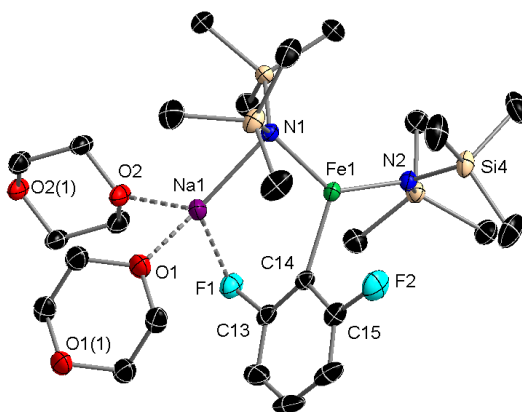
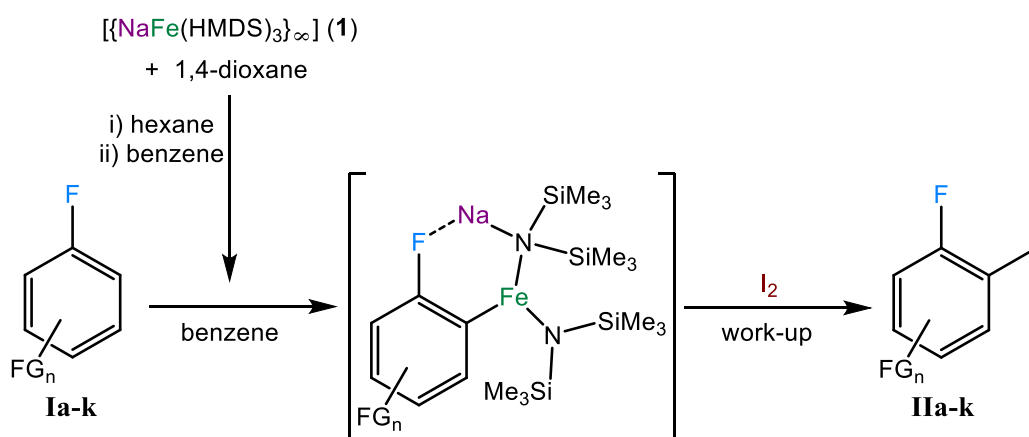


Figure 3.8 – Molecular structure of complex **19** with extra equivalent of dioxane shown in the asymmetric unit. Hydrogen atoms are omitted for clarity. Thermal ellipsoids displayed at 50% probability level. Selected bond distances (\AA) and angles ($^{\circ}$): Fe1-C14 2.1157(18), Fe1-N1 2.0018(14), Fe1-N2 1.9425(14), Fe1---Na1 3.0686(7), Na1-F1 2.3437(13), Na1-N1 2.4392(16), Na1-O1 2.3136(14), Na1-O2 2.2967(14); C14-Fe1-N1 113.45(6), C14-Fe1-N2 116.05(6), N1-Fe1-N2 130.10(6), Na1-N1-Fe1 86.83(5), Na1---Fe1-N2 154.04(4), Na1---F1-C13 97.51(9), N1-Na1-F1 114.85(5), N1-Na1-O1 131.29(6), N1-Na1-O2 121.99(5), O1-Na1-F1 98.31(5), O1-Na1-O2 91.72(5), O2-Na1-F1 88.84(5).

The structure of **19** is almost identical to that of **18**, the clear formation of a new Fe-C σ -bond *ortho* to both F atoms and 1,4-dioxane bridging between monomeric units to form a 1-D ‘zigzag’ polymer chain. A large six-membered $\{\text{NaNFeCCF}\}$ ring is present again, now that 1,3-difluorobenzene bridges between Fe and Na. In another example of *ancillary vs anchoring* bonding, the distance of the Na-F electrostatic contact in **19** is noticeably longer than the corresponding length in **18** (2.3437(13) vs 2.206(3) \AA , respectively) whilst the Fe-C bond distances are very similar (2.1157(18) and 2.102(4) \AA , respectively).

3.2.3.1 Methodology for Ferration and Electrophilic Iodination of Fluorinated Aryl Substrates

The synthesis and characterisation of metallated intermediates **18** and **19** set the scene for the exploration of direct ferration of fluorinated aryl substrates. The achievement of metallating mildly activated and comparatively unreactive fluorobenzene led us to postulate that we could similarly promote the direct ferration of other fluorobenzenes.



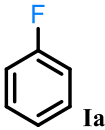
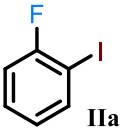
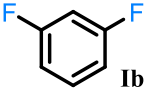
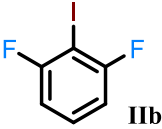
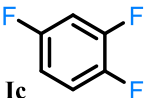
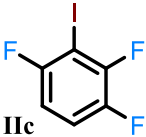
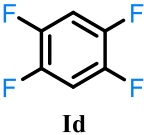
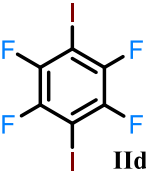
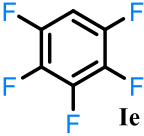
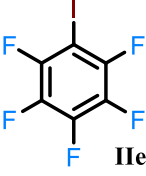
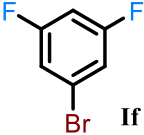
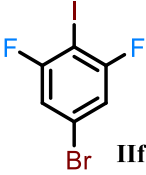
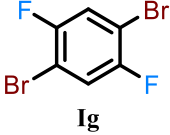
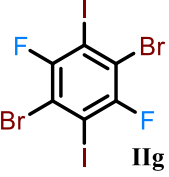
Scheme 3.11 – Methodology for the direct ferration of fluorinated aryls with a sodium ferrate base and electrophilic interception with I_2 .

Accordingly, an array of fluorinated aryl substrates (**Ia-k**) were subject to direct ferration and electrophilic interception (I_2) via the following methodology:

- i. A solution of $[\{\text{NaFe}(\text{HMDS})_3\}_\infty]$ (**1**) is prepared in hexane and stirred for one hour
- ii. One equivalent of 1,4-dioxane is added and stirring is continued for one hour
- iii. Hexane is removed under vacuum and the solid product, $[\text{dioxane}\cdot\text{NaFe}(\text{HMDS})_3]$ (**17a**), is dissolved in benzene (or the neat substrate for less activated fluoroaryls)
- iv. The substrate is added to the solution and reacted for the appropriate length of time and at the appropriate temperature
- v. At ambient temperature the electrophilic interception is carried out using five equivalents of I_2 and left to stir for an hour
- vi. Quenching of the reaction is undertaken by addition of saturated $\text{Na}_2\text{S}_2\text{O}_3$ solution before extracting the organic product with diethyl ether (3 x 50 mL), washing with brine, drying over magnesium sulfate and removing the solvents under vacuum

The results of the direct ferrations and subsequent iodinations are presented in Table 3.2 below. For a number of reactions starting material was recovered when conducted on a 1:1 scale, thus these reactions were run with an extra equivalent of base present (see entries 2-4, 9, 10). Reactions that were run in neat substrate are indicated in the conditions column in Table 3.1.

Table 3.1 – Direct ferration and iodination of a variety of fluorinated arenes.

Entry	Substrate	Base Eq.	Conditions	Product	Isolated Yield (%)
1	 Ia	1	Neat, 50°C 16 hr	 IIa	74
2	 Ib	2	RT 16 hr	 IIb	84
3	 Ic	2	RT 16 hr	 IIc	80
4	 Id	3	RT 16 hr	 IIId	88
5	 Ie	1	RT 16 hr	 IIe	91
6	 If	1	0°C, 1 hr then RT, 16 hr	 IIIf	80
7	 Ig	2	RT 16 hr	 IIg	85

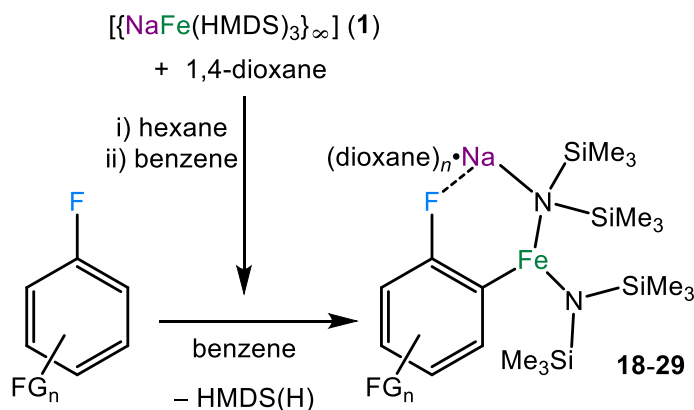
8		1	50°C 2 d		40
9		2	50°C 16 hr		78
10		2	50°C 5 d		45 ^a
11		1	Neat, 50°C 16 hr	 5:1 	24 ^b

^aNMR spectroscopy conversion with a 10% ferrocene internal standard. ^bThe isomers were obtained in a 5:1 ratio (major:minor).

The results highlight the excellent levels of regioselectivity of this metallation approach where in all cases the Fe-H exchange process occurs at the position *ortho* to a F atom. For 1,3-difluorobenzene and 1,2,4-trifluorobenzene (entries 2 and 3), ferration occurs exclusively at the doubly activated position (in 84% and 80% yields, respectively), *ortho* to two fluorine substituents, as opposed to any other available *ortho* position. Employing three equivalents of the **17a**, 1,2,4,5-difluorobenzene (entry 4), holding two doubly activated positions, can captivantly be di-metallated in a high 88% yield. With a single equivalent of base present deprotonation is exclusively regioselective *ortho* to both F atoms for 1-bromo-3,5-difluorobenzene (entry 6) in an 80% yield, though this is to be expected considering the weaker inductive strength of Br versus that of F. However, the positions between F and Br are sufficiently activated that di-deprotonation of 1,4-dibromo-2,5-difluorobenzene (entry 7) is achieved with a stoichiometric two equivalents of sodium ferrate (85% yield). 4-fluorobenzonitrile (entry 8), possessing a strongly electron withdrawing nitrile group, is metallated exclusively *ortho* to fluorine although in this case the reaction takes place in a modest yield (40%). Whilst 3-fluoroanisole (entry 9) is metallated at the C2 position (78%), 4-fluoroanisole (entry 10) displays regioselective deprotonation *ortho* to strongly inducting F as opposed to the strongly coordinative methoxy group, though even after 5 days at 50°C the yield was a relatively low 45%. 3-fluorotoluene (entry 11) gave two products in an overall

low 24% yield, showing preferential deprotonation *para* to the CH₃ group (and *ortho* to F), likely a result of steric effects.

3.2.4 Synthesis, Isolation and Structural Characterisation of Ferrated Intermediates

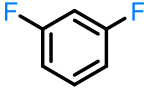
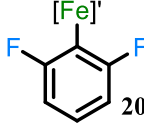
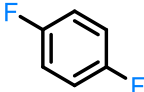
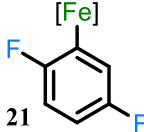
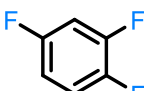
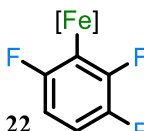
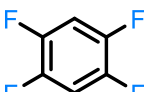
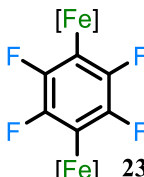
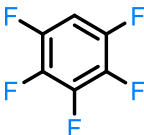
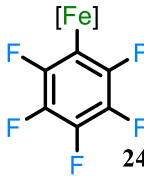
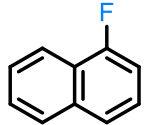
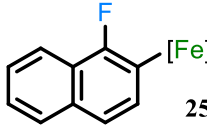
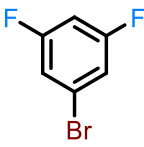
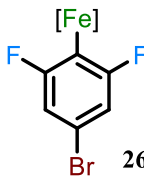
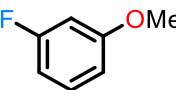
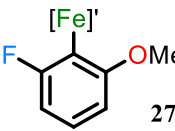
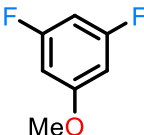
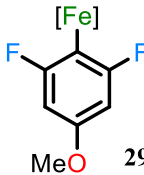


Scheme 3.12 – Generalised methodology for the synthesis of ferrated fluoroaromatic intermediates complexes.

In order to gather a better understanding of the direct *ortho*-ferration reactions we endeavoured to isolate and structurally characterise a number of ferrated intermediates prior to electrophilic interception. Satisfyingly, ferrated intermediate complexes were successfully isolated for a range of fluoroaromatic substrates and characterised by X-ray crystallography, ¹H NMR spectroscopy and elemental analysis. Complexes were synthesised via the generalised methodology outlined in Scheme 3.12, many in a stoichiometric 1:1 (base:substrate) ratio. The results of the reactions are summarised in Table 3.2 below.

Table 3.2 – Direct ferration of a variety of fluorinated arenes.

Entry	Substrate	Conditions ^a	Product ^b	Crystalline Yield (%)
1		Neat, 50°C, 16 hr		82
2		50°C, 16 hr		66

3 ^b		4 eq. 17a , 50°C, 16 hr		36
4		Neat, 50°C, 20 min		38
5		RT, 16 hr		51
6 ^d		2 eq. 17a , 80°C, 1 hr		76
7		0°C to RT, 4 hr		90
8		Neat, 50°C, 16 hr		26
9		0°C to RT, 2 hr		60 ^e
10		50°C, 16 hr		20 ^f
11		RT, 16 hr		51

^aStandard conditions: $[\{\text{NaFe}(\text{HMDS})_3\}_\infty]$ (**1**) prepared in hexane *in situ* to which 1 eq. of 1,4-dioxane was added. Solvent removed *in vacuo* and solid (**17a**) redissolved in benzene after which 1 eq. substrate is added. Neat reactions carried out in the substrate as solvent. ^b[Fe] = $\{(\text{dioxane})_n \cdot \text{NaFe}(\text{HMDS})_2\}$; [Fe]' = $\{(\text{dioxane})_n \cdot \text{Na}_2\text{Fe}(\text{HMDS})_2\}$ ^c4 eq. of **17a** to 1 eq. of substrate. ^d2 eq. of **17a** to 1 eq. of substrate. ^eMaximum possible yield of 66.67% due to 1.5 eq. of 1,4-dioxane required. ^fMaximum possible yield of 50% due to 2 eq. of **17a** required.

Summarising the results, using 10 different substrates, the synthesis, isolation and characterisation of 11 ferrated intermediate structures was achieved at generally moderate temperatures within 16 hours. In all cases, a new (or multiple, see entry **6**) Fe-C σ -bond *ortho* to a fluorine atom is formed with the same F atom engaging in an electrostatic interaction with Na and the formation of large six-membered {NaNFeCCF} ring apparent. Ferration occurs at the most highly inductively activated position on the ring, *ortho* to two F atoms where possible.

Compounds **18** and **19** covered earlier were isolated in good yields of 82% and 66%, respectively (entries **1** and **2**). Investigating whether further metallation of 1,3-difluorobenzene was possible, utilising 4 eq. of **17a**, SSIP complex **20** (containing two Na atoms within the cation, each interacting with a F atom) was obtained in a somewhat low 36% yield (entry **3**). Relatively unactivated 1,4-difluorobenzene was reacted neat with **17a** furnishing crystals of **21** in a 38% yield (entry **4**), whilst more activated 1,2,4-trifluorobenzene gave ferrated product **22** in a higher 51% yield on a 1:1 scale (entry **5**). The di-metallated product **23** was recovered in a good yield (76%) from the reaction of 1,2,4,5-tetrafluorobenzene and 2 eq. of **17a** (entry **6**). Ferrated pentafluorobenzene product **24** was isolated in an excellent 90% yield (entry **7**). Polycyclic (though reasonably unactivated) 1-fluoronaphthalene was ferrated in a low 26% yield, though the necessity to utilise the neat substrate with a high boiling point (215°C) hindered efforts to concentrate the solution to obtain more of product **25** (entry **8**). 1-bromo-3,5-difluorobenzene was ferrated at the 4-position between the F atoms and the product **26** was isolated in a very good 60% yield, where the maximum obtainable yield was 66.67% under the conditions (entry **9**). Reaction of **17a** with 3-fluoroanisole (entry **10**) generated SSIP complex **27** in a 20% yield (maximum possible yield 50%). Metallation at the 4-position (between the F atoms) was achieved with **17a** and 3,5-difluoroanisole, with complex **29** recovered in a 51% yield (entry **11**).

Further to X-ray crystallographic analysis of complexes **18-29**, supplementary characterisation by ^1H NMR spectroscopy and elemental analysis was successful. Though significant efforts were made, unfortunately $^{19}\text{F}\{^1\text{H}\}$ NMR spectroscopy was found not to be a reliable diagnostic tool for these paramagnetic complexes (most probably because of rapid relaxation),²⁵⁰ as spectra either showed merely resonances corresponding to free substrate starting material or no signal at all. Additionally complexes **17-19**, **23** and **24** were subject to magnetometry studies.

3.2.4.1 Structural and Spectroscopic Studies on Metallated Intermediates of Direct Ferration Reactions: (a) Polyfluoroarenes

Probing whether a second ferration on the aryl ring of 1,3-difluorobenzene would be possible, 4 equivalents of base **17a** were employed. Di-ferration was not achieved but instead the separated ion-pair structure $[\{(dioxane)_2 \cdot Na_2Fe(1,3-C_6H_3F_2)(HMDS)_2\}^+ \{Fe(HMDS)_3\}^-]_\infty$ (**20**) was recovered in a 36% crystalline yield (Figure 3.9).

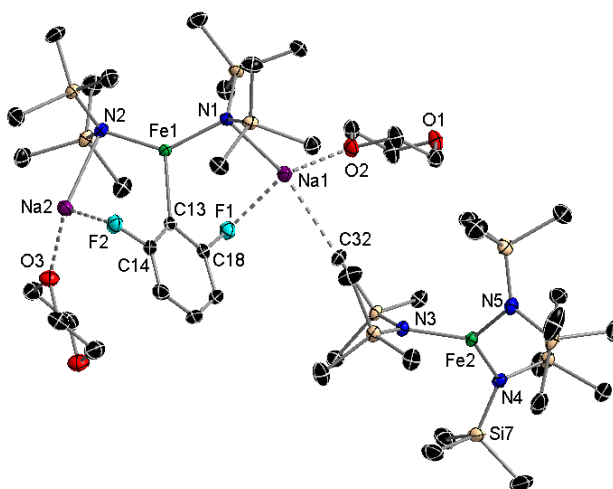


Figure 3.9 – Asymmetric unit of complex **20**. Hydrogen atoms and solvent omitted for clarity. Thermal ellipsoids displayed at 50% probability level. Selected bond distances (Å) and angles (°): Fe1-C13 2.1026(17), Fe1-N1 1.9865(14), Fe1-N2 1.9804(14), Fe1---Na1 3.5651(7), Fe1---Na2 3.2888(7), Fe2-N3 1.9853(14), Fe2-N4 1.9867(14), Fe2-N5 1.9845(14), Na1-F1 2.3308(13), Na1-N1 2.5484(15), Na1-O2 2.3792(14), Na1---C32 2.854(1), Na2-F2 2.3573(13), Na2-N2 2.5654(16), Na2-O3 2.3439(14), Na2-O1(1) 2.3312(14); C13-Fe1-N1 110.60(6), C13-Fe1-N2 113.34(6), N1-Fe1-N2 136.06(6), N3-Fe2-N4 119.84(6), N3-Fe2-N5 118.87(6), N4-Fe2-N5 121.25(6), Na1-N1-Fe1 102.95(6), Na1---Fe1-N2 149.35(4), Na1-F1-C18 117.73(9), N1-Na1-F1 93.94(5), N1-Na1-O2 124.04(5), N1-Na1---C32 143.896(1), O2-Na1-F1 131.12(5), O2-Na1---C32 83.525(1), C32---Na1-F1 80.125(1), Na2-N2-Fe1 91.77(5), Na2---Fe1-N1 166.45(4), Na2-F2-C14 97.80(9), N2-Na2-F2 99.66(5), N2-Na2-O3 131.27(5), N2-Na2-O1(1) 139.74(5), O3-Na2-F2 109.55(5), O3-Na2-O1(1) 81.35(5), O1(1)-Na2-F2 86.76(5).

As previously discussed for **18** and **19**, the 2-position has been deprotonated with Fe residing in the former proton's place, though now the aryl moiety is supported by two sodium atoms, present in the cation, each forming a contact to an F atom. Here two fused six-membered $\{NaNFeCCF\}$ rings are present, joined by the central Fe1-C13 bond. The counter anion is that of $\{Fe(HMDS)_3\}^-$, previously encountered in the homoleptic SSIP structures **5**, **7**, **8** and **13** (*vide supra*). Na1 achieves coordinative stabilisation by coordination to F1, HMDS nitrogen N1, 1,4-dioxane O2 and a long electrostatic to HMDS methyl C32 of the anion (Na1---C32 2.854(1) Å; c.f. Na1---C13 2.727(2) Å in **8**). Similarly Na2 *ancillary* bonds to F2,

HMDS nitrogen N2, 1,4-dioxane O3 and to a second equivalent of 1,4-dioxane to propagate a linear 1-D chain.

The ^1H NMR spectra of **19** and **20** were measured in C_6D_6 . With a 2:1 integration of the *meta* to the *para* H atoms, these signals can be assigned with confidence (**19**: 104.40 [*meta*, 2H], -66.65 [*para*, 1H] ppm; **20**: 104.99 [*meta*, 2H], -66.37 [*para*, 1H] ppm). Though overlapping due to their inherent broadness, two distinct signals are seen in the spectrum of **20** for the two sets of inequivalent HMDS groups at -1.76 and -4.78 ppm.

1,4-difluorobenzene was found to be suitably less activated than 1,3-difluorobenzene, failing to show evidence of metallation on a 1:1 scale. Its $\text{p}K_{\text{a}}$ is in fact calculated higher than that of fluorobenzene (40.1 vs 36.8, respectively),²⁴⁷ presumably due to the symmetrically competing inductive effect at each end of the aryl ring. Thus, the reaction was carried out in neat 1,4-difluorobenzene to form $[\text{dioxane}\cdot\{\text{NaFe}(1,4\text{-C}_6\text{H}_3\text{F}_2)(\text{HMDS})_2\}_2]_{\infty}$ (**21**) in a 38% yield. (Figure 3.10).

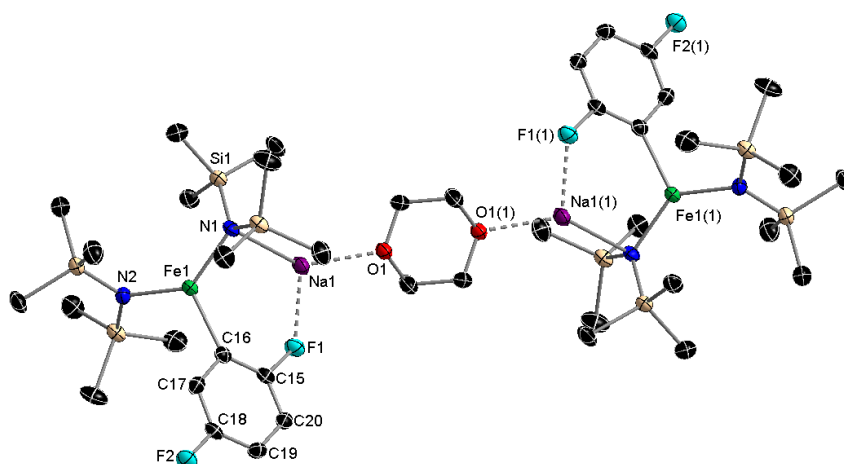


Figure 3.10 – Structure of complex **21**. Hydrogen atoms and co-crystallised 1,4-difluorobenzene solvent are omitted for clarity. Thermal ellipsoids displayed at 50% probability level. Selected bond distances (Å) and angles (°): Fe1-C16 2.094(3), Fe1-N1 1.995(3), Fe1-N2 1.957(3), Fe1---Na1 3.2561(14), Na1-F1 2.256(2), Na1-N1 2.524(3), Na1-O1 2.357(3), Na1---F2(2) 2.359(2); C16-Fe1-N1 115.92(12), C16-Fe1-N2 112.52(13), N1-Fe1-N2 131.56(11), Na1-N1-Fe1 91.46(10), Na1---Fe1-N2 141.17(7), Na1---F1-C15 129.06(17), N1-Na1-F1 107.47(9), O1-Na1-N1 140.17(10), O1-Na1-F1 104.88(9).

Complex **21** is dimeric consisting with 1,4-dioxane bridging between two units of $\{\text{NaFe}(1,4\text{-C}_6\text{H}_3\text{F}_2)(\text{HMDS})_2\}$. Interestingly, Na1 is able to accommodate two electrostatic Na-F contacts; an *intramolecular* contact to F1 (2.256(2) Å) and a longer *intermolecular* contact to *para* fluorine F2(2) (2.359(2) Å) from a second dimeric unit giving rise to 2-D fused ring

network of interconnected dimers, with each ring involving six Na atoms, 4 units of ferrated 1,4-difluorobenzene and two 1,4-dioxane units (Figure 3.11).

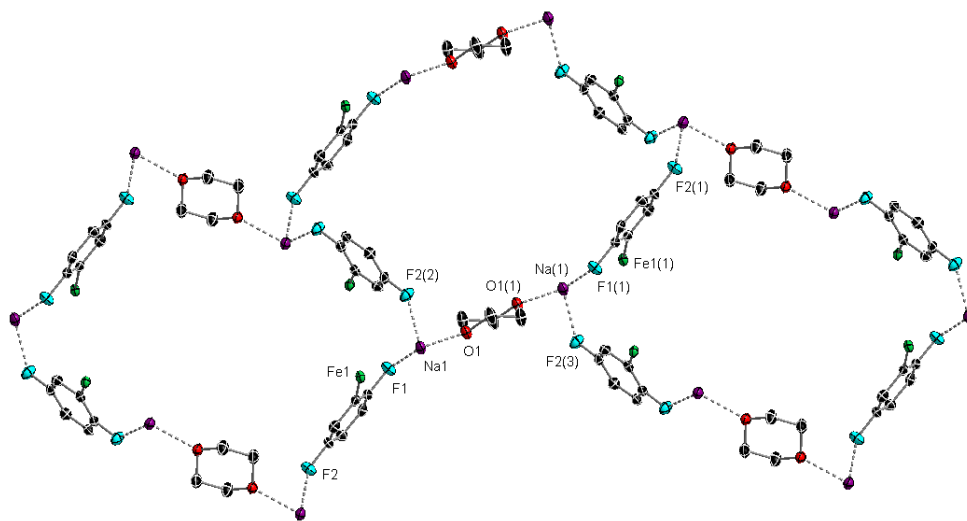


Figure 3.11 – Expanded structure of complex **21**. Hydrogen atoms, HMDS groups and co-crystallised 1,4-difluorobenzene solvent are omitted for clarity. Thermal ellipsoids displayed at 50% probability level. Selected bond distances (Å): Na1-F1 2.256(2), Na1---F2(2) 2.359(2).

The ^1H NMR spectrum of **21** in C_6D_6 features an extremely downfield shifted signal for one of the aryl H atoms at 213.44 ppm, with the remaining aryl hydrogen resonances appearing at 141.36 and -56.51 ppm. The broad HMDS resonance appears at -2.74 ppm.

With an extra fluorine added to the ring, 1,2,4-trifluorobenzene has a doubly activated position the arene ring, with a lower calculated $\text{p}K_{\text{a}}$ (26.1) than that of 1,3-difluorobenzene (28.7). Hence, the reaction with the sodium ferrate base could be carried out stoichiometrically and even without the application of heat as immediately a white precipitate was formed and the solution changed colour from green to orange. Large yellow brick crystals recovered were analysed by X-ray crystallography revealed the structure [dioxane $\cdot \{\text{NaFe}(1,2,4\text{-C}_6\text{H}_2\text{F}_3)(\text{HMDS})_2\}_2\}_\infty$ (**22**) (Figure 3.12) in 51% yield.

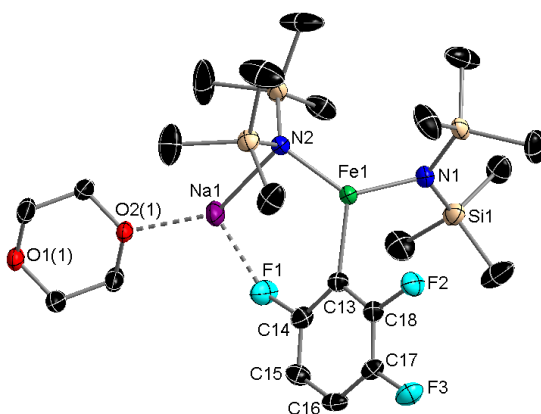


Figure 3.12 – Monomeric unit of complex **22** with an extra half equivalent of 1,4-dioxane shown. Hydrogen atoms, co-crystallised fluorobenzene solvent and disorder in one TMS group are omitted for clarity. Thermal ellipsoids displayed at 50% probability level. Selected bond distances (Å) and angles (°): Fe1-C13 2.114(2), Fe1-N1 1.9490(18), Fe1-N2 2.0039(18), Fe1---Na1 3.3683(9), Na1-F1 2.2173(18), Na1-N2 2.523(2), Na1-O2(1) 2.2984(16), Na1---F9(2) 2.4615(18); C13-Fe1-N1 111.52(8), C13-Fe1-N2 118.86(8), N1-Fe1-N2 129.38(8), Na1-N2-Fe1 95.46(7), Na1-Fe1-N1 145.71(6), Na1-F1-C14 131.64(14), N2-Na1-F1 104.71(6), N2-Na1-O2(1) 140.17(10), N2-Na1-F9(2) 114.25(7), F1-Na1-O2(1) 108.13(7), F1-Na1-F9(2) 80.52(6), O2(1)-Na1-F9(2) 79.21(6).

The monomeric unit is of similar motif to the other ferrated fluorinated arenes but the expanded structure is somewhat more complex. There exists three monomeric units within the asymmetric unit in addition to three equivalents of co-crystallised fluorobenzene, two of which coordinates through F to Na (Na1-F11(1) 2.749(2) Å, Na3-F10 2.903(4) Å). Similar to complex **21**, the metallated aryl moiety, with F atoms in *para* and *meta* positions, allows for enhanced coordination via secondary Na---F contacts. Na1 holds a primary interaction with *ipso* F1 (2.2173(18) Å) within its monomer, a secondary contact with *para* F9(2) (2.4615(18) Å) of a second monomer and a long contact with co-crystallised fluorobenzene solvent F11(1) (2.749(2) Å) as well as a bond with O2(1) of 1,4-dioxane (2.2984(16) Å). Na3 possess the same bonding modes as Na1, to *ipso* F7, *para* F6, fluorobenzene F10 (due to disorder only a 65% occupancy) and O1. Na2 differs slightly as it holds no interaction with any co-crystallised fluorobenzene but resides closer to a second monomer unit allowing for interaction with *meta* F2 as well as *para* F3; these are in addition to its primary coordination to *ipso* F4 and 1,4-dioxane's O3. Thus, the outcome of these *ancillary* bonding interactions by Na is a 2-D sheet network of fused rings (Figure 3.13). Each large ring is comprised of six Na atoms, four ferrated 1,2,4-trifluorobenzene units and two 1,4-dioxane rings; note that between the 2-D sheets, no observable bonding is present.

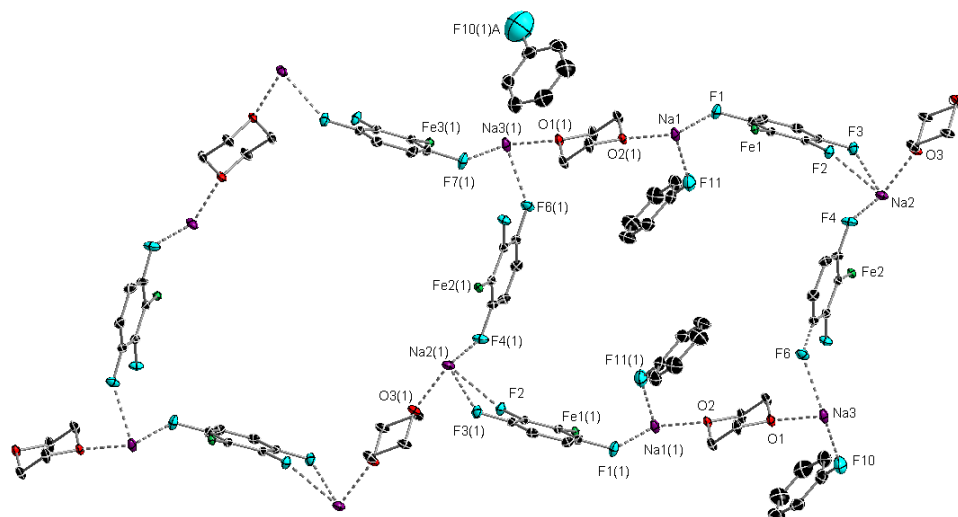


Figure 3.13 – The expanded 2-D sheet fused ring structure of complex **22**. Hydrogen atoms, HMDS groups and some co-crystallised fluorobenzene solvent groups are omitted for clarity. Disordered fluorobenzene component (F10/F10(1)A) shown in both modelled positions, 65%/35% occupancy, respectively. Thermal ellipsoids displayed at 25% probability level. Selected bond distances (Å): Na1-F1 2.2173(18), Na1-F11 2.749(2), Na1-O2(1) 2.2984(16), Na1-F9(2) 2.4615(18) (not pictured), Na2-F2 2.8763(17), Na2-F3 2.3556(18), Na2-F4 2.2868(18), Na2-O3 2.3138(17), Na3-F6 2.4406(19), Na3-F10 2.903(4), Na3-O1 2.3124(17), Na3-F7 2.2419(19) (not pictured).

The aryl H atoms are observed in the ^1H NMR spectrum of **22** in C_6D_6 at chemical shifts of 119.63 and -58.60 ppm. The broad resonance corresponding to HMDS is centred at -1.32 ppm.

1,2,4,5-tetrafluorobenzene presented an interesting case as it possesses two equally suitable positions on the ring for deprotonation each with a low calculated $\text{p}K_{\text{a}}$ value of 23.1.²⁴⁷ Hence, we decided to investigate whether we could deprotonate both positions with the application of two equivalents of sodium ferrate base. Refluxing the reaction for one hour and slow cooling yielded orange needle-like crystals of $[\{\text{dioxane}\cdot\text{NaFe}(\text{HMDS})_2\}_2(1,2,4,5\text{-C}_6\text{F}_4)]_{\infty}$ (**23**) (Figure 3.14) in a 76% yield.

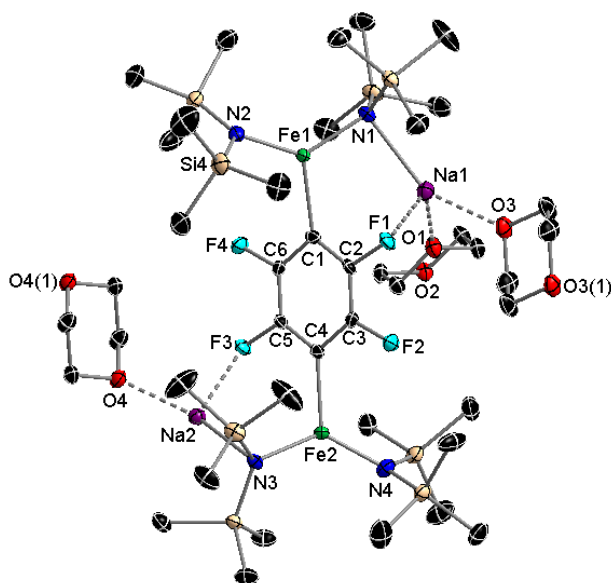


Figure 3.14 – Molecular structure of complex **23** with an extra equivalent of 1,4-dioxane shown. Hydrogen atoms and disorder in one SiMe₃ group are omitted for clarity. Thermal ellipsoids displayed at 50% probability level. Selected bond distances (Å) and angles (°): Fe1-C1 2.140(3), Fe1-N1 2.012(2), Fe1-N2 1.951(3), Fe1---Na1 3.3435(13), Na1-N1 2.503(3), Na1-F1 2.334(2), Na1-O1 2.384(2), Na1-O3 2.352(3), Fe2-C4 2.128(3), Fe2-N3 2.007(2), Fe2-N4 1.954(3), Fe2---Na2 3.3886(12), Na2-N3 2.525(3), Na2-F3 2.261(2), Na2-O4 2.315(2), Na2-O2(1) 2.364(2); C1-Fe1-N1 113.56(11), C1-Fe1-N2 115.31(11), N1-Fe1-N2 130.74(11), Na1-N1-Fe1 94.94(10), Na1---Fe1-N2 166.21(8), Na1-F1-C2 100.69(16), N1-Na1-F1 99.18(8), N1-Na1-O1 124.34(9), N1-Na1-O3 146.37(10), O1-Na1-O3 85.34(9), O1-Na1-F1 105.43(8), O3-Na1-F1 85.62(8), C4-Fe2-N3 110.92(11), C4-Fe2-N4 118.77(11), N3-Fe2-N4 130.31(11), Na2-N3-Fe2 96.11(10), Na2---Fe2-N4 142.99(8), Na2-F3-C5 125.72(16), N3-Na2-F3 104.58(8), N3-Na2-O4 148.75(9), N3-Na2-O2(1) 125.96(9), O4-Na2-O2(1) 79.94(8), O4-Na2-F3 93.87(8), O2(1)-Na2-F3 85.04(8).

Splendidly, di-ferration of 1,2,4,5-tetrafluorobenzene was achieved under these conditions. The structure of the monomeric unit reveals opposing Fe-C bonds at C1 and C4 positions on the aryl ring, similarly Na-F contacts are made at positions *para* to one another. With the arene capped on both sides, opportunity for secondary Na---F interactions is unobtainable however 1,4-dioxane plays a role in the wider structure. Expanded, **23** is a 2-D network structure with propagation along the *x* axis by 1,4-dioxane oxygen atoms O3(1) and O4(1) and propagation along the *y* axis through O2. The net result is a honeycomb structure with two sizes of ring present.

Accordingly, the ¹H NMR spectrum of **23** displays no highly shifted signals for aryl H atoms, just a broad signal and very broad signal for 1,4-dioxane and HMDS H atoms, respectively around the expected chemical shifts (4.06 and -2.49 ppm, respectively).

To put complex **23** into context, only two structurally characterised examples exist featuring a di-metallated 1,2,4,5-C₆F₄ ring (Figure 3.15, left). The dinuclear nickel complex [1,4-

$\{\text{Ni}(\text{}^i\text{Pr}_2\text{Im})_2(\text{Cl})\}_2(\text{C}_6\text{F}_4)$] was synthesised by a two-fold C-F activation (oxidative addition) process of hexafluorobenzene with $[\text{Ni}_2(\text{}^i\text{Pr}_2\text{Im})_4(\text{COD})]$ and subsequent transhalogenation at Ni with Me_3SiCl .²⁵¹ Interestingly, the other example is a dinuclear iron(II) complex, $[\text{1,2,4,5-C}_6\text{F}_4(\text{Fp}^\ddagger)_2]$ (where $\text{Fp}^\ddagger = (\eta^5\text{-C}_5\text{H}_5)\text{Fe}(\text{CO})_2$) (Figure 3.15, right),²⁵² though this complex was synthesised via di-lithiation of 1,4-dibromotetrafluorobenzene and reaction with $\text{Fp}^\ddagger\text{I}$.²⁵³

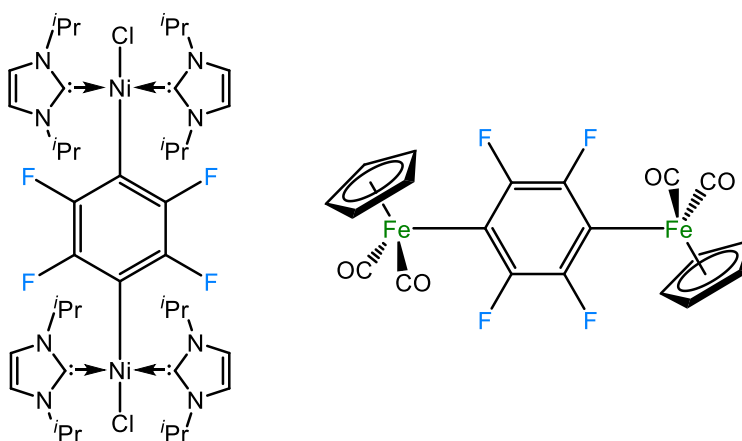


Figure 3.15 – Structurally characterised examples of di-metallated 1,2,4,5- C_6F_4 rings by Ni^{251} and Fe^{252}

Due to time constraints mono-metallation of 1,2,4,5-tetrafluorobenzene was not attempted, though it would be reasonable to assume this could be achieved with a single equivalent of base at low temperature (0°C), certainly when one considers latter results detailed *vide infra* (see Section 4.2.1). Direct mono-C-H activation has been achieved and structurally authenticated by Au ,²⁵⁴ Ni ,²⁵⁵ Pt ,²⁵⁶ Re ²⁵⁷ and Rh ²⁵⁸ complexes.

Pentafluorobenzene offers only one site for deprotonation, which was satisfyingly achieved by the sodium ferrate. Large green crystals obtained from the reaction were analysed by X-ray crystallography to reveal $[\text{dioxane}\cdot\{\text{NaFe}(\text{C}_6\text{F}_5)(\text{HMDS})_2\}_2]_\infty$ (**24**) in a 90% yield (Figure 3.16).

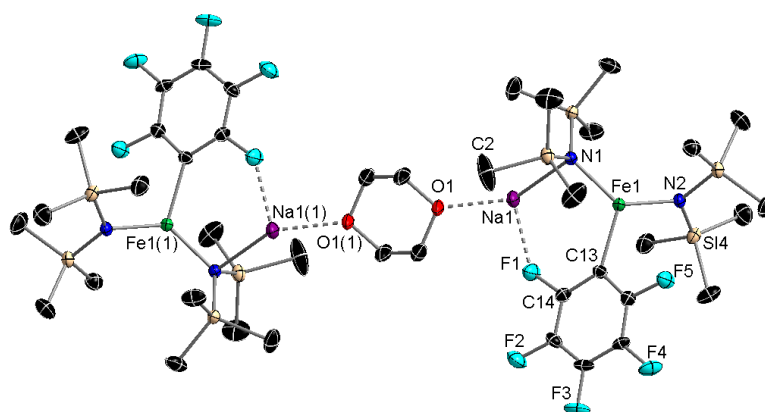


Figure 3.16 – Molecular structure of complex **24**. Hydrogen atoms and a molecule of co-crystallised benzene solvent omitted for clarity. Thermal ellipsoids displayed at 50% probability level. Selected bond distances (Å) and angles (°): Fe1-C13 2.117(3), Fe1-N1 1.995(2), Fe1-N2 1.941(2), Fe1---Na1 3.3427(11), Na1-F1 2.261(2), Na1-N1 2.491(2), Na1-O1 2.268(2), Na1---C2 3.078(4), Na1---F4(2) 2.463(2); C13-Fe1-N1 115.83(10), C13-Fe1-N2 112.70(10), N1-Fe1-N2 131.08(10), Na1-N1-Fe1 95.69(9), Na1---Fe1-N2 137.27(7), Na1-F1-C14 135.03(16), N1-Na1-F1 102.94(8), O1-Na1-F1 98.28(8), O1-Na1-N1 143.03(9).

The structure of compound **24** is almost identical to that of complex **21**. The symmetrically equivalent dimer unit is centrally bridged by 1,4-dioxane with the metallated rings anti-periplanar to one another. Na1 holds a secondary electrostatic contact to F4(2) on a separate perpendicular dimer unit (2.463(2) Å), the result of this is that like complex **21**, complex **24** exists as a 2-D fused ring network of interconnected dimers (Figure 3.18).

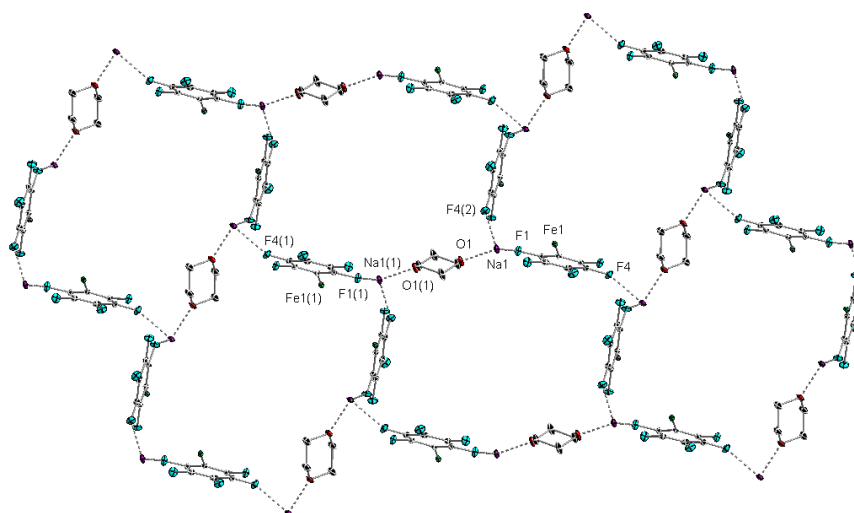


Figure 3.17 – Expanded polymeric structure of complex **24**. Hydrogen atoms, HMDS groups and co-crystallised benzene solvent omitted for clarity. Thermal ellipsoids displayed at 25% probability level. Selected bond distances: Na1-F1 2.261(2), Na1---F4(2) 2.463(2).

With no remaining aryl H atoms the ^1H NMR spectrum of **24** simply displays resonances for 1,4,-dioxane and HMDS H atoms at 3.60 and -1.91 ppm, respectively.

3.2.4.2 Structural and Spectroscopic Studies on Metallated Intermediates of Direct Ferration Reactions: (b) Other Substituted Fluoroarenes

Moving away from increasing fluorine atoms on the aromatic ring, we were curious to see whether polycyclic 1-fluoronaphthalene could be ferrated. Possessing just one hydrogen *ortho* to a single F atom (thus rendering the position fairly unactivated), it was decided to run the reaction in neat 1-fluoronaphthalene, heating overnight at 50°C. Green rod crystals obtained were subjected to X-ray crystallography uncovering the structure [$\{dioxane \cdot NaFe(1-C_{10}H_6F)(HMDS)_2\}_\infty$] (**25**) (Figure 3.18), synthesised in a low 26% yield (due in part to the high boiling point 1-fluoronaphthalene, which did not allow for adequate concentration of the solution).

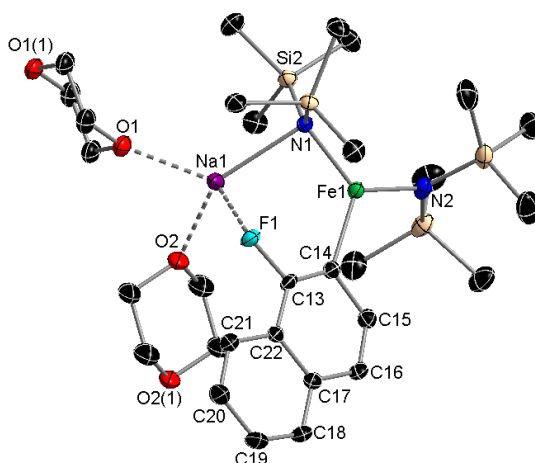


Figure 3.18 – Molecular structure of complex **25** with extra equivalent of 1,4-dioxane shown in the asymmetric unit. Hydrogen atoms omitted for clarity. Thermal ellipsoids displayed at 50% probability level. Selected bond distances (Å) and angles (°): Fe1-C14 2.0029(16), Fe1-N1 2.0029(16), Fe1-N2 1.9552(16), Fe1---Na1 3.3122(8), Na1-F1 2.2277(14), Na1-N1 2.4805(17), Na1-O1 2.3404(16), Na1-O2 2.3203(16); C14-Fe1-N1 116.47(7), C14-Fe1-N2 117.86(8), N1-Fe1-N2 125.55(7), Na1-N1-Fe1 94.66(6), Na1---Fe1-N2 149.78(5), Na1-F1-C13 119.80(11), N1-Na1-F1 90.44(5), O1-Na1-O2 84.11(6).

As observed in Figure 3.18 direct ferration occurs at the C2 position, whilst the Na atom engages with the F atom. The extended structure of **25**, a 1D ‘zigzag’ polymeric chain, is essentially isostructural with complexes **18** and **19**, made up by Na-O dative bonding involving the dioxane ligands and neighbouring $\{NaFe(1-C_{10}H_6F)(HMDS)_2\}$ units.

Resonances for the five of the six aromatic H atoms were found in the 1H NMR spectrum of **25** in C_6D_6 , ranging from 70.63 to -20.12 ppm. Broad resonances for 1,4-dioxane and HMDS

H atoms appear at 4.13 and -2.98 ppm, respectively; it is certainly conceivable the sixth ring H atom signal may be completely hidden underneath the very broad HMDS signal.

In order to assess the influence of heteroatoms present on the aryl ring and explore a little further the sodium ferrate system's affinity for fluorine and C-H activation *ortho* to F a number of fluorobenzenes with heteroatoms present were explored as substrates.

1-bromo-3,5-difluorobenzene has three possible reaction sites for metallation on the ring; two of its H atoms are between Br and F and the third H is between two F atoms. The latter site is likely to be the most activated considering F atoms higher electronegativity and thus stronger inductive effect, indeed this position is favoured by LiTMP which upon carboxylation yields a single product in an 84% yield.²²⁵ One equivalent of 1-bromo-3,5-difluorobenzene was reacted with sodium ferrate **17a** in benzene at 0°C and stirred for two hours with the metallation occurring regioselectivity at the H that is located between the two F atoms. Stirring was stopped and the solution was left to reach ambient temperature overnight upon which green block crystals were formed. X-ray crystallography revealed the structure [dioxane·{dioxane·NaFe(1-Br-3,5-C₆H₂F₂)(HMDS)₂}₂] (**26**) (Figure 3.19), recovered in a 60% yield (maximum possible yield 66.67% due to 1.5 eq. of 1,4-dioxane required).

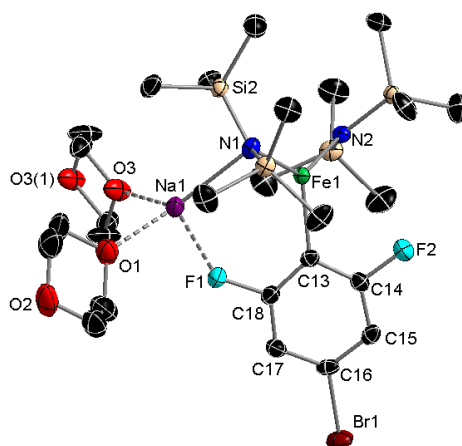


Figure 3.19 – Asymmetric unit of complex **26** with an extra half equivalent of 1,4-dioxane shown. Hydrogen atoms and disorder in one 1,4-dioxane group and one TMS group are omitted for clarity. Thermal ellipsoids displayed at 50% probability level. Selected bond distances (Å) and angles ($^{\circ}$): Fe1-C13 2.093(2), Fe1-N1 1.9902(17), Fe1-N2 1.9429(17), Fe1---Na1 3.3158(9), Na1-F1 2.3170(16), Na1-N1 2.507(2), Na1-O1 2.3010(19), Na1-O3 2.3407(18); C13-Fe1-N1 119.46(8), C13-Fe1-N2 112.67(8), N1-Fe1-N2 127.48(7), Na1-N1-Fe1 94.30(7), Na1---Fe1-N2 137.56(5), Na1---F1-C18 134.13(13), N1-Na1---F1 104.09(6), O1---Na1-N1 134.34(7), O1-Na1-F1 100.68(7), O1-Na1-O3 89.62(7), O3-Na1-N1 126.02(7), O3-Na1-F1 93.29(7).

The structure is a discreet dimer, bridging through 1,4-dioxane molecule. Na completes its coordination sphere by engaging with a second molecule of 1,4-dioxane, which is terminal and does not bridge.

A heated 3:1 (**17a**:substrate) reaction with 1-bromo-3,5-difluorobenzene is discussed in Section 4.2.6.

In order to explore and assess the coordinative and inductive effects of the methoxy group in comparison to fluorine substituents on the aryl ring, anisole and fluoroderivatives 3-fluoroanisole and 3,5-difluoroanisole were chosen as substrates.

Incorporating oxygen into the substrate, 3-fluoroanisole has a doubly activated hydrogen position between the methoxy and fluorine groups, providing an interesting scenario as to whether Na will coordinate preferentially to O or F. A 1:1 reaction at 50°C overnight provided large green crystals which were found to be $[\{(dioxane)_2 \cdot Na_2Fe(3-C_6H_3FOMe)(HMDS)_2\}^+ \{Fe(HMDS)_3\}^-]_\infty$ (**27**) (Figure 3.20).

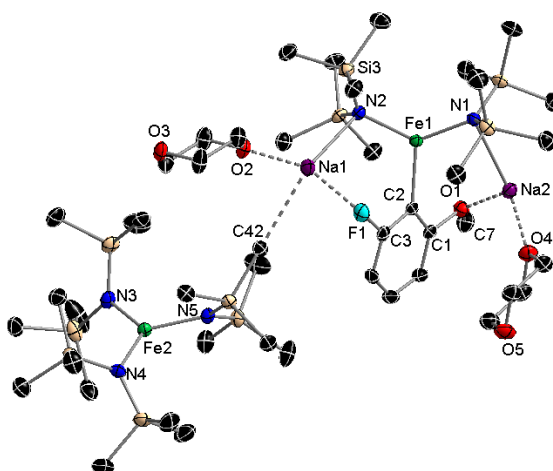


Figure 3.20 – Asymmetric unit of complex **27**. Hydrogen atoms and solvent omitted for clarity. Thermal ellipsoids displayed at 50% probability level. Selected bond distances (Å) and angles (°): Fe1-C2 2.106(3), Fe1-N1 1.986(2), Fe1-N2 1.998(2), Fe1---Na1 3.5063(12), Fe1-Na2 3.2664(12), Fe2-N3 1.995(2), Fe2-N4 1.989(2), Fe2-N5 1.991(2), Na1-F1 2.309(2), Na1-N2 2.549(3), Na1-O2 2.376(2), Na1---C42 2.9272(1), Na2-O1 2.403(2), Na2-N1 2.599(3), Na2-O4 2.365(2), Na2-O3(1) 2.387(2); C2-Fe1-N1 114.80(10), C2-Fe1-N2 110.72(10), N1-Fe1-N2 134.44(10), N3-Fe2-N4 120.39(10), N3-Fe2-N5 118.76(10), N4-Fe2-N5 120.81(10), Na1-N2-Fe1 100.22(9), Na1---Fe1-N1 149.83(7), Na1-F1-C3 110.57(15), N2-Na1-F1 96.24(8), N2-Na1-O2 124.44(9), N2-Na1---C42 143.567(2), O2-Na1-F1 124.66(8), O2-Na1---C42 82.334(2), C42---Na1-F1 84.219(2), Na2-N1-Fe1 89.83(9), Na2---Fe1-N2 164.58(7), Na2-O1-C1 97.96(16), N1-Na2-O1 100.56(8), N1-Na2-O4 128.12(9), N1-Na2-O3(1) 135.60(9), O4-Na2-O1 110.56(9), O4-Na2-O3(1) 80.28(8), O3(1)-Na2-O1 98.22(8).

Interestingly, we see sodium accomplishing coordination with both substituents by means of a disodium ferrate cation, $\{(\text{dioxane})_2 \cdot \text{Na}_2\text{Fe}(\text{3-C}_6\text{H}_3\text{FOMe})(\text{HMDS})_2\}^+$, (balanced by a $\{\text{Fe}(\text{HMDS})_3\}^-$ anion) in this SSIP structure. The structure of **27** is very similar to that of complex **20**; here we see Na1 bonding with F, 1,4-dioxane (O2) and HMDS (N2), alike with the other ferrated fluoroarene structures, but it completes its coordination sphere via a long electrostatic contact to a methyl group of the $\{\text{Fe}(\text{HMDS})_3\}^-$ anion (Na1---C42 2.9272(1) Å), an appreciably longer Na---C distance than observed in either **20** or **8** (2.854(1) and 2.727(2) Å, respectively). The second sodium atom, Na2, is coordinated by the methoxy group oxygen (Na2-O1 2.403(2) Å) in addition to the other HMDS group bridging to Fe1, a terminal 1,4-dioxane group (O4) and a bridging 1,4-dioxane group (O3) of a second monomeric unit, resulting in 1-D linear chain for the cationic units.

The methoxy group hydrogens resonance is visible in the ^1H NMR spectrum of **27**, upfield at a chemical shift of -14.75 ppm whilst aryl H atom resonances are visible at 105.39, 99.84 and -69.48 ppm. Two very broad resonances for the inequivalent HMDS groups overlap, peaking at -2.56 and -4.76 ppm whilst the signal for 1,4-dioxane appears at 8.22 ppm.

Acknowledging that in complex **27**, sodium forms an electrostatic contact to the methoxy group for the ferration of 3-fluoroanisole, we questioned whether the fluorine group is necessary for metallation of the aryl ring and whether the OMe would be sufficiently activating enough to facilitate direct *ortho*-ferration.

Anisole's *ortho* hydrogens have an estimated $\text{p}K_{\text{a}}$ of 39.0,^{259–261} thus it was hypothesised that with a single OMe group present, *ortho* H atoms may not be sufficiently acidified (alike with fluorobenzene) and so ferration was attempted in neat anisole. When anisole was reacted with sodium ferrate **17a** no metallation was observed. Cooling down of the solution in neat anisole led to the isolation of coordination complex $[\text{dioxane} \cdot \{\text{Na}(\text{PhOMe})_3\}_2]^{2+}[\{\text{Fe}(\text{HMDS})_3\}_2]^{2-}$ (**28**) (Figure 3.21) in a 20% yield (maximum possible yield 50% due to 2:1 base to substrate required).

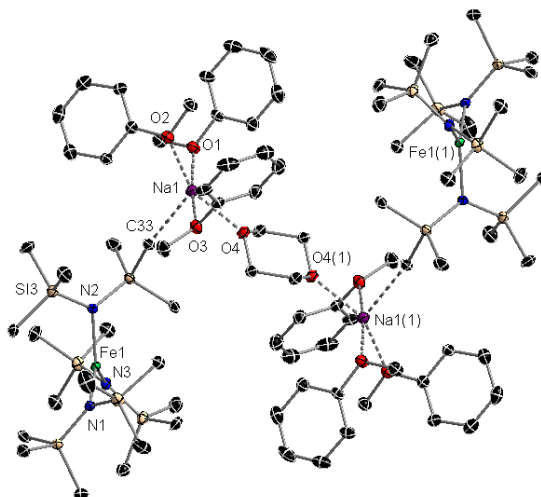


Figure 3.21 – Structure of complex **28**. Hydrogen atoms and solvent omitted for clarity. Thermal ellipsoids displayed at 30% probability level. Selected bond distances (Å) and angles (°): Fe1-N1 1.9781(17), Fe1-N2 1.9924(16), Fe1-N3 1.9798(18), Na1-O1 2.3824(18), Na1-O2 2.3852(17), Na1-O3 2.3780(18), Na1-O4 2.3419(16), Na1---C33 2.8978(1); N1-Fe1-N2 119.50(7), N1-Fe1-N3 120.93(7), N2-Fe1-N3 119.55(7), O1-Na1-O2 89.18(6), O1-Na1-O3 171.71(7), O1-Na1-O4 95.70(6), O1-Na1---C33 85.111(2), O2-Na1-O3 85.93(6), O2-Na1-O4 151.53(7), O2-Na1---C33 129.210(2), O3-Na1-O4 85.53(6), O3-Na1---C33 103.165(2), O4-Na1---C33 79.221(2).

Exhibiting a SSIP structure, **28**, contains a Na centre solvated by three molecules of anisole and a molecule of 1,4-dioxane (half equivalent). In addition Na forms a long distance electrostatic contact (Na1---C33 2.8978(1) Å) with a Me group on the $\{\text{Fe}(\text{HMDS})_3\}^-$ anionic unit. Here Na resides in a pseudo square-based pyramidal geometry with the O atoms providing the base of the pyramid and Me as the peak (sum of O angles around Na = 356.34°, range 85.53 to 89.18°). 1,4-dioxane bridges between symmetrically equivalent Na atoms resulting in an overall dimeric structure.

In order to counter the strong coordinating effect of the anisole that results in the abstraction of the Na atom away from Fe, an equimolar reaction in benzene was attempted, heating overnight at 50°C. Like fluorobenzene however (when metallation was attempted on an equimolar scale), the only crystals recovered were that of **17** and no evidence of metallation was observed by ^1H NMR spectroscopy of the solid.

To assess the optional site selectivity of the sodium ferrate base, the ferration of 3,5-difluoroanisole was attempted. When considering the reactions with anisole and 3-fluoroanisole, would ferration occur preferentially at either of the two positions flanked by the

superior coordinating OMe group and F or at the single site between the two more inductive F atoms.

Stirring for an hour before leaving sedentary overnight resulted in a change of solution colour from green to tan/brown from which crystals of [dioxane·{NaFe(3,5-C₆H₂F₂OMe)(HMDS)₂}]₂ (29) (Figure 3.22) were recovered at 5°C in a 51% yield.

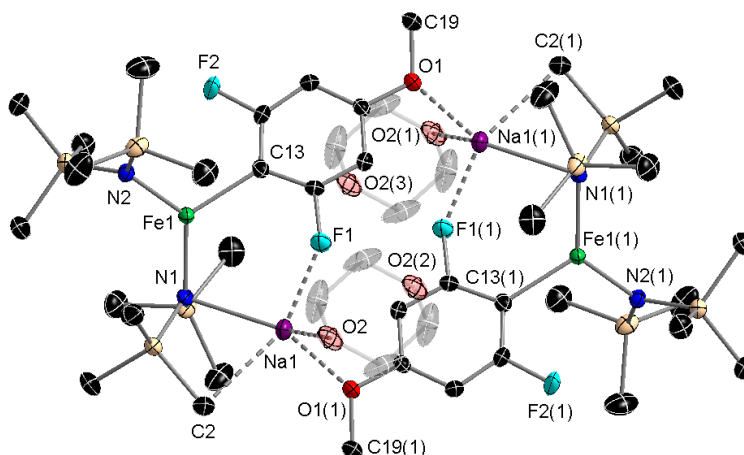


Figure 3.22 – Dimeric unit of complex **29**. Hydrogen atoms and solvent omitted and 1,4-dioxane transparent for clarity. Thermal ellipsoids displayed at 50% probability level. Selected bond distances (Å) and angles (°): Fe1-C13 2.1078(17), Fe1-N1 2.0077(14), Fe1-N2 1.9395(14), Fe1---Na1 3.5442(7), Na1-F1 2.2450(12), Na1-N1 2.5257(15), Na1-O2 2.3397(14), Na1-C2 2.7535(1), Na1-O1(1) 2.3745(14); C13-Fe1-N1 117.57(6), C13-Fe1-N2 115.02(6), N1-Fe1-N2 127.41(6), Na1-N1-Fe1 102.25(6), Na1---Fe1-N2 149.63(4), Na1---F1-C18 139.46(9), N1-Na1-F1 96.18(5), N1-Na1-O2 132.11(6), N1-Na1-O1(1) 133.81(5), O2-Na1-F1 78.55(5), O2-Na1-O1(1) 91.28(5), O1(1)-Na1-F1 109.40(5).

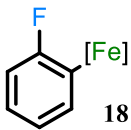
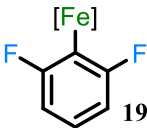
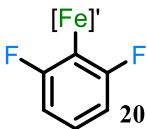
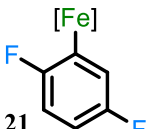
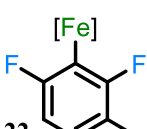
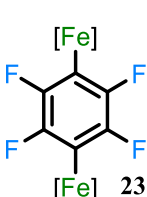
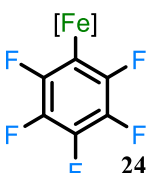
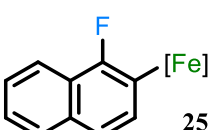
Clear preference is established for metallation at the 4-position between the two F atoms with construction of a single new Fe-C bond (2.1078(17) Å). Interestingly however, the methoxy group is still able to achieve coordination, O1 bonding to Na1(1) of a second ferrated unit at a distance of 2.3745(14) Å creating a dimeric structure with a 12-membered {NaFCCCO}₂ ring. The expanded structure is a linear 1-D network of cyclodimers where propagation is facilitated by 1,4-dioxane (through O2(2) and O2(3)) bridging between sodium atoms.

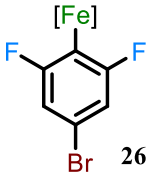
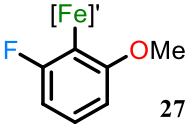
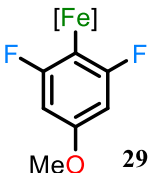
Considering these three results in addition to that of 4-fluoroanisole (Table 3.1, entry 10), it can be concluded sodium ferrate base [dioxane·NaFe(HMDS)₃] (**17a**) follows with the trend of fully complexed bases (e.g. ⁿBuLi/PMDETA and superbasic mixtures) in favouring attack at the most inductively activated position, *ortho* to F. Indeed when we consider substrates which failed to show evidence of ferration (*vide infra*, Section 3.2.7) we postulate that fluorine and the establishment of a strong Na-F interaction plays a major role in facilitating ferration.

3.2.5 Structural Summary

Table 3.3 below summarises the Fe-C σ -bond distances and the bond lengths of the primary and secondary Na---F electrostatic interactions for the structurally characterised ferrated intermediate complexes.

Table 3.3 – Fe-C and Na-F Bond lengths (Å) for isolated ferrated fluoroarenes.

Compound ^a	Bond Length	
	Fe-C	Na-F ^b
 18	2.102(4)	2.206(3)
 19	2.1157(18)	2.3437(13)
 20	2.1026(17)	2.3308(13) (Na1-F1) 2.3573(13) (Na2-F2)
 21	2.094(3)	2.256(2) (Na1-F1) 2.359(2) (Na1---F2(2))
 22	2.114(2)	2.2173(18) (Na1-F1) 2.4615(18) (Na1---F9(2))
 23	2.140(3) (Fe1-C1) 2.128(3) (Fe2-C4)	2.334(2) (Na1-F1) 2.261(2) (Na2-F3)
 24	2.117(3)	2.261(2) (Na1-F1) 2.463(2) (Na1---F4(2))
 25	2.0029(16)	2.2277(14)

	2.093(2)	2.3170(16)
	2.106(3)	2.309(2)
	2.1078(17)	2.2450(12)
Longest	2.140(3) (23)	2.3437(13) (19) 2.463(2) (Na1---F4(1)) (24)
Shortest	2.0029(16) (25)	2.206(3) (18)
Mean	2.1019	2.2820 ^c 2.3093 ^d

^a[Fe] = {(dioxane)_n·NaFe(HMDS)₂}; [Fe]' = {(dioxane)_n·Na₂Fe(HMDS)₂} ^bNa---F denotes a secondary polymer propagating interaction; ^cAverage of primary Na-F bonds; ^dAverage of primary Na-F and secondary Na---F bonds.

Di-ferrated 1,2,4,5-tetrafluorobenzene (**23**) contains the longest Fe-C bond lengths of any of the ferrated fluorobenzene complexes at lengths of 2.140(3) and 2.128(3) Å. Ferrated 1-fluoronaphthalene (**25**) displays the shortest Fe-C bond distance of 2.0029(16) Å, a difference of 0.1371 Å from the longest Fe-C bond length. The mean Fe-C bond length is 2.1019 Å.

On average these Fe-C distances are longer than those observed in other structurally characterised examples of Fe(II) bonded to a fluoroarene. For example [Fe{C₆F₄C(O)Me-2}(η⁵-C₅H₅)(PMe₃)] contains an Fe-C bond of distance 1.929(3) Å (Figure 3.23, top left)²⁶² and a reported Fe-fluorophenylarylimine complex²⁶³ (Figure 3.23, top right) possesses an Fe-C bond length of 1.991 Å whilst conversely, complex [{(Ph₂CN)₂C₂H₄}Fe(CH₂SiMe₃)C₆F₅] has a noticeably longer bond length of 2.132(7) Å (Figure 3.23, bottom).²⁶⁴

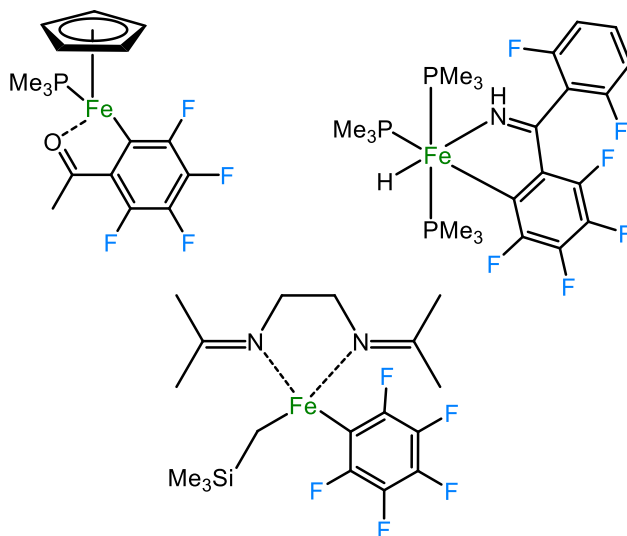


Figure 3.23 – A selection of complexes where an Fe(II) centre is bonded to a fluoroaryl moiety.

If one discounts the secondary intermolecular (polymer propagating) Na---F interactions, the difference between the longest and shortest primary Na-F electrostatic interaction bond lengths is 0.1377 Å, very similar to the difference between the longest and shortest Fe-C bond lengths. The shortest Na-F distance is displayed in ferrated fluorobenzene complex **18** at 2.206(3) Å, whilst the longest is shown by ferrated 1,3-difluorobenzene complex **19** (2.3437(13) Å). All the Na-F dative interactions are well within the sum of the van der Waals radii for Na and F (2.27 + 1.47 = 3.74 Å, respectively).²⁶⁵ For reference, the Na-F bond distance in pure NaF is 1.9260 Å (determined by microwave spectroscopy).²⁶⁶

According to the CCDC, 127 crystallographically characterised compounds to date containing a Na-F bond (Na---F, any bond) have been reported; the longest bond length stands at 3.039 Å, observed in [$\{\text{Na}(3\text{-(thiophen-2'-yl)-phen})\text{BF}_4\}_\infty$]²⁶⁷ and the shortest is recorded at 1.991 Å in $[(\text{Cp}^*\text{Rh})_4(\mu\text{-thym})_4\text{Na}]^+[\text{PF}_6]^-$ (Cp* = pentamethylcyclopentadienyl, thym = thymine²⁻).²⁶⁸ The mean Na-F bond distance between all 127 compounds is 2.4128 Å; clearly the Na-F electrostatic interactions in the ferrated structures are towards the shorter end of the scale with a mean distance of 2.3093 Å. The Na-F distance reported for the zincated²⁴³ α,α,α -trifluorotoluene structure noticeably longer at 2.435 Å, as are the distances of the sodiated²⁴⁴ α,α,α -trifluorotoluene structures (see Section 3.1.1) at 2.6415(7) and 2.6750 Å (TMEDA and PMEDTA complexes, respectively).

Of the 11 ferrated intermediate structures, only complex **26** exists as a discrete dimer whilst the others exhibit structural diversity through a variety of supramolecular motifs facilitated by

intermolecular interactions of Na with either O or F. Compounds **18**, **19**, **20**, **25** and **27** exist as infinite 1D polymer chains propagating via Na-1,4-dioxane interactions. **21**, **22** and **24** are all very similar, displaying 2-D supramolecular motifs of dimers arranged in fused rings of equal size, whereas complex **23** exhibits two rings of unequal size in a 2-D arrangement. Complex **29** exists as 1-D polymer chain of repeating cyclodimeric units.

3.2.6 Magnetometry Studies of Ferrated Fluoroaromatic Complexes

The electronic structures of the Fe(II) centres in complexes **17-19** and **24** were studied through bulk magnetisation measurements. Molar paramagnetic susceptibility (χ_M) data was collected on microcrystalline samples in the warming mode from 2 to 300 K under a constant magnetic field of 0.5 T (0.3 T in the case of **24**). Additionally, this study was complemented with magnetisation measurements at 2 K under variable magnetic field (0 to 5 T). Resulting $\chi_M T$ vs T and $M/N\mu_B$ vs H curves together with their best fits are shown in Figure 3.24.

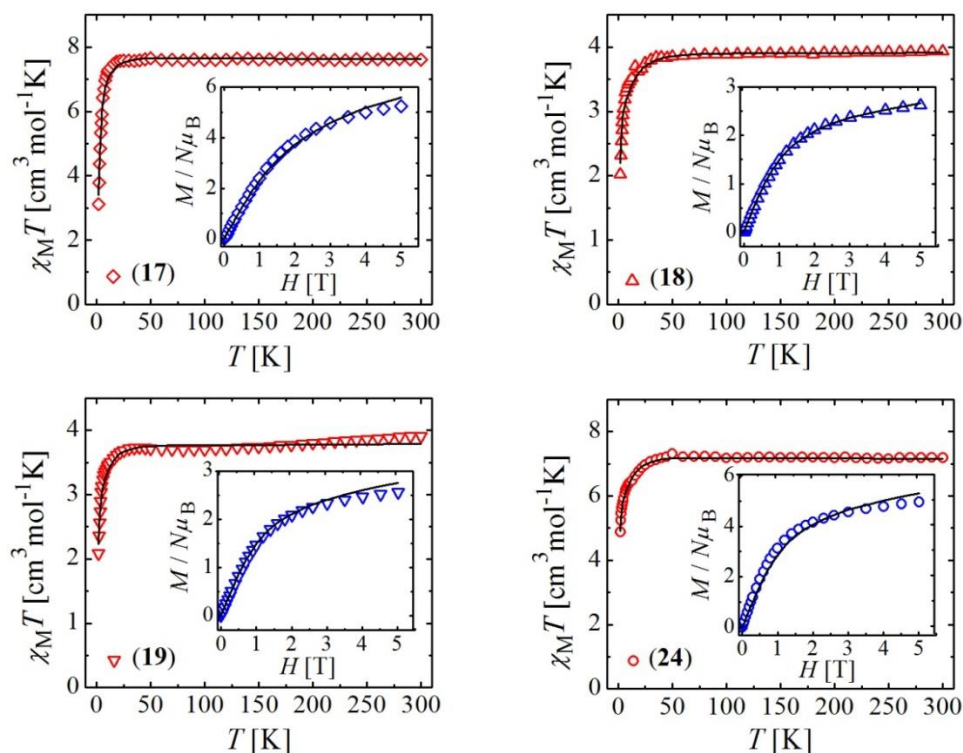


Figure 3.24 – $\chi_M T$ vs T and $M/N\mu_B$ vs H (inset) curves of compounds **17-19** and **24**. Measurement setup: warming mode (2→300 K), $B = 0.5$ T (0.3 T for **24**); $T_{\text{mag}} = 2$ K. Solid black lines represent the result of the fits.

In all cases, the displayed magnetic behaviour is as expected for compounds containing isolated high-spin iron(II) centres. At 300 K, the χ_{MT} product for compounds **18** and **19** is slightly higher than the expected value ($3.00 \text{ cm}^3 \text{ K mol}^{-1}$ for $g = 2.0$) for one uncoupled high-spin ($S = 2$) iron(II) centre (measured 3.93 and $3.90 \text{ cm}^3 \text{ K mol}^{-1}$, respectively). Similarly, compounds **17** and **24** with two isolated iron(II) centres in their magnetic unit exhibit higher values of χ_{MT} product (7.19 and $7.61 \text{ cm}^3 \text{ K mol}^{-1}$, respectively) from the expected value of $6.00 \text{ cm}^3 \text{ K mol}^{-1}$ ($g = 2.0$). The estimated g values using the Curie Law for the ambient temperature data are $g = 2.25$ (**17**), 2.29 (**18**), 2.28 (**19**) and 2.19 (**24**), suggesting the presence of unquenched angular momentum coupled to the electronic spin. Second-order spin orbit coupling is often observed for the trigonal-planar compounds of iron(II), where the ground state, lacking any orbital angular momentum ($L = 0$), is allowed to mix with low-lying excited electronic states with non-zero L .¹⁰⁶

Upon lowering the temperature, the χ_{MT} product remains practically constant down to 40 K. Sharp decreases are observed for all the products at the lowest temperatures, leading to χ_{MT} values of 3.11 , 2.02 , 2.09 and $4.88 \text{ cm}^3 \text{ K mol}^{-1}$ (for **17**, **18**, **19**, and **24**, respectively) at 2 K. The displayed behaviour can be explained as a manifestation of the zero-field splitting effects which additionally are obvious from the variable field magnetisation measurements at 2 K. For all compounds, $M/N\mu_B$ vs H curves stay far from saturation even at the highest magnetic fields (expected $4 \mu_B$ for one and $8 \mu_B$ for two $S = 2$ centres and $g = 2$). The measured magnetisation at 5 T for dinuclear compounds **17** and **24** are 5.26 and $4.96 \mu_B$, whereas for mononuclear compounds **18** and **19** the highest values of magnetisation were 2.62 and $2.56 \mu_B$, respectively.

In order to quantify the ZFS effects, the experimental data (χ_{MT} vs T and $M/N\mu_B$ vs H) were fit simultaneously using the program PHI¹⁴⁸ by matrix diagonalisation of the (perturbative) anisotropic spin Hamiltonian defined in Equation (3.1):

$$\hat{H} = D \left(\hat{S}_z^2 - \frac{1}{3} \hat{S}^2 \right) + E \left(\hat{S}_x^2 - \hat{S}_y^2 \right) + \mu_B \hat{S} g B \quad (3.1)$$

In this equation, D and E stand for axial and rhombic ZFS parameters, respectively, \hat{S} is the total spin operator of the individual Fe(II) ion and \hat{S}_i ($i = x, y, z$) are the operators of its components. B is the magnetic induction and μ_B is the Bohr magneton. Although the anisotropic g factor defined as $g_x = g_y \neq g_z$ was considered, only the isotropic g value was used

in order to avoid the overparameterisation of spin Hamiltonian. Contribution of intra- and intermolecular interactions (zJ) was also considered taking into account the connectivity between the spin carriers as well as the long-range ordering in the crystal structure. The results obtained from the fitting are presented in Table 3.4.

Table 3.4 – Fitting Parameters for compounds **17-19** and **24**.

Compound	$\chi_M T^a$ at r.t. (g)	μ_{eff}^b at r.t	$\chi_M T^a$ at 2 K	g	D (cm ⁻¹)	$ E $ (cm ⁻¹)	$ E /D$	zJ (cm ⁻¹)
17	7.61 (2.25)	11.02	3.11	2.25	9.3	1.7	0.18	0.05
18	3.93 (2.29)	5.61	2.02	2.27	-12.0	3.3	0.27	0.07
19	3.90 (2.28)	5.58	2.09	2.22	-9.1	2.9	0.32	0.07
24	7.19 (2.19)	10.73	4.88	2.18	-9.6	2.9	0.30	0.04

^aIn units of cm³ K mol⁻¹ ^bIn units of Bohr magnetons.

For compound **17**, the best fits reveal the presence of zero-field splitting with a positive value for the axial parameter D (9.3 cm⁻¹) and with a significant contribution from rhombic parameter $|E| = 1.7$ cm⁻¹ ($|E|/D = 0.18$). On the other hand, fits of the magnetic data for compounds with heteroleptic {Fe(HMDS)₂(Ar)} cores (Ar = aryl) led to the negative D values (-9.1 to -12.0 cm⁻¹) with larger rhombicity ($0.27 \leq |E|/D \leq 0.32$). The latter can be correlated with the structural data since the larger deviations of the iron(II) coordination environment from ideal three-fold symmetry are witnessed in the heteroleptic compounds containing fluorine substituted aryl ligands. Interestingly, the observed change from positive anisotropy in homoleptic compound **17** to negative anisotropy in heteroleptic {Fe(HMDS)₂(Ar)} complexes **18**, **19** and **24** confirms our previous findings¹⁹³ and agrees with reported data for similar compounds.^{85,111,189,208,269}

Di-ferrated 1,2,4,5-tetrafluorobenzene complex **23** was also subject to bulk magnetic measurements under the same conditions. Resulting $\chi_M T$ vs T and $M/N\mu_B$ vs H curves are shown in Figure 3.25.

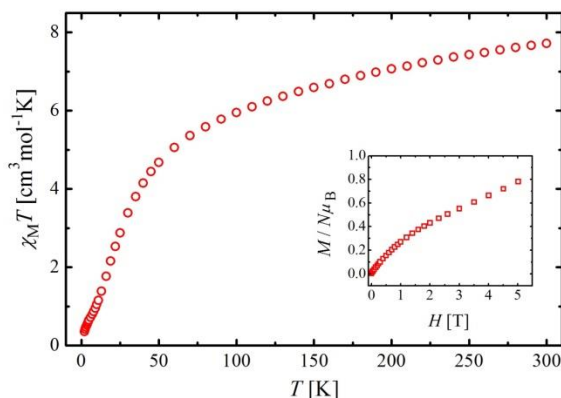


Figure 3.25 – $\chi_M T$ vs T and $M/N\mu_B$ vs H (inset) curves of compound **23**. Measurement setup: warming mode (2→300 K), $B = 0.5$ T; $T_{\text{mag}} = 2$ K.

At 300 K, the $\chi_M T$ product is higher than the expected spin-only value ($6.00 \text{ cm}^3 \text{ K mol}^{-1}$ for $g = 2.0$) for two uncoupled high-spin ($S = 2$) iron(II) centres (measured $7.72 \text{ cm}^3 \text{ K mol}^{-1}$). In the high temperature region from 150 K to 300 K, the $\chi_M T$ product linearly decreases upon cooling. Below 150 K ($6.59 \text{ cm}^3 \text{ K mol}^{-1}$), a more pronounced decline is present, resulting in an abrupt fall below 60 K ($5.06 \text{ cm}^3 \text{ K mol}^{-1}$). The final value of the $\chi_M T$ at 2 K is $0.36 \text{ cm}^3 \text{ K mol}^{-1}$. The behaviour displayed here indicates the existence of antiferromagnetic exchange interactions between two spin carriers in the molecule, possibly assisted by zero-field splitting effects. Variable field magnetisation measurements at 2 K show that the $M/N\mu_B$ vs H curve stays far from expected $8 \mu_B$ for two uncoupled $S = 2$ centres ($g = 2$). Measured magnetisation at 5 T of only $0.78 \mu_B$ additionally confirms the presence of antiferromagnetic interactions. In order to quantify the magnitude of observed coupling, experimental data was fit using the program PHI¹⁴⁸ by matrix diagonalisation of the spin Hamiltonian defined in Equation (3.2):

$$\hat{H} = -2J(\hat{S}_1\hat{S}_2) + \mu_B B \sum_i g_i \hat{S}_i \hat{H} + D \sum_i \left(\hat{S}_{iz}^2 - \frac{1}{3} \hat{S}_i^2 \right) \quad (3.2)$$

where J is the exchange constant, \hat{S}_i ($i = 1, 2$) is the total spin operator of the individual Fe(II) ions (\hat{S}_{iz} is the operator of its z -component), B is the magnetic induction, μ_B is the Bohr magneton, g is the isotropic g factor and D stands for the axial ZFS parameter. Unfortunately, a reasonable fit could not be obtained for the entire temperature range. The high temperature region (150-300 K) proved problematic and could only be modelled by using unreasonable temperature-independent paramagnetism contributions ($\text{TIP} > 0.001 \text{ cm}^3 \text{ mol}^{-1}$). The presence

of a small amount of antiferromagnetically coupled impurity in the measured sample could be the source of this problem. Nevertheless, fits of the experimental data below 150 K were successful (Figure 3.26) and yielded a set of reasonable parameters: fixed g factor at 2.25, exchange constant $J = -3.34 \text{ cm}^{-1}$ and $D = -3.58 \text{ cm}^{-1}$.

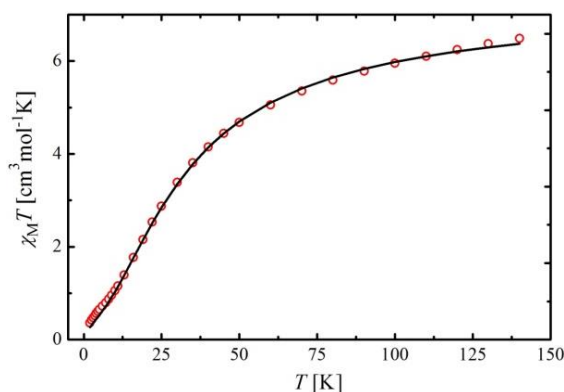


Figure 3.26 – $\chi_M T$ vs T and (2-150 K) curve of compound **23** with best fit (solid line). Measurement setup: warming mode (2→300 K), $B = 0.5 \text{ T}$.

The obtained exchange constant is slightly larger than the one reported for the compound $[\text{Na}_4\text{Fe}_2(\text{TMP})_6(\text{C}_6\text{H}_4)]$ ($J = -2.28 \text{ cm}^{-1}$, $g = 2.15$).⁸² The source of this difference could be the application of different g values, since a higher g will produce the higher exchange constant J . Secondly, it is possible that the close contacts between the sodium cations and iron coordinated carbon atoms from the phenyl bridge in $[\text{Na}_4\text{Fe}_2(\text{TMP})_6(\text{C}_6\text{H}_4)]$ slightly weaken the coupling between two iron sites. The DFT calculations reported for this compound indicate that the exchange coupling involves the interaction between the σ -orbitals of benzene and d orbitals of the iron(II) centres. Moreover, in the case of **23**, any additional contribution through the π -spin polarisation will increase the strength of antiferromagnetic interactions. Similarly, antiferromagnetic coupling through spin polarisation has been reported for pyrazine linked metal centres.^{270,271}

3.2.7 Negative Results

A number of other substrates were reacted with sodium ferrate **17a** in attempts to achieve direct ferration, the results of which were either inconclusive or showed no (or little) evidence of metallation.

Stimulated by the reported successful zincation²⁴³ and sodiation²⁴⁴ of α,α,α -trifluorotoluene (see Section 3.1.1), 1:1 and neat reactions of the substrate and **17a** were conducted but only starting material was recovered. Although the CF_3 group is strongly electron withdrawing, its inductive effect is less than that of F directly attached to the benzene ring,²⁷² demonstrated in one sense by the *ortho* position of α,α,α -trifluorotoluene which has a $\text{p}K_{\text{a}}$ of 39.7 versus that of fluorobenzene where it is 36.8.²⁴⁷ Additionally, with the involvement of an extra atom (C) between F and the ring it is also possible that even if an F engages with Na, sterically, the substrate may not be primed for *ortho*-ferration (i.e. the *ortho* C may be located too far from the Fe centre), though it must be said this was no barrier in the case of the sodium zincate where $[(\text{TMEDA})\text{NaZn}(\text{C}_6\text{H}_4\text{CF}_3)(\text{TMP})(^i\text{Bu})]$ displays a 7-membered $\{\text{NaFCCCZnN}\}$ ring.²⁴³

The tertiary amide group, $\text{C}(\text{O})\text{N}(^i\text{Pr})_2$, is regarded as one of the strongest directing groups for directed *ortho*-lithiation²⁷³ but reaction of *N,N*-diisopropylbenzamide with sodium ferrate **17a** (1:1, 50°C, 16 hr) produced no metallated product. Though mildly activating through inductive electron withdrawal, the coordinative effects of the tertiary amide group are chiefly responsible for its strong directing effect.

Reactions of **17a** with chloro and bromo substrates were not positive in promoting direct ferration. Reaction of **17a** in neat chlorobenzene (50°C, 16 hr) furnished no ferration product, nor did 1,3,5-trichlorobenzene or 3-bromobenzonitrile on at 1:1 stoichiometries under the same conditions.

Reaction of **17a** with 3-fluoropyridine on a 1:1 scale at 50°C for 3 hours and quenching with I_2 did show new products; iodination at the 2- and 4-positions in conversions of 14% and 8%, respectively. Noting the immediate colour change, reaction at ambient temperature for 5 minutes showed solely to the 4-position product in a marginally improved albeit low yield of 17%. Though an immediate change of colour for the solution from green to yellow was observed with 4-methoxypyridine (1:1, 50°C, 16 hr) no conversion to shown to any other iodinated product upon quenching. 1:1 reactions with pyrazine, 3-fluoronitrobenzene and benzothiazole showed solution colour changes but likely degradation of the sodium ferrate in the case of the former two (black solutions) and no ferrated products were obtained. With sensitive functional groups and moieties present such as nitriles, pyridines, etc. it is possible that these may coordinatively interact with either (or both) of the metal centres in such a way

that hinders or precludes direct ferration, possibly favouring the formation of less reactive SSIP intermediates.

Considering these observations coupled with the direct ferration results obtained with fluorobenzenes, a number of conclusions can be drawn about the reactivity of sodium ferrate base **17a**. Ferration has not been achieved with any non-fluorinated, yet moderately activated, aryl substrates, nor with any other halogen (Cl, Br) containing aryl substrates. Thus it appears that an activated ring proton with a suitable pK_a is not the sole requirement but the presence of an F atom is crucial for direct ferration. Fluorine's presence on the ring delivers a strong inductive effect, most strongly activating the *ortho* proton(s) towards deprotonative metallation. Secondly, when using base **17a**, fluorine's high electronegativity is highly attractive to electropositive, relatively hard cation Na^+ , as in all the structurally characterised ferrated intermediates a strong Na-F dative interaction is observed. This key interaction is the likely initiator for direct ferration in solution, bringing the substrate into close proximity to the Fe centre (pre-coordination) for deprotonative metallation (via the loss of HMDS(H)) and stabilising the newly ferrated aryl ring via the construction of a large 6-membered {NaNFeCCF} ring.

3.2.8 Other Structures Obtained from C-H Activation Studies

Throughout the course of investigations into direct ferration of fluorinated aryl substrates, a number of crystallographically characterised structures were obtained which do not display metallation of any fluorinated substrate but are nonetheless related.

3.2.8.1 Importance of Air and Moisture in Ferration Processes

Whilst the rigorous exclusion of molecular oxygen and atmospheric water is of highest priority to any chemist working with air-sensitive compounds it is a challenging task to control every aspect involved in synthesis to minimise the appearance of adventitious O_2 and H_2O to the last ppm. Oxo-inverse crown ether $[Na_2Fe_2(HMDS)_4(O)]$ (**30**) (Figure 3.27) has appeared numerous times during the syntheses of HMDS-based sodium ferrate species from the synthesis of homoleptic and solvent-free **1** to the metallations of fluorinated aryls.

Attempts to rationally prepare **30** by exposing reaction mixtures to oxygen using a drying tube containing CaCl_2 that precluded the presence of moisture were unsuccessful. Contrastingly, by adding H_2O (1 eq.) to $[\{\text{NaFe}(\text{HMDS})_3\}_\infty]$ (**1**) led to the isolation of **30** in an 81% yield.

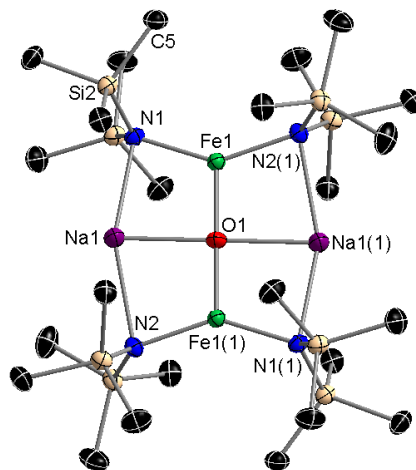


Figure 3.27 – Molecular structure of complex **30** which is centrosymmetric at O1. Hydrogen atoms omitted for clarity. Thermal ellipsoids displayed at 50% probability level. Selected bond distances (Å) and angles (°): Fe1-O1 1.8480(3), Fe1-N1 2.0016(16), Fe1-N2(1) 2.0000(16), Fe1---Na1 2.9462(9), Fe1---Na1(1) 3.0155(9), Na1-O1 2.3391(8), Na1-N1 2.5142(18), Na1-N2 2.5623(18); Fe1-O1-Fe1(1) 180.000(1), Na1-O1-Na1(1) 180, N1-Fe1-N2(1) 143.19(7), N1-Fe1-O1 109.30(5), Fe1-N1-Na1 80.58(6), Fe1-O1-Na1 88.63(2), N1-Na1-N2 155.33(6), N1-Na1-O1 80.57(4), Na1-N2-Fe1(1) 81.74(6), N2-Na1-O1 78.46(4), Na1-O1-Fe1(1) 91.37(2).

30 displays a cationic eight-membered $\{\text{NaNFeNNaNFen}\}$ ring which hosts at its core an oxo anion. O^{2-} resides as the “guest” in this inverse crown ether, situated centrally between the metal atoms, showing no deviation from the $\{\text{Na1Fe1Na1(1)Fe1(1)}\}$ plane. Fe resides closer to O at distance of 1.8480(3) Å whilst the Na1-O1 bond length is considerably longer at 2.3391(8) Å. The HMDS ligands reside at the four corner positions bridging between the iron and sodium atoms. Nitrogens N1 and N2 deviate 0.2826(1) and 0.2859(1) Å, respectively, below the $\{\text{Na1Fe1Na1(1)Fe1(1)}\}$ plane on one side of the square whilst the symmetrically equivalent nitrogens deviate the same distances above the plane on the opposing side of the square. Within the asymmetric unit, Na1 is positioned slightly closer to N1 (2.5142(18) Å) than to N2 (2.5623(18) Å), leading to two unequal angles of Na1-O1-Fe1 at 88.63(2)° and Na1-O1-Fe1(1) 91.37(2)°, which sum together to give a perfectly linear Fe1-O1-Fe1(1) angle of 180.000(1)° and by extension the same angle of 180.000(1)° for Na1-O1-Na1(1).

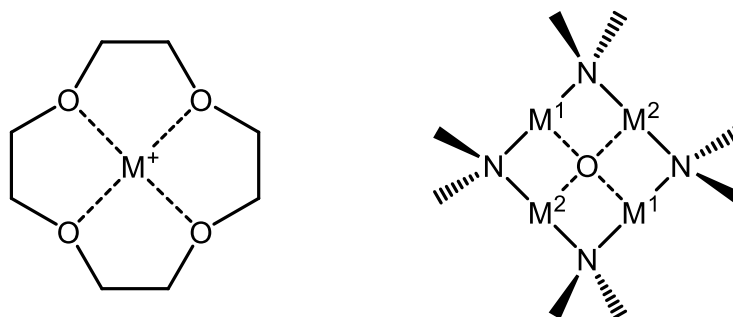


Figure 3.28 – Structural representations of a traditional crown ether and an inverse crown ether complex.

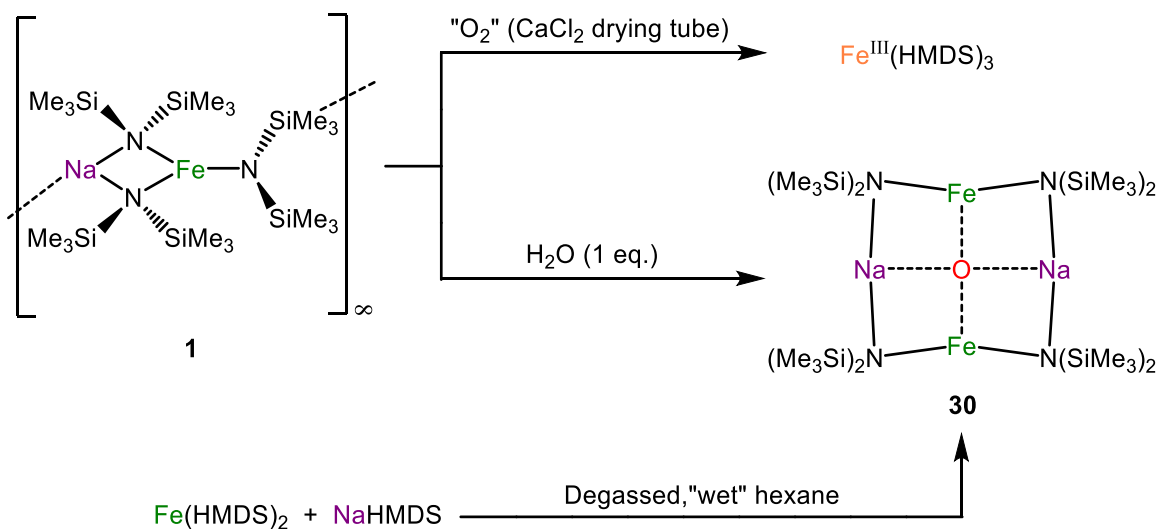
Recalling the introduction of inverse crown ether (ICE) complexes in Section I.I, these complexes are termed as such due to the role reversal present from conventional crown ether complexes (Figure 3.28). The encompassing ring of an ICE is Lewis acidic consisting of metal atoms and (generally amido) supporting ligands whereas the central “guest atom” is a Lewis basic oxygen species.^{29,30} As far as we can ascertain, **30** represents the first example of an inverse crown ether complex containing iron. Examples of Na-HMDS ICEs have been formerly reported with Mg²⁷⁴, Mn¹⁹⁴ and Zn²⁷⁵. All three examples are isostructural to **30** with the sodium atoms deviating from linearity (N-Na-N) whilst the lower polarity metal atoms are drawn into the square and the superoxo core remains perfectly central between the metal centres. On comparison of the bond lengths (Table 3.5), structure **30** possesses the longest Na-O distance of any of the Na-HMDS ICEs in addition to the shortest mean Na-N and M²-O bond lengths (where M² is the secondary metal).

Table 3.5 - Comparison of bond lengths (given in Ångstroms) between Na-HMDS inverse crown ether complexes. M² = Fe, Mg, Mn or Zn.

Bond	Na/Fe (30)	Na/Mg ²⁷⁴	Na/Mn ¹⁹⁴	Na/Zn ²⁷⁵
Na-O	2.3391(8)	2.3278(7)	2.3262(6)	2.265(2)
M ² -O	1.8480(3)	1.8575(4)	1.9272(2)	1.873(1)
Na-N1	2.5142(18)	2.549(1)	2.5269(13)	2.541(3)
Na-N2	2.5623(18)	2.595(1)	2.5627(14)	2.597(3)
Mean Na-N	2.5383	2.572	2.5448	2.569

Na/Fe inverse crown ether **30** crystallises with extreme ease at ambient and sub-ambient temperatures and is frequently easily identifiable as very well-formed and often large, emerald green rhombuses, which appear to be stable in air for several minutes.

In order to uncover the source of oxygen in **30** a series of reactions were run with hexane solutions of **1** (Scheme 3.13).



Scheme 3.13 – Reactions of **1** with “O₂”, H₂O or degassed “wet” hexane.

To the first solution of **1** (Scheme 3.13, top), a CaCl₂ filled drying tube was attached to the Schlenk and the argon flow was stopped whilst stirring was continued for three hours resulting in a noticeable darkening of the green solution. Dark green, thin rod crystals obtained from this reaction were analysed by X-ray crystallography and ¹H NMR spectroscopy confirming the synthesis of oxidation product Fe^{III}(HMDS)₃.^{125,276,277}

Evaluating water, addition of one equivalent of H₂O to a solution of **1** lead to a slight darkening of the green solution for which stirring was continued for one hour. Crystals formed from this reaction were found, after analysis by X-ray crystallography and ¹H NMR spectroscopy, to be that of complex **30**. Corroborating this result, crystals of **30** were obtained from the attempted synthesis of **1** in “wet”, degassed hexane. Hexane was taken straight from the bottle and was degassed by the freeze-pump-thaw method²⁷⁸ (three times in total) but not dried by any process. 20 mL of this hexane was added to Fe(HMDS)₂ and NaHMDS to synthesise **1**; Fe(HMDS)₂ was immediately solubilised giving a dark green/brown solution to which NaHMDS entered after an hour of stirring. After slow cooling, the solution furnished crystals of **30**. Collectively these results strongly suggest that the presence of moisture, and not O₂, is the likely origin for the formation of oxo-ICE **30** in HMDS sodium ferrate reactions.

The ^1H NMR spectrum of **30** in d_8 -tol shows a single broad resonance at -0.81 ppm. Owing to the ease of formation of **30**, a resonance at around this chemical shift can be seen in the ^1H NMR spectra of a number of other sodium ferrate species, corresponding to minor degradation of the sample or the presence of a small quantity of atmospheric moisture during synthesis, though in some cases it may be overlapping with or completely masked by a broad HMDS signal below 0 ppm for the principal sodium ferrate species measured.

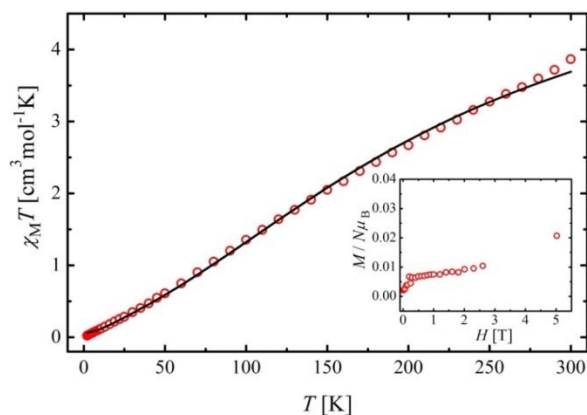


Figure 3.29 – $\chi_M T$ vs T and $M/N\mu_B$ vs H (inset) curves of compound **30**. Measurement setup: warming mode ($2 \rightarrow 300$ K), $B = 0.5$ T; $T_{\text{mag}} = 2$ K. Solid line represents the result of the fit.

Compound **30** was also characterised by SQUID magnetometry where molar paramagnetic susceptibility (χ_M) data was collected on microcrystalline samples in the warming mode from 2 to 300 K under a constant magnetic field of 0.5 T; resulting $\chi_M T$ vs T and $M/N\mu_B$ vs H curves are displayed in Figure 3.31. The results confirmed the presence of two paramagnetic Fe(II) centres within **30** which were found to display magnetic behaviour characteristic of a dinuclear complex with antiferromagnetic interactions between the spin carriers (i.e. the two Fe(II) centres).

At 300 K the value of $\chi_M T$ product of $3.87 \text{ cm}^3 \text{ K mol}^{-1}$ is significantly lower than expected for two non-interacting high-spin ($S = 2$) Fe(II) centres (the expected value is $6.00 \text{ cm}^3 \text{ K mol}^{-1}$ taking into account $g = 2.0$). Additionally, a pronounced and almost linear decrease of the $\chi_M T$ product is observed upon cooling ending at the final value of $0.023 \text{ cm}^3 \text{ K mol}^{-1}$ at 2 K. In order to quantify the magnitude of the observed coupling, experimental data were fit using the program PHI¹⁴⁸ by matrix diagonalisation of the anisotropic spin Hamiltonian defined in Equation (3.3).

$$\hat{H} = -2J(\hat{S}_1\hat{S}_2) + g\mu_B B\hat{S}_i + D\left(\hat{S}_{iz}^2 - \frac{1}{3}\hat{S}_i^2\right) \quad (3.3)$$

where J is the exchange constant, \hat{S} is the total spin operator (\hat{S}_z is the operator of its z -component), $\hat{S}_1 = \hat{S}_2 = 2$ are the spin operators of the individual Fe(II) ions, B is the magnetic induction, μ_B is the Bohr magneton while D stands for the axial zero-field splitting parameter. In order to avoid the overparameterisation of the spin Hamiltonian, only isotropic g values were considered. The best fit of the experimental data was with a fixed g factor at 2.08 and 2% of paramagnetic impurity ($S = 2$) which yielded the exchange constant $J = -24.05\text{cm}^{-1}$ and an axial ZFS component $D = -18.10\text{ cm}^{-1}$ as the most reasonable parameters. Obtained values of J and D indicate the moderate antiferromagnetic coupling of high-spin ($S = 2$) Fe(II) ions with considerable orbital angular momentum. Due to the consequential mixing of S levels, attempts to model the magnetic data with a solely Heisenberg-Dirac-Van Vleck Hamiltonian, $\hat{H} = -2J(\hat{S}_1\hat{S}_2)$, failed to reproduce the low temperature behaviour well.

The sign and absolute value of the obtained axial ZFS parameter are similar to those expected for compounds containing Fe(II) ions in distorted trigonal-planar environment where second order spin-orbit coupling occurs by mixing of ground state ($L = 0$) with an electronic excited states with a non-zero L .¹⁰⁶ Similar values of D have been previously reported for other [Fe(HMDS)₂L] ($L = \text{ligand}$) systems.^{85,111,189,193,208,269}

On the other hand, the observed exchange coupling within the linear $\{\text{Fe}^{\text{II}}_2(\mu_2\text{-O})\}$ core is to the best of our knowledge first ever reported. Very weak antiferromagnetic coupling was observed in compound $[\text{Fe}_3(\text{Ap}^{\text{TMS}})_6\text{Li}_2\text{O}]^4$ ($\text{Ap}^{\text{TMS}} = 4\text{-methyl-2-}[(\text{trimethylsilyl})\text{amino}]\text{pyridyl}$) where oxide anion bridges three trigonal-planar iron(II) centres and two Li cations ($g = 2.48$, $J = -2.7\text{ cm}^{-1}$, temperature-independent paramagnetism = $200 \times 10^{-6}\text{ cm}^3\text{ mol}^{-1}\text{ K}$, 5% of paramagnetic impurity $S = 2$).¹⁵⁸ A similar J value was reported also in a complex with a linear $\{\text{Fe}^{\text{II}}_2(\mu_2\text{-F})\}$ core with trigonal bipyramidal iron(II) centres bound by poly(pyrazolyl)methane ligands ($g = 2.11$, $J = -16.3\text{ cm}^{-1}$, $D = -10.0\text{ cm}^{-1}$, 0.04% of paramagnetic impurity $S = 2$).²⁷⁹ Furthermore, a diamagnetic ground state, as a consequence of antiferromagnetic coupling, was confirmed for the first oxo-diiron(II) complex reported by Holland and co-workers (via DFT calculations and Mössbauer spectroscopy).²⁸⁰ The same study revealed the existence of substantial unquenched orbital angular momenta for the ferrous ions.

In conclusion, the magnitude of coupling for the linear $\{\text{Fe}^{\text{II}}_2(\mu_2\text{-O})\}$ core in **30** is significantly smaller than $|J| > 100 \text{ cm}^{-1}$ found for numerous oxo-diiron(III) complexes.^{281,282} Following the magneto-structural correlations of Lippard²⁸¹ and Weihe and Güdel,²⁸² this observation can be rationalised partially with longer Fe(II)–O bonds in **30** (1.848 Å). Secondly, dinuclear iron(III) systems contain mostly unsupported μ_2 -oxo bridges while here the reported iron(II) dimer holds the μ_4 -oxo bridge where the coordination of two sodium ions reduces the capacity of oxide ligand to moderate the coupling. Likewise, a decrease in J was reported for oxo-diferric compounds upon metalation, alkylation and protonation of the μ -O bridge.²⁸¹

3.2.8.2 A Polymeric NaHMDS 1,4-Dioxane Solvate

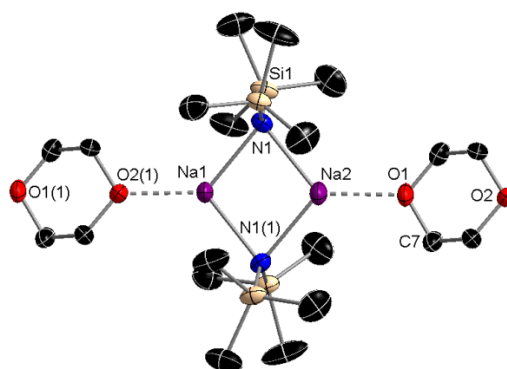


Figure 3.30 – Crystal structure of complex **31** with an extra equivalent of 1,4-dioxane shown. Hydrogen atoms, one equivalent of co-crystallised benzene solvent and disorder in one 1,4-dioxane group omitted for clarity.

Thermal ellipsoids displayed at 50% probability level. Selected bond distances (Å) and angles (°): Na1–N1 2.382(3), Na1–N1(1) 2.382(3), Na1–O2(1) 2.283(6), Na1---Na2 3.008(2), Na2–N1 2.394(3), Na2–N1(1) 2.394(3), Na2–O1 2.305(5); Na1–N1–Na2 54.88(4), N1–Na1–N1(1) 102.29(18), O2(1)–Na1–N1 129.611(3), O2(1)–Na1–N1(1) 126.944(3), N1–Na2–N1(1) 101.58(18), O1–Na2–N1 129.1(2), O1–Na2–N1(1) 128.1(2), O1–Na2–Na1 170.52(14), O2(1)–Na1–Na2 170.805(2).

Crystals of $[\{\text{dioxane}\cdot(\text{NaHMDS})_2\}_\infty]$ (**31**) (Figure 3.30) have been found as the product of several reactions including the attempted metallations of 4-methoxypyridine and 4-fluorobenzonitrile and also when attempting to form **17** directly from benzene. It is possible addition of too much 1,4-dioxane to the reaction favours the formation of this complex or that with the highly coordinating functional groups present (pyridine, nitrile), interaction with the Fe centre could allow for and promote the formation of **31**. Via rational synthesis, addition of a half molar equivalent of 1,4-dioxane to a benzene solution of NaHMDS, complex **31** can be isolated in a 67% yield.

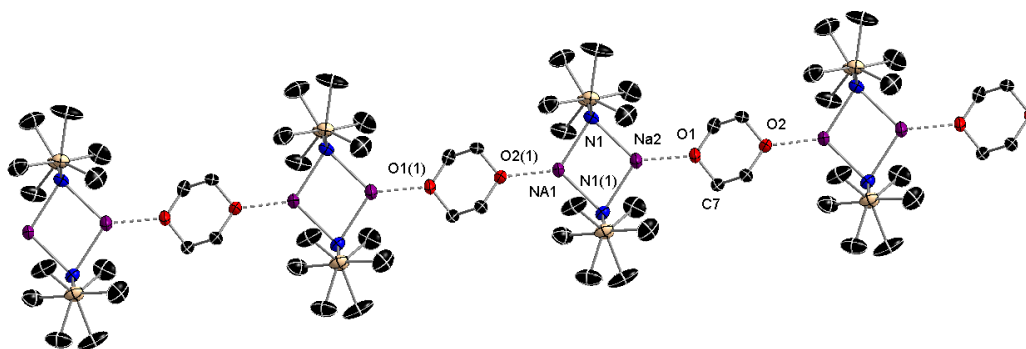


Figure 3.31 – Section of the polymeric chain in complex **31**. Hydrogen atoms, co-crystallised benzene solvent and disorder in 1,4-dioxane groups omitted for clarity. Thermal ellipsoids displayed at 50% probability level.

In **31**, a cyclodimer of $\{(\text{NaHMDS})_2\}$ can be seen, solvated by an equivalent of 1,4-dioxane attached to one of the Na atoms. The remaining O of 1,4-dioxane binds to a neighbouring Na atom giving rise to a linear 1-D chain structure (Figure 3.31).

Whilst unsolvated NaHMDS holds a cyclic trimeric structure^{89,90} (see Chapter 1), dimeric arrangements have been reported for THF mono-solvated²⁸³ and bi-solvated²⁸⁴ $\{(\text{NaHMDS})_2\}$ cyclodimers (Figure 3.32) which are precluded from polymerisation. The HMDS groups in **31** are symmetrically equivalent though the Na atoms are not; this is reflected in the bond lengths where Na1 is more closely bonded to N1 and O2(1) (2.382(3) and 2.283(6) Å, respectively) than Na2 is to N1 and O1 (2.394(3) and 2.305(5) Å, respectively).

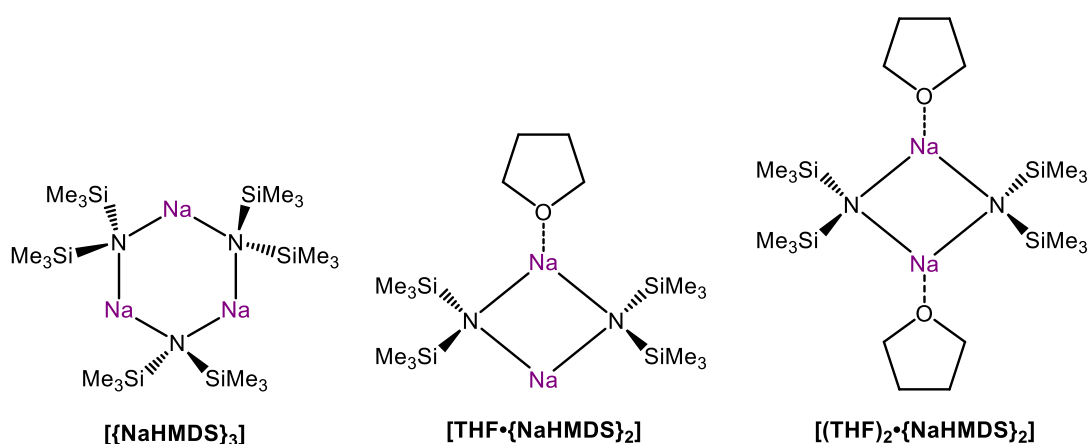


Figure 3.32 – Structural representations of unsolvated $[\{\text{NaHMDS}\}_3]$ ^{89,90} and THF mono-solvated²⁸³ and bi-solvated²⁸⁴ $\{(\text{NaHMDS})_2\}$ cyclodimers.

The only structurally authenticated 1,4-dioxane adduct of NaHMDS to be reported is $[(\text{dioxane})_2 \cdot \text{NaHMDS}]_\infty$ (Figure 3.33) by Stalke and co-workers in 1992.²⁸⁵ Here a

monomeric unit of NaHMDS is solvated by four 1,4-dioxane groups, each of which bridge to other monomeric units of NaHMDS resulting in a 3-dimensional polymeric network.

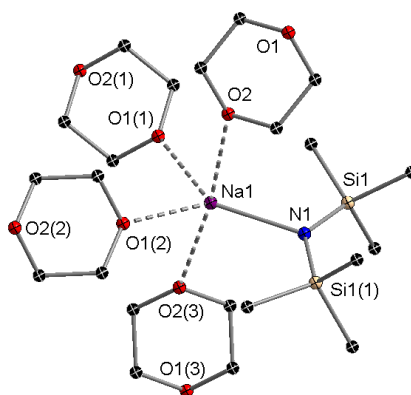
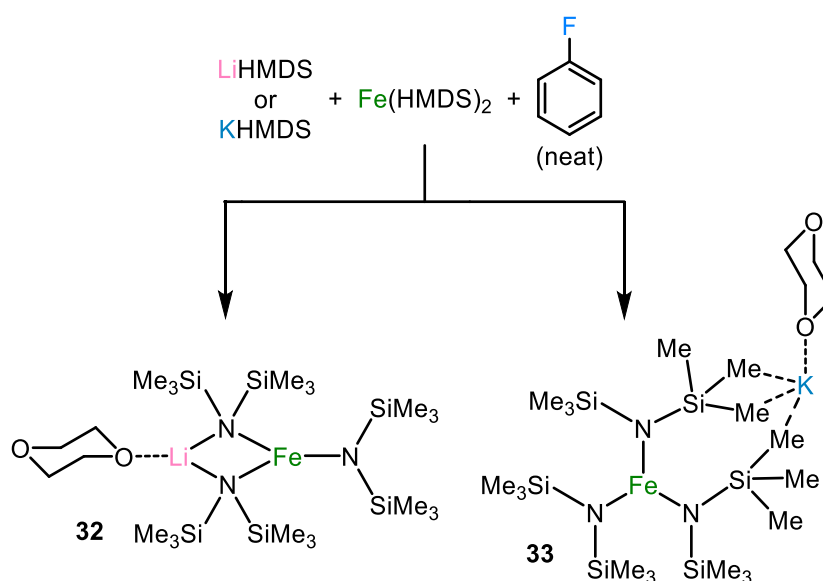


Figure 3.33 – Structure of $[(\text{dioxane})_2 \cdot \text{NaHMDS}]_\infty$. Hydrogen atoms omitted for clarity.²⁸⁵

3.2.8.3 Exploring the Alkali Metal Effect

Preliminary investigations into the alkali metal effect, within the context of the ferration of fluorinated aryl substrates, were carried out by employing LiHMDS and KHMDS in place of NaHMDS as a partner for $\text{Fe}(\text{HMDS})_2$. As such, the same methodologies were applied for the attempted metallations of fluorobenzene (Scheme 3.14) and 1,3-difluorobenzene.



Scheme 3.14 – Synthesis of Li and K Fe-tris(HMDS)-dioxane congeners in neat fluorobenzene.

Crystals analysed from a 1:1:1 reaction of LiHMDS, Fe(HMDS)₂ and 1,4-dioxane reaction in neat fluorobenzene solvent were found to be discrete monomer [dioxane·LiFe(HMDS)₃] (**32**) (Figure 3.34), isolated in a 70% yield.

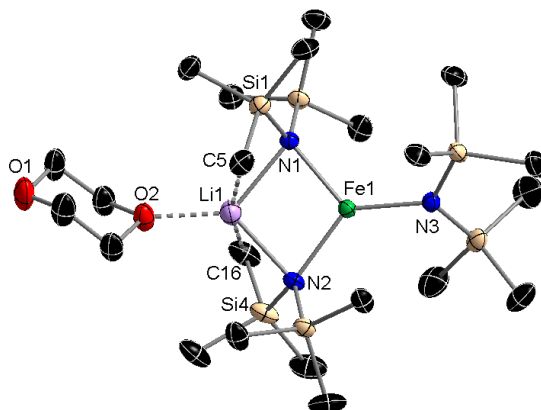


Figure 3.34 – Asymmetric unit of complex **32**. Hydrogen atoms omitted for clarity. Thermal ellipsoids displayed at 50% probability level. Selected bond distances (Å) and angles (°): Fe1-N1 2.0474(19), Fe1-N2 2.0548(18), Fe1-N3 1.9604(19), Fe1---Li1 2.665(4), Li1-N1 2.133(5), Li1-N2 2.135(5), Li1-O2 1.991(5), Li1---C5 2.7847(2), Li1---C16 2.8292(2); N1-Fe1-N2 103.41(8), N1-Fe1-N3 125.99(8), N2-Fe1-N3 130.39(8), Li1-N1-Fe1 79.19(13), Li1-N2-Fe1 78.97(13), Li1---Fe1-N3 171.39(11), N1-Li1-N2 97.93(18), O2-Li1-Fe1 174.6(2), O2-Li1-N1 132.4(2), O2-Li1-N2 129.7(2).

NMR analysis of the filtrate confirmed that no metalation of fluorobenzene had occurred in this instance. 1,4-dioxane has coordinated to monomeric {LiFe(HMDS)₃} and curiously does not bridge between lithium atoms as it does between sodium atoms in compound **17**. Geometrical parameters of **32** compare well with those previously reported [THF·LiFe(HMDS)₃].⁹⁶ Should the ferration of fluorobenzene be dependent on a strong alkali metal–fluorine interaction it can be postulated that in **32**, lithium may be less sterically accessible to facilitate a strong AM-F interaction than sodium is capable of in complex **17/17a**. Comparatively, the smaller Li atom is ‘sunk’ further into the steric sphere of the {Fe(HMDS)₃} moiety, in closer proximity to Fe at a distance of 2.665(4) Å (Na1---Fe1 2.9995(6) Å in **17**) and finds stabilisation by bonding closer to HMDS nitrogens (mean Li-N bond distance 2.134 Å) and 1,4-dioxane oxygen (Li1-O2 1.991(5) Å) than Na can respectively achieve in **17** (mean Na-N 2.4645 Å, Na1-O1 2.2828(12) Å). Additionally, Li also forms long distance electrostatic contacts with two Me groups (C5 and C16 at distances of 2.7847(2) and 2.8292(2) Å, respectively) each of them belonging to the two bridging HMDS ligands, whilst the analogous Na---Me distances in **17** are all longer than 3 Å.

Even when more activated 1,3-difluorobenzene was employed no colour change in the reaction was observed and no evidence of metallation was forthcoming with only crystals of oxidation product $\text{Fe}^{\text{III}}(\text{HMDS})_3$ grown from the reaction, verified by X-ray crystallography and ^1H NMR spectroscopy analysis.^{125,276,277}

Moving to the heavier alkali metal potassium, under the same reaction conditions as those employed for the synthesis of **32**, ferration of fluorobenzene was also not evident in this case. Crystals collected from the reaction were found to be that of $[\{\text{dioxane}\cdot\text{KFe}(\text{HMDS})_3\}_\infty]$ (**33**) (Figure 3.35) in a 64% yield. Though the connectivity of the structure could be established by X-ray crystallographic analysis, the accuracy of the structure is compromised by significant disorder present in the 1,4-dioxane and HMDS groups. The formation of **33** is however supported by ^1H and $^{13}\text{C}\{^1\text{H}\}$ NMR spectroscopy (in d_8 -tol) and elemental analysis. The ^1H NMR spectrum displays a very broad resonance at -2.54 ppm assigned to the HMDS H atoms and a resonance at 3.15 ppm assigned to 1,4-dioxane H atoms. The $^{13}\text{C}\{^1\text{H}\}$ NMR spectrum shows just two signals, one in the far downfield region at 344.71 ppm (HMDS) and one much further upfield at 67.11 ppm (1,4-dioxane).

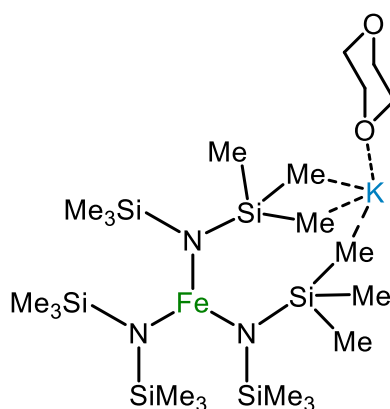


Figure 3.35 – ChemDraw Representation of $[\{\text{dioxane}\cdot\text{KFe}(\text{HMDS})_3\}_\infty]$ (**33**).

Without the addition of 1,4-dioxane, solvent-free $[\{\text{KFe}(\text{HMDS})_3\}_\infty]$ (**34**) (Figure 3.36) can be produced. KHMDS and $\text{Fe}(\text{HMDS})_2$ were combined in toluene and stirred for two hours before crystallisation from fluorobenzene with a hexane layer to produce crystals in a low 15% yield.

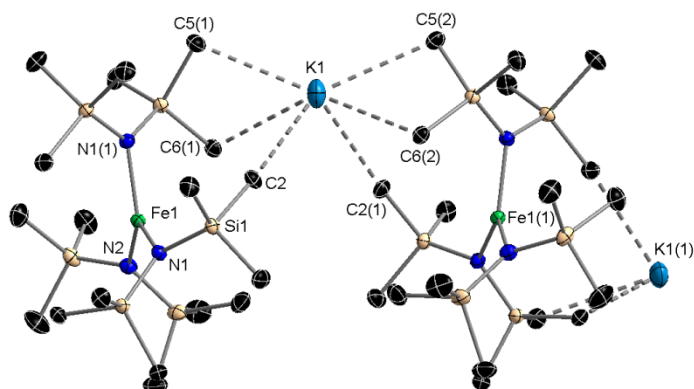


Figure 3.36 – Crystal structure of complex **34**. Hydrogen atoms and co-crystallised fluorobenzene solvent molecules omitted for clarity. Thermal ellipsoids displayed at 50% probability level. Selected bond distances (Å) and angles (°): Fe1-N1 1.981(2), Fe1-N2 1.986(3), Fe1-N1(1) 1.981(2), Fe1---K1 5.4301(2), K1---C2 3.313(3), K1---C5(1) 3.224(3), K1---C6(1) 3.315(3), K1---C2(3) 3.313(3), K1---C5(2) 3.224(3), K1---C6(2) 3.315(3); N1-Fe1-N2 121.39(6), N1-Fe1-N1(1) 117.22(12), N2-Fe1-N1(1) 121.39(6), C2---K1---C5(1) 80.13(7), C2---K1---C6(1) 71.09(6), C2---K1---C2(3) 94.76(10), C2---K1---C5(2) 135.22(7), C2---K1---C6(2) 80.69(7), C5(1)---K1---C6(1) 55.41(6), C5(1)---K1---C2(3) 135.22(7), C5(1)---K1---C5(2) 133.14(10), C5(1)---K1---C6(2) 148.55(7), C6(1)---K1---C2(3) 80.69(7), C6(1)---K1---C5(2) 148.55(7), C6(1)---K1---C6(2) 137.94(10), C2(3)---K1---C5(2) 80.13(7), C2(3)---K1---C6(2) 71.09(6), C5(2)---K1---C6(2) 55.41(6).

Compound **34** is a 1-D polymeric chain (Figure 3.37) in the solid-state where distorted trigonal planar $\{\text{Fe}(\text{HMDS})_3\}^-$ anionic units are interspersed by bridging K^+ cations which achieve coordinative stabilisation through electrostatic contacts to six Me groups, three per anionic unit. No evidence of metallation fluorobenzene was observed during the synthesis of **34**. Highly disordered molecules of co-crystallised $\text{C}_6\text{H}_5\text{F}$ were removed from the crystal structure applying the SQUEEZE routine within PLATON,²⁸⁶ with the F atom making a close approach to K, thus **34** cannot be considered a completely solvent-free ate complex.

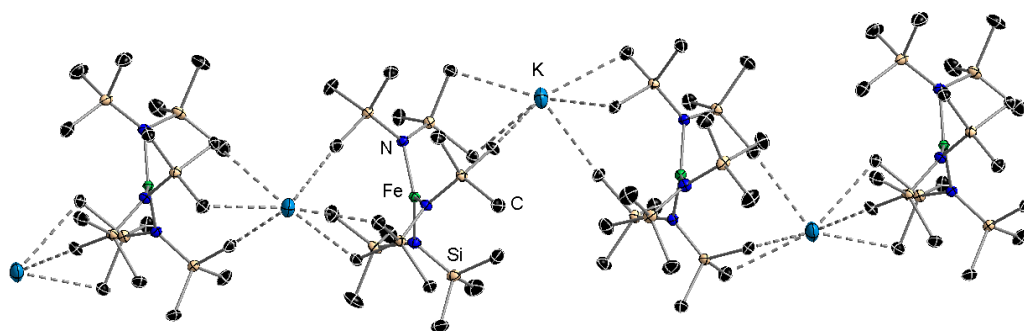


Figure 3.37 – Section of the polymeric chain in complex **34**. Hydrogen atoms and co-crystallised fluorobenzene solvent molecules omitted for clarity. Thermal ellipsoids displayed at 50% probability level.

3.2.8.4 Synthesis of a Heteroleptic Sodium Ferrate Dioxane Base

Initial studies were carried out to explore inclusion of the CH_2SiMe_3 monosilyl group into the sodium ferrate base system and assess its reactivity. With complex **12** firmly in mind (see Section 2.3.1), we looked first to synthesise and characterise the related dioxane base. $\text{NaCH}_2\text{SiMe}_3$ was used in place of NaHMDS as a synthetic procedure analogous to that for the synthesis of **17** was carried out. Crystals of isostructural (with respect to **17**) [dioxane: $\{\text{NaFe}(\text{HMDS})_2(\text{CH}_2\text{SiMe}_3)\}_2$] (**35**) (Figure 3.38) were obtained from benzene in a 31% yield.

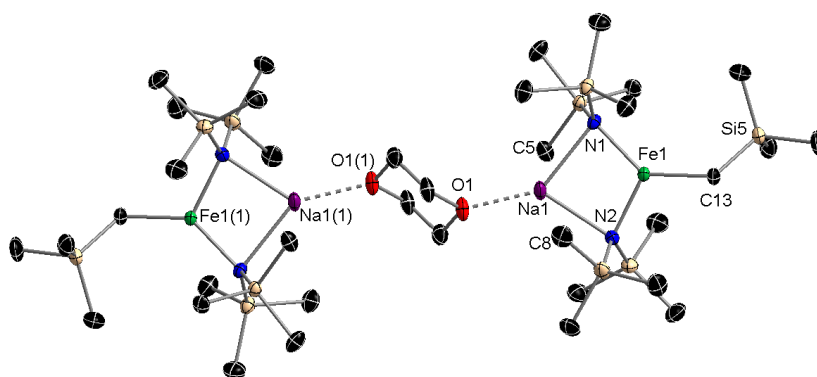


Figure 3.38 – Dimeric unit of complex **35**. Hydrogen atoms omitted for clarity. Thermal ellipsoids displayed at 50% probability level. Selected bond distances (Å) and angles (°): Fe1-N1 2.0264(14), Fe1-N2 2.0260(14), Fe1-C13 2.0487(18), Fe1---Na1 2.9578(7), Na1-N1 2.4585(16), Na1-N2 2.4321(16), Na1-O1 2.2506(14), Na1---C5 2.7255(1), Na1---C8 2.811(2); N1-Fe1-N2 109.15(6), N1-Fe1-C13 134.46(7), N2-Fe1-C13 116.00(7), Na1-N1-Fe1 81.91(5), Na1-N2-Fe1 82.59(5), Na1---Fe1-C13 163.09(5), N1-Na1-N2 84.94(5), O1-Na1-N1 141.79(6), O1-Na1-N2 132.95(6).

The ferration of 1,3-difluorobenzene was attempted applying the same methodology as before (see Section 3.2.3), but with $\text{NaCH}_2\text{SiMe}_3$ in place of NaHMDS . Though a significant change in solution colour was apparent (green to dark red/brown) after stirring overnight at 50°C , no crystals or even dry solid product could be produced from the reaction, only oily products were forthcoming. ^1H NMR spectra of these products were inconclusive.

3.3 Conclusions

Demonstrated here are genuine examples of sodium-mediated ferration. Aided by 1,4-dioxane, the unique metallating power of the homoleptic HMDS sodium ferrate has been uncovered when reacted with fluoroaromatic substrates, indicating the stronger potential metallating abilities of CIP sodium ferrate complexes in comparison to their SSIP counterparts. Encouraged by the unprecedented direct *ortho*-ferration of fluorobenzene and subsequently 1,3-difluorobenzene, a methodology was developed allowing for the direct *ortho*-ferration and electrophilic interception with I₂ of an array of fluorobenzenes. Whilst less activated substrates (e.g. fluorobenzene, 4-fluoroanisole) required neat conditions or extended reaction times, more activated substrates (e.g. pentafluorobenzene, 1-bromo-3,5-difluorobenzene) could be metallated stoichiometrically. Stoichiometric di-ferration was achieved for 1,2,4,5-tetrafluorobenzene and 1,4-dibromo-2,5-difluorobenzene which each hold two highly activated proton positions on the ring. Generally, good yields were achieved with excellent regioselectivity, under mild reaction conditions. Under these conditions no NaF elimination or benzyne formation is observed.

Isolation and structural characterisation of ferrated intermediate species uncovered the molecular crystal structures of a number of complexes. In all cases the loss of HMDS(H) enables the formation of a new Fe-C σ -bond *ortho* to F and the same F atom forms a dative bond with Na resulting in a six-membered {NaNFeCCF}. With polyfluoroaromatic substrates containing an F atom para to that coordinated by Na secondary Na---F interactions are possible resulting in extended 1-D and 2-D polymeric structures. Optional site selectivity of the sodium ferrate base was demonstrated with anisole and two anisole fluoro derivatives, showing clear preference for metallation *ortho* to inductively activating fluorine rather than the superiorly coordinating methoxy group. Considering the accumulated results, including the substrates which failed to be ferrated, ferration can be achieved with **17a** for fluorine containing aromatic substrates where fluorine plays a dual role in inductively activating the *ortho* proton position and forming a strong dative electrostatic interaction with Na that aides ferration and stabilises the product.

Magnetometry studies revealed a change in anisotropy between homoleptic tris(HMDS) complex **17** (holding a positive *D* value) and complexes **18**, **19** and **24** that contain heteroleptic {Fe(HMDS)₂(Ar)} cores (which exhibit negative *D* values), results that echo

those observed for the NHC ferrate complexes in Chapter 2. Dinuclear complex **23** was found to exhibit antiferromagnetic coupling between the high-spin Fe(II) centres.

The requirement for vigilant exclusion of air and atmospheric water from sodium ferrate reactions has been highlighted by the synthesis and isolation oxo-inverse crown ether **30**. Magnetic studies exposed novel antiferromagnetic coupling between two paramagnetic Fe(II) centres within the linear $\{\text{Fe}^{\text{II}}(\mu_2\text{-O})\}$ core of **30**. A new cyclodimeric polymer (**31**) has been synthesised from NaHMDS and 1,4-dioxane.

Evidencing a dramatic alkali metal effect, attempts to effect the direct *ortho*-ferration of fluorobenzene and 1,3-difluorobenzene with Li and K ferrate congeners were unsuccessful, allowing for the isolation of [dioxane·(AMFe(HMDS)₃)] complexes.

Finally, replacing an HMDS group with alkyl CH_2SiMe_3 led to the isolation of heteroleptic ferrate [dioxane·{NaFe(HMDS)₂(CH₂SiMe₃)₂}] (**35**). Attempts to ferrate 1,3-difluorobenzene with this new complex were inconclusive however.

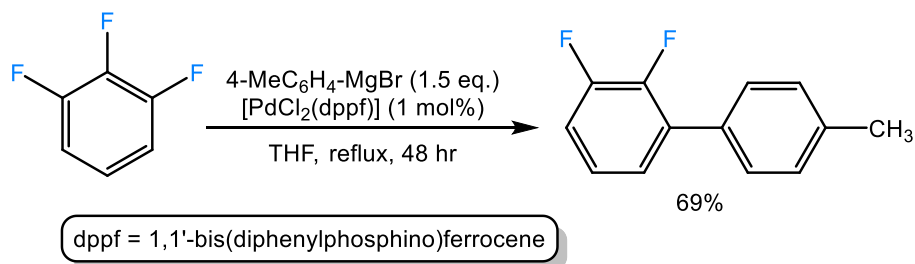
Chapter 4 – C-H and C-F Activation of 1,3,5-Trifluorobenzenes

4.1 Introduction to C-F Bond Activation

Having already conferred the great importance of fluorinated aromatic molecules and their C-H activation in Section 3.1, with the results to follow in this chapter it is judicious to now discuss the importance of C-F activation of these molecules.

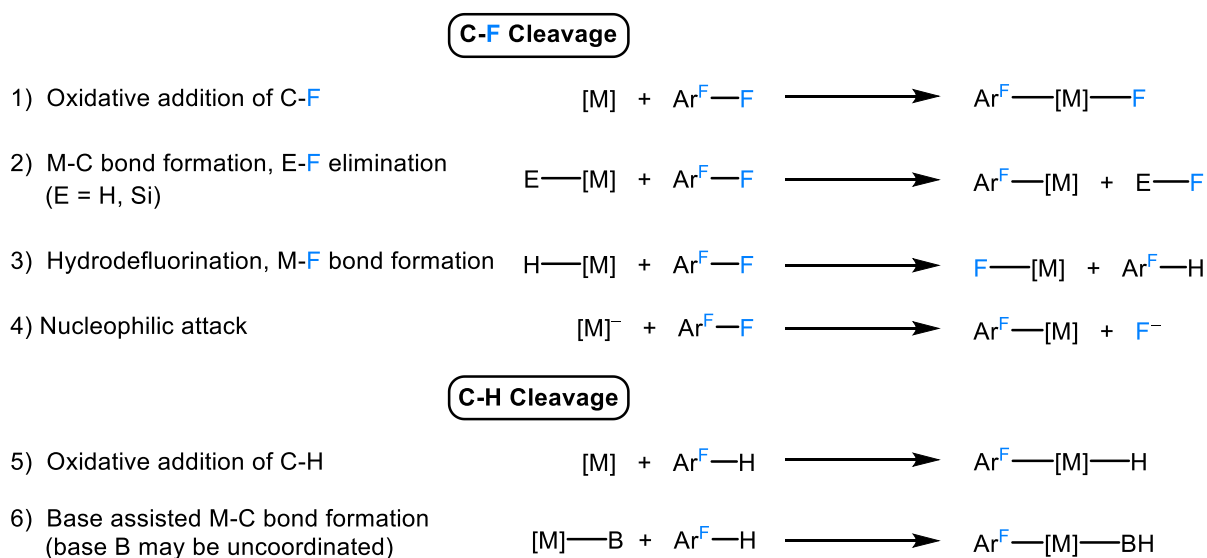
With the exception of the Si-F bond (bond dissociation energy = 576.4 kJ/mol), the C-F bond is empirically the strongest single bond in organic chemistry with a diatomic bond dissociation energy of 513.8 kJ/mol.²⁶⁶ In spite of the high polarity between δ^+ C and δ^- F, the consequential strong electrostatic attraction between the atoms is what provides the C-F bond with its strength and stability.²¹⁰ Exploitation of this high strength and general inertness is manifested in useful chemical products such as PTFE (polytetrafluoroethylene, commonly known as Teflon), whose omniphobic, heat resistance and dielectric properties lends itself to a host of beneficial applications including non-stick cookware coatings, wiring insulation and lubricants.²⁸⁷

Yet despite this, the C-F bond can be broken (activated) and accordingly much research has been devoted to this challenging area of chemistry and the variety of approaches available.^{211,288} C-F activation has not only allowed for the construction of key organofluorine molecules using polyfluorinated precursors^{212,289} (Scheme 4.1) but methods have also been sought for the defluorination of environmentally harmful substances, specifically chlorofluorocarbons (CFCs) which have heavily contributed to atmospheric ozone depletion and for the synthesis of environmentally benign replacements, hydrofluorocarbons (HFCs).^{290,291}



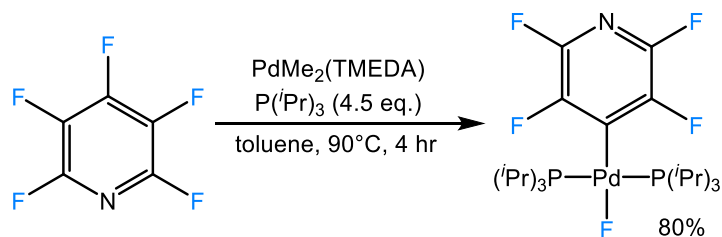
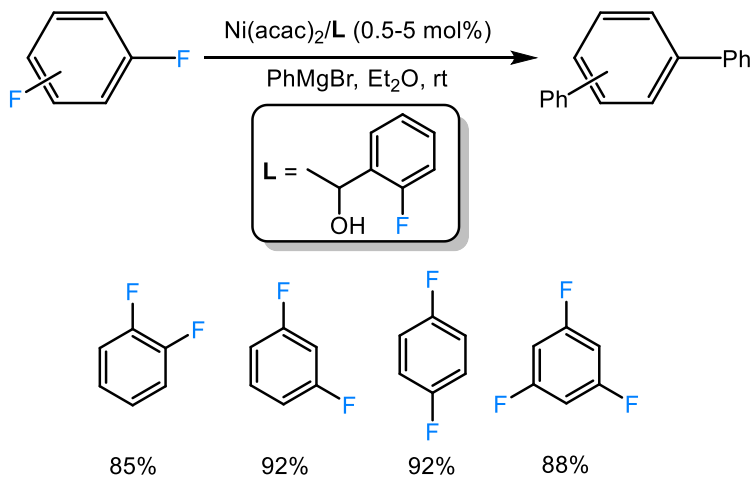
Scheme 4.1 – Polyfluoro building block construction via Pd-catalysed C-F activation and cross-coupling.²⁹² The reaction proceeds via the common Pd-catalysis oxidative addition-reductive elimination pathway but is chemoselective for F over H.

Numerous efforts in the field have centred on the activation of fluorinated aromatic molecules and the construction of new C-C bonds using low valent and electron rich transition metal centres.^{211,288} In a 2011 review article, Perutz and co-authors classed stoichiometric reactions of fluoroaromatics at transition metals that cleave C-F bonds into four distinct types, as shown in Scheme 4.2.²⁹³ In addition, they identified competing C-H activation processes to operate via either oxidative addition or base-assisted cleavage.

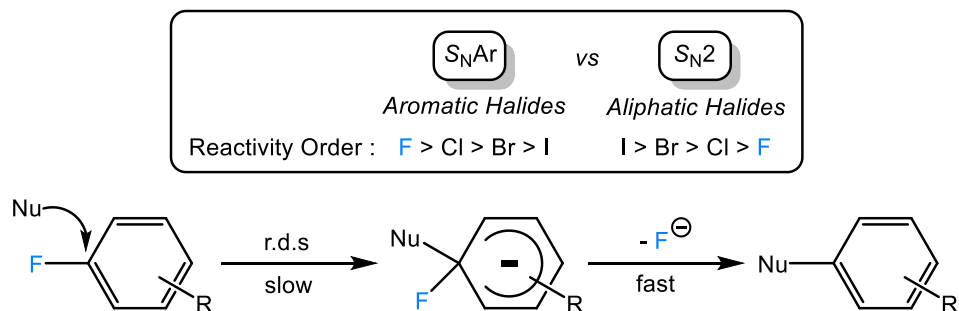


Scheme 4.2 – C-F and C-H cleavage reactions of fluoroaromatics (Ar^F) at transition metal centres. [Scheme adapted from Perutz *et al.*].²⁹³

C-F cleavage via oxidative addition (Scheme 4.3) has certainly been the most prominent pathway observed in the literature with transition metals such as Ni, Pt, Pd and Rh at the forefront of these processes, many operating catalytically (Scheme 4.4).^{212,216,293}

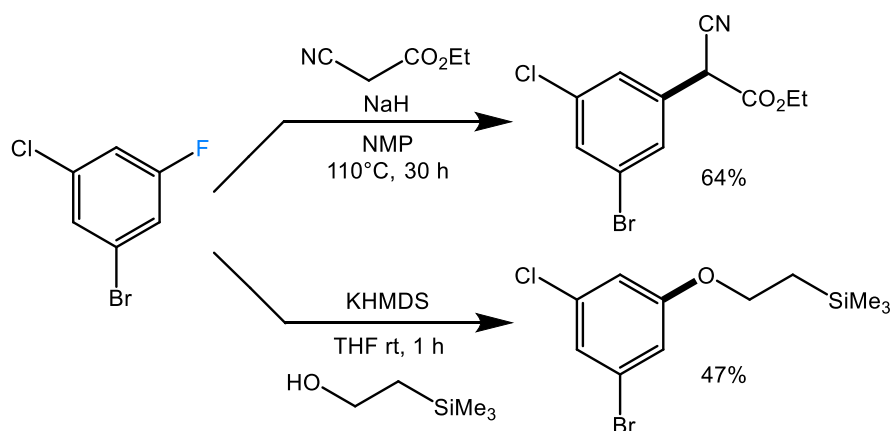
Scheme 4.3 – C-F cleavage via oxidative addition of pentafluoropyridine with a palladium complex.²¹¹Scheme 4.4 – Nickel-catalysed cross-couplings of polyfluorobenzenes. [Scheme adapted from Love and Sun].²¹⁶

This approach has primarily focused on the subsequent use of nucleophilic reagents (e.g. Grignard reagents) as cross-coupling partners for reductive elimination to create new C-C bonds (see Scheme 4.1).^{212,216} Methods for the construction of C-X (X = heteroatom) bonds from C-F bonds are scarcer however, principally restricted to nucleophilic aromatic substitution with high fluorinated or activated fluoroaromatics which are predisposed towards this pathway due to fluorine's electronegativity and leaving group ability (Scheme 4.5).^{211,288,290}



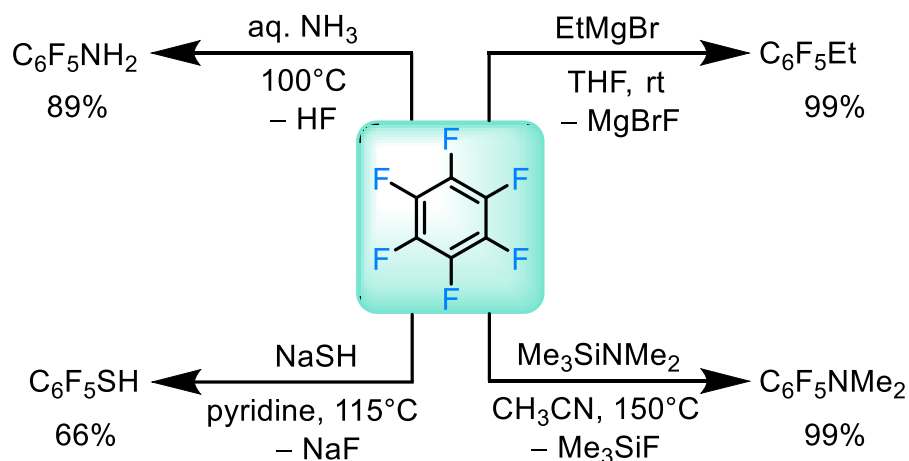
Scheme 4.5 – Opposite reactivity trends with halogen substituents for nucleophilic aromatic substitution and S_N2 nucleophilic substitution (r.d.s = rate determining step). [Scheme adapted from Amii and Uneyama].²¹¹

The entirely opposite reactivity pattern is observed with aromatic halides for Nucleophilic Aromatic Substitution (S_NAr) (where fluorine is the most favoured leaving group) compared to aliphatic halides in S_N2 nucleophilic substitution (where F is the least favoured) (Scheme 4.5). Two representative examples of this S_NAr reactivity are displayed in Scheme 4.6 where clear preference for attack at the fluorine position is established over the Cl and Br substituents.^{294,295}



Scheme 4.6 – Preferential nucleophilic aromatic substitution at the F position of 1-bromo-3-chloro-5-fluorobenzene.^{294,295}

A number of examples of nucleophilic substitution of hexafluorobenzene have been shown with alkali metal reagents and organic nucleophiles to produce new C-X bonds (Scheme 4.7).^{285,291–294} Perfluoroarenes are particularly susceptible to nucleophilic attack due to the strong electron-withdrawing effect of F which dramatically lowers the energy of the π^* orbitals.²¹¹



Scheme 4.7 – Reactions of hexafluorobenzene with a range of nucleophiles to create new C-X bonds.^{287,290,296–299}

As seen in Scheme 4.7, aside from the strongly nucleophilic Grignard reagent (top right), the rather weak nucleophiles require forcing conditions ($>100^{\circ}\text{C}$) to successfully attack a δ^+ C on hexafluorobenzene and remove an F atom.

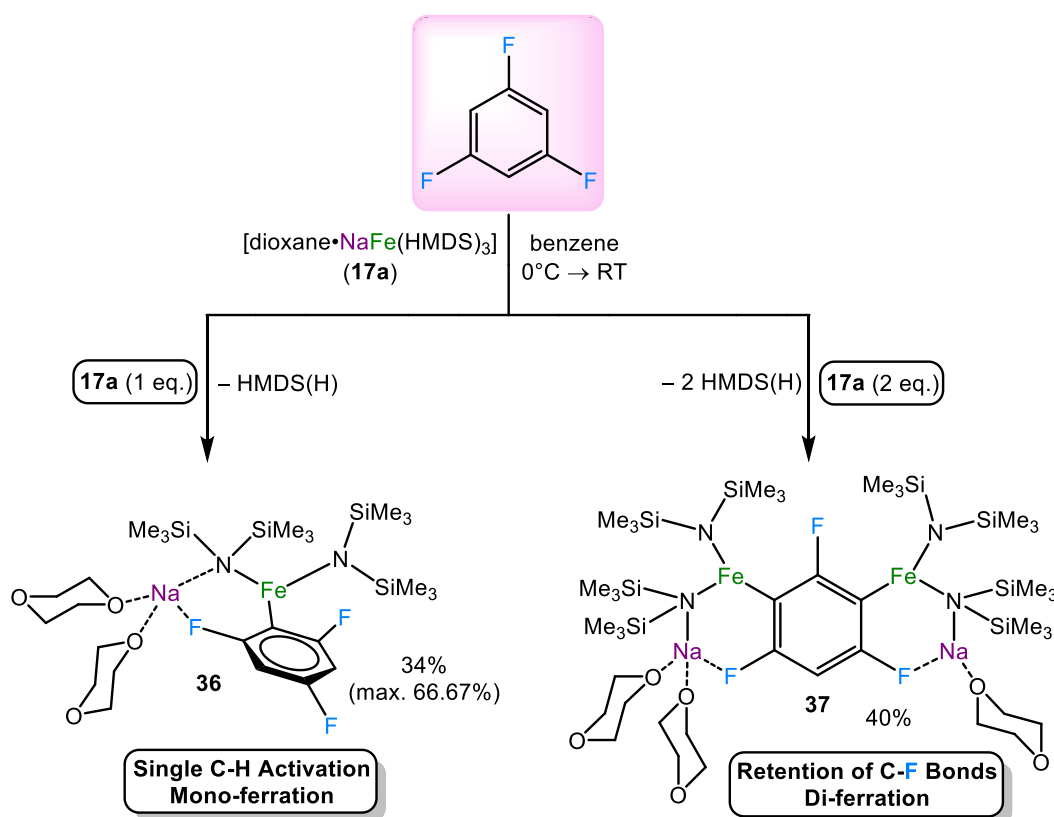
In this final chapter we aim to explore the unprecedented C-F and C-H activations of 1,3,5-trifluorobenzenes with sodium ferrate base **17a**. Uncovered are the dynamics of the reaction of **17a** with 1,3,5-trifluorobenzene with variable stoichiometry and temperature. Along with invaluable structural studies, aspects of the reaction and the development of a proposed mechanism are investigated via NMR spectroscopy and the use of halo-derivative substrates.

4.2 Results and Discussion

Through the course of investigations into the C-H activations of fluorinated aryl substrates, 1,3,5-trifluorobenzene presented a unique set of results. The substrate has three symmetric, doubly activated (by two adjacent F atoms) ring H atoms with a calculated pK_a of 31.5.²⁴⁷ We explored variation of reaction temperature and stoichiometry which led to three very different outcomes.

4.2.1 Mono- and Di-Ferration

In separate reactions of 1:1 and 2:1 stoichiometries (base:substrate), bimetallic base **17a** was reacted with 1,3,5-trifluorobenzene at 0°C in benzene, stirring for one hour before leaving static overnight and allowing to reach ambient temperature (Scheme 4.8). In both cases, clear solution colour changes were observed from green to yellow/brown and the formation of crystals was apparent.



Scheme 4.8 – Low temperature reactions of sodium ferrate base **17a** with 1,3,5-trifluorobenzene.

From the 1:1 reaction, colourless block crystals revealed the mono-metallated structure $[\{(dioxane)_{1.5} \cdot NaFe(1,3,5-C_6H_2F_3)(HMDS)_2\}_2]$ (**36**) (Figure 4.1) in a 34% yield (where the maximum attainable yield was 66.67% according to 1.5 equivalents of 1,4-dioxane in the structure).

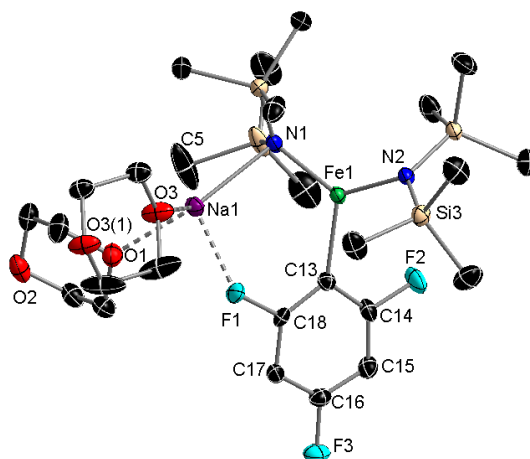


Figure 4.1 – Asymmetric unit of complex **36** featuring an extra half equivalent of 1,4-dioxane. Hydrogen atoms are omitted for clarity. Thermal ellipsoids displayed at 50% probability level. Selected bond distances (Å) and angles (°): Fe1-C13 2.092(2), Fe1-N1 1.9927(17), Fe1-N2 1.9435(16), Fe1---Na1 3.3876(8), Na1-F1 2.2523(15), Na1-N1 2.5256(17), Na1-O1 2.3192(17), Na1-O3 2.3354(16), Na1---C5 2.976(3); C13-Fe1-N1 115.73(7), C13-Fe1-N2 116.06(7), N1-Fe1-N2 128.09(7), Na1-N1-Fe1 96.42(7), Na1---Fe1-N2 143.05(5), Na1-F1-C18 130.09(11), N1-Na1-F1 103.98(6), N1-Na1-O1 145.67(7), N1-Na1-O3 127.44(7), O1-Na1-F1 86.61(6), O1-Na1-O3 84.06(6), O3-Na1-F1 90.98(6).

Interestingly, when the reaction was carried out using two molar equivalents of **17a**, the brown solution obtained deposited yellow needle crystals of $[\{dioxane \cdot NaFe(HMDS)_2\}_2(1,3,5-C_6HF_3)]$ (**37**) (Figure 4.2) in a 40% crystalline yield, resulting from the unprecedented di-metallation of the substrate at the C2 and C6 positions.

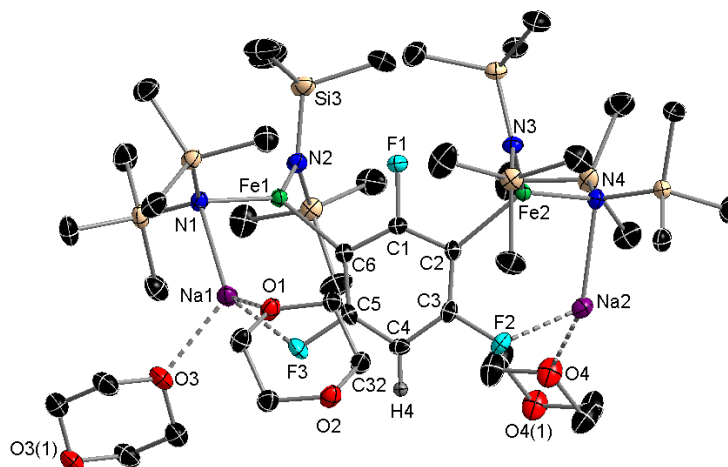


Figure 4.2 – Molecular structure of complex **37** shown with an extra equivalent of 1,4-dioxane in the asymmetric unit. Hydrogen atoms and a molecule of co-crystallised benzene solvent are omitted for clarity. Thermal ellipsoids displayed at 50% probability level. Selected bond distances (Å) and angles (°): Fe1-C6 2.118(3), Fe1-N1 2.007(2), Fe1-N2 1.946(3), Fe1---Na1 3.1764(13), Na1-N1 2.452(3), Na1-F3 2.328(2), Na1-O1 2.362(3), Na1-O3 2.362(3), Fe2-C2 2.103(3), Fe2-N3 1.945(3), Fe2-N4 2.017(3), Fe2---Na2 3.2322(13), Na2-N4 2.463(3), Na2-F2 2.343(2), Na2-O4 2.324(3), Na2-O2(1) 2.376(2), Na2---C32(1) 3.053(3), F1-C1 1.388(3), F2-C3 1.401(3), F3-C5 1.401(3); C6-Fe1-N1 113.42(11), C6-Fe1-N2 117.86(11), N1-Fe1-N2 127.60(11), Na1-N1-Fe1 90.26(10), Na1---Fe1-N2 155.46(9), Na1-F3-C5 100.97(16), N1-Na1-F3 112.23(9), N1-Na1-O1 127.52(10), N1-Na1-O3 122.36(10), O1-Na1-O3 95.95(10), O1-Na1-F3 97.76(8), O3-Na1-F3 93.92(9), C2-Fe2-N3 116.91(11), C2-Fe2-N4 114.53(11), N3-Fe2-N4 128.20(11), Na2-N4-Fe2 91.80(10), Na2---Fe2-N3 147.50(8), Na2-F2-C3 110.11(17), N4-Na2-F2 112.40(9), N4-Na2-O4 136.52(10), N4-Na2-O2(1) 125.27(10), O4-Na2-O2(1) 87.53(9), O4-Na2-F3 85.88(9), O2(1)-Na2-F2 98.55(8).

The molecular structures of complexes **36** and **37** were established by X-ray crystallography and demonstrate clear mono- and di-ferration of 1,3,5-trifluorobenzene correspondingly. The primary bond lengths and angles present in structures **36** and **37** are presented in Table 4.1 below.

Table 4.1 - Selected geometrical parameters of compounds **36**, and **37**. Bond distances are given in Ångstroms and bond angles given in degrees (°).

Bond/Angle	36	37	
		Left Side (Fe1)	Right Side (Fe2)
Fe-C	2.092(2)	2.118(3)	2.103(3)
Fe-N _{bridging}	1.9927(17)	2.007(2)	2.017(3)
Fe-N _{terminal}	1.9435(16)	1.946(3)	1.945(3)
Fe---Na	3.3876(8)	3.1764(13)	3.2322(13)
Na-F	2.2523(15)	2.328(2)	2.343(2)

Na-N_{bridging}	2.5256(17)	2.452(3)	2.463(3)
C-F(-Na)	1.397(2)	1.401(3)	1.401(3)
N_{bridging}-Fe-N_{terminal}	128.09(7)	127.60(11)	128.20(11)
N_{bridging}-Fe-C	115.73(7)	113.42(11)	114.53(11)
N_{terminal}-Fe-C	116.06(7)	117.86(11)	116.91(11)
Σ(N-Fe-N/C) angles	359.88	358.88	359.64
Na-N-Fe	96.42(7)	90.26(10)	91.80(10)
Na-F-C	130.09(11)	100.97(16)	110.11(17)

In complexes **36** and **37** only very minor variation in bond length is observed between the Fe-C σ -bonds whilst the Na-F dative bonds are clearly more diverse in length over the different Na centres. The Fe-C bond distances in **36** and **37** (2.092(2); 2.118(3) and 2.103(3) Å, respectively) are close to the average Fe-C bond distance of 2.1019 Å observed for the ferrated fluoroaromatic complexes in Chapter 3. The Na-F distance of 2.2523(15) Å in **36** is noticeably shorter than the Na-F lengths of 2.328(2) and 2.343(2) Å in **37** (Na1-F3 and Na2-F2, respectively) which are very much towards the longer end of the scale for the lengths observed in complexes **18-27** and **29** (see Table 3.3). The bond angles around the Fe centres in all cases sum very close to 360° with iron in a trigonal planar geometry. The Na-N-Fe angles in **37** (90.26(10)° and 91.80(10)°) are noticeably more acute than the corresponding angle in **36** (96.42(7)°), though this is likely a result of steric crowding between the two terminal HMDS groups. Once again the formation of six-membered {NaNFeCCF} rings is apparent, with two present in complex **37** fused to the central aryl ring, thus displaying strong engagement of the bimetallic system with the substrate.

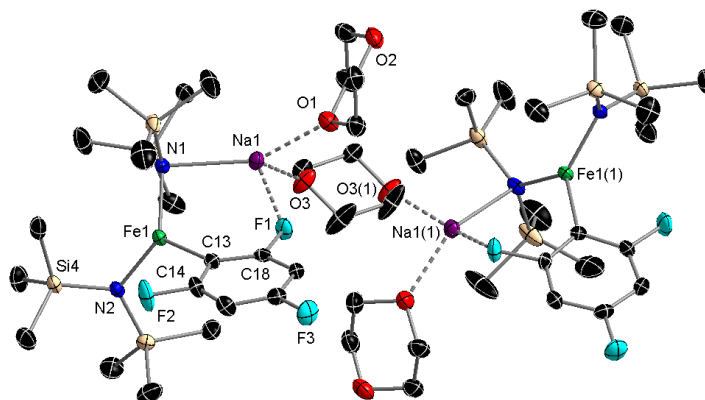


Figure 4.3 – Dimeric structure of complex **36**. Hydrogen atoms are omitted for clarity. Thermal ellipsoids displayed at 50% probability level.

Supramolecularly, complex **36** exists as a discrete dimer with an equivalent of 1,4-dioxane bridging between Na atoms (O3/O3(1)) and no secondary Na---F interactions (Figure 4.3). Dinuclear **37** meanwhile, polymerises through three distinct 1,4-dioxane units attached to the two Na atoms (Figure 4.4). The O1/O2 unit allows for dimerisation with a second dinuclear unit, the O3/O3(1) unit bridges between these dimers of dinuclear units along the *x* axis and the O4/O4(1) unit does the same along the *y* axis; thus the net result is a 2-D sheet of fused rings of two different sizes.

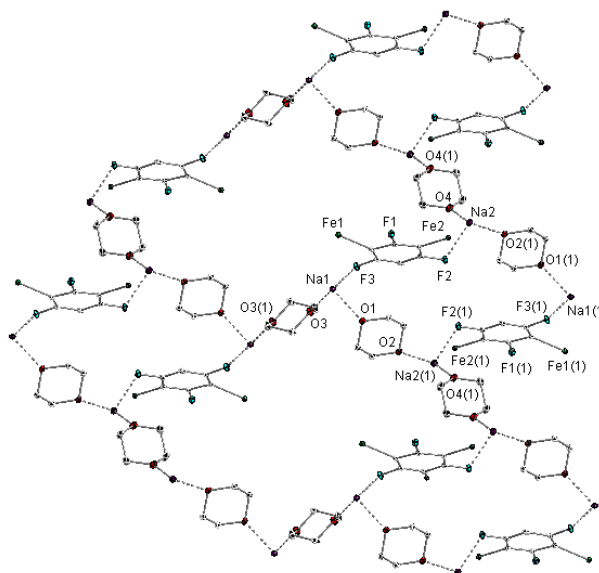


Figure 4.4 – Supramolecular 2-D polymeric structure of complex **37**. Hydrogen atoms, HMDS groups and co-crystallised benzene solvent are omitted for clarity. Thermal ellipsoids displayed at 20% probability level.

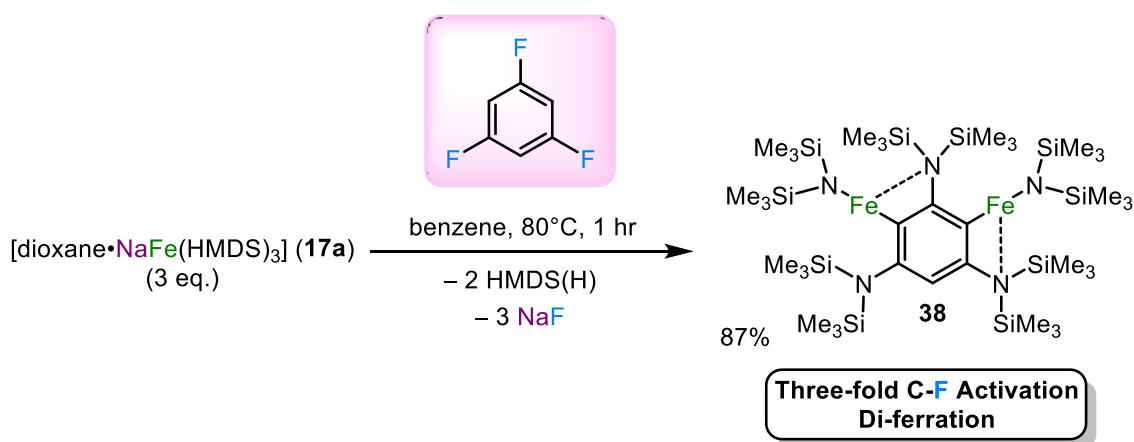
Complexes **36** and **37** represent the first recorded examples of ferration of 1,3,5-fluorobenzene. A search in the CCDC revealed that at present there are 23

crystallographically characterised examples 1,3,5-trifluorobenzene bonded by C to a metal, featuring metals Au, Pt, Pd, Hg, Rh and Ir. Whilst the majority of the reported complexes are synthesised via either transmetallation or oxidative addition of 1,3,5-trifluorobenzene, an example with gold³⁰⁰ and two with rhodium^{301,302} are examples of direct metallation of the substrate. There are no structurally recorded examples of di-metallated 1,3,5-trifluorobenzene.

36 and **37** were characterised by ¹H NMR spectroscopy (in C₆D₆) and displayed very broad resonances at -2.26 and -3.14 ppm, respectively, for the HMDS H atoms and are within the range (0 to -5 ppm) observed for ferrated complexes detailed in Chapter 3. Broad resonances at 4.85 and 2.49 ppm (**36** and **37**, respectively) are assigned to 1,4-dioxane. The spectrum of **36** showed a singlet peak at 101.64 ppm for the two equivalent ring H atoms whilst the spectrum of **37** displayed a singlet at 177.56 ppm corresponding to its sole remaining ring proton.

4.2.2 Di-Ferration and Three-Fold C-F Activation

With the ambition of metallating all three ring proton positions on 1,3,5-trifluorobenzene after successful mono- and di-metallations, a 3:1 stoichiometry reaction was carried out (Scheme 4.9). Refluxing for one hour produced a clear colour change in solution from green to yellow/brown and large flat yellow rod crystals were generated by slow cooling of the solution, along with a small quantity of brown precipitate.



Scheme 4.9 – Synthesis of C-F activation product **38** with 3 eq. of sodium ferrate base **17a** and 1,3,5-trifluorobenzene.

The crystals were analysed by X-ray crystallography to reveal the structure of homometallic [1,3-bis(FeHMDS)-2,4,6-tris(HMDS)-C₆H] (**38**) (Figure 4.5), recovered in an 87% yield. Astonishingly, 1,3,5-trifluorobenzene has undergone a two-fold C-H activation and a remarkable three-fold C-F activation to yield a 1,3-di-ferrated and penta-substituted aryl ring. Accompanying the loss of three fluorine atoms, three new C-N bonds have been formed by HMDS groups inserting into the former F positions on the ring.

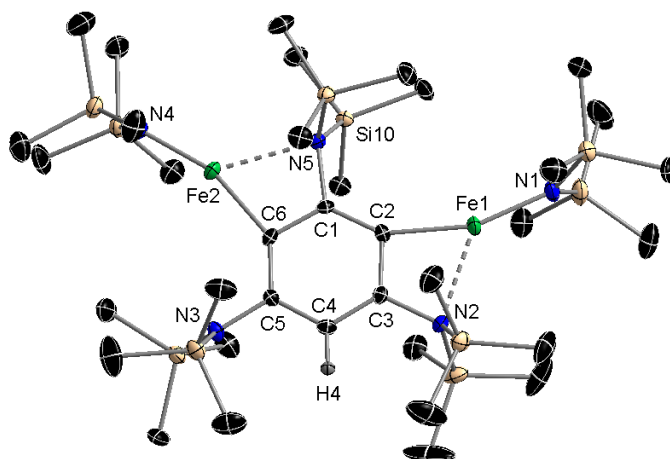
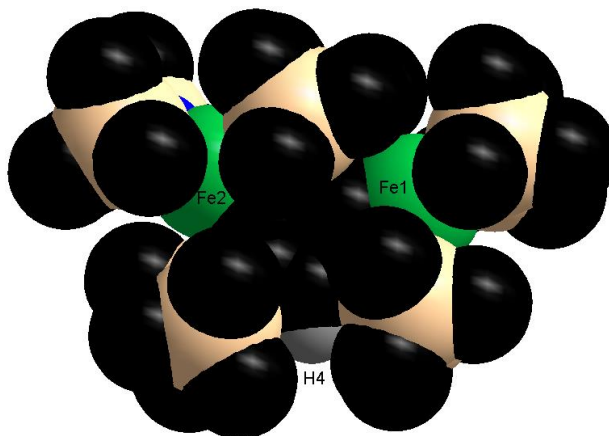
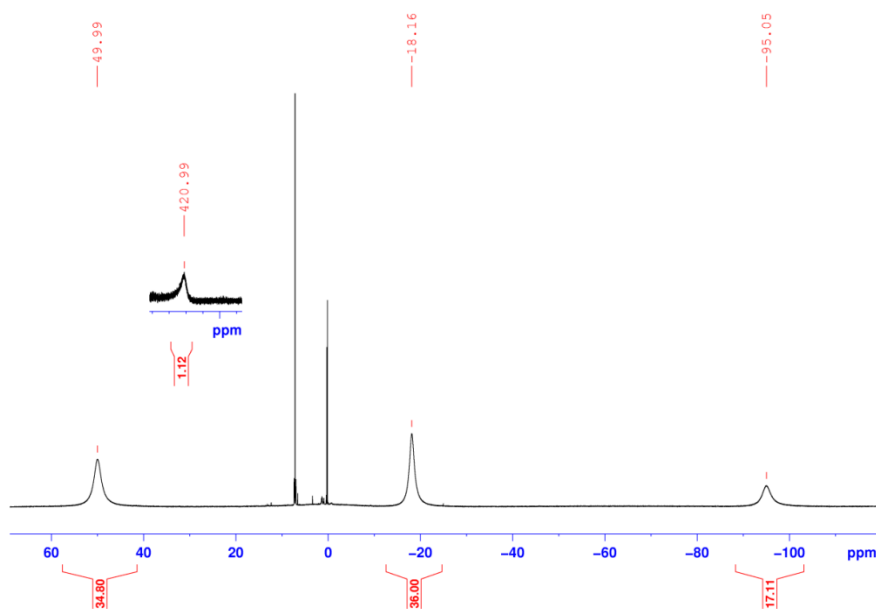


Figure 4.5 – Molecular structure of complex **38**. Hydrogen atoms (except H4) are omitted for clarity. Thermal ellipsoids displayed at 50% probability level. Selected bond distances (Å) and angles (°): Fe1-C2 2.033(3), Fe1-N1 1.916(3), Fe1---N2 2.360(2), Fe2-C6 2.016(3), Fe2-N4 1.922(3), Fe2---N5 2.418(3), N2-C3 1.483(4), N3-C5 1.444(4), N5-C1 1.491(3); C2-Fe1-N1 159.43(12), N1-Fe1---N2 133.77(10), C2-Fe1---N2 66.59(10), C3-C2-Fe1 97.1(2), N2-C3-C2 114.1(3), N2-C3-C4 122.1(3), C2-C3-C4 123.8(3), N3-C5-C4 118.9(3), N3-C5-C6 120.7(3), C4-C5-C6 120.4(3), C6-Fe2-N4 161.06(12), N4-Fe2---N5 133.88(10), C6-Fe2---N5 64.96(10), C1-C6-Fe2 100.5(2), N5-C1-C6 112.3(2), N5-C1-C2 122.7(3), C6-C1-C2 125.0(3).

The two Fe atoms are formally two-coordinate, bridging between a ring carbon and a terminal HMDS group. However, a long distance electrostatic interaction with the N atom of a neighbouring HMDS bonded to the aryl ring is observable for each Fe centre (Fe1---N2 2.360(2) Å, Fe2---N5 2.418(3) Å), manifesting itself in a deviation from linearity between ring carbon C, Fe and HMDS N atoms (C2-Fe1-N1 159.43(12)°, C6-Fe2-N4 161.06(12)°). As seen in the space-filling model (Figure 4.6), **38** is a very densely crowded system with the steric bulk of HMDS groups providing protection for the low coordinate Fe(II) centres.

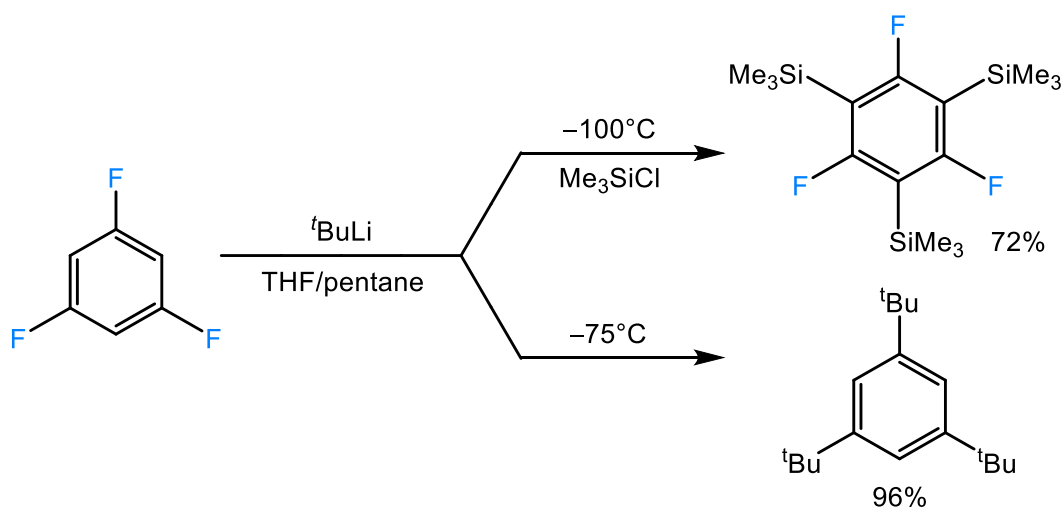
Figure 4.6 – Space-filling model of complex **38**.

The ^1H NMR spectrum in C_6D_6 of complex **38** (Figure 4.7) reveals a remarkable downfield shifted resonance at 420.99 ppm for the sole remaining ring H atom. A very broad and upfield shifted signal is visible at -95.05 ppm integrating to 18H, that is tentatively assigned to the HMDS attached to C1. A further two very broad resonances of equal integration (36H) appear at 49.99 and -18.16 ppm, either of which may correspond to the HMDS groups at C3 and C5 or the HMDS groups attached to Fe. Despite efforts made to unambiguously assign resonances, including the use of truncated driven NOESY,³⁰³ it was not possible in this case.

Figure 4.7 – ^1H NMR spectrum of complex **38** in C_6D_6 .

Recall that the use of organolithium reagents with fluorobenzenes often led to unavoidable benzyne formation via *ortho*-metallation and consequential LiF salt elimination (see Section

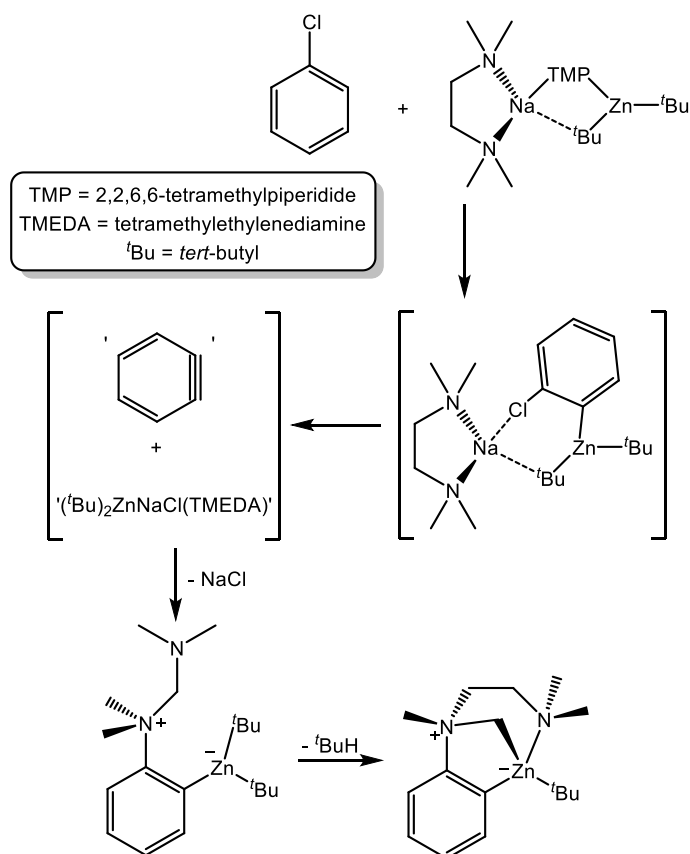
3.1.1) at temperatures above -50°C . *Ortho*-metallation and nucleophilic substitution with fluoroarenes can, under certain circumstances, be competing events as Gilman *et al.* showed that below -100°C strongly nucleophilic $t\text{BuLi}$ exclusively lithiates the *ortho* positions on the ring of 1,3,5-trifluorobenzene whilst at -75°C the fluorine positions are replaced by $t\text{Bu}$ groups (Scheme 4.10).^{304,305}



Scheme 4.10 – C-H vs C-F activation of 1,3,5-trifluorobenzene with $t\text{BuLi}$.^{304–306}

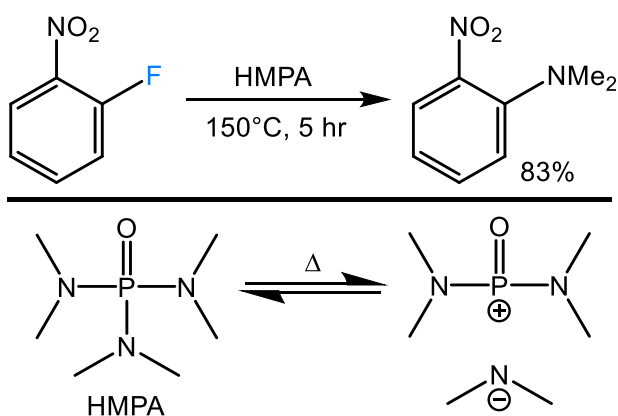
The top pathway is thought not to proceed via tri-lithiation as first proposed³⁰⁵ but via a series of mono-metallated intermediates and the bottom pathway via a cascade of LiF eliminations and $t\text{BuLi}$ additions (di-lithiation/benzyne formation).³⁰⁶

To compare and contrast the syntheses of **36**, **37** and **38** with Gilman's work and the reported reactivity of bimetallic base $[(\text{TMEDA})\text{NaZn}(\text{TMP})(t\text{Bu})_2]$ with chlorobenzene (Scheme 4.11, also see Section 3.1.1),²⁴² the reaction of sodium ferrate base **17a** and 1,3,5-trifluorobenzene can furnish solely ferrated intermediate products **36**, **37** and **38** at temperatures of 0°C and above which are stable enough to be isolated and characterised. Furthermore, though there is the removal of halogens (F) in the case of **38**, the reactions carried out provided no evidence of benzyne formation by the absence of any further reaction products (e.g. isomers, 1,2-addition products) that would have arisen if that were the case.



Scheme 4.11 – Proposed mechanistic pathway of zincation of chlorobenzene followed by benzyne formation and isolation of α -zincated N ylides.²⁴²

C-F to C-N nucleophilic aromatic substitution has been previously observed with 1-fluoro-2-nitrobenzene and hexamethylphosphoramide (HMPA), as shown in Scheme 4.12.³⁰⁷

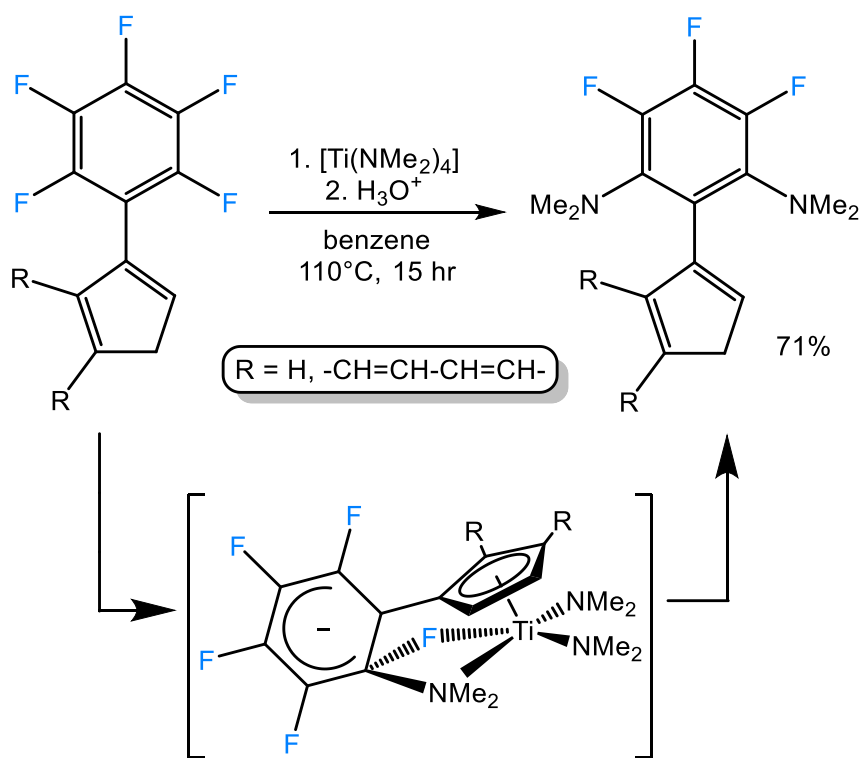


Scheme 4.12 – C-F to C-N transformation via nucleophilic aromatic substitution.³⁰⁷

HMPA is reasoned to exhibit some ionic character at elevated temperatures, releasing a suitably labile -NMe_2 unit which can add to the aromatic ring and release F^- , not to mention

the substituted NO_2 group is known to activate *ortho*-F positions towards nucleophilic aromatic substitution.^{212,289,307}

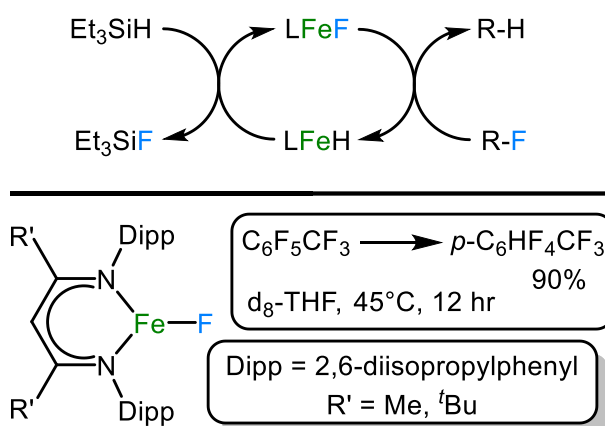
Very much related is the proposed intramolecular C-F to C-N nucleophilic aromatic substitution that has been reported with titanium complex $[\text{Ti}(\text{NMe}_2)_4]$ (Scheme 4.13).³⁰⁸ Reaction of pentafluorophenylcyclopentadiene and pentafluorophenylindene with the Ti complex affords the doubly aminated products where NMe_2 has been substituted at the *ortho* positions on the 6-membered ring. Three similar examples of proposed intramolecular fluorine/amine exchange have been reported at Mo ,³⁰⁹ Zr ³¹⁰ and Hf ³¹¹ early transition-metal centres.



Scheme 4.13 – Intramolecular nucleophilic fluorine/amine exchange with a titanium complex.³⁰⁸ [Figure adapted from Braun *et al.*].²⁸⁹

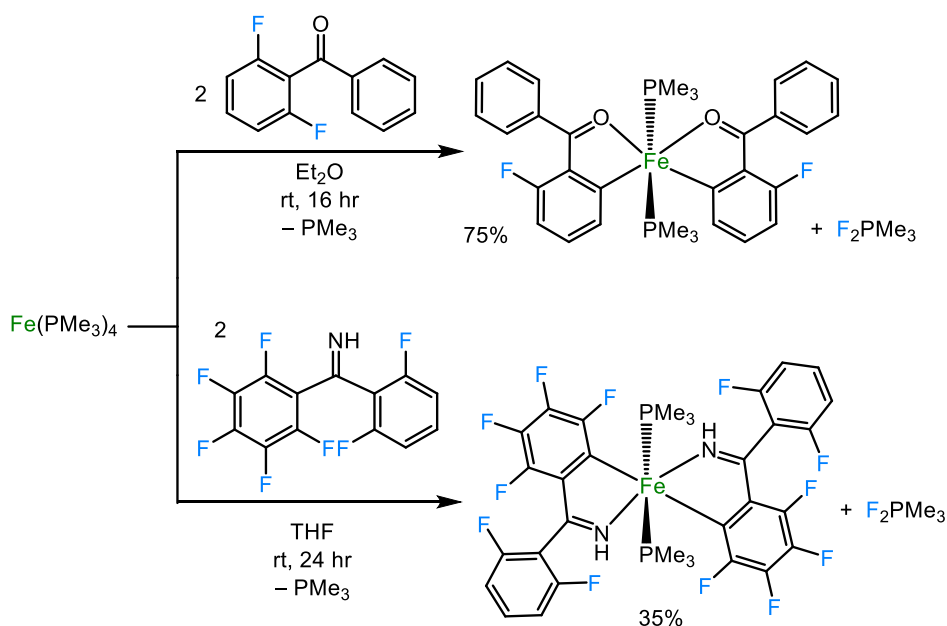
The reported involvement of iron in C-F activation reactions is currently extremely scarce; the only apparent reports before 1995 are concerned with heterogeneous or gas-phase C-F activations with Fe (a number of which are summarised in a review by Richmond *et al.*).²⁸⁸ Muir has reported intramolecular C-F activation with perfluorovinylidiron complexes involving fluoride migration and attack by primary and secondary amines³¹² and phosphine nucleophiles.³¹³ Catalytic hydrodefluorination of a range of pefluorinated aromatics and

olefins has been reported by Holland with Fe(II) complex [LFeF] (L = β -diketamine ligand) and Et₃SiH (Scheme 4.14).²⁵⁰



Scheme 4.14 – Fe-catalysed hydrodefluorination of fluorohydrocarbons.²⁵⁰

Li and co-workers have reported two instances of C-F activation by Fe(PMe₃)₄ with a fluoroarylketone³¹⁴ and fluoroarylimine^{263,315} substrates, generating new Fe(II) complexes (Scheme 4.15). Identification of an equivalent quantity of F₂PMe₃ in the reaction via ¹⁹F{¹H} and ³¹P{¹H} NMR spectroscopy lead the authors to propose a Fe(0)/Fe(II) redox mechanism progressing through Fe(I) and Fe(III) transition states with oxidative addition and removal of F by the labile PMe₃ ligands.



Scheme 4.15 – Fe(0) to Fe(II) C-F activation with fluoroarylketone³¹⁴ and fluoroarylimine²⁶³ substrates.

Complex **38** comprises of not one but two di-coordinate Fe centres. Recently there has been a high degree of interest in stable two-coordinate, open-shell transition metal complexes, noted as some of the rarest and most unexplored compounds in coordination chemistry.³¹⁶ Exhibiting high degrees of coordinative unsaturation, complexes of this class habitually demonstrate unique physical properties and reactivities.³¹⁶ Furthermore, linearly coordinated complexes command a great deal of attention because of their potential to exhibit interesting and unusual magnetic behaviour,^{317–319} particularly Fe(II) complexes which have been the most heavily researched.³¹⁶ Two-coordinate transition metal complexes may display highly anisotropic internal magnetic fields, high orbital angular momenta and high zero-field splittings, all of which can lead to high barriers to spin flipping which are required for single-molecule magnet (SMM) behaviour.^{205,316} One such complex that exhibits such characteristics is linear two-coordinate $[\text{Fe}\{\text{C}(\text{SiMe}_3)_2\}]$,³¹⁷ which exists as a monomer^{320,321} in the solid-state unlike its HMDS congener at ambient temperature which has a dimeric structure (Figure 4.8).⁹²

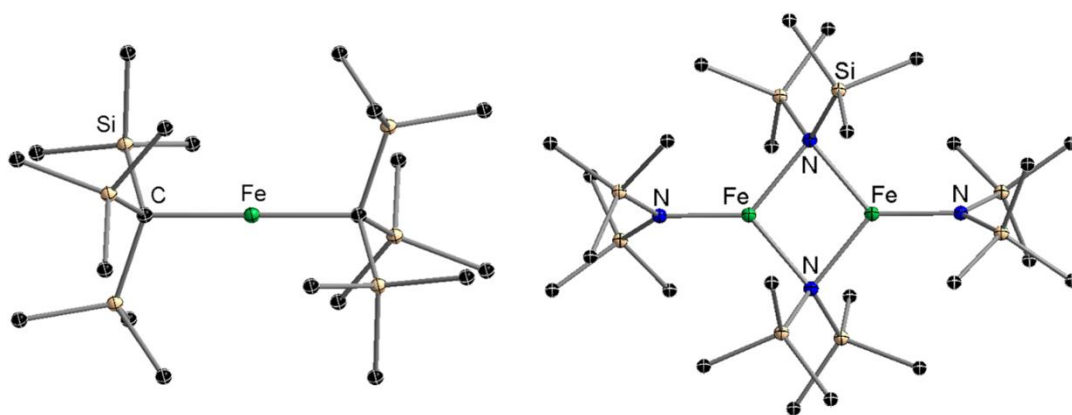
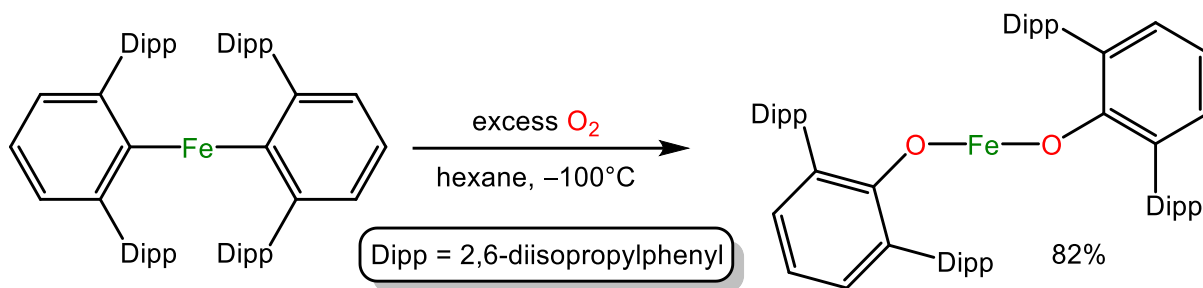


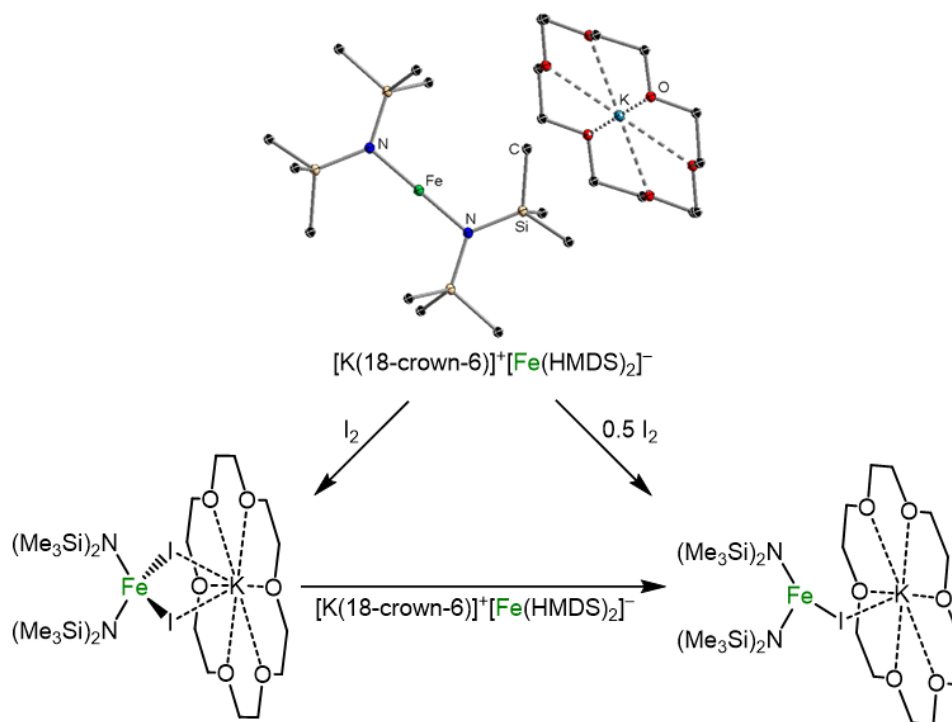
Figure 4.8 – Solid-state structures of monomeric $[\text{Fe}\{\text{C}(\text{SiMe}_3)_2\}]$ ^{320,321} (right) and dimeric $[\{\text{Fe}(\text{HMDS})_2\}_2]$ ⁹² (left).

As an example of reactivity, two-coordinate Fe(II) diaryl complex $\text{Fe}(\text{Ar}')_2$ ($\text{Ar}' = \text{C}_6\text{H}_3\text{-2,6-}(\text{C}_6\text{H}_3\text{-2,6-}^i\text{Pr}_2)_2$) can activate O_2 to generate the bis(aryloxide) derivative, $\text{Fe}(\text{OAr}')_2$ (Scheme 4.16), that is resistant to further oxidation with excess O_2 ; this is in contrast to most Fe complexes that participate in non-heme O_2 activation which generally undergo oxidation to yield Fe(III) complexes.³²²



Scheme 4.16 - Insertion of oxygen into two-coordinate Fe(II) diaryl complex to yield the bis(aryloxy) derivative.³²²

As **38** possesses two linearly di-coordinated Fe metal centres in close proximity this should only seek to enhance the potential magnetic behaviour as coupling between the metal centres should be possible (see Section 4.2.5 for magnetometry studies). The formal coordination number of the Fe centres in **38** are however up for debate when considering the secondary Fe---N interactions present, especially as the coordination number of other primarily two-coordinate Fe complexes have been disagreed upon in the past.^{323,324} The secondary Fe---N electrostatic interactions are of lengths of 2.360(2) and 2.418(3) Å (for Fe1---N2 and Fe2---N5, respectively) and induce roughly a 20° divergence from linearity for the Fe centres between the aryl C and HMDS N atoms (C2-Fe1-N1 159.43(12)°, C6-Fe2-N4 161.06(12)°). Whilst a number of Fe---C_{aryl} weak secondary interactions have been reported for formally di-coordinate Fe complexes possessing aryl ligand substituents (ranging from 3.068 Å³²² to 2.389(2) Å³²⁵), reports of Fe---N secondary interactions appear to be scarce, adding a unique property to **38**. The lengths of these secondary Fe---N interactions are however considerably longer than the bond distances observed between Fe and its terminal HMDS group and the aryl ring in **38**; 1.916(3) and 1.922(3) Å for Fe1-N1 and Fe2-N4, respectively, and Fe-C bond lengths of 2.033(3) and 2.016(3) Å for Fe1-C2 and Fe2-C6, respectively. For comparable reference, the average Fe-N_{terminal} bond length in [$\{\text{Fe}(\text{HMDS})_2\}_2$] is 1.925 Å⁹² and the average Fe-C_{terminal} bond length in [$\{\text{Fe}(\text{Mes})_2\}_2$] is 2.024 Å,³²⁶ though both these complexes are formally tri-coordinate.



Scheme 4.17 – Crystal structure of [K(18-crown-6)]⁺[Fe(HMDS)₂]⁻ and 1e⁻ and 2e⁻ oxidations with I₂.³²⁷ Hydrogen atoms are omitted for clarity.

Sabo-Etienne and co-workers have recently reported the synthesis of linear two-coordinate Fe(I) HMDS salts.³²⁷ Starting from [$\{Fe(HMDS)_2\}_2$] they can access potassium salt complexes via reduction with KC₈ in the presence of either 18-crown-6 or 2,2,2-crypt, even from trigonal planar [Fe(HMDS)₂(PCy₃)], demonstrating two-coordinate geometry of the Fe(II) precursor is not compulsory to access a two-coordinate Fe(I) derivative. The Fe(I) potassium salts display single-molecule magnet behaviour and 1e⁻ and 2e⁻ oxidations of [K(18-crown-6)]⁺[Fe(HMDS)₂]⁻ were achieved by adding 0.5 eq. and 1 eq. of I₂, respectively (Scheme 4.17).

It has been logically concluded in the preceding literature that the notable hard acid/hard base interactions of the type M---F-C (where M = Na for ferrated complexes in Chapter 3 and complexes **36** and **37** in this chapter) may facilitate cleavage of the C-F bond.^{210,288,328,329} A demonstrable example of this is [Na(OCH(CF₃)₂)] whose solid state structure displays considerable Na---F-C interactions; chemical vapour deposition of the complex onto silica at 285°C deposits pure NaF.³³⁰

To assess if the formation of **38** occurs with the concomitant elimination of NaF, NMR spectroscopic analysis of the accompanying brown solid recovered from the synthesis of **38** was successfully carried out. The solid proved to be completely insoluble in deuterated organic solvents, however it dissolved well in D₂O. A comparison of the ¹⁹F{¹H} NMR spectra of this brown solid with that of a standard of NaF strongly suggests that this solid is indeed NaF with the former exhibiting a single resonance at -122.30 ppm and the latter a single resonance at -122.57 ppm (Figure 4.9). It is interesting to conclude that sodium, which is instrumental in stabilising all of the ferrated fluoroaryl complexes through dative Na-F interactions, appears to also be now a major player in the activation of these strong C-F bonds. The formation of NaF is not entirely surprising though, given the highly energetically favourable lattice formation enthalpy of NaF (-930 kJ/mol).²⁶⁶

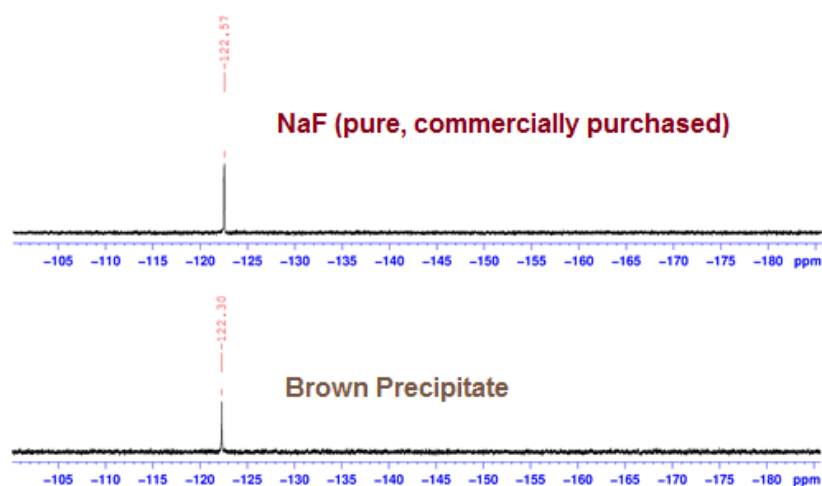


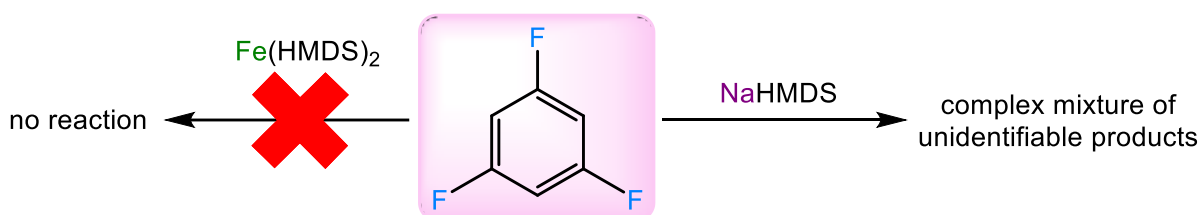
Figure 4.9 – ¹⁹F{¹H} NMR spectra comparison of pure NaF and isolated brown precipitate in D₂O from the reaction of **17a** (3 eq.) and 1,3,5-trifluorobenzene.

4.2.3 Mechanistic Investigations

In order to understand more about the complex C-F activation of 1,3,5-trifluorobenzene with sodium ferrate base **17a** we sought a multi-platform approach to investigate the mechanism of this complex reaction.

4.2.3.1 Assessing the Reaction of 1,3,5-Trifluorobenzene with Single-Metal Components of **17a**

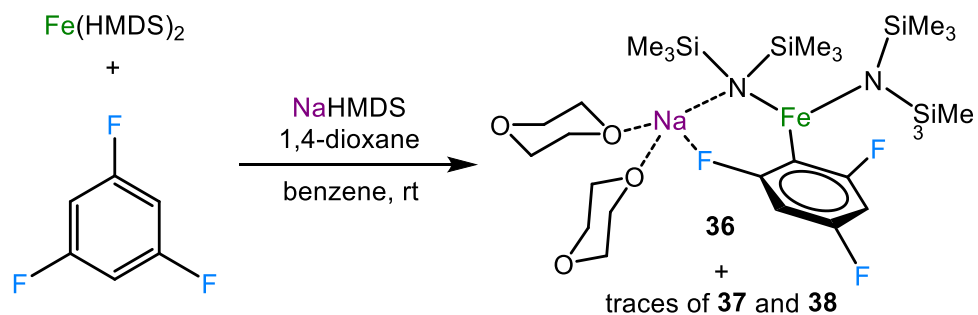
Firstly, it was prudent to assess the reaction of NaHMDS and $\text{Fe}(\text{HMDS})_2$, single-metal components of **17a**, with 1,3,5-trifluorobenzene which were investigated by X-ray crystallography and NMR spectroscopy (Scheme 4.18). Addition of 0.33 eq. of the substrate to a 1 mmol hexane solution $\text{Fe}(\text{HMDS})_2$ produced solely crystals of $\text{Fe}(\text{HMDS})_2$ (even after refluxing at 80°C) and showed no evidence of reaction by ^1H NMR spectroscopy.



Scheme 4.18 – Monometallic reagent effects with 1,3,5-trifluorobenzene.

A 1:1 mixture of NaHMDS and 1,3,5-trifluorobenzene in C_6D_6 was monitored by ^1H , $^{13}\text{C}\{^1\text{H}\}$, $^{19}\text{F}\{^1\text{H}\}$ NMR spectroscopy over 4 days at ambient temperature. In the ^1H and $^{13}\text{C}\{^1\text{H}\}$ NMR spectra, the corresponding resonances for 1,3,5-trifluorobenzene and NaHMDS slowly diminished over this time period with a concomitant increasing signal for HMDS(H). After this time period, in the ^1H NMR spectra, there are multiple overlapping signals of very low intensity present in the baseline around the aromatic region and additionally the $^{19}\text{F}\{^1\text{H}\}$ NMR spectrum now shows multiple peaks. Thus, it can be suggested that 1,3,5-trifluorobenzene is likely metallated by NaHMDS to some degree but extremely inefficiently, leading to many unidentifiable products; evidence of NaF formation or addition of HMDS to the ring was not forthcoming.

Addition of 1 eq. of 1,3,5-trifluorobenzene to a benzene solution of $\text{Fe}(\text{HMDS})_2$ showed no reaction but upon addition of equimolar quantities of NaHMDS and 1,4-dioxane the emergence of mono-metallated product **36** became apparent in the ^1H NMR spectrum along with traces of di-metallated **37** and C-F activation product **38** (Scheme 4.19).



Scheme 4.19 – Equimolar reaction of $\text{Fe}(\text{HMDS})_2$ and 1,3,5-trifluorobenzene with subsequent addition of NaHMDS and 1,4-dioxane leading to an *in-situ* formation of **17a** which furnishes **36** predominately with traces of **37** and **38**.

4.2.3.2 Dynamic Nature of the Reaction

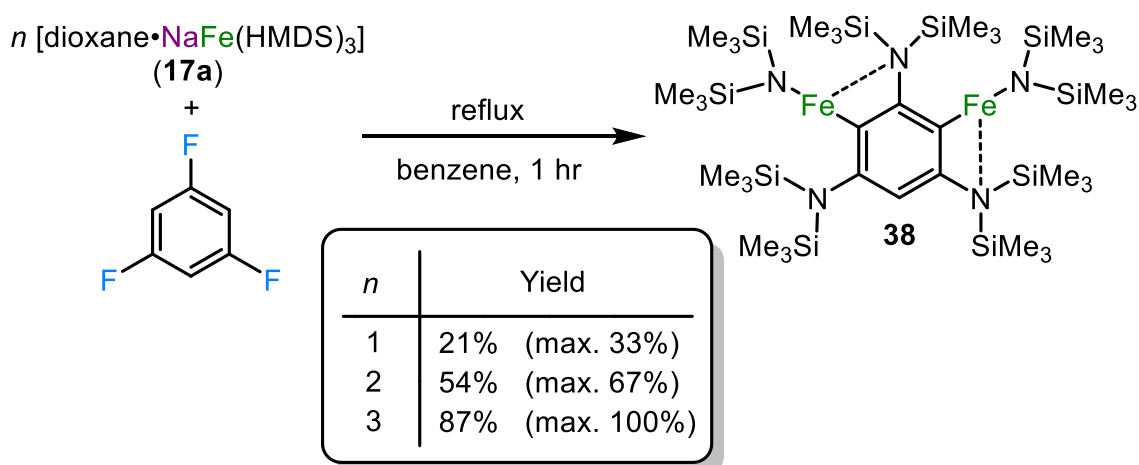
During the course of investigations into the synthesis of complexes **36**, **37** and **38** it became apparent that the pathways to each product were not static and that at points in time, mixtures of all three products could be found in the reaction mixture, regardless of stoichiometry. ^1H NMR data allowed us to observe the presence of a three products in solution via their characteristic resonances, which are summarised in Table 4.2.

Table 4.2 – ^1H NMR spectroscopic chemical shift values (in ppm) of isolated complexes **36**, **37** and **38** in C_6D_6 .

Complex	^1H Chemical Shift (ppm)		
	Aryl H	HMDS	1,4-dioxane
36	101.64 (2H)	-2.26	4.85
37	177.56	-3.14	2.49
38	420.99	49.99 -18.16 -95.05	-

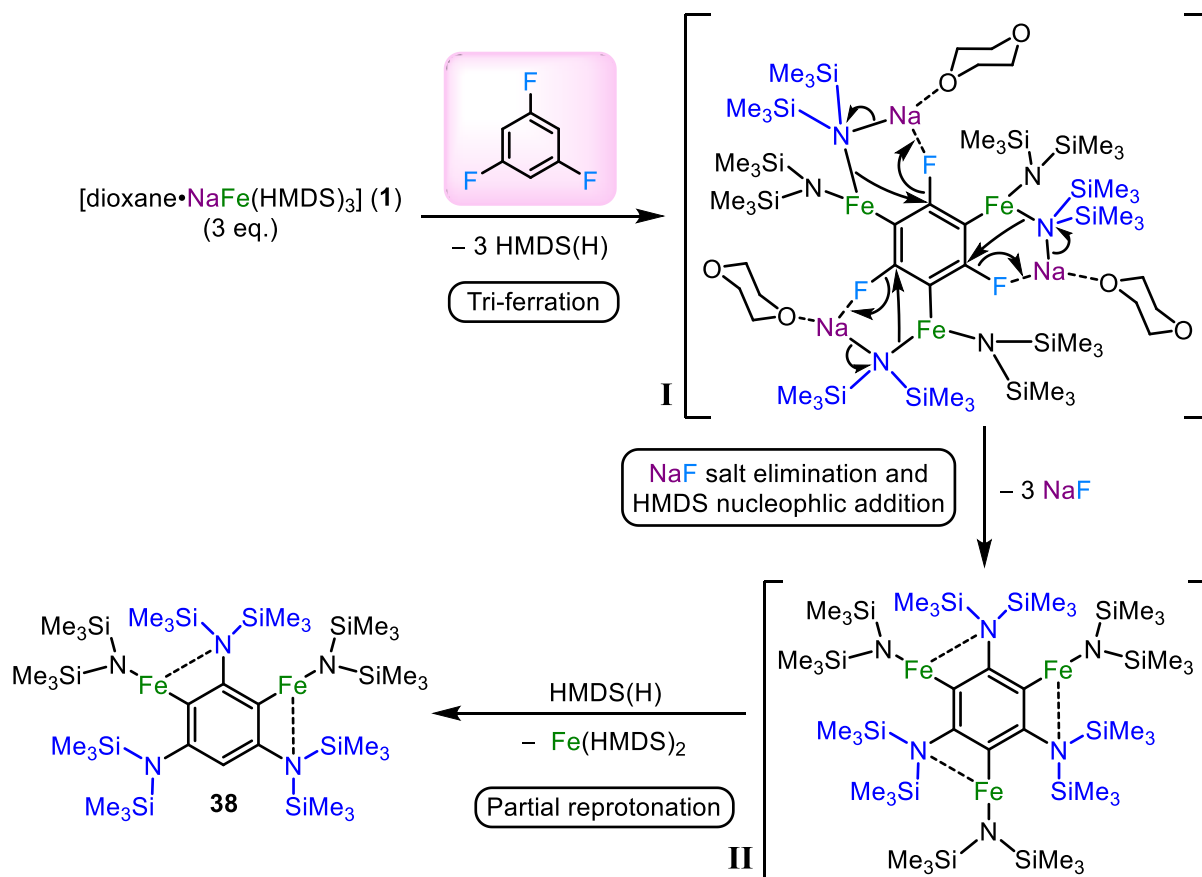
Scheme 4.8 and Scheme 4.9 (see above) represent the ideal (and stoichiometrically correct) conditions to promote and favour the formation of each product, which are essence is purified by crystallisation allowing for each to be isolated in a pure form. Heating solutions of **17a** and 1,3,5-trifluorobenzene, regardless of stoichiometry, promoted the formation of C-F activation product **38**. At stoichiometries of 1:1 and 2:1, above 0°C , **38** could be recovered in yields of 54% and 21%, respectively (where maximum possible yields are 66.67% and 33.33%, respectively) (Scheme 4.20). Conducting the syntheses of **36** and **37** at 0°C was

necessary to suppress the formation of **38** (and to a degree, the formation of **37** in the case of **36**).



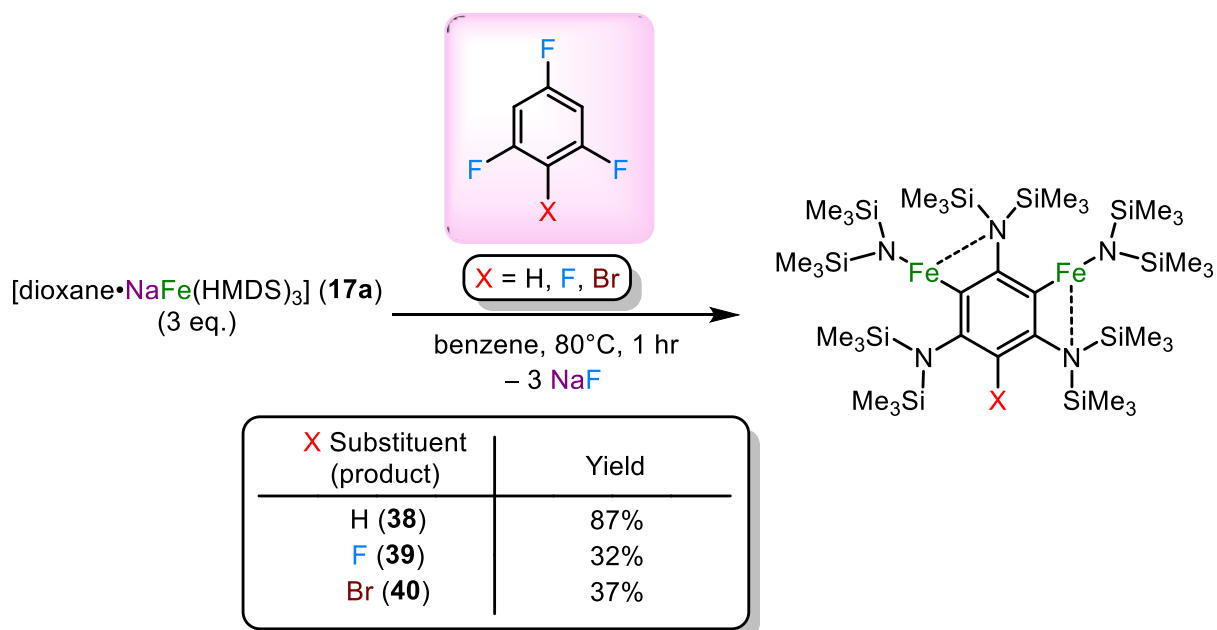
Scheme 4.20 – Synthesis of **38** at different stoichiometries.

Considering di-metallated product **37** and the elimination of NaF and formation of three new C-N bonds in **38**, a possible explanation could be the tri-ferration of 1,3,5-trifluorobenzene, affording a highly reactive intermediate (**I**) with subsequent elimination of 3 eq. of NaF, which would favour the intramolecular nucleophilic attack of the aryl ring by three HMDS groups (attached Fe atoms) to give intermediate **II**. Intermediate **II** could react with some of the free amine, HMDS(H), generated in the ferration step to give Fe(HMDS)₂ and final product **38** (Scheme 4.21).

Scheme 4.21 – Postulated tri-ferration mechanism for the formation of **38**.

4.2.3.3 Extension to 1,3,5-Trifluorobenzene Derivatives

Precluding a tri-metallation mechanism however, are the products of reactions with respective fluoro- and bromo-derivatives 1,2,3,5-tetrafluorobenzene and 1-bromo-2,4,6-trifluorobenzene, where one of the available ring hydrogen positions is now occupied by either F or Br (Scheme 4.22).



Scheme 4.22 – C-H and C-F activation of 1,3,5-trifluorobenzenes.

1 mmol of 1,2,3,5-tetrafluorobenzene was added to a 3 mmol solution of **17a** and refluxed for one hour. Upon reaching reflux the solution changed colour from green to brown/dark red and flat yellow needle-like crystals were grown from it over several hours at $\sim 5^\circ\text{C}$. X-ray crystallography revealed the structure as [1,3-bis(FeHMDS)-2,4,6-tris(HMDS)-C₆F] (**39**) (Figure 4.10), formed in a 32% yield.

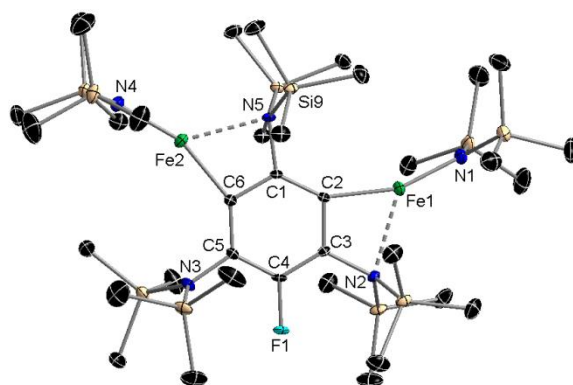


Figure 4.10 – Molecular structure of complex **39**. Hydrogen atoms are omitted for clarity. Thermal ellipsoids displayed at 50% probability level. Selected bond distances (Å) and angles (°): Fe1-C2 2.0344(13), Fe1-N1 1.9139(12), Fe1---N2 2.4136(11), Fe2-C6 2.0259(13), Fe2-N4 1.9250(12), Fe2---N5 2.3999(11), N2-C3 1.4770(16), N3-C5 1.4386(16), N5-C1 1.4935(15), F1-C4 1.3704(14); C2-Fe1-N1 159.73(5), N1-Fe1---N2 133.68(5), C2-Fe1---N2 66.15(4), C3-C2-Fe1 97.27(8), N2-C3-C2 115.83(11), N2-C3-C4 123.02(11), C2-C3-C4 121.14(11), N3-C5-C4 119.37(11), N3-C5-C6 122.50(11), C4-C5-C6 118.13(11), C6-Fe2-N4 159.48(5), N4-Fe2---N5 135.15(4), C6-Fe2---N5 65.28(4), C1-C6-Fe2 99.87(8), N5-C1-C6 112.01(10), N5-C1-C2 122.71(10), C6-C1-C2 125.26(11).

Similarly, to a 1 mmol solution of **17a**, 0.33 mmol of 1-bromo-2,4,6-trifluorobenzene was added and the solution refluxed for one hour, exhibiting a colour change from green to brown and furnishing thin yellow rod crystals. X-ray crystallographic analysis uncovered the structure as [1,3-bis(FeHMDS)-2,4,6-tris(HMDS)-C₆Br] (**40**) (Figure 4.11), formed in a 37% yield.

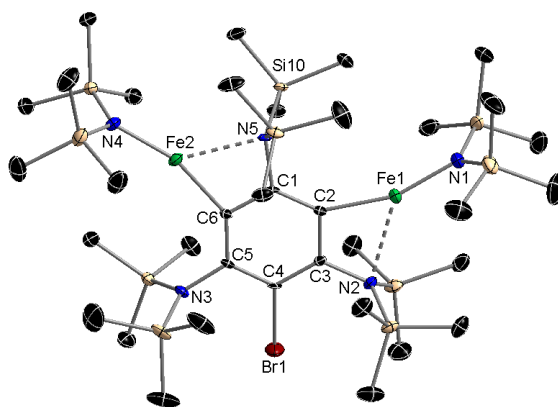


Figure 4.11 – Molecular structure of complex **40**. Hydrogen atoms are omitted for clarity. Thermal ellipsoids displayed at 50% probability level. Selected bond distances (Å) and angles (°): Fe1-C2 2.040(2), Fe1-N1 1.924(2), Fe1---N2 2.5351(22), Fe2-C6 2.028(2), Fe2-N4 1.930(2), Fe2---N5 2.4808(21), N2-C3 1.480(3), N3-C5 1.448(3), N5-C1 1.501(3), Br1-C4 1.926(2); C2-Fe1-N1 161.26(10), N1-Fe1---N2 134.553(89), C2-Fe1---N2 63.725(80), C3-C2-Fe1 101.12(16), N2-C3-C2 115.2(2), N2-C3-C4 124.1(2), C2-C3-C4 120.7(2), N3-C5-C4 120.3(2), N3-C5-C6 120.9(2), C4-C5-C6 118.8(2) C6-Fe2-N4 161.39(10), N4-Fe2---N5 134.647(89), C6-Fe2---N5 63.849(82), C1-C6-Fe2 102.37(16), N5-C1-C6 111.8(2), N5-C1-C2 123.1(2), C6-C1-C2 125.0(2).

As can clearly be seen, refluxed reactions of 3:1 stoichiometry with 1,2,3,5-tetrafluorobenzene and 1-bromo-2,4,6-trifluorobenzene lead to C-F activation products **39** and **40**, respectively, both of which are isostructural with C-F activation product **38**. This structural similarity and the retention of F or Br at the position *meta* to both Fe atoms all but rules out a tri-metallation mechanism. Furthermore, these dinuclear complexes appear to be the first structurally characterised examples of systems possessing two pseudo-linear Fe(II) centres.

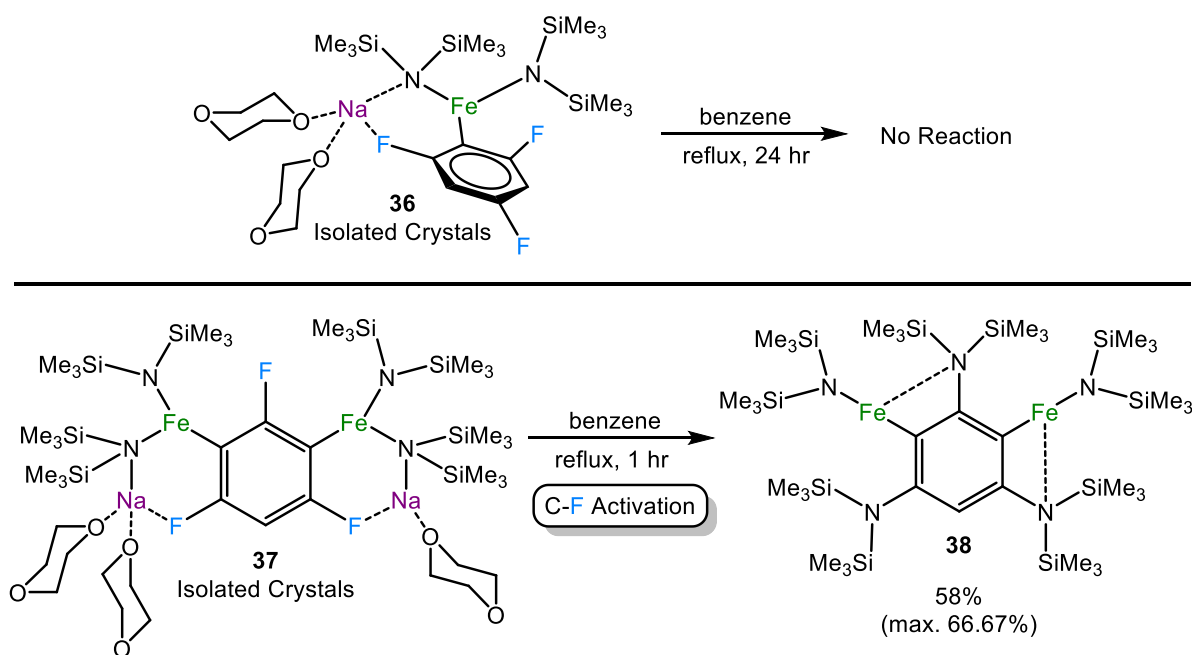
Table 4.3 - Selected geometrical parameters of compounds **38**, **39** and **40**. Bond distances are given in Ångstroms and bond angles given in degrees (°).

Bond/Angle	38	39	40
Fe1-C2	2.033(3)	2.0344(13)	2.040(2)
Fe2-C6	2.016(3)	2.0259(13)	2.028(2)
Mean Fe-C	2.025	2.0302	2.034
Fe1-N1	1.916(3)	1.9139(12)	1.924(2)
Fe2-N4	1.922(3)	1.9250(12)	1.930(2)
Mean Fe-N	1.919	1.9195	1.927
Fe1---N2	2.360(2)	2.4136(11)	2.5351(22)
Fe2---N5	2.418(3)	2.3999(11)	2.4808(21)
Mean Fe---N	2.389	2.4068	2.5080
N2-C3	1.483(4)	1.4770(16)	1.480(3)
N3-C5	1.444(4)	1.4386(16)	1.448(3)
N5-C1	1.491(3)	1.4935(15)	1.501(3)
Mean N-C	1.473	1.4697	1.476
C2-Fe1-N1	159.43(12)	159.73(5)	161.26(10)
C6-Fe2-N4	161.06(12)	159.48(5)	161.39(10)
C2-Fe1---N2	66.59(10)	66.15(4)	63.725(80)
C6-Fe2---N5	64.96(10)	65.28(4)	63.849(82)

Comparing the geometries of complexes **38**, **39** and **40** (Table 4.3), little difference is observed between the primary bond lengths and angles. The substituent atom at C4 (H, F or Br) has essentially no effect on the structural geometry.

4.2.3.4 Thermal Stabilities of Complexes **36** and **37**

Speculating whether mono- and di-ferrated complexes **36** and **37** could evolve to **38** under forcing reaction conditions, the thermal stabilities of these compounds were evaluated by refluxing benzene/ C_6D_6 solutions of each, prepared from pure isolated crystalline material (Scheme 4.23). The reactions were monitored by 1H NMR spectroscopy and X-ray crystallography. Compound **36** demonstrated a great thermal stability and after 24 hours at $80^\circ C$ it does not convert into any other species.



Scheme 4.23 – Thermal stability assessment of complexes **36** and **37**.

Contrastingly, it was found that refluxing a benzene solution of di-ferrated **37** for 1 hour or indeed by leaving a C_6D_6 solution of **37** for several days without the application of heat (*ca.* 5 days for full consumption of **37**) lead to the evolution of C-F activation product **38**. Crystals of **38** were obtained in a 58% isolated yield from a 1 mmol scale reaction. Furthermore, addition of 1 or 2 eq. of **17a** to the solution of robust mono-metallated complex **36** led to the same result with consumption of the **17a**, visualised by the disappearance of the **17a**'s HMDS

resonance at -4.72 ppm in the ^1H NMR spectra. The addition of 1 eq. of **17a** to a solution of **37** also showed consumption of **17a** with the simultaneous formation of complex **38** along with $\text{Fe}(\text{HMDS})_2$. Thus, whilst the isolated mono-ferrated product **36** is stable in benzene, it appears **37** is a meta-stable product which over time evolves to **38** in solution.

4.2.3.5 From Di-metallation to C-F Activation

Evaluating at this point, it appears sodium ferrate base **17a** is required to perform the ferration and C-F of 1,3,5-trifluorobenzene and that under refluxing conditions, di-ferrated product **37** is fully consumed furnishing the C-F activation product **38**.

Heating the solution of pure and prior isolated **37**, the corresponding ^1H NMR spectroscopy resonances for **37** completely disappear with formation of the three new HMDS signals for **38** (Figure 4.12). Stoichiometrically there is a mismatch, going from 4 HMDS groups (**37**) to 5 HMDS groups (**38**), suggesting that **38** is formed as a consequence of a redistribution process, although other possible Fe-containing species could not be confidently characterised.

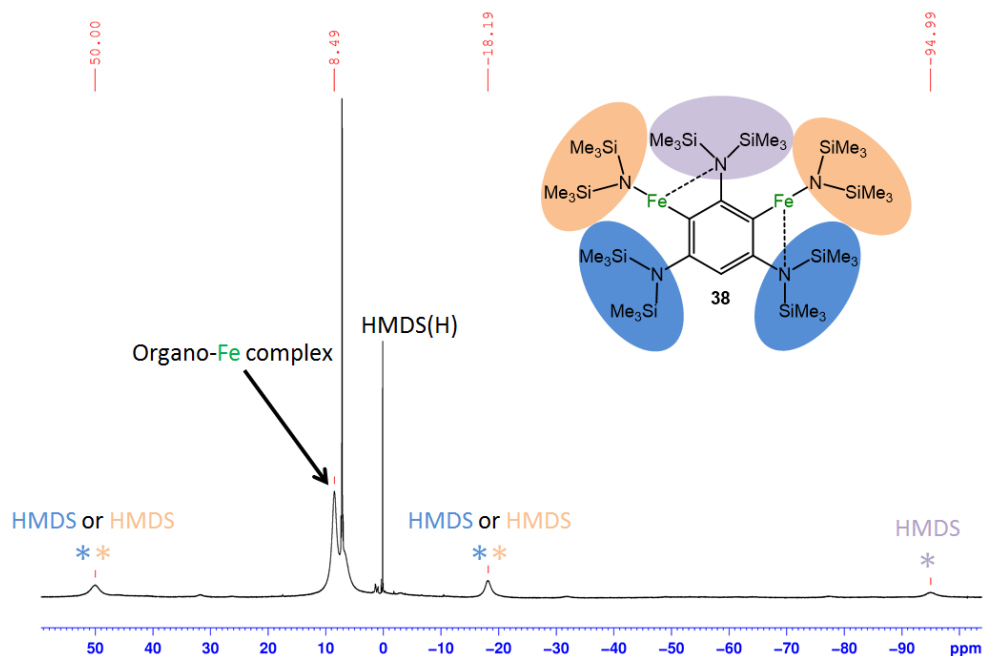
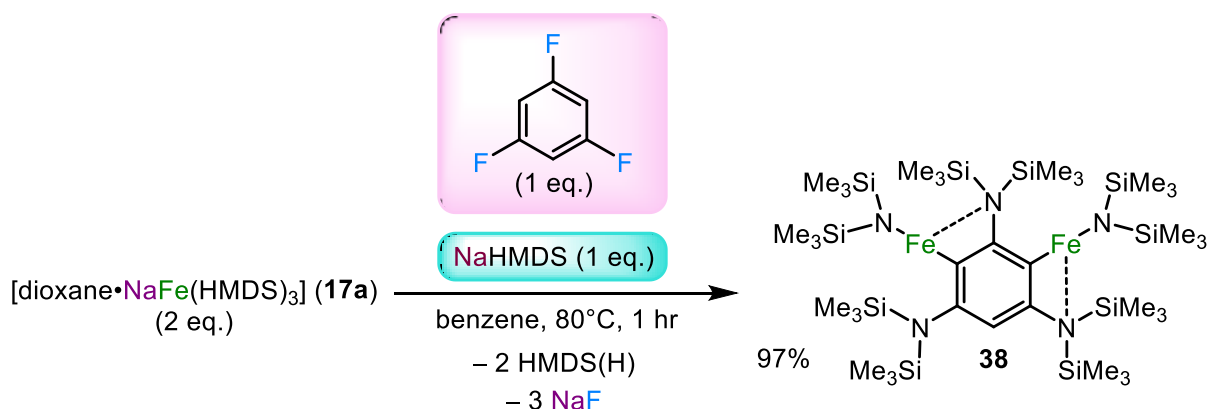


Figure 4.12 – ^1H NMR spectrum of **38** from the refluxed solution of **37**. The broad resonance at 8.49 ppm is proposed to correspond to an unknown organo-Fe complex.

From the reactions with **37**, apart from the three HMDS resonances attributed to **38**, the only other significant signal in the ^1H NMR spectra is an unknown broad resonance (Figure 4.12),

its peak centred anywhere from ~15 to ~5 ppm, which would belong to this unknown Fe complex.

Illuminatingly, it was found that the addition of 1 eq. of NaHMDS to a C₆D₆ solution of di-metallated complex **37** and refluxing quantitative showed conversion to complex **38** with the consumption of NaHMDS. Stoichiometrically the reaction is balanced with three Na atoms to liberate the three ring F atoms and five units of HMDS present which are preserved in the structure of **38**. This result suggests that in the absence of any excess NaHMDS some of **37** could undergo redistribution, eliminating some NaHMDS which in turn could react with some of **37** to give **38**.

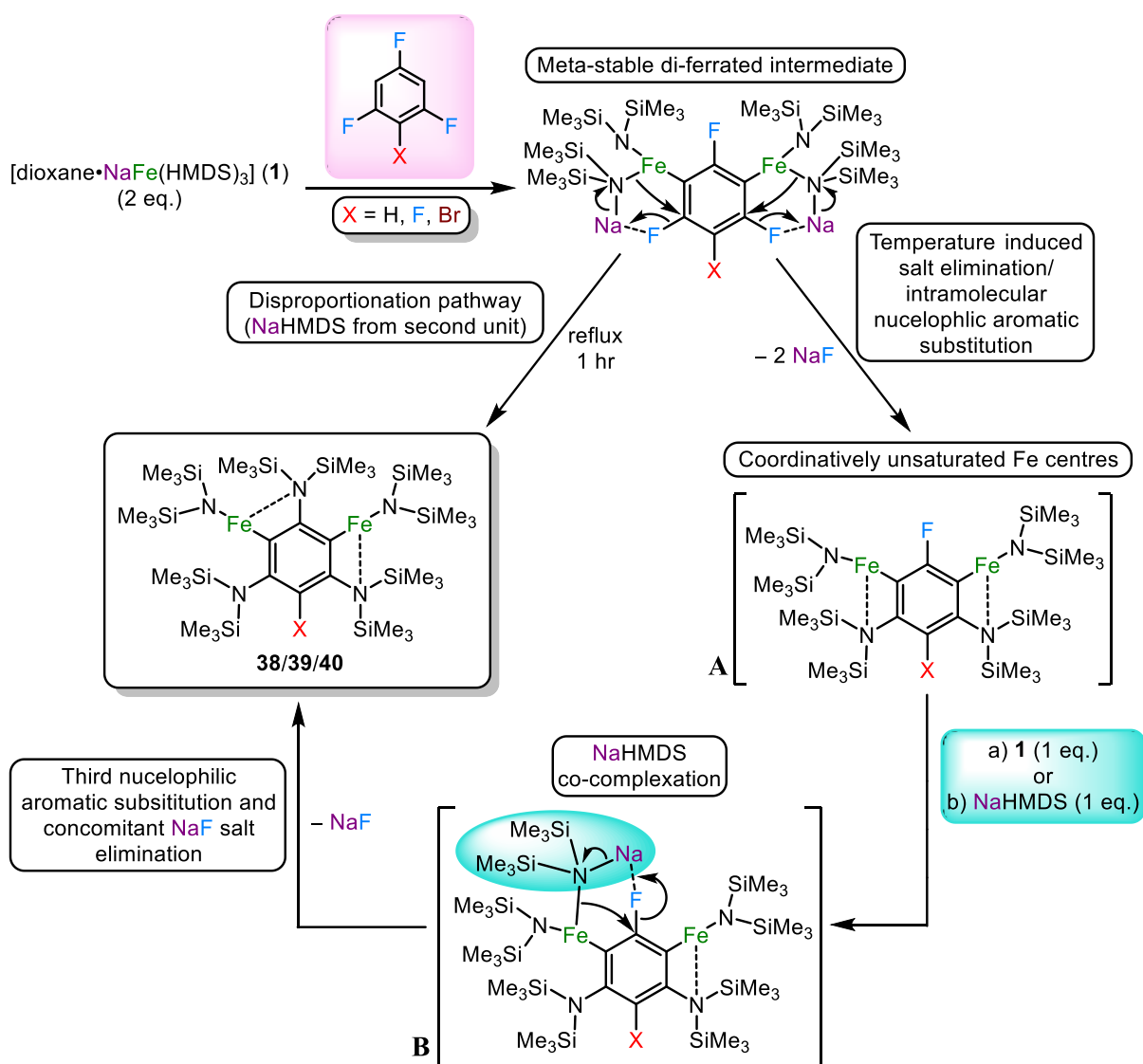


Scheme 4.24 – Stoichiometrically correct reaction where two eq. of **17a** and 1 eq. of NaHMDS are required to attain a near quantitative yield of compound **38**.

Finally, a benzene mixture of 2 eq. of **17a**, 1 eq. of NaHMDS and 1 eq. of 1,3,5-trifluorobenzene was refluxed for 1 hour, after which the mixture was filtered hot to remove NaF and the filtrate allowed to crystallise (Scheme 4.24). All volatiles were removed under vacuum and the combination of crystalline and amorphous solid product was collected. The sole product was confirmed by ¹H NMR spectroscopy as complex **38** which was obtained in a 97% yield, supporting that a 2:1:1 (base:NaHMDS:substrate) combination leads to the quantitative formation of the C-F activation product **38**.

4.2.3.6 Mechanistic Proposal: Cascade Reaction

Considering knowledge accrued from our investigations, the following mechanism can be proposed for the di-ferration and subsequent C-F activation of 1,3,5-trifluorobenzene with sodium ferrate base **17a** (Scheme 4.25).



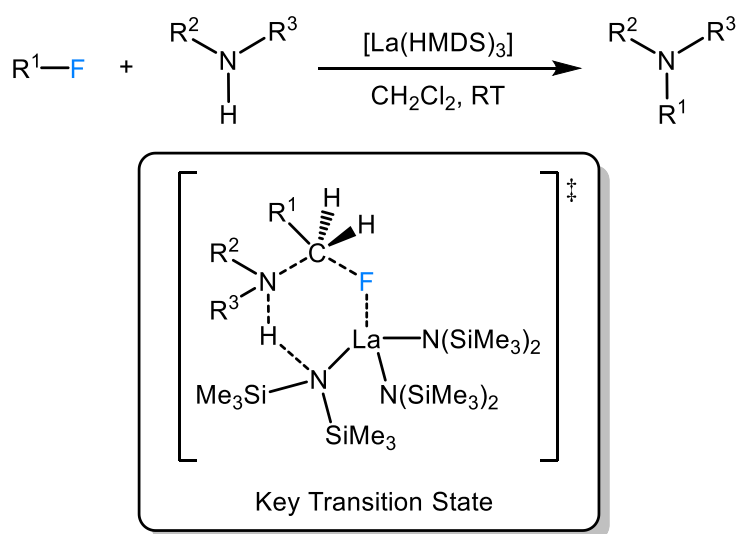
Scheme 4.25 – Proposed mechanism for the di-ferration and C-F activation of 1,3,5-trifluorobenzenes.

In order to access C-F activation product **38**, 1,3,5-trifluorobenzene is required to be di-metallated by two equivalents of sodium ferrate base **17a** to synthesise meta-stable product **37**. At this point it is proposed the thermally induced NaF elimination occurs as a consequence of HMDS intramolecular nucleophilic substitution to form putative intermediate **A** where Fe is coordinatively unsaturated. An equivalent of NaHMDS could then undergo co-

complexation with one of the Fe centres, to form intermediate **B**, where now Na can engage with the third ring F. NaHMDS could come from either i) another di-metallated unit in solution (disproportionation), ii) another equivalent of base **17a** present or iii) the presence of 1 eq. of NaHMDS added to the reaction. Resulting from this NaHMDS can facilitate the removal of the third F atom, again eliminating NaF, with concomitant insertion of HMDS at the vacant site.

To compare with Gilman's work with monometallic reagent $t\text{BuLi}$ and 1,3,5-trifluorobenzene (see Section 4.2.2, Scheme 4.10),^{304,305} with bimetallic base **17a**, Fe and Na work in synchronised cooperation to achieve C-H activation(s) where Fe occupies the site vacated by the removed proton and Na stabilises the complex by an electrostatic interaction to F. The two metals also work together to achieve the C-F activation of 1,3,5-trifluorobenzene where the di-metallation and stabilisation with Na/Fe provides the necessary activation to remove F and insert HMDS. It is also interesting to note the C-F activation of 1,3,5-trifluorobenzene with **17a** occurs at ambient temperature or above and not via a benzyne reaction pathway.

A recent relevant example of C-F to C-N conversion has been demonstrated with aliphatic organofluorines and secondary amines mediated by $\text{La}(\text{HMDS})_3$.³³¹ The authors propose a cyclic six-membered transition state where electron poor and fluorophilic lanthanum facilitates the abstraction of the F atom whilst HMDS acts as a base, deprotonating the secondary amine (Scheme 4.26).



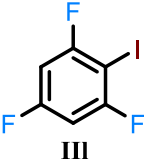
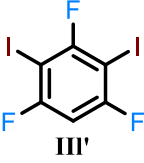
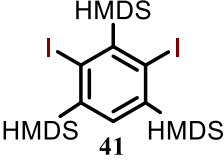
Scheme 4.26 – Proposed mechanistic transition state for the C-F to C-N bond conversion of aliphatic organofluorides with secondary amines mediated by $\text{La}(\text{HMDS})_3$.³³¹

To compare and contrast this C-F to C-N conversion with the synthesis of **38**, it is Na that engages with F in di-metallated, eventually removing F from the aromatic ring via salt elimination (NaF) whilst HMDS is directly installed in the vacant position. Speculating on the role of Fe, from complex **37**, Fe provides some necessary activation of the ring via di-metallation and the framework required to install HMDS and indeed each Fe atom shows a clear attraction to an adjacent HMDS group on the ring.

4.2.4 Electrophilic Quenching

Electrophilic quenching of each of the three reaction pathways with 1,3,5-trifluorobenzene was undertaken with I₂ and is summarised in Table 4.4.

Table 4.4 – Reactions and electrophilic quenching (I₂) of **17a** and 1,3,5-trifluorobenzene at variable temperatures and stoichiometries.

Entry	Base Eq.	Conditions	Product	Conversion (%) ^a	Isolated Yield (%)
1	1	0°C 1 hr then RT 16 hr	 III	58	-
2	2	0°C 1 hr then RT 16 hr	 III'	68	56
3	3	^b RT, 16 hr	 41	80	73

^aNMR spectroscopy conversion with a 10% ferrocene internal standard. ^bThe reaction was gently heated for 5 minutes upon substrate addition.

Utilising the optimised conditions for the synthesis of each metallated product, the corresponding iodinated products could be obtained in high yields after quenching, organic work-up and purification by column chromatography.

As the di-iodo product of the C-F activation (complex **41**, Entry 3, Table 4.4) could be isolated as an off-white solid it was recrystallized and attempts were made to obtain a crystal structure. Though data could be obtained with relative ease and was of high quality, it is not a completely reliable model due to the (perceived) high symmetry of the molecule and consequential positional disorder of the iodine atoms as a result of crystallographic packing being dictated by the bulky HMDS groups (i.e. I atoms apparent at three ring positions). Characterisation of **41** by ^1H NMR spectroscopy in CDCl_3 though was successful; the ring hydrogen resonance appearing in the aromatic region at 6.59 ppm along with signals for the HMDS groups at 0.27 ppm (18H) and 0.14 ppm (36H). Further characterisation was provided by $^{13}\text{C}\{^1\text{H}\}$ NMR spectroscopy and High Resolution-Mass Spectrometry (HR-MS).

Gratifyingly however, the hydrolysis product of **38** could be crystallographically characterised; [1,3,5-tris(HMDS)- C_6H] (**42**) is shown in Figure 4.13 and was recovered in a 71% yield.

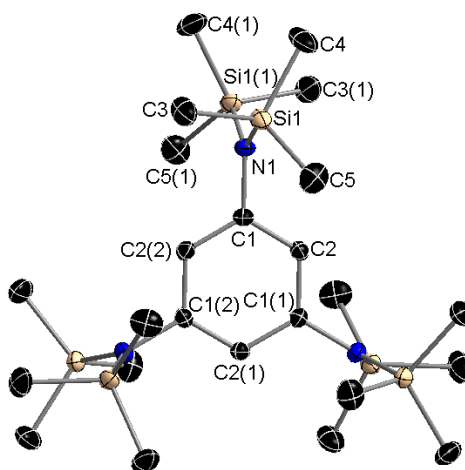


Figure 4.13 – Crystal structure of complex **42**. Hydrogen atoms are omitted for clarity. Thermal ellipsoids displayed at 50% probability level. Selected bond distances (Å) and angles (°): Si1-N1 1.7431(6), N1-C1 1.4419(18), C1-C2 1.3939(9).

Complex **42** is a novel, tri-substituted, bulky benzene derivative and is highly symmetrical. A ^1H NMR spectrum of **42** in CDCl_3 displays a singlet resonance at 6.21 ppm for the aromatic ring H atoms and a large singlet for the 54 equivalent HMDS H atoms at 0.06 ppm. The $^{13}\text{C}\{^1\text{H}\}$ NMR spectrum shows three resonances at 148.30, 127.96 and 2.42 ppm for the C1 carbons, C2 carbons and HMDS Me carbons, respectively.

4.2.5 Magnetometry Studies

4.2.5.1 Static Magnetic Properties of Complexes **38** and **39**

The electronic structures of the Fe(II) centres in complexes **38** and **39** were studied through bulk magnetisation measurements where molar paramagnetic susceptibility (χ_M) data was collected on microcrystalline samples in the warming mode from 2 to 300 K under a constant magnetic field of 0.5 T for **38** and 0.1 T in the case of **39**. Additionally, this study was complemented with magnetisation measurements at 2 K under variable magnetic field (0 to 5 T). Resulting $\chi_M T$ vs T and $M/N\mu_B$ vs H curves are shown in Figure 4.14.

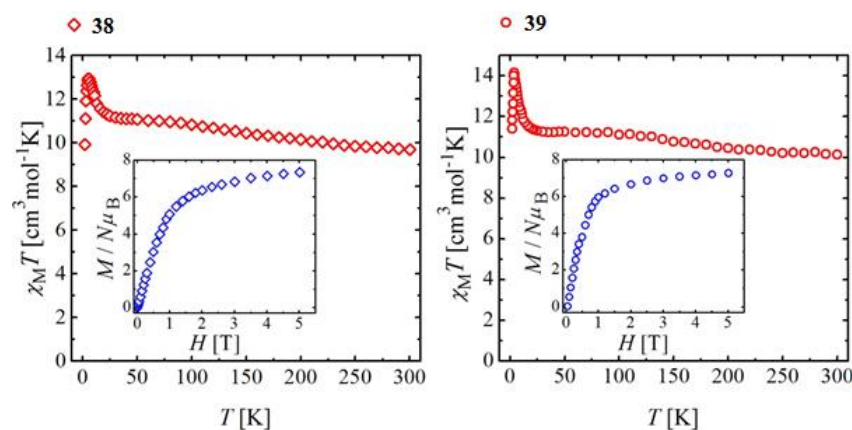


Figure 4.14 – $\chi_M T$ vs T and $M/N\mu_B$ vs H (inset) curves of compounds **38** and **39**. Measurement setup: warming mode (2→300 K), $B = 0.5$ T for **38** and 0.1 T for **39** (0.3 T ; $T_{\text{mag}} = 2$ K).

For both compounds, the displayed magnetic behaviour reveals the existence of ferromagnetic interactions between two highly anisotropic high-spin iron(II) centres. At 300 K, the $\chi_M T$ product for compounds **38** and **39** is significantly higher than the expected spin-only value ($6.00 \text{ cm}^3 \text{ K mol}^{-1}$ for $g = 2.0$) for two uncoupled high-spin ($S = 2$) iron(II) centres (measured at 9.70 and $10.14 \text{ cm}^3 \text{ K mol}^{-1}$, for **38** and **39**, respectively). These findings suggest a significant contribution of orbital angular momentum (L) to the magnetic moment as well as the existence of the first-order spin-orbit coupling. Thus, the most appropriate description for the electronic state of the Fe(II) centres in these two compounds would be a 5D_4 free-ion term ($S = 2, L = 2, J = 4$). Calculated g values employing the equation $\chi_M T = g^2 \cdot J \cdot (J+1)/8$ for the room temperature $\chi_M T$ products are $g = 1.39$ for **38** and $g = 1.42$ for **39**, indicating the presence of partially quenched orbital momentum. Taking into account the *quasi-linear* (or highly distorted trigonal planar) coordination environment of iron(II) centres in these structures, this observation agrees with previously reported magnetic studies of similar

mononuclear iron(II) compounds.^{208,332,333} For instance, similar room temperature values of the χ_{MT} product were reported by Murugesu *et al.* for distorted trigonal-planar iron(II) compound [Fe(HMDS)₂(PCy₃)] (5.16 cm³ K mol⁻¹)²⁰⁸ and by Chilton *et al.* for the bent linear compound [Fe(Ar^{Prⁱ})₂] (Ar^{Prⁱ} = C₆H₃-2,6(C₆H₃-2,6-ⁱpr₂)₂) (C–Fe–C angle 159°; 4.5 cm³ K mol⁻¹).³³²

Upon lowering the temperature, the χ_{MT} product in both cases steadily increases down to 70 K, followed by the plateau spread between 25 K and 70 K. Such a magnetic response is additional confirmation of significant orbital contribution to the magnetic moment. Below 25 K, the abrupt increment of the χ_{MT} product is taking place defining the maximum values of 12.94 cm³ K mol⁻¹ at 5 K for **38** and 14.16 cm³ K mol⁻¹ at 3.75 K for **39**. This sharp increase can be rationalised by the existence of weak ferromagnetic interactions between spin carriers which can be established via a spin-polarization mechanism through bridging *m*-phenyl ligands (i.e. an Fe2-N5-C1-C2-C3-N2-Fe1 pathway, see Figure 4.5). In the lowest temperature range, sharp decreases are observed for both compounds leading to χ_{MT} values of 9.93 and 11.40 cm³ K mol⁻¹ (for **38** and **39**, respectively) at 2 K. The displayed behaviour can be explained as a manifestation of the zero-field splitting effects and/or antiferromagnetic intermolecular interactions. Significant anisotropy of these compounds is evidenced also from the variable field magnetisation measurements at 2 K, with $M/N\mu_B$ vs H curves remaining far from the saturation even at the highest magnetic fields (expected 12 μ_B for two iron(II) centres with $J = 4$; $S = 2$; $L = 2$ and $g = 2$). The measured magnetisation values at 5 T for dinuclear compounds **38** and **39** are 7.35 and 7.25 μ_B , respectively.

In order to quantify the crystal field effects, ferromagnetic interactions between spin carriers and spin-orbit coupling, numerous attempts of fitting the experimental data (χ_{MT} vs T and $M/N\mu_B$ vs H) were carried out using the program PHI¹⁴⁸ by matrix diagonalisation of the (perturbative) anisotropic spin Hamiltonian defined in Equation (4.1):

$$\hat{H} = \sum_i \lambda_i (\sigma_i \hat{L}_i \cdot \hat{S}_i) + \sum_i \sigma_i^2 (B_2^0 \hat{O}_2^0 + B_2^2 \hat{O}_2^2) + \sum_i \sigma_i^4 (B_4^0 \hat{O}_4^0 + B_4^4 \hat{O}_4^4) \quad (4.1)$$

$$- 2J(\hat{S}_1 \hat{S}_2) + \mu_B B \sum_i (g_i \hat{S}_i + \sigma_i \hat{L}_i)$$

In this equation, the first component is the sum of the spin-orbit coupling, the second and third are the crystal field interactions and the fourth corresponds to the exchange coupling

while the last part of the sum defines the Zeeman effect. The parameters λ_i and σ_i are the spin-orbit coupling constant (-100.0 cm^{-1}) and the orbital reduction parameter, respectively, J is the exchange constant, \hat{S}_i ($S = 2$) is the total spin operator of the individual Fe(II) ions, \hat{L}_i ($L=2$) is their orbital angular momentum, B is the magnetic induction, μ_B is the Bohr magneton while $B_k^q \hat{O}_k^q$ are the Stevens operators defining the potential of C_1 crystal field. In order to avoid the overparameterisation of defined Hamiltonian the g factor was fixed at 2.0 and the same set of the parameters was used for both iron(II) sites. Unfortunately, due to the large number of variables as well as the high dimensionality of the system, it was not possible to find a unique model for the experimental data. The quality and the outcome of the fits were strongly dependent on the input values of the parameters, especially Stevens operator $B_2^0 \hat{O}_2^0$. As reported recently, the parameterisations where the largest contribution to the crystal field component comes from the negative $B_2^0 \hat{O}_2^0$ define the well isolated ground orbital doublet which cannot be depopulated to the excited states with the thermal energy available at the room temperature.³³² Therefore, the strong orbital splitting cannot be evaluated from the experimental data and subsequently neither is it possible to evaluate properly the ligand field parameters without the valid input from the theoretical calculations. However, attempts to model the experimental data enabled us to estimate of exchange constant (J) range between 0.3 and 0.45 cm^{-1} .

To the best of our knowledge, these compounds are the first characterised molecular systems possessing two *quasi*-linear iron(II) centres. The observation of the ferromagnetic interactions between them indicates that the *m*-phenyl linkages can provide an effective pathway for the spin polarisation mechanism similar to those reported previously for pyrimidine and *m*- N,N' -phenylene based systems.^{271,334–338} Based on these findings, a synthetic strategy employing the 1,3-aromatic connectors between two highly anisotropic metal centres could be used to access more complex molecular systems with higher spin ground states.

4.2.5.2 Dynamic Magnetic Properties of Complexes 38 and 39

Encouraged by the results from the direct current (DC) studies, the possible SMM behaviour of these complexes was investigated. Studies of the frequency (Figure 4.15 and Figure 4.16) and temperature dependence (Figure 4.17 and Figure 4.18) of the alternate current (AC)

magnetic susceptibility were completed in the temperature range from 1.8 (1.85 K for **39**) to 17 K and in the frequency range from 10 to 1488.1 Hz. The first measurements performed under zero DC field and 4 Oe AC field, showed for both compounds, superimposed curves for the in-phase AC susceptibility (χ_M') and very small signal at 1.8 K for the out-of-phase AC susceptibility (χ_M''). Application of the static field of 1000 Oe resulted in the appearance of a set of frequency dependent in- and out-of-phase AC susceptibility signals for both compounds.

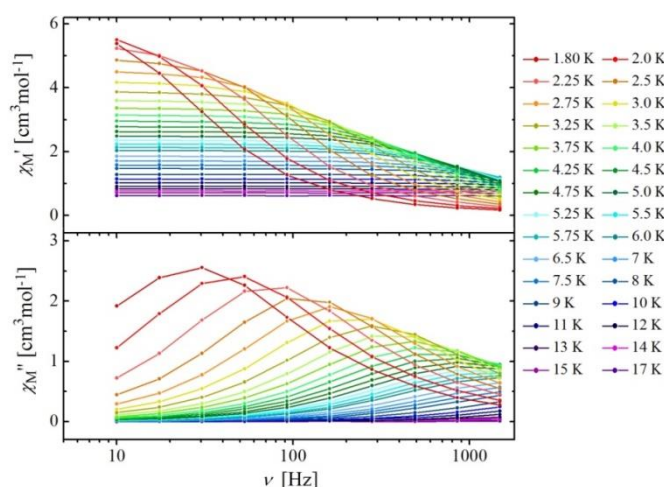


Figure 4.15 – Frequency dependence of the in- (χ_M') and out-of-phase (χ_M'') AC susceptibility for **38** under an applied DC field of 1000 Oe. The solid lines are a guide for the eye.

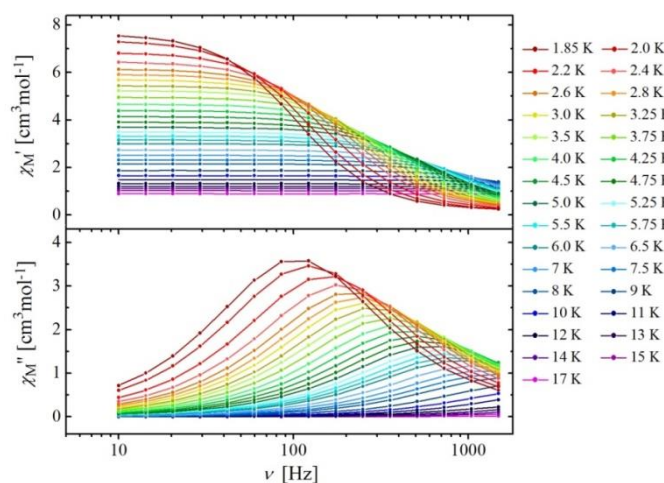


Figure 4.16 – Frequency dependence of the in- (χ_M') and out-of-phase (χ_M'') AC susceptibility for **39** under an applied DC field of 1000 Oe. The solid lines are a guide for the eye.

The described field-induced SMM behaviour for Fe(II) compounds is very common for non-Kramers ions since their slow relaxation of the magnetisation is significantly influenced by

the quantum tunnelling of the magnetisation.^{339,340} One of the possible reasons for this effect can be found in the existence of the rhombic anisotropy (E) which provides the tunnelling pathway through the spin-reversal barrier generated by mixing of the $\pm M_S$ energy levels (i.e. the electron tunnels through thermal barrier from $+M_S$ to $-M_S$). Application of the additional magnetic field removes the degeneracy of the $\pm M_S$ energy levels by Zeeman splitting and directly diminishes the tunnelling effects in favour of thermal relaxation. The applied magnetic field here was not optimised but instead was chosen as a reasonable assumption after analysis of AC magnetic studies of similar reported mononuclear Fe(II) SMMs.^{111,149,150,208,333,341,342}

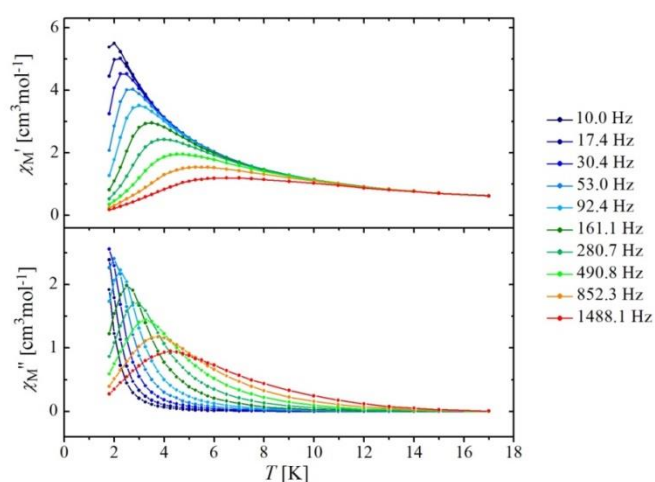


Figure 4.17 – Temperature dependence of the in- (χ_M') and out-of-phase (χ_M'') AC susceptibility for **38** under an applied DC field of 1000 Oe. The solid lines are a guide for the eye.

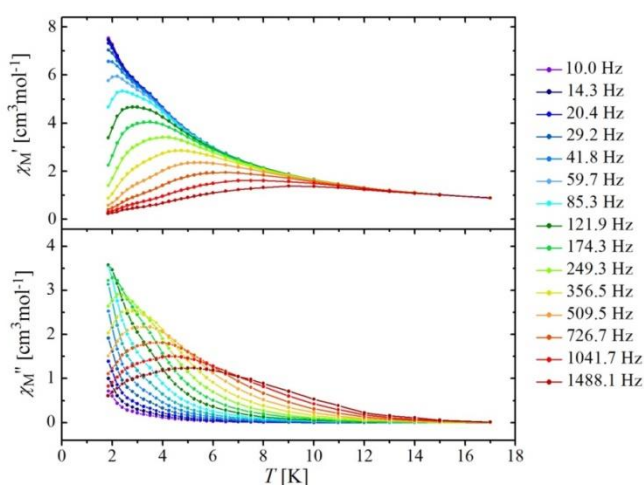


Figure 4.18 – Temperature dependence of the in- (χ_M') and out-of-phase (χ_M'') AC susceptibility for **39** under an applied DC field of 1000 Oe. The solid lines are a guide for the eye.

Frequency dependent sets of the out-of-phase AC susceptibility (χ''_M) show that the maxima of the χ''_M vs ν curves is shifted towards higher frequency value as the temperature is increased accompanied also by decaying intensity (Figure 4.15 and Figure 4.16). Similarly, the intensity of the in-phase AC susceptibility (χ'_M) systematically declines by increasing the frequency. The latter is clearly visible from the temperature dependence of the AC susceptibility data (Figure 4.17 and Figure 4.18) which also clearly indicates that the maximum for the χ''_M at the lowest temperature appears between 85.3 Hz and 121.9 Hz for **39** and very close to 30.4 Hz for **38**. Representation of the obtained results in the complex χ -plane, simplified as Cole-Cole (Argand) plots (Figure 4.19 and Figure 4.20), reveals a set of semicircles which lose their completeness and intensity upon increasing the temperature. Furthermore, the unique semicircle structures indicate the dominance of the single relaxation process.

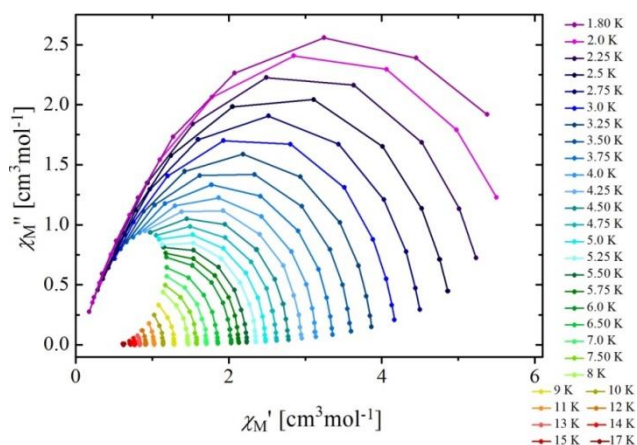


Figure 4.19 – Cole-Cole isotherms of the AC susceptibility for **38** under an applied DC field of 1000 Oe. The solid lines are a guide for the eye.

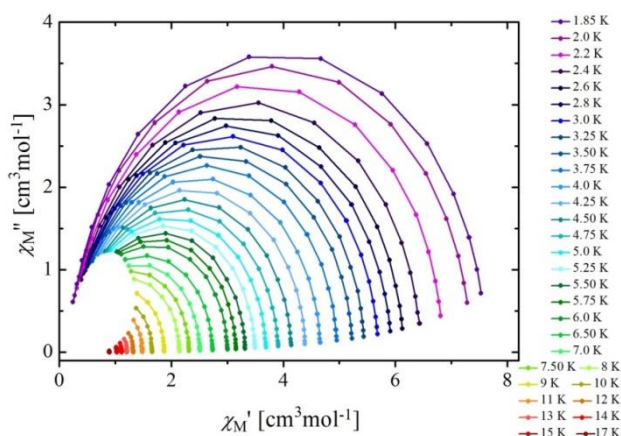


Figure 4.20 – Cole-Cole isotherms of the AC susceptibility for **39** under an applied DC field of 1000 Oe. The solid lines are a guide for the eye.

In order to quantify the dynamics of the magnetisation (relaxation time and the width of its distribution), χ_M' and χ_M'' data were fitted simultaneously to the generalised Debye model,³⁴³ shown in Equation (4.2):

$$\chi_{AC}(\omega) = \chi_S + \frac{\chi_T - \chi_S}{1 + (i\omega\tau)^{(1-\alpha)}} \quad (4.2)$$

In this equation, α is the Cole-Cole parameter ($0 < \alpha < 1$), τ is the Cole-Cole relaxation time, χ_T and χ_S are the isothermal and the adiabatic susceptibilities, respectively, while ω is the angular frequency ($\omega = 2\pi\nu$). The relaxation time τ is defined by the angular frequency (ω) at which the Cole-Cole plot reaches the maximum ($\tau = \omega^{-1}$). Parameter α directly describes the width of the distribution of the relaxation time where 0 value corresponds to the relaxation

with one time constant while larger α values correspond to the flatter distribution of the time constants around τ . The real component of this expression defines the in-phase AC susceptibility (χ_M') while the imaginary part defines the out-of-phase ac susceptibility (χ_M''). Parameters obtained by fitting the experimental data to described model are represented in Figure 4.21 and Figure 4.22 with the tabulated results shown in Table III-14 and Table III-15 in Section III.V for compounds **38** and **39**, respectively.

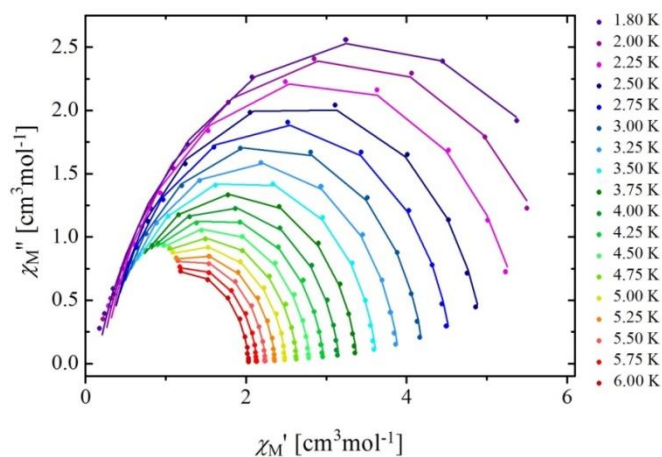


Figure 4.21 – Cole-Cole isotherms of the AC susceptibility for **38** under an applied DC field of 1000 Oe. Solid lines represent the results of the fits.

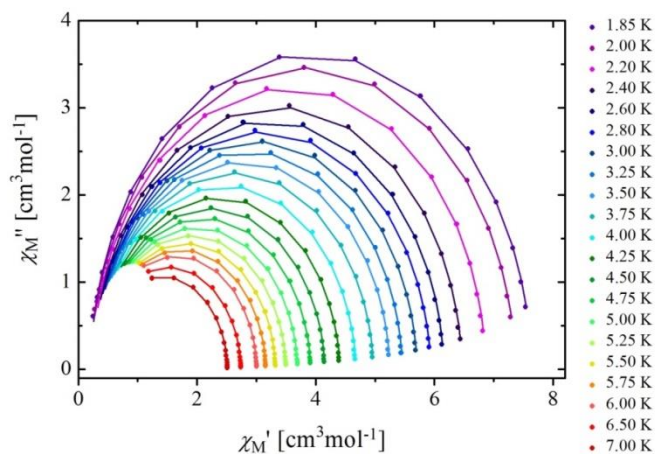


Figure 4.22 – Cole-Cole isotherms of the AC susceptibility for **39** under an applied DC field of 1000 Oe. Solid lines represent the results of the fits.

Analysing the fitted parameters of the slow relaxation of the **39** (Table III-15), it can be seen that the described model agrees very well with the experimental data and yields very low α values over the entire temperature range taking into consideration $0.017 < \alpha < 0.030$. On the other hand, the parameters obtained for the **38** (Table III-14) show a broad range of slightly

higher α values (0.08-0.17). The highest values are observed for the lowest temperatures (1.80-2.25 K) where $0.10 < \alpha < 0.17$ which could indicate that the quantum tunnelling of the magnetisation is not completely quenched (thus the applied magnetic field could be optimised). At the higher temperatures, fitted α parameters are below 0.1 which confirms that the applied Debye model for the single relaxation process is valid for the AC data for complex **38**. Also, it is important to point out that the crystal structure of the **38** contains three crystallographically inequivalent molecules which each possess different intrinsic anisotropy and thus can act as three slightly different single-molecule magnets. Consequently, a larger distribution of the relaxation time can be easily produced. Following this assumption, smaller values and narrower range of α observed for **39** nicely reflect the existence of the unique molecular structure. Comparing the obtained relaxation times (τ) for both compounds, it can be seen that the faster relaxation at higher temperatures occurs for the compound **38**.

In order to determine the exact pathway of the relaxation process, the dependence of the relaxation times and temperature was analysed. Evaluation of the effective barriers (U_{eff}) to magnetic relaxation and characteristic time (τ_0) can be derived from the high temperature regime using the Arrhenius expression $\tau = \tau_0 e^{(U_{\text{eff}}/k_B T)}$ (Boltzmann constant $k_B = 1.38065 \times 10^{-23} \text{ J K}^{-1}$). Linearisation of this expression in the form of $\ln(\tau)$ vs $1/T$ is shown in Figure 4.23.

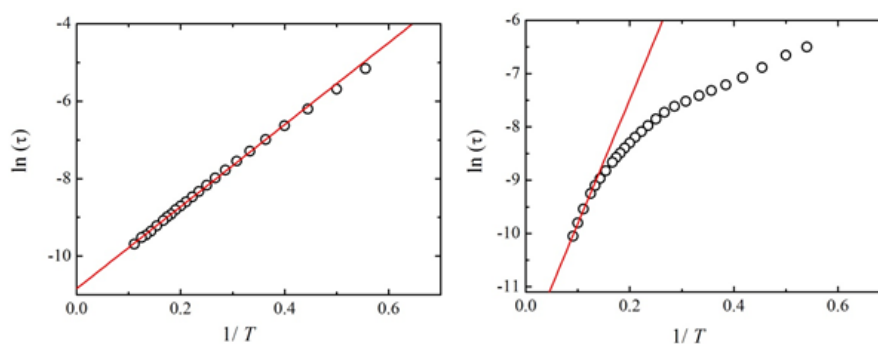


Figure 4.23 – Magnetisation relaxation time (τ) in form of Arrhenius $\ln(\tau)$ vs $1/T$ plots for the compounds **38** (left) and **39** (right). Solid red lines represent the fits of the linear part of the curve.

Temperature dependence of the natural logarithm of τ for **39** (Figure 4.23, right) follows the linearity only at the highest temperature region (above 7 K) while the curvature upon cooling indicates the change of the relaxation pathway from thermally activated over barrier to through barrier relaxation (i.e. Raman, quantum tunnelling). Least-square fit of the experimental data yielded the energy barrier $U_{\text{eff}} = 23.4 \text{ K} = 16.4 \text{ cm}^{-1}$ and the attempt

relaxation time $\tau_0 = 5.2 \times 10^{-6}$ s. The obtained value for the relaxation time is slightly larger than usually reported for the single-molecule magnets (10^{-7} - 10^{-10} s) suggesting that through barrier relaxation processes may still be slightly effective together with the thermally activated Orbach relaxation.^{340,344} The smaller U_{eff} values for **39** compared with other low coordinate Fe(II) SMMs can be related to the lower symmetry of this system and more importantly, the presence of magnetic coupling between two iron(II) centres within the molecule.^{111,149,150,208,333,341,342,345,346} Both effects can easily decrease the total anisotropy of the systems and therefore accelerate the relaxation.

On the other hand, the of $\ln(\tau)$ vs $1/T$ plot for **38** (Figure 4.23, left) shows linearity over almost the entire temperature range (small deviations are observed only at the lowest temperatures), thus indicating the Orbach process. Least-square fit of this dependence gave the energy barrier $U_{\text{eff}} = 10.6 \text{ K} = 7.4 \text{ cm}^{-1}$ and the attempt relaxation time $\tau_0 = 2.0 \times 10^{-5}$ s. The latter value is certainly somewhat larger than normal SMM relaxation times and may indicate that phonon bottleneck effects lead to slow relaxation of the magnetisation.³⁴⁷ Such unusual dynamics of the magnetisation was first reported for the iron(III) dimer $(\text{Et}_4\text{N})_3(\text{Fe}_2\text{F}_9)$ with an $S = 5$ ground state, axial anisotropy and an energy barrier of 2.40 K.³⁴⁷ As explained by authors, the poor thermal contact between sample and bath leads to a phonon bottleneck situation with appearance of the butterfly-shaped hysteresis loops below 5 K which can be reproduced using a microscopic model based on the interaction of the spins with resonant phonons. Similarly, the same effect enables the observation of the resonant quantum tunnelling of the magnetisation at 1.8 K, far above the blocking temperature for spin-phonon relaxation. AC magnetic susceptibility studies have shown that without an applied magnetic field no out-of-phase signal is detected (i.e. no SMM behaviour) while at 1000 Oe slow relaxation is easily observed. The reported relaxation time is temperature dependent and follows the Arrhenius law, thus indicating the Orbach process ($\tau_0 = 1.0 \times 10^{-5}$ and $U_{\text{eff}} = 12.6$ K). The relaxation process occurs over the barrier of combined system formed by the ground $S = 5$ and the first excited $S = 4$ state, where much higher density of levels eases the $\Delta S = \pm 1$ transitions induced by thermal phonons. In conclusion, similarity of the relaxation dynamics for **38** with the described system (along with the high spin ground state due to the weak ferromagnetic coupling) indicates that cooperativity between the ground and thermally available excited states generates the observed behaviour.

Improvement of the SMM behaviour of these systems can be achieved by judicious design of the substituted *m*-phenyl bridge which will allow the strictly linear symmetry of the local

coordination environment around Fe(II). An easier alternative for this challenging task would be the controlled reduction of the iron(II) precursors to their iron(I) equivalents. This simple one-electron modification of the structure will change the spin nature of the metal ions from non-Kramers $S = 2$ to Kramers $S = 3/2$ which can significantly suppress the effect of the quantum tunnelling of the magnetisation. Elegant realisation of this approach was first reported by Long *et al.* for the compound $[\text{Fe}\{\text{C}(\text{SiMe}_3)_2\}_2]$ and its reduced complex iron(I) salt $[\text{K}(\text{crypt-222})]^+[\text{Fe}\{\text{C}(\text{SiMe}_3)_2\}_2]^-$ where large increment of the energy barrier to magnetic relaxation was recorded passing from 146 cm^{-1} for the $S = 2$ system³³³ to record a barrier of 226 cm^{-1} for the $S = 3/2$ system.³⁴⁸

4.2.5.3 Static Magnetic Properties of Complexes 36 and 37

Complex **36** was subject to bulk magnetisation measurements under the same conditions as complexes **17-19** (Chapter 3, Section 3.2.6) where molar paramagnetic susceptibility (χ_M) data was collected on a microcrystalline sample in the warming mode from 2 to 300 K under a constant magnetic field of 0.5 T with additional magnetisation measurements at 2 K under variable magnetic field (0 to 5 T). Resulting $\chi_M T$ vs T and $M/N\mu_B$ vs H curves together with their best fits are shown in Figure 4.24.

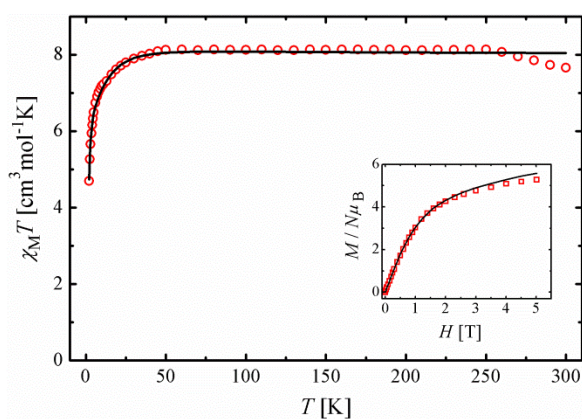


Figure 4.24 – $\chi_M T$ vs T and $M/N\mu_B$ vs H (inset) curves of compound **36**. Measurement setup: warming mode (2→300 K), $B = 0.5 \text{ T}$; $T_{\text{mag}} = 2 \text{ K}$. Solid black lines represent the result of the fits.

Complex **36**, possessing two isolated high-spin iron(II) centres in its magnetic unit, exhibits an $\chi_M T$ product of $7.66 \text{ cm}^3 \text{ K mol}^{-1}$, higher than the expected value of $6.00 \text{ cm}^3 \text{ K mol}^{-1}$ ($g = 2.0$) with an estimated g value (using the Curie Law for the room temperature data) of $g =$

2.26, suggesting the presence of unquenched angular momentum coupled to the electronic spin. A slight increase of $\chi_{\text{M}}T$ takes place upon cooling to 250 K ($8.13 \text{ cm}^3 \text{ K mol}^{-1}$), probably due to the decomposition of the sample arising from residual humidity of the gelatin capsule. Alike with complexes **17-19** and **24**, a sharp decrease of $\chi_{\text{M}}T$ is observed at the lowest temperatures to give an $\chi_{\text{M}}T$ value of $4.69 \text{ cm}^3 \text{ K mol}^{-1}$; behaviour as a result of the manifestation of the zero-field splitting effects which is additionally obvious from the variable field magnetisation measurement at 2K. The measured magnetisation at 5 T for dinuclear **36** is $5.27 \mu_{\text{B}}$.

To quantify the ZFS effects, the data for **36** was fit to the same equation at complexes **17-19** and **24** (see Equation (3.1), Section 3.2.6) with the all the results shown together in Table 4.5.

Table 4.5 – Fitting Parameters for compounds **17-19** and **24** and **36**.

Compound	$\chi_{\text{M}}T^a$ at r.t. (g)	μ_{eff}^b at r.t	$\chi_{\text{M}}T^a$ at 2 K	g	D (cm^{-1})	$ E $ (cm^{-1})	$ E /D$	zJ (cm^{-1})
17	7.61 (2.25)	11.02	3.11	2.25	9.3	1.7	0.18	0.05
18	3.93 (2.29)	5.61	2.02	2.27	-12.0	3.3	0.27	0.07
19	3.90 (2.28)	5.58	2.09	2.22	-9.1	2.9	0.32	0.07
24	7.19 (2.19)	10.73	4.88	2.18	-9.6	2.9	0.30	0.04
36	7.66 (2.26)	11.07	4.69	2.31	-10.5	3.2	0.30	0.04

^aIn units of $\text{cm}^3 \text{ K mol}^{-1}$ ^bIn units of Bohr magnetons.

The results obtained for complex **36** are similar to complexes **18**, **19** and **24** which all contain a heteroleptic $\{\text{Fe}(\text{HMDS})_2(\text{Ar})\}$ core. Although no direct correlation between the ligand field strength (tuned by the number of the fluorine substituents) and the anisotropy could be found, a small correlation can be seen between the ZFS components and the local coordination geometry around the Fe(II) centre. Compounds with the larger D and E values (**18** and **36**) have very similar ligand fields with slightly more acute N–Fe–N angles ($127.83(1)^\circ$ and $128.09(7)^\circ$, respectively) and slightly shorter Fe–C bond distances ($2.103(4) \text{ \AA}$ and $2.091(2) \text{ \AA}$, respectively) than compounds **19** and **24** which possess slightly more obtuse N–Fe–N angles and slightly longer Fe–C bond distances ($130.10(6)^\circ$ and $131.08(10)^\circ$; $2.116(2) \text{ \AA}$ and $2.117(3) \text{ \AA}$, respectively). The zero-field splitting parameters of latter pair are also quite similar and reflect nicely the local coordination environment of the Fe(II) centre.

Di-ferrated 1,3,5-trifluorobenzene complex **37** was also subject to bulk magnetisation measurements where molar paramagnetic susceptibility (χ_M) data was collected on a microcrystalline sample in the warming mode from 2 to 300 K under a constant magnetic field of 0.5 with additional magnetisation measurements at 2 K under variable magnetic field (0 to 5 T). Resulting $\chi_M T$ vs T and $M/N\mu_B$ vs H curves together with their best fits are shown in Figure 4.25.

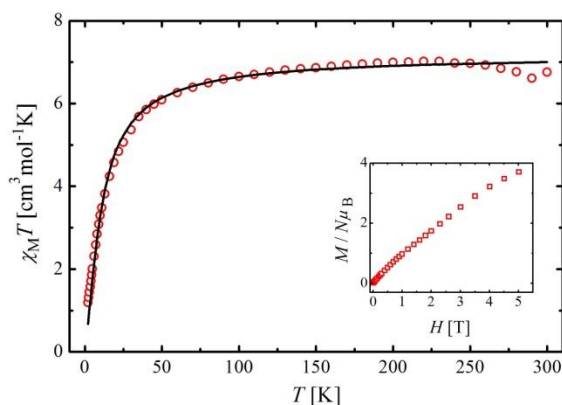


Figure 4.25 – $\chi_M T$ vs T and $M/N\mu_B$ vs H (inset) curves of compound **37**. Measurement setup: warming mode (2→300 K), $B = 0.5$ T; $T_{\text{mag}} = 2$ K. Solid black line represents the result of the fit.

At 300 K, the $\chi_M T$ product of $6.75 \text{ cm}^3 \text{ K mol}^{-1}$ is higher than the expected spin-only value ($6.00 \text{ cm}^3 \text{ K mol}^{-1}$ for $g = 2.0$) for two uncoupled high-spin ($S = 2$) iron(II) centres. The estimated g value using the Curie Law for the room temperature data is $g = 2.12$ suggesting the presence of unquenched angular momentum coupled to the electronic spin (second-order spin-orbit coupling).¹⁰⁶ Upon lowering the temperature, the $\chi_M T$ product slightly increases down to 250 K ($6.97 \text{ cm}^3 \text{ K mol}^{-1}$), likely due to the decomposition of the sample. Below that temperature, the $\chi_M T$ product steadily decreases down to 60 K ($6.26 \text{ cm}^3 \text{ K mol}^{-1}$) followed by an abrupt decline ending at the value of $1.19 \text{ cm}^3 \text{ K mol}^{-1}$ at 2 K. The displayed behaviour can be assigned to the existence of antiferromagnetic exchange interactions between two spin carriers in the molecule, but it can also be a consequence of the zero-field splitting effects. Variable field magnetisation measurements at 2K show that the $M/N\mu_B$ vs H curve stays far from saturation even at the highest magnetic fields (expected $8 \mu_B$ for two $S = 2$ centres and $g = 2$). The measured magnetisation at 5 T for is $3.70 \mu_B$ which additionally confirms the presence of antiferromagnetic interactions or strong ZFS effects. In order to quantify the magnitude of observed coupling, experimental data were fit using the program PHI¹⁴⁸ by matrix diagonalisation of the spin Hamiltonian as defined in Equation (4.3):

$$\hat{H} = -2J(\hat{S}_1\hat{S}_2) + \mu_B B \sum_i g_i \hat{S}_i \quad (4.3)$$

where J is the exchange constant, \hat{S}_i ($S = 2$; $i = 1, 2$) is the total spin operator of the individual Fe(II) ions, B is the magnetic induction, μ_B is the Bohr magneton while g is the isotropic g factor. The best fit (Figure 4.25) with a fixed g factor at 2.21 was optimised with the exchange constant $J = -0.99 \text{ cm}^{-1}$, intermolecular interaction $zJ = -0.07 \text{ cm}^{-1}$ and the small presence (3.3%) of mononuclear impurity (i.e complex **36**, $S = 2$). The obtained J value is reasonable taking into account the large intramolecular separation between the metals (Fe---Fe = 5.8596(5) Å).

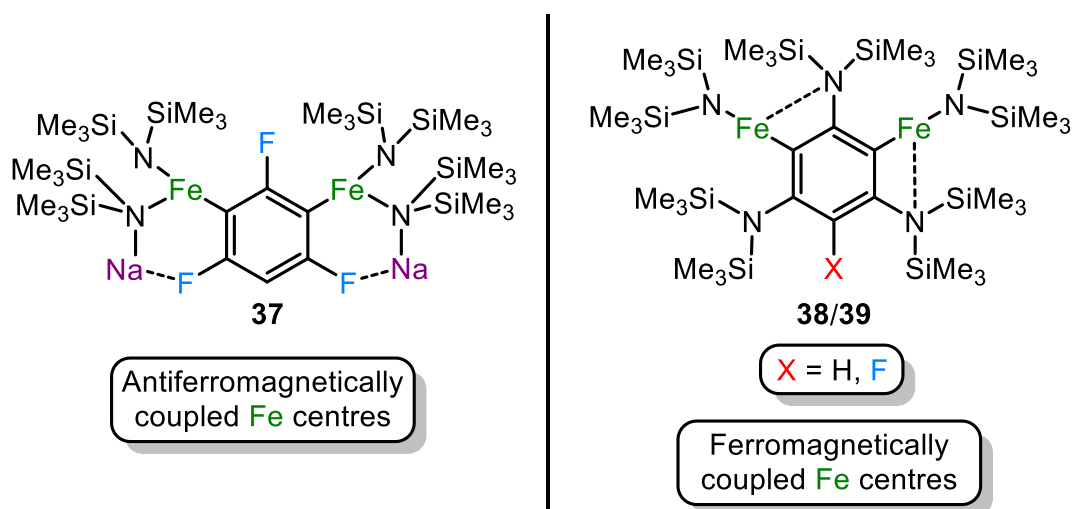


Figure 4.26 – Aryl ligand influence on the magnetic coupling of the Fe(II) centres in complex **37**, **38** and **39**.

Surprisingly, despite the similar Fe–C–C–C–Fe bridging fragment, the magnetic coupling between the two Fe(II) centres in the compound **37** is antiferromagnetic in contrast to complexes **38** and **39** which exhibit the ferromagnetic interactions (Figure 4.26). Obviously, the spin polarisation mechanism cannot be effective here, but the coupling of the metal centres can be also achieved via σ -type exchange pathway. The condition for establishing this kind of interaction between two metals is the d_{σ} - p_{σ} orbital overlap between the metal centres and coordinated donor atoms. Studies on pyrimidine bridged dinuclear compounds have shown that both exchange pathways can be effective and that the dominant one depends strongly on the electronic structure of the metal and the local coordination geometry.²⁷⁰ The corresponding DFT calculations of the spin density distribution showed that in the case of antiferromagnetic coupling (σ -type exchange), metal ions and coordinated N-donor atoms

from the pyrimidine ring have spin densities with the same positive sign. This was explained as a spin delocalisation effect with the resonance between $M(\uparrow\downarrow)-N(\uparrow)$ and $M(\uparrow)-N(\uparrow\downarrow)$. On the other hand, DFT calculations for the ferromagnetic coupling via spin polarisation mechanism have shown the classical spin alternation where the N-donor atoms from the pyrimidine ring carry the negative spin density, as in organic radicals.³³⁴ Relating those findings to the ligand structures in complexes **37-39**, it can be concluded that antiferromagnetic coupling observed for the 1,3-trifluorophenyl bridge (**37**) can be expected due to the fact that the fluorine substituents are strongly electron withdrawing, consequently decreasing the electron density of the aromatic ring and therefore it is easier to generate a positive spin density distribution. On the other hand, the structures of **38** and **39** have HMDS substituents which act as electron donors, therefore increasing the electron density of the aromatic bridge and suppressing the previously described effect. Secondly, the mechanism of spin polarisation involves magnetic interaction through the π -pathway. In the structures of **38** and **39** local coordination geometry around Fe(II) centres belongs to the same plane as the aromatic connector. Thus, Fe(II) d -orbitals perpendicular to the coordination plane are suitably positioned for π -overlap with the π -orbitals of the phenyl bridge. In the structure of **37** the coordination plane around Fe(II) is rotated around 60° outside the plane of the phenyl bridge and therefore no good π overlap can occur between the ligand and metal orbitals.

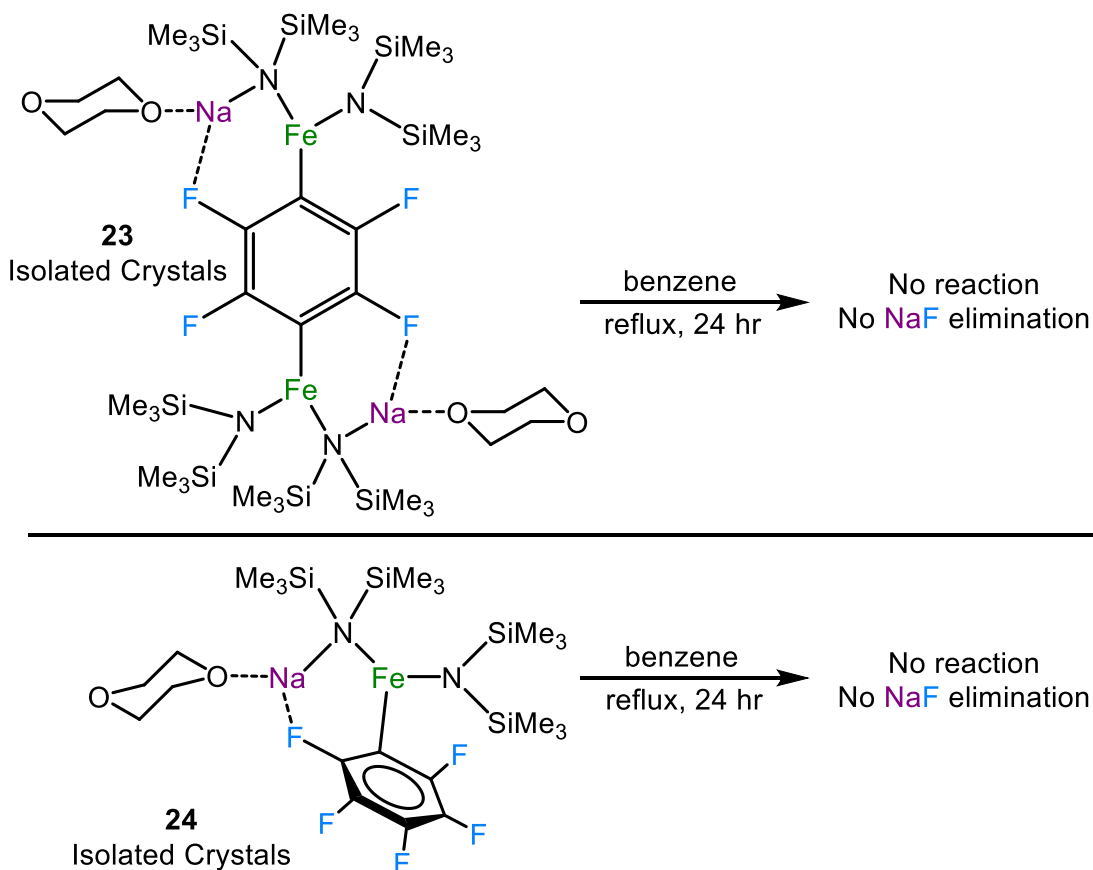
In conclusion, the antiferromagnetic coupling observed for the **37** can be characterised by a dominating through-bond superexchange mechanism (σ -pathway Fe1-C2-C1-C6-Fe2) while the ferromagnetic coupling observed for the **38** and **39** comes from dominating π -spin polarisation mechanism.

4.2.6 Other Associated Reactions

Through the course of this research into C-H and C-F activation of 1,3,5-trifluorobenzene with sodium ferrates a number of related reactions were conducted, the results of which are detailed forthwith.

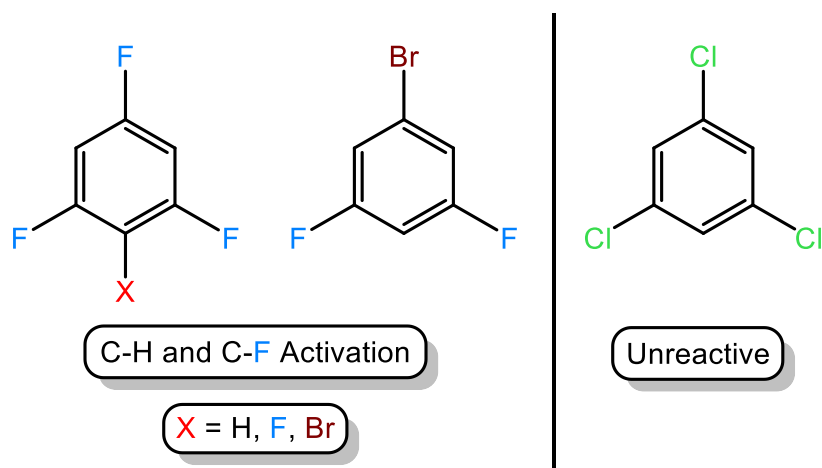
Heteroleptic sodium ferrate **35** was reacted with 1,3,5-trifluorobenzene on a 1:1 scale in benzene solvent and stirred at 50°C overnight. Like with 1,3-difluorobenzene however (see Section 3.2.8.4), only an oily product could be obtained.

Seeking to assess whether ferrated, highly fluorinated aryl complexes **23** and **24** (di-ferrated 1,2,4,5-tetrafluorobenzene and mono-ferrated pentafluorobenzene) could be energetically coaxed into C-F activation, benzene solutions of each were refluxed for several hours and the products examined by X-ray crystallography and ^1H NMR spectroscopy (Scheme 4.27). Neither compound gave any further product(s) from the reaction hence, it appears complexes **23** and **24** are thermally robust and do not undergo C-F activation with **17a**.



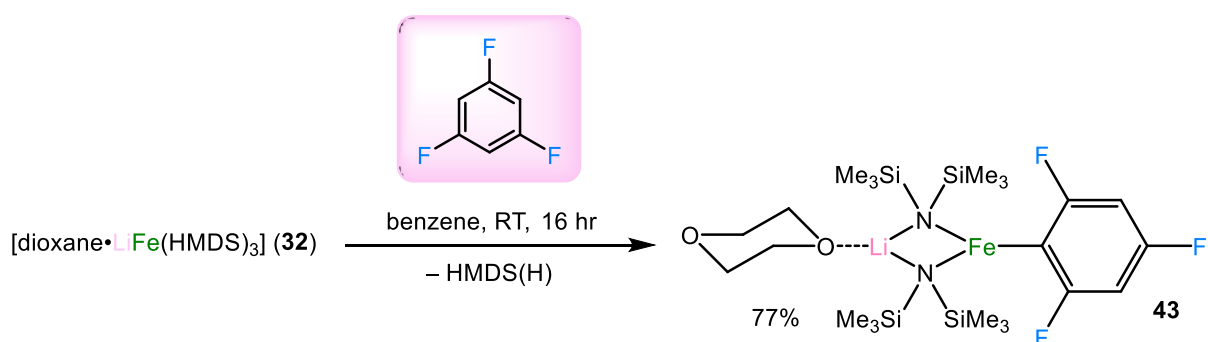
Scheme 4.27 – Thermal stability assessment of complexes **23** and **24**.

Attempts were made to induce C-H activation of 1,3,5-trichlorobenzene but no reactivity with **17a** was observed (Figure 4.27). No colour change was observed from a 1:1 reaction at 50°C stirred overnight and the only crystals to be grown from the reaction were that of O-ICE **30**. Repeating the reaction and quenching with I_2 yielded no product conversion.

Figure 4.27 – Reactivity of 1,3,5-trihalobenzene complexes with **17a**.

It was found that C-F activation product **38** could also be accessed from 1-bromo-3,5-difluorobenzene (Figure 4.27). Recall in Section 3.2.4.2, mono-ferration of 1-bromo-3,5-difluorobenzene was accomplished on a 1:1 scale at 0°C to yield complex **26**. On a 3:1 scale with heating, complex **38** was synthesised in a 43% yield. Conversely, the di-metallated product could not be obtained even on a 2:1 scale and adding the substrate at 0°C before heating gently at 40°C for 3 hours, only crystals of **26** were found.

After the exciting and unprecedented results with sodium ferrate **17a** and 1,3,5-trifluorobenzene, we sought to explore whether similar reactivity would be observed with a lithium system.

Scheme 4.28 – Mono-ferration of 1,3,5-trifluorobenzene with lithium ferrate **32**.

Having already isolated $[\text{dioxane} \cdot \text{LiFe}(\text{HMDS})_3]$ (**32**) (see Section 3.2.8.3) from the unsuccessful attempt to ferrate fluorobenzene, a 1 mmol solution of **32** was prepared to which

an equivalent of 1,3,5-trifluorobenzene was added (Scheme 4.28). No immediate colour change or precipitation was apparent (even after heating) so the solution was stirred overnight after which a colour change from green to yellow was apparent. Concentration of the solution produced large, flat yellow rod crystals which, subject to X-ray crystallographic analysis, revealed the structure [dioxane·LiFe(HMDS)₂(1,3,5-C₆H₂F₃)] (**43**) (Figure 4.28), recovered in a 77% yield.

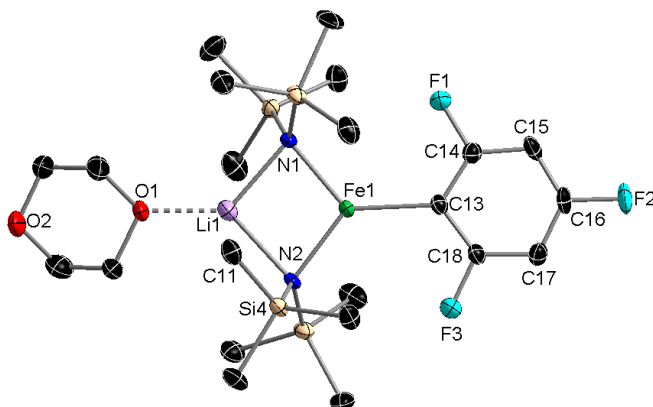


Figure 4.28 – Asymmetric unit of complex **43**. Hydrogen atoms omitted for clarity. Thermal ellipsoids displayed at 50% probability level. Selected bond distances (Å) and angles (°): Fe1-N1 2.007(3), Fe1-N2 2.017(3), Fe1-C13 2.078(4), Fe1---Li1 2.661(7), Li1-N1 2.080(8), Li1-N2 2.135(8), Li1-O1 1.943(8), Li1---C11 2.662(9); N1-Fe1-N2 102.72(13), N1-Fe1-C13 127.70(15), N2-Fe1-C13 129.57(14), Li1-N1-Fe1 81.2(2), Li1-N2-Fe1 79.7(2), Li1---Fe1-C13 178.29(19), N1-Li1-N2 96.4(3), N1-Li1-O1 130.9(4), N2-Li1-O1 132.3(4), O1-Li1---Fe1 175.3(4).

Successful mono-ferration of 1,3,5-trifluorobenzene has taken place, strikingly however, the fluoroaryl ring resides at the terminal position attached to Fe whilst the two bridging HMDS groups remain in place. Absolutely no Li-F contact of any form is present and **43** exists a discrete monomer in the solid state. Structurally, **43** compares well with complex **32** for the equivalent bond lengths and angles. Like in **32**, Li is ‘sunk’ further into the steric sphere of the {Fe(HMDS)₃} moiety than Na in similar complexes and forms an electrostatic contact with HMDS Me group C11 at a distance of 2.662(9) Å. No further reaction was observed upon heating **43**.

4.3 Conclusions

Following on from successful direct *ortho*-ferrations of fluorinated aryl substrates by sodium ferrate base **17a** in Chapter 3, unique reactivity was uncovered with 1,3,5-trifluorobenzene. By careful temperature and stoichiometric control, mono- and di-ferrated products **36** and **37** can be obtained, respectively. With 3 equivalents of **17a** and the application of heat, the unprecedented two-fold C-H activation and three-fold C-F activation of the fluoroaromatic substrate takes place accompanied by the concomitant elimination of NaF. Observed in complex **38** is the nucleophilic substitution of three HMDS groups to the aromatic ring at the sites previously occupied by F atoms. The structure also displays 1,3-di-ferration of the aromatic ring through two pseudo-linearly di-coordinate Fe centres, each exhibiting a third significant interaction to the N atom of a neighbouring HMDS group. Complex **38** represents an important contribution not only nucleophilic C-F activation but to the field of two-coordinate transition metal complex chemistry which is of great evolving interest.³¹⁶

Investigations of the reactions of **17a** with 1,3,5-trifluorobenzene established the dynamics present, namely that regardless of stoichiometry, with the application of heat C-F activation becomes favourable. Fluoro and bromo derivatives of **38** have been acquired in the form of complexes **39** and **40** with the substrates 1,2,3,5-tetrafluorobenzene and 1-bromo-2,4,6-trifluorobenzene, respectively; results that preclude any tri-metallation mechanism. These complexes appear to be the first characterised examples of systems possessing two pseudo-linear Fe(II) centres. Mono-metallated product **36** was found to be thermally robust whilst di-metallated **37** was identified as a meta-stable product. **37** is fully consumed upon refluxing to furnish **38** and an unidentifiable Fe-containing species, indicating a possible disproportionation process. The combination of two equivalents of **17a**, one equivalent of NaHMDS and one equivalent of 1,3,5-trifluorobenzene led to near quantitative formation of C-F activation product **38**. Thus, based on our observations we propose a cascade reaction mechanism triggered by the formation of di-ferrated **37** where the elimination of NaF may be a significant driving force. With a source of a unit of NaHMDS present (either another di-ferrated unit in solution or equivalent of base or pure NaHMDS) NaF salt elimination/HMDS insertion brings us through to complex **38**. The same product could also be accessed via 1-bromo-3,5-difluorobenzene.

Utilising the optimal conditions to form complexes **36**, **37** and **38**, electrophilic interception with I₂ furnished iodinated products of each. Hydrolysis of **38** yielded the novel and bulky tri-substituted benzene derivative [1,3,5-tris(HMDS)-C₆H] (**42**).

Magnetometry studies revealed that whilst fluoro-substituted **37** displayed antiferromagnetic coupling between its two Fe(II) centres, HMDS-substituted complexes **38** and **39** showed ferromagnetic interactions between its two highly anisotropic Fe(II) centres along with single-molecule magnet behaviour. The magnetic behaviour of **36** was found to be similar to that of ferrated intermediates **18**, **19** and **24** and though no obvious correlation between the number of fluorine substituents and the anisotropy was found, a small relationship between the geometry around the Fe centres and ZFS components is apparent.

Ferrated and highly fluorinated complexes **23** and **24** have shown themselves as thermally robust, giving no evidence of C-F activation.

Exploring the alkali metal effect, results with potassium were inconclusive whilst monoferration of 1,3,5-trifluorobenzene was found (but no C-F activation) when using [dioxane·LiFe(HMDS)₃] (**32**) in place of **17a**. Occupying the terminal position on the Fe centre with no Li---F contact present, the Li congener base likely operates in a different manner to its sodium equivalent.

II – Conclusions and Further Work

II.1 Conclusions

An intensive and wide-ranging exploration into the synthesis, characterisation and reactivity of novel alkali metal ferrate complexes has been undertaken with many successes achieved and surprises found. This original work and the results presented have explored an area of chemistry where previously only little attention has been paid and has uncovered unexpected reactivities and properties.

The overall project sought to build upon the great successes in cooperative heterobimetallic chemistry observed with alkali metal/main-group complexes and firmly introduce transition metals to this cooperative chemistry. Though synthetic chemists have been keen to move away from a number of transition metals, those of which that are scarce, expensive and often toxic, the use of iron is not only highly attractive because of its excellent economical, ecological and biological profiles but highly interesting given its preceding accomplishments in synthesis and open-shell character which brings a new dynamic to the field of cooperative bimetallic chemistry.

New valuable insights have been gained on co-complexation reactions of sodium reagents and $\text{Fe}(\text{HMDS})_2$, which afforded a range of new sodium ferrates with notable structural diversity.

Attempts to accessing anionic NHC complexes have revealed that while bimetallic systems fail to deprotonate unsaturated NHC IPr, sequential reactivity, where the carbene was first treated with a sodium alkyl, followed by the introduction of the Fe bis(amide) led to the isolation of a novel heteroleptic ferrate containing an anionic NHC ligand. This compound reacts with MeOTf, eliminating NaOTf, undergoing selective methylation at the C2 position to form a novel *abnormal* NHC-Fe complex.

In Chapter 3 the unprecedented metallating capability of a sodium ferrate base towards fluoroaromatic substrates was uncovered. A wide range of fluorinated aryl substrates were subject to successful direct *ortho*-ferration and electrophilic interception with I_2 , achieving good yields with excellent regioselectivity under mild reaction conditions. Furthermore, a number of key ferrated intermediate species were isolated and characterised by X-ray crystallography and ^1H NMR spectroscopy. The structures revealed in all cases the formation of a new Fe-C σ -bond *ortho* to F, which in turn establishes a strong electrostatic interaction

with Na, resulting in a six-membered {NaNFeCCF} ring. These interactions appear to be significant in stabilising the organometallic intermediate.

This bimetallic showed a great stoichiometric control for tri- and tetrafluoro-substituted aromatics, affording di-ferrated products when two equivalents of the base were employed.

A dramatic alkali metal effect has been noted in these reactions; thus switching Na with either Li or K inhibited the Fe-H exchange processes.

Interestingly, studies on the reaction of 1,3,5-trifluorobenzene with sodium ferrate [dioxane·NaFe(HMDS)₃] (**17a**) have revealed a unique activation process where the organic substrate undergoes two-fold metallation and three-fold C-F activation, affording a novel di-iron complex, which contains two low-coordinate Fe centres in a W conformation connected by an aryl fragment where each F atom has been replaced by a N(SiMe₃)₂ group. The formation of this new complex appears to be the result of a cascade reaction, with the concomitant elimination of NaF. Excitingly, two complexes have shown single-molecule magnet behaviour.

Overall, significant progress has been made in the underdeveloped area alkali metal ferrate chemistry, with findings that have implications bridging a number of diverse fields of chemistry. Following in the footsteps of highly successful alkali metal main-group cooperative heterobimetallic complexes, the uncovered alkali metal ferrates have demonstrated diverse structural variety, stimulating magnetic properties and exciting reactivity with N-heterocyclic carbenes and fluorinated aryl substrates.

X-ray crystallography has been an essential tool to structurally characterise a large number of compounds allowing for insight into their structural diversity and in cases uncovering their unique reactivity. Despite the presence of high-spin Fe(II) paramagnetic centres good quality NMR spectra have been obtained and informative in confirming the synthesis of pure products and monitoring certain reactions. Collaborative efforts in undertaking SQUID magnetometry studies and EPR spectroscopy have provided excellent information on the magnetic properties that a number of these ferrates hold.

II.II Further work

Reflecting on what we have come to learn about alkali metal ferrates thus far, there is a great deal of potentially interesting routes of further research.

Though preliminary investigations into lithium and potassium ferrates have been explored and discussed here, it would be interesting to investigate these complexes further to compliment the more extensive work with sodium ferrates. An exploration of structural diversity could be helpful in understanding the differences between the alkali metal ferrates and give indications of their reactivity; in Chapter 3 it is shown that lithium ferrate **32** is incapable of ferrating fluorobenzene and 1,3-difluorobenzene which we propose is due to smaller Li being ‘sunken’ further into the steric sphere of the CIP structure and unable to establish any interaction with F. The known π -affinity¹³² of larger and softer K could prove interesting for potassium ferrates where flexible aryl arms could be introduced or in solution with aromatic substrates. Moving even further forward, the synthesis and characterisation of alkaline earth metal ferrates could be very fruitful, particularly magnesium ferrates with a view to uncovering potential bimetallic active catalytic species operating in Fe-catalysed cross-coupling reactions with Grignard reagents (see Section I.III).

Assessing the results disclosed in Chapter 1, along with the difference in reactivity observed between CIP **17a** and SSIP **5** towards fluorobenzene (see Section 3.2.2), it would be judicious to further observe the differences in reactivity between CIP and SSIP sodium ferrate complexes in instances of metallation and beyond which could perhaps highlight the importance of Na and Fe connected via bridging ligand. Acknowledging the relative ease of in the introduction of DPA to the sodium ferrate system (see Section 1.1.4) there is certainly scope for the introduction of other ligand sets which could amplify magnetic properties, enhance reactivity and exhibit interesting and unusual structural motifs. Previous reports of ferrates with the tetramethylpiperdine ligand have shown exciting reactivity for cross-coupling⁸⁶ and direct C-H metallation.⁸²

Continuing the successful introduction ferrates to N-heterocyclic carbene IPr, there are a wealth of other NHCs and carbenic substrates to explore in a similar fashion. Regarding complex **15**, as well as functionalisation at C2 with other electrophilic reagents (such as TMSCl, allyl bromide or SiPh₂Cl₂) which could be very interesting, the Fe-C4 bond could be exploited for backbone functionalisation. The use of K and Fe could prove interesting with

IPr (or other aryl substituted NHCs) considering a recently reported K/Mg anionic NHC featuring significant K-aryl π -interactions in an unusual polymeric structure.

The stimulating reactivity of sodium ferrate mediated C-H activation of fluorinated aromatic substrates reported in Chapter 3 opens the door to an array of possibilities for further research. Concerning the direct *ortho*-ferration of fluoroaromatics with dioxane sodium ferrate base **17/17a**, other structurally characterised CIP sodium ferrate complexes (i.e. those detailed in Chapter 1) should be assessed as to whether they display the same or similar reactivity towards fluoroaryls or whether 1,4-dioxane is a vital component for C-H activation. Though SSIP complex **5** was unreactive towards fluorobenzene, reacting SSIP sodium ferrates with more activated fluoroarene substrates may uncover different results and should be investigated. Electrophilic quenching with I₂ provided a good proof of concept and so now we should look further to identify whether a methodology for sodium ferrate mediated cross-coupling reactions could be developed. Further investigations into Li, K and heteroleptic ferrates could prove valuable as only a small number of reactions were carried out during this project concerning these complexes. Looking beyond fluoroaromatics, other (non-fluorinated) aryl substrates, possibly those bearing substituents with a significant inductive effect and affinity to sodium, may be amenable to direct ferration. Hydrofluoroolefins, currently of high interest as “fourth generation refrigerants” with a far superior ecological profile to HFCs,^{349,350} could prove very interesting as substrates for direct ferration (or even C-F activation), and if successful, for further functionalisation.

Complexes **38-40**'s two-coordinate Fe centres are likely to be highly reactive thus investigations into reactions of these complexes with small molecules like O₂ (akin to O insertion with Fe(Ar')₂, see Section 4.2.2) may lead to some interesting results, as would an assessment of the lability of the terminal HMDS groups attached to Fe (e.g. transamination). Of high interest, the addition of alkali metal reagents (such as ⁿBuLi, NaCH₂SiMe₃, etc.) to compounds **38-40** could result in a number of outcomes like instigating the formation of a heteroleptic ferrate system by interaction with an Fe centre, deprotonation of the remaining aryl proton in the case of **38**, AM/halogen exchange or nucleophilic aromatic substitution with **39** and **40** or even the deprotonation of a HMDS methyl unit could be possible. Regarding diferrated complex **37**, given that one equivalent of NaHMDS is required to transform **37** into **38** in a stoichiometrically manner, the addition of an alternative alkali metal reagent could facilitate the insertion of a different R group onto the ring at the 2-position between the Fe-substituted C atoms. Based on the observed magnetic data, tuning the framework of

complexes **38-40** could enhance or alter their magnetic behaviour, in addition to attempts to reduce the Fe(II) centres to Fe(I) centres to alter the spin state from $S = 2$ to $S = 3/2$ to suppress quantum tunnelling effects. Novel and bulky tri-substituted compound **42** could find use as a bulky ligand and may well be responsive to deprotonative metallation by simple alkali metal reagents at one of its three ring C-H sites. Pursuing further studies of Li and K ferrates with 1,3,5-trifluorobenzene would also be worthwhile. As regards to the terminally bonded 1,3,5-trifluorobenzene in **43**, further equivalents of base could facilitate deprotonation of the remaining aryl H atoms.

III – Experimental

III.I General Experimental Techniques

III.I.I Schlenk Techniques

The majority of organometallic materials used within this project are sensitive to air and moisture sensitive including a number of reagents which are pyrophoric. As such, Standard Schlenk techniques were utilised for the synthetic work under a dry, inert atmosphere of purified argon gas. All glassware was oven-dried at 125°C prior to use.



Figure III-1 – A Schlenk line with vacuum pump and solvent trap.

The Schlenk line (Figure III-1) is a dual manifold piece of glass apparatus with one pathway connected to a vacuum pump with a solvent trap (cooled by liquid N₂) to condense any volatile solvents removed from reaction flasks under vacuum and the other, to a supply of argon gas with paraffin oil-filled Drechsel bottles at the outlet to prevent overpressure. Taps at the five separate connectors allow for the interchange between Ar and vacuum to any connected glass apparatus (e.g. Schlenk tubes, addition tubes, filter sticks). All taps and joints were lubricated with high-vacuum Apiezon N Grease prior to use. Before carrying out reactions vacuum was applied to remove air and atmospheric moisture from an oven-dried Schlenk tube for 5 minutes before refilling with argon gas. This process was repeated three times in total to guarantee an oxygen and moisture-free environment to carry out reactions in.

III.I.II Glove Box

For the storage and handling of solid materials including the weighing of reagents and isolated products, as well as the preparation of NMR spectroscopy elemental analysis samples, an MBraun MB10 compact glove box with an argon gas recirculation and purification system was used to provide an inert argon atmosphere (Figure III-2).



Figure III-2 – MBraun MB10 compact glove box.

A large chamber fitted with a plastic window and sealed rubber gloves is the working area where chemicals can and equipment can be stored and manipulated. Conveniently, this model contains a freezer (on the left side) for storage of reagents or products which necessitate a cold climate for storage or are very volatile or reactive. At the right side of the box is a separate sealed chamber with a door to the working area and a door to the outside. Through this port chemicals and equipment can be introduced to or taken out of the glove box. Before taking any apparatus inside the working area the chamber is evacuated of air by vacuum and refilled with argon gas. Vacuum is applied for 10 minutes before refilling with Ar, as with glassware on the Schlenk line this process is repeated three times in total. Manipulations inside the box were carried out with <0.5 ppm of O_2 and H_2O present.

III.I.III Solvent Drying and Purification

It is important not only to ensure the atmosphere around solid reactants is free from air and moisture but also that the solvents used are dry and free from O₂. Accordingly, solvents used in synthesis were distilled under an inert nitrogen atmosphere over sodium wire and benzophenone to remove any traces of moisture and dissolved oxygen. The Na-benzophenone mixture produces a radical anion ketyl species which acts as an effective oxygen and water scavenger, turning the solution a blue, green or purple colour.³⁵¹ Distillation of the solvent after the point at which the mixture has turned coloured affords oxygen-free, pure and dry solvent. The primary solvents dried by this method and used during this project were *n*-hexane, toluene, diethyl ether, tetrahydrofuran and benzene. Additionally, *n*-hexane and toluene were available to use dried and degassed by Grubbs column³⁵² (PureSolv micro solvent purification system, Innovative Technologies); this source of dry *n*-hexane was preferable for the synthesis of alkali metal ferrates. Fluorobenzene was dried over P₂O₅ for 3 days before fractionally distilling and storing over 4 Å molecular sieves. The following reagents were dried by distillation over CaH₂ under a nitrogen or argon atmosphere and stored over 4 Å molecular sieves: 1,4-dioxane, TMEDA, DTEDA, PMDETA, Me₆TREN, fluorobenzene, 1,3-difluorobenzene, 1,4-difluorobenzene, 1,2,4-trifluorobenzene, 1,2,4,5-tetrafluorobenzene, pentafluorobenzene 1-fluoronaphthalene, 1-bromo-3,5,-difluorobenzene, anisole, 3-fluoroanisole, 1,3,5-trifluorobenzene, 1,2,3,5-tetrafluorobenzene and 1-bromo-2,4,6-trifluorobenzene. Deuterated solvents such as C₆D₆, d₈-THF, d₈-toluene and d₅-pyridine for NMR spectroscopy were stored over 4 Å molecular sieves in the glove box prior to use.

III.I.IV Commercial Reagents

Commercially available reagents and solvents were purchased from the following suppliers: Sigma Aldrich, Alfa Aesar, Manchester Organics and Fluorochem.

III.I.V Preparation of Starting Materials

IPr,¹⁹⁶ NaCH₂SiMe₃³⁵³ and [(IPr)Fe(HMDS)₂]¹⁸⁹ were prepared according to the reported methods.

Fe(HMDS)₂

Fe(HMDS)₂ was prepared according to a modified literature procedure from Lappert *et al.*⁹¹ FeBr₂ (9.251 g, 43 mmol) was reacted directly with LiHMDS (14.390 g, 86 mmol) in Et₂O solvent (80 mL) at 0°C as opposed to first synthesising the THF adduct, guaranteeing a THF-free final product. Diethyl ether was removed under vacuum and the mixture was redissolved in 50 mL of hexane to leave LiBr as a precipitate which was removed via filtration over Celite/glass wool into a three-neck round-bottomed flask with a single 20 mL wash-through of hexane. Hexane was removed under vacuum to leave a dark green oil. The oil was distilled into a second three-neck round-bottom flask under dynamic vacuum at 120°C with the aid of a heat gun. The product was a bright emerald green oil which slowly darkened and crystallised at ambient temperature (13.76 g, 87% yield). The product was stored within a glove-box at -35°C for convenient use as a solid.

¹H NMR (C₆D₆, 300 K) δ (ppm) = 60.27 [vbs, SiMe₃]

S=PPh₃

2.62 g (10 mmol) of PPh₃ was added to an oven-dried Schlenk tube and dissolved in 20 mL of toluene. 0.32 g (10 mmol) of Sulfur flowers (S₈) was added via solid addition tube and quickly entered solution after which a white precipitate began to form. The mixture was left to stir overnight before removing toluene under vacuum to isolate 2.71 g (92% yield) of the white precipitate.

¹H NMR (d₈-THF, 300 K) δ (ppm) = 7.76-7.71 [m, *ortho* aryl CH's, 6H], 7.53-7.49 [m, *para* aryl CH's, 3H], 7.46-7.42 (6H) [m, *meta* aryl CH's, 6H]

¹³C{¹H} NMR (d₈-THF, 300 K) δ (ppm) = 135.28-134.44 [d, *ipso* aryl C's], 133.15-133.05 [d, *ortho* aryl CH's], 132.09-132.06 [d, *para* aryl CH's], 129.19-129.07 [d, *meta* aryl CH's]

³¹P{¹H} NMR (d₈-THF, 300 K) δ (ppm) = 44.17 [s, S=PPh₃]

III.I.VI NMR Spectroscopy

All samples for NMR spectroscopy were prepared inside the inert argon atmosphere of the glove-box. ¹H (400.13 MHz), ²H (61.41 MHz), ⁷Li (155.47 MHz), ¹³C{¹H} (100.59 MHz) ¹⁹F{¹H} (376.40 MHz) and ³¹P{¹H} (161.93 MHz) NMR spectra were recorded on either a

Bruker AV400 or AV3 spectrometer using TopSpin software (v2.1, Bruker Biospin, Karlsruhe) at 300 K. ^1H and $^{13}\text{C}\{^1\text{H}\}$ NMR spectra were referenced internally to the corresponding residual solvent peaks. LiCl in D_2O ($\delta = 0$ ppm) was used as an external standard for ^7Li NMR spectroscopy. CFCl_3 ($\delta = 0$ ppm) was used as an external reference for $^{19}\text{F}\{^1\text{H}\}$ NMR. 85% (w/w) H_3PO_4 in D_2O was used as an external standard at 0 ppm for $^{31}\text{P}\{^1\text{H}\}$ NMR spectra. The following deuterated solvents were used: C_6D_6 , d_8 -THF, d_8 -toluene, d_5 -pyridine, D_2O and CDCl_3 . All NMR spectroscopy samples for organometallic compounds were measured in tubes equipped with a James Young valve.

III.I.VII Magnetometry Studies

Magnetic studies were undertaken in collaboration with Dr Guillem Aromi and Ivana Borilovic at the Universitat de Barcelona. Sections concerning magnetometry studies in this thesis have been adapted from reports authored by Ivana Borilovic. Variable temperature magnetic susceptibility data were obtained on powdered polycrystalline samples with a Quantum Design MPMS5 SQUID magnetometer at the “Unitat de Mesures Magnètiques” at the Universitat de Barcelona. Pascal’s constants were used to estimate diamagnetic corrections to the molar paramagnetic susceptibility and a correction was applied for the sample holder. Taking into account extreme air and moisture sensitivity of the compounds, samples were prepared in a glovebox and transferred to a Schlenk before transporting them to the SQUID. Samples were held within gelatin capsules during measurements. Results of SQUID measurements ($\chi_{\text{M}}T$ vs T curves) were fitted using the program PHI (v2.0).¹⁴⁸ X-Band (9.42 GHz) EPR spectra of powdered samples were determined on a Bruker ESP300E spectrometer, equipped with a liquid helium cryostat. EPR samples were stored in a Wilmad quartz EPR sample tube (4 mm thin wall, 25 cm long) which was sealed in a glovebox with a tip-off manifold.

Solution magnetic susceptibilities (where possible) were determined by the Evans method at 300 K.^{102,103} Pascal’s constants were used to estimate diamagnetic corrections to the molar paramagnetic susceptibility.

III.I.VIII Organic Work-Up

The general procedure for organic work-up (see products **IIa-I'** and compounds **41** and **42**) was thus; addition of 5 equivalents of I_2 (or H_2O in the case of **42**) in THF and stirring for one

hour before quenching with saturated sodium thiosulfate solution. The organic compound was extracted with diethyl ether (3 x 50 mL) and the combined organic fractions were washed with brine, dried over magnesium sulfate and the solvents were removed under vacuum.

III.I.IX Gas Chromatography-Mass Spectrometry

Gas Chromatography-Mass Spectrometry (GC-MS) samples were measured on an Agilent Technologies 5975C GC/MS detector fitted with an RXi[®]-5Sil column. High Resolution-Mass Spectrometry (HR-MS, GC/EI-MS) for products **41**, **IIc**, **IIg** and **IIh** was conducted on a Thermo Scientific LTQ Orbitrap XL mass spectrometer at the EPSRC National Mass Spectrometry Facility in Swansea.

III.I.X Elemental Analysis

Elemental analyses were performed on a Perkin Elmer 2400 Series II CHNS/O Analyser. Samples were prepared in the glove box sealing 3 x 1-3 mg of crystalline solid within tin capsules before transporting quickly to the instrument.

III.II Synthesis and Characterisation of Numbered Inorganic Compounds

III.II.I Chapter 1

[{NaFe(HMDS)₃}_∞] (1)

0.377 g (1 mmol) of Fe(HMDS)₂ and 0.184 g NaHMDS were added to an oven-dried Schlenk tube. 20 mL of hexane was added resulting in near instant dissolution of the Fe(HMDS)₂ and the suspension of the NaHMDS. The suspension was gently heated and left to stir for one hour till complete dissolution of the NaHMDS was apparent and the solution had changed colour from light green to dark green. Green needle-like crystals could be obtained by reducing the volume of the solution to half *in vacuo* and slowly cooling to -30°C (0.45 g, 80% yield).

^1H NMR (C_6D_6 , 300 K) δ (ppm) = -4.72 [vbs, SiMe_3]

$^{13}\text{C}\{^1\text{H}\}$ NMR (C_6D_6 , 300 K) δ (ppm) = 333.41 [SiMe_3]

Anal. Calcd for $\text{C}_{18}\text{H}_{54}\text{FeN}_3\text{NaSi}_6$: C 38.61, H 9.72, N 7.51 Found: C 38.64, H 9.99, N 8.04

Solution Magnetic Moment (d_8 -tol, 300 K) = $4.72 \mu_{\text{B}}$

[THF·NaFe(HMDS)₃] (2)

0.08 mL (1 mmol) of THF was added *in situ* to a freshly synthesised solution of **1** in hexane. This resulted in the immediate precipitation of a white solid. Stirring was continued for one hour before slow cooling to -30°C to yield green plate-like crystals. The combined yield of the precipitate and crystals was 83% (0.526 g).

N.B. [THF·NaFe(HMDS)₃] was originally found as a side-product during the synthesis of **1**. The presence of the THF was unexpected and it is likely to have originated from $\text{Fe}(\text{HMDS})_2$, indeed Power *et al.* crystallographically characterised [THF·Fe(HMDS)₂].⁹² The original batch used was synthesised according to Lappert's method from 1988; principally by making FeBr_2 more soluble by stirring in THF to generate $\text{FeBr}_2\cdot(\text{THF})_2$ followed by a metathesis reaction with two equivalents of LiHMDS in diethyl ether (Et_2O) solvent.⁹¹ THF-free $\text{Fe}(\text{HMDS})_2$ can be synthesised using FeBr_2 directly rather than the $\text{FeBr}_2\cdot(\text{THF})_2$. A polymorph of **2** has previously been synthesised and reported by Lerner and co-workers.¹¹⁶

^1H NMR (C_6D_6 , 300 K) δ (ppm) = 10.86 [vbs, $\text{CH}_2(2,5)$, 4H], 6.35 [bs, $\text{CH}_2(3,4)$, 4H], -4.74 [vbs, SiCH_3 , 54H]

$^{13}\text{C}\{^1\text{H}\}$ NMR (C_6D_6 , 300 K) δ (ppm) = 330.32 [SiMe_3], not observed [THF CH_2 's]

Anal. Calcd for $\text{C}_{22}\text{H}_{62}\text{FeN}_3\text{NaOSi}_6$: C 41.80, H 9.89, N 6.65 Found: C 41.52, H 10.09, N 6.55

Solution Magnetic Moment (C_6D_6 , 300 K) = $4.84 \mu_{\text{B}}$

[Et₂O·NaFe(HMDS)₃] (3)

0.1 mL (1 mmol) of Et₂O was added *in situ* to a freshly synthesised solution of **1** in hexane and stirred overnight. The solution was concentrated to ~10 mL before slow cooling to -30°C. Small green crystals were yielded after several days (0.4915 g, 78% yield).

¹H NMR (C₆D₆, 300 K) δ (ppm) = 10.18 [bs, Et₂O CH₂'s, 4H], 4.52 [bs, Et₂O CH₃'s, 6H], -4.81 [vbs, SiMe₃, 54H]

¹³C{¹H} NMR (C₆D₆, 300 K) δ (ppm) = 327.22 [SiMe₃], 4.52 [Et₂O CH₃'s], not observed [Et₂O CH₂'s]

Anal. Calcd for C₂₂H₆₄FeN₃NaOSi₆: C 41.67, H 10.17, N 6.63 Found: C 41.24, H 9.99, N 7.16

Solution Magnetic Moment (C₆D₆, 300 K) = 5.71 μ_B

[PPh₃=S·NaFe(HMDS)₃] (4)

To a freshly prepared solution of **1** in hexane, 0.294 g (1 mmol) of S=PPh₃ was added via a solid addition tube, gently heated and stirred for 1 hour. A large quantity of crystalline material was generated upon cooling to -30°C. Excess solvent was removed via a syringe and the off-white crystalline material was dried under vacuum (0.62 g, 72% yield).

¹H NMR (C₆D₆, 300 K) δ (ppm) = 10.22 [bs, *ortho* aryl CH's, 6H], 7.90 [s, *meta* aryl CH's, 6H], 7.45 [s, *para* aryl CH's, 3H], -4.70 [vbs, SiMe₃, 54H]

¹³C{¹H} NMR (C₆D₆, 300 K) δ (ppm) = 327.62 [SiMe₃], 136.54 [*ipso* aryl C's], 133.32 [*para* aryl CH's], 130.62 [*ortho* aryl CH's], obscured by solvent signal [*meta* aryl CH's]

³¹P{¹H} NMR (C₆D₆, 300 K) δ (ppm) = no visible resonances

Anal. Calcd for C₃₆H₆₉FeN₃NaOPSSi₆: C 50.61, H 8.14, N 4.92 Found: C 50.63, H 8.11, N 5.91

[Na(TMEDA)₂]⁺[Fe(HMDS)₃]⁻ (5)

To a freshly prepared solution of **1** in hexane, 0.30 mL (2 mmol) of TMEDA was added resulting in the immediate precipitation of a white solid and a slow colour change of the

solution from green to light brown. The mixture was stirred for 2 hours before removing all hexane under vacuum and redissolving the precipitate in 6 mL of C₆H₅F and layering with 20 mL of hexane. Storage overnight yielded a crop of large, light green, needle-like crystals. Excess solvent was removed via a syringe and the crystals were subsequently dried under vacuum (0.64 g, 80% yield).

¹H NMR (d₈-THF, 300 K) δ (ppm) = 2.31 [s, TMEDA CH₂, 8H], 2.16 [s, TMEDA CH₃, 24H], -2.37 [vbs, SiMe₃, 54H]

¹³C{¹H} NMR (d₈-THF, 300 K) δ (ppm) = 347.81 [SiMe₃], 58.77 [TMEDA CH₂], 46.11 [TMEDA CH₃]

Anal. Calcd for C₃₀H₈₆FeN₇NaSi₆: C 50.45, H 11.37, N 10.84 Found: C 49.86, H 11.51, N 10.53

[Na(DTEDA)₂]⁺[Fe(HMDS)₃]⁻ (6)

To a freshly prepared solution of **1** in hexane, 0.28 mL (2 mmol) of DTEDA was added resulting in the immediate precipitation of a white solid. The mixture was left to stir overnight before removing all hexane was removed under vacuum and the precipitate was redissolved in 6 mL of C₆H₅F and cooled to -30°C. Storage overnight yielded a crop of large, light yellow crystals which were subsequently dried under vacuum. The yield of the crystalline powder was 79% (0.7152 g).

¹H NMR (d₈-THF, 300 K) δ (ppm) = 2.57 [s, DTEDA CH₂, 8H], 1.04 [s, DTEDA CH₃, 36H], -2.37 [vbs, SiMe₃, 54H], not observed [DTEDA NH, 4H]

¹³C{¹H} NMR (d₈-THF, 300 K) δ (ppm) = 347.81 [SiMe₃], 50.25 [DTEDA C(CH₃)₃], 44.17 [DTEDA CH₂], 29.56 [DTEDA CH₃]

Anal. Calcd for C₃₈H₁₀₂FeN₇NaSi₆: C 50.45, H 11.37, N 10.84 Found: C 49.86, H 11.51, N 10.53

[Na(PMDETA)₂]⁺[Fe(HMDS)₃]⁻ (7)

0.41 mL (2 mmol) of PMDETA was added *in situ* to a solution of **1** in hexane producing a colour change of solution from green to brown along with the formation of a white

precipitate. After an hour stirring all volatiles were removed under vacuum and the remaining solid redissolved in 6 mL of C₆H₅F. Upon slow cooling and storage at –30°C crystals were obtained after 3 days (0.732 g, 81% yield)

¹H NMR (d₈-THF, 300 K) δ (ppm) = 2.40 [bs, PMDETA NCH₂CH₂N(CH₃)₂, 8H], 2.30 [bs, PMDETA CH₂N(CH₃)₂, 8H], 2.14 [bs, PMDETA CH₃, 30H], –2.42 [vbs, SiMe₃, 54H]

¹³C{¹H} NMR (d₈-THF, 300 K) δ (ppm) = 347.05 [SiMe₃], 58.77 [PMDETA CH₂], 57.21 [PMDETA CH₂], 46.19 [PMDETA CH₃], 43.29 [PMDETA N(CH₃)₂]

Anal. Calcd for C₃₆H₁₀₀FeN₉NaSi₆: C 47.69, H 11.21, N 13.90 Found: C 47.72, H 10.89, N 14.46

[Me₆TREN·Na]⁺[Fe(HMDS)₃][–] (8)

To a freshly prepared solution of **1** in hexane, 0.26 mL (1 mmol) of Me₆TREN was added resulting in the precipitation of a white solid and inducing a colour change from green to sandy brown in the solution. After 1 hour of stirring hexane was removed *in vacuo* and the remaining solid dissolved in 6 mL of fluorobenzene. The solution was cooled slowly to –30°C and stored in the freezer for several days to obtain large colourless crystals (0.6656 g, 84%).

¹H NMR (d₈-THF, 300 K) δ (ppm) = 2.40 [bs, Me₆TREN NCH₂CH₂N(CH₃)₂, 6H], 2.24 [bs, Me₆TREN NCH₂CH₂N(CH₃)₂, 6H], 2.09 [bs, Me₆TREN CH₃, 18H], –2.46 [vbs, SiMe₃, 54H]

¹³C{¹H} NMR (d₈-THF, 300 K) δ (ppm) = 348.19 [SiMe₃], 58.45 [Me₆TREN CH₂], 57.74 [Me₆TREN CH₂], 45.97 [PMDETA CH₃], 43.29 [Me₆TREN N(CH₃)₂]

Anal. Calcd for C₃₀H₈₃FeN₇NaSi₆: C 45.59, H 10.71, N 12.41 Found: C 45.56, H 11.02, N 13.48

[{Fe(HMDS)(DPA)}₂] (9)

Fe(HMDS)₂ (0.377 g, 1 mmol) and DPA(H) (0.171 g, 1 mmol) were added to a Schlenk tube along with 20 mL of hexane. Upon stirring a brown solution with off-white precipitate was formed which was stirred at ambient temperature overnight. Addition of 8 mL of THF

dissolved the precipitate and gave a black solution which was cooled to -30°C . This yielded orange plate-like crystals (0.15 g, 38% yield).

^1H NMR (C_6D_6 , 300 K) δ (ppm) = 47.15 [bs, DPA aryl $\text{CH}'\text{s}$, 2H], 25.00 [bs, DPA aryl $\text{CH}'\text{s}$, 2H], 21.27 [bs, DPA aryl $\text{CH}'\text{s}$, 2H], 17.01 [vbs, SiMe_3 , 54H], -14.31 [bs, DPA aryl $\text{CH}'\text{s}$, 2H]

Anal. Calcd for $\text{C}_{32}\text{H}_{52}\text{Fe}_2\text{N}_8\text{Si}_4$: C 49.73, H 6.78, N 14.50 Found: C 49.94, H 6.78, N 14.80

Solution Magnetic Moment (C_6D_6 , 300 K) = $5.37 \mu_{\text{B}}$

$[(\text{THF})_2 \cdot \text{NaFe}(\text{DPA})(\text{HMDS})_2]$ (10)

To a 1 mmol hexane solution of **1** 0.171 g of DPA(H) (1 mmol) was added via solid addition tube resulting in the immediate formation of sticky tan/brown solid residue at the base of the Schlenk tube in the green solution. After stirring overnight at ambient temperature this residue was a dark brown suspension in the green solution, addition of 2 mL of THF gave a black solution. Cooling to -30°C allowed for the isolation of orange plate-like crystals (0.43 g, 60%).

^1H NMR (C_6D_6 , 300 K) δ (ppm) = 6.39 [vbs], 4.97 [bs], 2.12 [bs], rational integration and assignment of resonances not possible

Anal. Calcd for $\text{C}_{26}\text{H}_{52}\text{FeN}_5\text{NaOSi}_4$ (loss of 1 THF): C 41.67, H 10.17, N 6.63 Found: C 41.24, H 9.99, N 7.16

$[\{\text{THF} \cdot \text{NaFe}(\text{DPA})_3\}_\infty]$ (11)

To a 1 mmol solution of **1** in hexane 0.513 g of DPA(H) (3 mmol) was added via solid addition tube resulting in the immediate formation of sticky tan/brown solid residue at the base of the Schlenk tube in the green solution. After stirring overnight at ambient temperature there was a mustard coloured suspension in a dark brown solution. All volatiles were removed under vacuum and the mustard coloured solid residue was redissolved in 15 mL of toluene and 5 mL of THF. Cooling to -30°C allowed for the isolation of yellow plate-like crystals (0.35 g, 18% yield).

^1H NMR (C_6D_6 , 300 K) δ (ppm) = rational assignment of hydrogen signals is not possible

Anal. Calcd for $C_{75}H_{72}Fe_2N_{18}Na_2O_2$ (2 monomer units + 1 eq. of co-crystallised toluene): C 63.65, H 5.13, N 17.82 Found: C 63.54, H 5.13, N 18.14

III.II.II Chapter 2

$[NaFe(HMDS)_2(CH_2SiMe_3)]_\infty$ (12)

0.377 g (1 mmol) of $Fe(HMDS)_2$ and 0.110 g $NaCH_2SiMe_3$ were added to an oven-dried Schlenk tube and cooled to 0°C. 20 mL of hexane was added producing a very pale green solution in which a white suspension appeared after several minutes that could be dissolved with gentle heating. Blue/green block-like crystals were obtained by slowly cooling the solution from ~50°C (0.36 g, 73% yield).

1H NMR (C_6D_6 , 300 K) δ (ppm) = 13.51 [vbs, CH_2SiMe_3 , 9H], -8.57 [vbs, HMDS $SiMe_3$, 36H], not observed [CH_2SiMe_3]

$^{13}C\{H\}$ NMR (C_6D_6 , 300 K) δ (ppm) = 342.71 [HMDS $SiMe_3$], 265.23 [CH_2SiMe_3], not observed [CH_2SiMe_3]

Anal. Calcd for $C_{16}H_{47}FeN_2NaSi_5$: C 39.48, H 9.73, N 5.75 Found: C 39.64, H 9.77, N 6.19

Attempts to measure the solution magnetic moment of 12 via the Evans method were unsuccessful due to irreproducible chemical shift differences between the internal reference sample and residual protic solvent producing exceedingly large μ_{eff} values.

$[Na(IPr)_2]^+[Fe(HMDS)_3]^-$ (13)

To a freshly prepared solution of **1** in hexane, 0.776 g (2 mmol) of IPr was added via a solid addition tube. The solution turned from green to light brown with an off-white precipitate whilst stirring was continued for one hour. Hexane was removed *in vacuo* and the solid was redissolved in 10 mL of C_6H_5F . The solution was cooled slowly to -30°C and a crop of green crystals were dried *in vacuo* and collected after several days (0.97 g, 73% yield).

1H NMR (d_8 -THF, 300 K) δ (ppm) = 7.36 [t, IPr, *p-CH*, 4H], 7.27-7.25 [d, IPr, *m-CH*, 8H], 7.18 [s, IPr, *NCH*, 4H], 2.83 [m, IPr, $CHMe_2$, 8H], 1.21-1.16 [IPr, $CHMe_2$, 48H], -2.39 [vbs, $SiMe_3$, 54H]

$^{13}\text{C}\{\text{H}\}$ NMR (d_8 -THF, 300 K) δ (ppm) = 346.74 [SiMe_3], 220.74 [IPr, im-C2], 146.53 [IPr, *o*-CH], 139.46 [IPr, *i*-CH], 128.98 [IPr, *p*-CH], 123.98 [IPr, *m*-CH], 122.32 [IPr, NCH], 29.02 [IPr, CHMe_2], 23.55 [IPr, CHMe_2]

Anal. Calcd for $\text{C}_{72}\text{H}_{126}\text{FeN}_7\text{NaSi}_6$: C 64.67, H 9.50, N 7.33 Found: C 64.47, H 9.87, N 7.77

Solution Magnetic Moment (d_5 -pyr, 300 K) = $4.90 \mu_{\text{B}}$

$(\text{THF})_3 \cdot \text{NaIPr}^+ [\text{Fe}(\text{HMDS})_2(\text{CH}_2\text{SiMe}_3)]^-$ (14)

To 1 mmol of **12** (0.487 g) in 10 mL of hexane, 1 mmol of IPr (0.387 g) was added along with a further 10 mL of hexane to wash the substrate into solution. With gentle heating, IPr enters solution with the colour turning from dark red to sandy brown with the formation of a precipitate. Upon addition of 0.5 mL of THF along with gentle heating an orange solution was produced along with a small quantity of a black oily substance. These were separated by filtration over Celite/glass wool and the orange solution began to afford pale green crystals immediately upon cooling back to ambient temperature. The crystals were washed with 3 x 5 mL of cold hexane and dried (0.76 g, 70% yield).

^1H NMR (d_8 -THF, 300 K) δ (ppm) = 13.51 [vbs, CH_2SiMe_3 , 9H], 7.37-7.18 [IPr, *p*- and *m*-CH + NCH, 10H], 2.80 [s, IPr, CHMe_2 , 4H], 1.15 [IPr, CHMe_2 , 24H], -3.77 [vbs, SiMe_3 , 36H], not observed [CH_2SiMe_3]

Anal. Calcd for $\text{C}_{51}\text{H}_{99}\text{FeN}_4\text{NaO}_2\text{Si}_5$ (1 single unit – 1 THF molecule lost under vacuum): C 60.08, H 9.79, N 5.49 Found: C 60.13, H 10.00, N 5.97

Solution Magnetic Moment (C_6D_6 , 300 K) = $4.40 \mu_{\text{B}}$

$(\text{THF})_3 \cdot \text{Na}[\text{C}\{\text{N}(\text{2,6-}^i\text{Pr}_2\text{C}_6\text{H}_3)_2\text{CHCFe}(\text{HMDS})_2\}]$ (15)

0.777 g (2 mmol) of IPr was suspended in hexane before adding 0.22 g (2 mmol) of $\text{NaCH}_2\text{SiMe}_3$ resulting in a quick colour change from peach to intense orange and the formation of a precipitate. After stirring for 1 hour, a solution of 0.754 g (2 mmol) of $\text{Fe}(\text{HMDS})_2$, dissolved in 10 mL of hexane, was added which induced a colour change from orange to red with the formation of a white precipitate. After stirring the mixture for 2 hours, 2 mL of THF was added which allowed the precipitate to enter solution and give a deep red coloured oil. This mixture was gently heated and placed in a hot water Dewar flask ($\sim 50^\circ\text{C}$).

Overnight the solution afforded pale green crystals which were collected by filtration after washing with cold hexane (3 x 10 mL). The crystalline yield was 60% (1.3737 g).

^1H NMR (d_8 -THF, 300 K) δ (ppm) = 10.59 [*m*-CH, 2H], 10.04 [*p*-CH, 1H], 8.29 [*p*-CH, 1H], 7.89 [*m*-CH, 2H], 5.27 [s, CHMe₂, 2H], 3.85 [CHMe₂, 6H], 3.03 [THF 2,5-CH₂, 12H], 3.03 [THF 3,4-CH₂, 12H], 0.86 [CHMe₂, 6H], -2.06 [CHMe₂, 2H], -4.21 [SiMe₃, 36H], -6.94 [CHMe₂, 12H], -26.37 [C5-H, 1H]

Anal. Calcd for C₅₅H₁₀₃FeN₄NaO₄Si₄ (1 monomeric unit + 1 eq. of co-crystallised THF): C 61.42, H 9.65, N 5.21 Found: C 61.32, H 9.90, N 5.74

Solution Magnetic Moment (C₆D₆, 300 K) = 4.86 μ_B

[CH₃C{[N(2,6-*i*-Pr₂C₆H₃)]₂CHCFe(HMDS)₂}] (16)

1.0756 g (1 mmol with 1 eq. co-crystallised THF) of **15** was suspended in 20 mL of toluene and cooled to -78°C. To this, 0.1477 g (0.9 mmol) of MeOTf in 5 mL of toluene was added and the solution was stirred and allowed to warm to ambient temperature over 1 hour. A white precipitate in a yellow solution was visible and thus the solution was filtered via a cannula. Volatiles were removed by vacuum from the filtrate and the solid was redissolved in a 1:1 mixture of hexane and toluene (total 20 mL). Slow cooling from 50°C produced yellow plate-like crystals which were isolated by filtration and washed with cold hexane (3 x 5 mL). The low crystalline yield obtained was 28% (based on 0.9 eq. MeOTf, 0.1979 g), due in part to loss during washing.

^1H NMR (d_8 -tol, 300 K) δ (ppm) = 29.37 [C2-CH₃, 3H], 10.78 [*p*-CH, 1H], 9.64 [*m*-CH, 2H], 8.58 [*p*- and *m*-CH, 3H], 4.53 [CHMe₂, 6H], 1.34-0.88 [CHMe₂, 4H], -0.98 [CHMe₂, 6H], -3.40 [CHMe₂, 6H], -5.05 [SiMe₃, 36H], -6.96 [CHMe₂, 6H], -33.29 [C5-H, 1H]

Anal. Calcd for C₄₀H₇₄FeN₄Si₄: C 61.65, H 9.57, N 7.19 Found: C 61.85, H 9.61, N 7.63

Solution Magnetic Moment (C₆D₆, 300 K) = 4.78 μ_B

III.II.III Chapter 3

[dioxane·{NaFe(HMDS)₃}₂] (17)

To a freshly prepared 1 mmol solution of [$\{\text{NaFe}(\text{HMDS})_3\}_\infty$] (**1**) in 20 mL of hexane, 0.085 mL (1 mmol) of 1,4-dioxane was added producing an off-white precipitate. The mixture was stirred for 1 hour before removing all volatiles *in vacuo*. The remaining green/white solid was redissolved in 5 mL of benzene then concentrated till precipitate appeared, warmed and then cooled slowly to generate large, green crystals (0.41 g, 63% yield based on Fe with 1 eq. of co-crystallised benzene).

N.B. Though the combination of equimolar equivalents of **1** and 1,4-dioxane crystallises as hemisolvate **17**, it is found that a full equivalent of 1,4-dioxane is retained in the green/white amorphous solid when the solution is subject to vacuum. Thus, **17a** shall refer to [dioxane·NaFe(HMDS)₃].

¹H NMR (d₈-tol, 300 K) δ (ppm) = 6.17 [bs, 1,4-dioxane, 4H], -4.72 [vbs, SiMe₃, 54H]

¹³C{¹H} NMR (d₈-tol, 300 K) δ (ppm) = 338.57 [SiMe₃], 76.32 [1,4-dioxane]

Anal. Calcd for C₄₃H₁₁₉Fe₂N₆Na₂O₂Si₁₂ (0.5 eq. of co-crystallised benzene per dimer): C 41.41, H 9.62, N 6.74 Found: C 41.26, H 9.51, N 6.66

[{dioxane·NaFe(C₆H₄F)(HMDS)₂}_∞] (18)

A 1 mmol solution of **1** was prepared in 20 mL of hexane before removing all solvent under vacuum. The green/white solid was redissolved in 2 mL of fluorobenzene (21.3 mmol) and stirred overnight at 50°C with a colour change from dark green to light brown apparent. The solution was cooled slowly to -30°C and stored at that temperature to obtain large, colourless crystals after several days (0.3175 g, 47% yield; at ambient temperature, stirring overnight without heating; with 1 equivalent of C₆H₅F co-crystallised solvent). On a 10 mmol scale, with stirring overnight at 50°C, 5.582 g of crystalline material was recovered to give 82% yield.

N.B. Metallation is possible at ambient temperature without stirring at 50°C, however poorer yields are obtained and usually stirring for an increased quantity of time is required.

^1H NMR (C_6D_6 , 300 K) δ (ppm) = 181.84 [s, aryl CH, 1H], 134.22 [s, aryl CH, 1H], 70.60 [s, aryl CH, 1H], 3.35 [s, 1,4-dioxane, 8H], -2.88 [vbs, SiMe_3 , 36H], -56.11 [s, aryl CH, 1H]

Anal. Calcd for $\text{C}_{94}\text{H}_{197}\text{F}_2\text{Fe}_4\text{N}_8\text{Na}_4\text{O}_8\text{Si}_{16}$ (4 monomeric units + 1 eq. of co-crystallised $\text{C}_6\text{H}_5\text{F}$): C 46.51, H 8.18, N 4.62 Found: C 46.56, H 8.77, N 4.69

Solution Magnetic Moment (C_6D_6 , 300 K) = $4.95 \mu_{\text{B}}$

[{(dioxane)·NaFe(1,3-C₆H₃F₂)(HMDS)₂}]_∞ (19)

A 1 mmol solution of **17a** was prepared in 20 mL of hexane before removing all solvent under vacuum. The green/white solid was redissolved in 5 mL of benzene to which 0.10 mL (1 mmol) of 1,3-difluorobenzene was added and stirred overnight at 50°C with a colour change from dark green to green/brown apparent. Removal of solvent until precipitate appeared, warming and slow cooling allowed for the isolation of large green crystals. The solution was removed via a syringe and the crystals washed 3 x 3 mL of cold hexane and dried (0.40 g, 66% yield).

^1H NMR (C_6D_6 , 300 K) δ (ppm) = 104.40 [s, *meta* aryl CH's, 2H], 5.20 [s, 1,4-dioxane, 8H], -1.86 [vbs, SiMe_3 , 36H], -66.65 [s, *para* aryl CH, 1H]

Anal. Calcd for $\text{C}_{22}\text{H}_{47}\text{F}_2\text{FeN}_2\text{NaO}_2\text{Si}_4$: C 43.98, H 7.89, N 4.66 Found: C 43.80, H 8.20, N 4.94

[{(dioxane)₂·Na₂Fe(1,3-C₆H₃F₂)(HMDS)₂}⁺{Fe(HMDS)₃}⁻]_∞ (20)

A 2 mmol solution of **17a** was prepared in 30 mL of hexane before removing all solvent under vacuum. The green/white solid was redissolved in 10 mL of benzene to which 0.05 mL (1 mmol) of 1,3-difluorobenzene was added and stirred overnight at 50°C. Removal of solvent until precipitate appeared, warming and slow cooling allowed for the isolation of large green crystals. The solution was removed via a syringe and the crystals washed 1 x 2 mL of cold hexane and dried (0.4131 g, 35.88% yield, accounting for loss of 1 eq. of 1,4-dioxane).

^1H NMR (C_6D_6 , 300 K) δ (ppm) = 104.99 [s, *meta* aryl CH's, 2H], 8.33 [bs, 1,4-dioxane, 8H], -1.76 & -4.78 [overlapping vbs, SiMe_3 , 90H], -66.37 [s, *para* aryl CH, 1H]

Anal. Calcd for $C_{40}H_{101}F_2Fe_2N_5Na_2O_2Si_{10}$ (loss of 1 eq. of 1,4,-dioxane): C 41.39, H 8.77, N 6.03 Found: C 41.50, H 8.83, N 6.58

Solution Magnetic Moment (d_8 -tol, 300 K) = $5.40 \mu_B$

[dioxane·{NaFe(1,4- $C_6H_3F_2$)(HMDS) $_2$ } $_2$] $_{\infty}$ (21)

A 1 mmol solution of **17a** was prepared in 20 mL of hexane before removing all solvent under vacuum. The green/white solid was redissolved in 5 mL of 1,4-difluorobenzene and stirred for 20 minutes at 50°C with a colour change from dark green to yellow. Removal of solvent until precipitate appeared, warming and slow cooling allowed for the isolation of very large green stick crystals. The solution was removed via a syringe and the crystals washed 2 x 2 mL of cold hexane and dried (0.24 g, 38% yield, 1 dimer + 1 eq. co-crystallised $C_6H_4F_2$).

1H NMR (C_6D_6 , 300 K) δ (ppm) = 213.44 [vbs, aryl CH, 1H], 141.36 [bs, aryl CH, 1H], 3.52 [s, 1,4-dioxane, 4H], -2.74 [vbs, SiMe $_3$, 36H], -56.51 [bs, aryl CH, 1H]

Anal. Calcd for $C_{46}H_{90}F_6Fe_2N_4Na_2O_2Si_8$ (1 dimer + 1 eq. co-crystallised $C_6H_4F_2$): C 45.01, H 7.39, N 4.56 Found: C 45.08, H 7.56, N 5.31

[dioxane·{NaFe(1,2,4- $C_6H_2F_3$)(HMDS) $_2$ } $_2$] $_{\infty}$ (22)

A 1 mmol solution of **17a** was prepared in 20 mL of hexane before removing all solvent under vacuum. The green/white solid was redissolved in 5 mL of benzene to which 0.101 mL (1 mmol) of 1,2,4-trifluorobenzene was added. A white precipitate was immediately formed and with gentle heating the solution turned from green to orange with more precipitate apparent. Stirring was continued overnight, benzene was removed under vacuum and the solid was redissolved in 10 mL of fluorobenzene and slowly cooled from ~50°C. This yielded large yellow brick crystals which were washed 2 x 2 mL of cold hexane and dried The solution was removed via a syringe and the crystals washed 2 x 2 mL of cold hexane and dried (0.3233 g, 50.61% yield, based on 1 dimer + 2 eq. co-crystallised C_6H_5F).

1H NMR (d_8 -tol, 300 K) δ (ppm) = 119.63 [bs, aryl CH, 1H], 4.13 [bs, 1,4-dioxane, 4H], -1.32 [vbs, SiMe $_3$, 36H], -59.60 [bs, aryl CH, 1H]

Anal. Calcd for $C_{72}H_{136}F_{11}Fe_3N_6Na_3O_3Si_{12}$ (1.5 dimers + 2 eq. co-crystallised C_6H_5F): C 45.13, H 7.15, N 4.39 Found: C 45.78, H 7.03, N 5.20

[{dioxane·NaFe(HMDS)₂}₂(1,2,4,5-C₆F₄)]_∞ (23)

A 2 mmol solution of **17a** was prepared in 30 mL of hexane before removing all solvent under vacuum. The green/white solid was redissolved in 10 mL of benzene to which 0.11 mL (1 mmol) of 1,2,4,5-tetrafluorobenzene was added and heated at reflux for one hour. Upon reaching reflux the green solution turned dark brown with a small quantity of off-white precipitate produced. After slowly cooling, small orange needle crystals were apparent. The excess solution was removed via a syringe and the off-white precipitate and small quantity of crystals were washed 1 x 3 mL of cold hexane and dried (0.86 g, 76% yield).

¹H NMR (C₆D₆, 300 K) δ (ppm) = 4.06 [bs, CH₂, 1,4-dioxane, 16H], -2.49 [vbs, SiMe₃, 72H]

Anal. Calcd for C₃₈H₈₈F₄Fe₂N₄Na₂O₄Si₈: C 40.63, H 7.90, N 4.99 Found: C 41.12, H 7.09, N 5.18

Solution Magnetic Moment (d₈-tol, 300 K) = 5.40 μ_B

[dioxane·{NaFe(C₆F₅)(HMDS)₂}]_∞ (24)

A 3 mmol solution of **17a** was prepared in 20 mL of hexane before removing all solvent under vacuum. The green/white solid was redissolved in 15 mL of benzene and cooled to 0°C to which 0.33 mL (3 mmol) of pentafluorobenzene was added and stirred for 4 hours. Upon warming to ambient temperature the solution exhibited a distinct colour change from green to green/brown with the formation of a precipitate. 20 mL more of benzene was added and the solution was heated to dissolve all precipitate before slowly cooling overnight. A clear deep red solution was apparent with large green rectangular plate crystals. The crystals were washed 2 x 5 mL of cold hexane and dried. A second set of crystals and some solid product were obtained from the filtrate; both show identical NMR spectra to that of the primary crystals (1.87 g, 90% yield).

¹H NMR (C₆D₆, 300 K) δ (ppm) = 3.60 [s, 1,4-dioxane, 4H], -1.91 [vbs, SiMe₃, HMDS, 36H]

Anal. Calcd for C₅₂H₉₂Fe₂N₄Na₂O₂Si₈ (1 dimeric unit + 2 eq. of co-crystallised benzene solvent): C 45.34, H 6.73, N 4.07 Found: C 45.25, H 6.60, N 4.92

[{dioxane·NaFe(1-C₁₀H₆F)(HMDS)₂}]_∞ (25)

A 1 mmol solution of **17a** was prepared in 20 mL of hexane before removing all solvent under vacuum. The green/white solid was redissolved in 5 mL of 1-fluoronaphthalene and stirred at 50°C overnight. Bright green rod crystals were obtained at 5°C. The excess solution was removed via a syringe and the crystals washed 3 x 3 mL of cold hexane and dried (0.17 g, 26% yield).

¹H NMR (C₆D₆, 300 K) δ (ppm) = 70.63 [bs, aryl CH, 1H], 24.08 [s, aryl CH, 1H], 19.47 [s, aryl CH, 1H], 4.19 [bs, CH₂, 1,4-dioxane, 8H], -2.98 [vbs, SiMe₃, 36H], -16.33 [bs, aryl CH, 1H], -20.12 [s, aryl CH, 1H]

Reliable elemental analysis for **25** could not be obtained due to co-crystallisation of [Na₂Fe₂(HMDS)₄(O)] (**30**).

[dioxane·{dioxane·NaFe(1-Br-3,5-C₆H₂F₂)(HMDS)₂}]₂ (26)

A 1 mmol solution of **17a** was prepared in 20 mL of hexane before removing all solvent under vacuum. The green/white solid was redissolved in 5 mL of benzene and cooled to 0°C whereupon 0.12 mL (1 mmol) of 1-bromo-3,5-difluorobenzene was added and stirred for two hours. Stirring was stopped and the solution was allowed to reach ambient temperature and left overnight. The now dark yellow solution was cooled to 5°C, producing green block crystals. The excess solution was removed via a syringe and the crystals washed 1 x 1.5 mL of cold hexane and dried (0.44 g, 60% yield, max possible 66.67% due to 1.5 eq. of 1,4-dioxane required).

¹H NMR (C₆D₆, 300 K) δ (ppm) = 103.92 [bs, aryl CH's, 2H], 4.89 [bs, CH₂, 1,4-dioxane, 12H], -1.99 [vbs, SiMe₃, 36H]

Anal. Calcd for C₂₄H₅₀BrF₂FeN₂NaO₃Si₄ (half of dimer): C 39.83, H 6.96, N 3.87 Found: C 40.00, H 6.72, N 4.29

Solution Magnetic Moment (d₈-tol, 300 K) = 4.22 μ_B

[{(dioxane)₂·Na₂Fe(3-C₆H₃FOMe)(HMDS)₂}⁺{Fe(HMDS)₃}⁻]_∞ (27)

A 1 mmol solution of **17a** was prepared in 20 mL of hexane before removing all solvent under vacuum. The green/white solid was redissolved in 5 mL of benzene to which 0.11 mL

(1 mmol) of 3-fluoroanisole was added and stirred overnight at 50°C with a colour change from dark green to dark orange apparent. Removal of solvent until precipitate appeared, warming and slow cooling allowed for the isolation of large green block crystals. The excess solution was removed via a syringe and the crystals washed 3 x 3 mL of cold hexane and dried (0.26 g, 20% yield, max possible 50% due to 2:1 base to substrate required).

^1H NMR (C_6D_6 , 300 K) δ (ppm) = 105.39 [bs, aryl CH, 1H], 99.84 [bs, aryl CH, 1H], 8.22 [bs, 1,4-dioxane, 16H], -2.56 & -4.76 [vbs overlapping, SiMe_3 , 90H], -14.75 [bs, OMe, 3H], -69.48 [bs, aryl CH, 1H]

Anal. Calcd for $\text{C}_{45}\text{H}_{112}\text{FFe}_2\text{N}_5\text{Na}_2\text{O}_5\text{Si}_{10}$: C 42.86, H 8.95, N 5.55 Found: C 42.82, H 9.12, N 6.59

Solution Magnetic Moment ($\text{d}_8\text{-tol}$, 300 K) = 5.01 μ_{B}

[dioxane·{Na(PhOMe)₃}₂]²⁺[{Fe(HMDS)₃}₂]²⁻ (28)

A 1 mmol solution of **17a** was prepared in 20 mL of hexane before removing all solvent under vacuum. The green/white solid was redissolved in 5 mL of anisole and stirred overnight after which the solution became green/brown. Cooling to -30°C allowed for the isolation of colourless block crystals. The excess solution was removed via a syringe and the crystals washed 3 x 3 mL of cold hexane and dried (0.45 g, 48% yield).

^1H NMR (C_6D_6 , 300 K) δ (ppm) = 7.23-7.20 [t, *meta* aryl CH's, 6H], 7.08-7.06 [d, *ortho* aryl CH's, 6H], 6.92-6.89 [t, *para* aryl CH's, 3H], 3.55 [s, OMe, 9H], -4.77 [vbs, SiMe_3 , 54H], not observed (lost under vacuum) [1,4-dioxane]

$^{13}\text{C}\{^1\text{H}\}$ NMR (C_6D_6 , 300 K) δ (ppm) = 329.12 [SiMe_3], 160.59 [*ipso* aryl C's], 129.84 [*meta* aryl C's], 121.05 [*para* aryl C's], 114.70 [*ortho* aryl C's], 55.03 [OMe], not observed (lost under vacuum) [1,4-dioxane]

Anal. Calcd for $\text{C}_{39}\text{H}_{78}\text{FeN}_3\text{NaO}_3\text{Si}_6$ (loss of 1,4-dioxane): C 52.96, H 8.89, N 4.75 Found: C 52.44, H 8.71, N 5.43

[dioxane·{NaFe(3,5-C₆H₂F₂OMe)(HMDS)₂}₂]_∞ (29)

A 1 mmol solution of **17a** was prepared in 20 mL of hexane before removing all solvent under vacuum. The green/white solid was redissolved in 5 mL of benzene and 0.12 mL (1 mmol) of 3,5-difluorobenzene was added and stirred for 1 hour before leaving sedentary overnight after which period the solution has changed from green to tan/brown. Cooling to 5°C allowed for the isolation of clear rectangular plate crystals. The excess solution was removed via a syringe and the crystals washed 3 x 3 mL of cold hexane and dried (0.2968 g, 51% yield).

¹H NMR (C₆D₆, 300 K) δ (ppm) = 99.97 [bs, aryl CH's, 2H], 9.35 [bs, OMe, 3H], 5.40 [bs, 1,4-dioxane, 4H], -2.24 [vbs, SiMe₃, 36H]

Anal. Calcd for C₂₁H₄₅FeN₂NaO₂Si₄: C 42.99, H 7.73, N 4.77 Found: C 42.03, H 7.62, N 5.32

Solution Magnetic Moment (d₈-tol, 300 K) = 5.88 μ_B

[Na₂Fe₂(HMDS)₄(O)] (30)

0.009 mL (0.5 mmol) of water was added via syringe to a freshly prepared solution of **1** in hexane and stirred overnight. The solution was concentrated to around 10 mL and cooled to 0°C. Bright emerald green rhomboidal plate crystals were grown overnight (0.33 g, 81% yield).

¹H NMR (d₈-tol, 300 K) δ (ppm) = -0.81 [vbs, SiMe₃]

Anal. Calcd for C₂₄H₇₂Fe₂N₄Na₂O₂Si₈: C 35.36, H 8.90, N 6.87 Found: C 35.32, H 9.13, N 7.49

[{dioxane·(NaHMDS)₂}_∞] (31)

To 0.184g NaHMDS (1 mmol) in 5 mL of benzene 0.04 mL (0.5 mmol) of 1,4-dioxane was added and stirred overnight generating a white precipitate. All volatiles were removed under vacuum to leave a bright white powdered solid. (0.15 g, 67% yield).

¹H NMR (C₆D₆, 300 K) δ (ppm) = 3.33 [s, 1,4-dioxane, 8H], 0.15 [s, SiMe₃, 36H]

¹³C {¹H} NMR (C₆D₆, 300 K) δ (ppm) = 67.11 [1,4-dioxane], 6.96 [SiMe₃]

Anal. Calcd for $C_{16}H_{44}N_2O_2NaSi_4$: C 42.25, H 9.75, N 6.16 Found: C 42.13, H 9.28, N 6.06

[dioxane·LiFe(HMDS)₃] (32)

0.167 g (1 mmol) of LiHMDS and 0.377 g (1 mmol) of Fe(HMDS)₂ were combined in a Schlenk tube with 20 mL of hexane and stirred for an hour. 0.17 mL (2 mmol) of 1,4-dioxane was added to the solution resulting in the precipitation of a white solid, stirring was continued for a further 1 hour. All hexane was removed by vacuum till dryness. The remaining solid was redissolved in 5 mL of C₆H₅F, stirred for 1 hour and then cooled slowly to -30°C and stored in the freezer. Green, rectangular, plate-like crystals were obtained after several days (0.44 g, 70% yield).

¹H NMR (d₈-THF, 300 K) δ (ppm) = 3.85 & 2.00 [1,4-dioxane resonances overlapping with solvent resonances], -2.34 [vbs, SiMe₃]

¹³C{¹H} NMR (d₈-THF, 300 K) δ (ppm) = 346.95 [SiMe₃], 1,4-dioxane obscured by solvent resonances

⁷Li NMR (d₈-THF, 300 K) δ (ppm) = 0.89

Anal. Calcd for C₂₂H₆₂FeLiN₃O₂Si₆: C 41.81, H 9.89, N 6.65 Found: C 41.91, H 10.15, N 6.39

[{dioxane·KFe(HMDS)₃}_∞] (33)

0.199 g (1 mmol) of KHMDS and 0.377 g (1 mmol) of Fe(HMDS)₂ were combined in a Schlenk tube with 20 mL of toluene and stirred for one hour before addition with the solution turning from green to clear yellow in 15 minutes. 0.085 mL (1 mmol) of 1,4-dioxane was added producing a darker yellow solution and an off-white precipitate. Stirring was continued for 1 hour before all toluene was removed by vacuum till dryness and the solid was redissolved in 5 mL of fluorobenzene. Gentle heating and slow cooling produced large colourless plate-like crystals (0.4285 g, 64% yield).

¹H NMR (d₈-tol, 300 K) δ (ppm) = 3.15 [s, 1,4-dioxane, 8H], -2.54 [vbs, SiMe₃]

¹³C{¹H} NMR (d₈-tol, 300 K) δ (ppm) = 344.71 [SiMe₃], 67.11 [1,4-dioxane]

Anal. Calcd for C₂₂H₆₂FeKN₃O₂Si₆: C 39.78, H 9.41, N 6.33 Found: C 39.73, H 9.01, N 6.32

[{KFe(HMDS)}₃]_∞] (34)

0.199 g (1 mmol) of KHMDS and 0.377 g (1 mmol) of Fe(HMDS)₂ were combined in a Schlenk tube with 20 mL of toluene and stirred for two hours. All toluene was removed by vacuum till dryness and the solid was redissolved in 5 mL of fluorobenzene to give a brown/green solution. Layering the solution with 20 mL of hexane produced large colourless needle crystals (0.09 g, 15% yield). Crystals were also produced at ~5°C in toluene with hexane layering.

¹H NMR (d₈- THF, 300 K) δ (ppm) = -2.13 [vbs, SiMe₃]

¹³C{¹H} NMR (d₈-THF, 300 K) δ (ppm) = 349.58 [SiMe₃]

Anal. Calcd for C₂₅H₆₂FeKN₃Si₆ (1 monomeric unit + 1 eq. of co-crystallised toluene solvent): C 44.93, H 9.12, N 6.29 Found: C 45.18, H 9.12, N 7.08

[dioxane·{NaFe(HMDS)₂(CH₂SiMe₃)₂}] (35)

To a 1 mmol solution of [{NaFe(HMDS)₂(CH₂SiMe₃)₂]_∞] (12) in 20 mL hexane, 0.085 mL (1 mmol) of 1,4-dioxane was added producing an off-white precipitate. The mixture was stirred for one hour before removing all volatiles *in vacuo*. The remaining sandy brown solid was redissolved in 5 mL of benzene then concentrated till precipitate appeared, warmed and then cooled slowly to generate large green brick crystals (0.16 g, 31% yield).

¹H NMR (C₆D₆, 300 K) δ (ppm) = 13.52 [bs, CH₂SiMe₃, 9H], 6.05 [bs, CH₂ 1,4-dioxane, 4H], -8.56 [vbs, HMDS SiMe₃, 36H], CH₂SiMe₃ H atoms not observed

¹³C{¹H} NMR (C₆D₆, 300 K) δ (ppm) = 343.53 [HMDS SiMe₃], 256.63 [CH₂SiMe₃], 71.15 [CH₂ 1,4-dioxane], CH₂SiMe₃ carbon not observed

Anal. Calcd for C₃₆H₁₀₂Fe₂N₄Na₂O₂Si₁₀: C 40.72, H 9.68, N 5.28 Found: C 40.77, H 9.42, N 5.79

III.II.IV Chapter 4

[{(dioxane)_{1.5}·NaFe(1,3,5-C₆H₂F₃)(HMDS)₂}]₂ (36)

A 1 mmol solution of **17a** was prepared in 20 mL of hexane before removing all solvent under vacuum. The green/white solid was redissolved in 5 mL of benzene and cooled to 0°C. 0.11 mL (1 mmol) of 1,3,5-trifluorobenzene was added and the solution was stirred at this temperature for 1 hour before allowing to reach ambient temperature overnight without stirring. A clear colour change of the solution from green to yellow was apparent with the appearance of a small quantity of crystals. Benzene was removed via syringe and the crystals washed 2 x 2 mL of cold hexane and dried (0.223 g, 34% yield with respect to 1,3,5-trifluorobenzene, maximum possible yield 66.67%).

¹H NMR (C₆D₆, 300 K) δ (ppm) = 101.64 [s, *meta* aryl C-*H*'s, 2H], 4.85 [s, CH₂, 1,4-dioxane, 12H], -2.26 [vbs, SiMe₃, 36H]

Anal. Calcd for C₂₄H₅₀F₃FeN₂NaO₃Si₄: C 43.49, H 7.60, N 4.23 Found: C 43.64, H 7.66, N 4.18

Solution Magnetic Moment (d₈-tol, 300 K) = 4.40 μ_B

[{(dioxane·NaFe(HMDS)₂}]₂(1,3,5-C₆HF₃)]_∞ (37)

A 2 mmol solution of **17a** was prepared in 20 mL of hexane before removing all solvent under vacuum. The green/white solid was redissolved in 10 mL of benzene and cooled to 0°C. 0.11 mL (1 mmol) of 1,3,5-trifluorobenzene was added and the solution was stirred at this temperature for 1 hour before allowing to reach ambient temperature overnight without stirring. A clear colour change of the solution from green to yellow/brown was apparent with the appearance of yellow needle crystals. Benzene was removed via syringe and the crystals washed 2 x 3 mL of cold hexane and dried (0.47 g, 40% yield, based on 1 eq. of co-crystallised benzene solvent per di-metallated unit).

¹H NMR (C₆D₆, 300 K) δ (ppm) = 177.56 [s, *para* aryl C(4)-*H*, 1H], 2.49 [s, CH₂, 1,4-dioxane, 16H], -3.14 [vbs, SiMe₃, 72H]

Anal. Calcd for C₄₄H₉₅F₃Fe₂N₄Na₂O₄Si₈ (1 di-metallated unit + 1 eq. of co-crystallised benzene solvent): C 44.65, H 8.09, N 4.73 Found: C 44.74, H 7.56, N 4.83

[1,3-bis(FeHMDS)-2,4,6-tris(HMDS)-C₆H] (38)

3:1 - A 1 mmol solution of **17a** was prepared in 20 mL of hexane before removing all solvent under vacuum. The green/white solid was redissolved in 5 mL of benzene to which 0.034 mL (0.33 mmol) of 1,3,5-trifluorobenzene was added. The solution was refluxed for one hour and exhibited a distinct colour change from green to yellow. Solvent was removed till precipitate appeared and the solution was heated and left to cool and crystallise slowly from ~50°C. Large yellow rectangular plate crystals were obtained which were washed 3 x 2 mL of cold hexane and dried (0.28 g, 87% yield with respect to 1,3,5-trifluorobenzene).

2:1 – A 1 mmol solution of **17a** was prepared in 20 mL of hexane before removing all solvent under vacuum. The green/white solid was redissolved in 5 mL of benzene to which 0.052 mL (0.55 mmol) of 1,3,5-trifluorobenzene was added. The solution exhibited a distinct colour change from green to yellow after stirring overnight. Solvent was removed till precipitate appeared and the solution was heated and left to cool and crystallise slowly from ~50°C. Large yellow rectangular plate crystals were obtained which were washed 3 x 2 mL of cold hexane and dried (0.27 g, 54% yield with respect to 1,3,5-trifluorobenzene, maximum possible yield 66.67%).

1:1 - A 1 mmol solution of **17a** was prepared in 20 mL of hexane before removing all solvent under vacuum. The green/white solid was redissolved in 5 mL of benzene to which 0.11 mL (1 mmol) of 1,3,5-trifluorobenzene was added. The solution exhibited a distinct colour change from green to yellow within minutes, stirring was continued overnight. Solvent was removed till precipitate appeared and the solution was heated and left to cool and crystallise slowly from ~50°C. Large yellow rectangular plate crystals were obtained which were washed 3 x 2 mL of cold hexane and dried (0.21 g, 21% yield with respect to 1,3,5-trifluorobenzene, maximum possible yield 33.33%).

¹H NMR (C₆D₆, 300 K) δ (ppm) = 420.99 [vbs, C-H (C4), 1H], 49.99 [vbs, SiMe₃, Fe-HMDS or HMDS (4,6), 36H], -18.16 [vbs, SiMe₃, Fe-HMDS or HMDS (4,6), 36H], -95.05 [vbs, SiMe₃, HMDS (2), 18H]

Anal. Calcd for C₃₆H₉₁Fe₂N₅Si₁₀: C 43.82, H 9.30, N 7.10 Found: C 43.43, H 9.33, N 7.52

[1,3-bis(FeHMDS)-2,4,6-tris(HMDS)-C₆F] (39)

A 3 mmol solution of **17a** was prepared in 40 mL of hexane before removing all solvent under vacuum. The green/white solid was redissolved in 10 mL of benzene to which 0.11 mL (1 mmol) of 1,2,3,5-tetrafluorobenzene was added and the solution was refluxed for one hour. Upon reaching reflux the solution turned from green to brown/dark red. The solution was slowly cooled to ~5°C upon which flat yellow needle-like crystals were formed over several hours. Benzene was removed via syringe and the crystals were washed 2 x 2 mL of cold hexane and dried (0.3243 g, 32.28% yield with respect to 1,2,3,5-tetrafluorobenzene).

¹H NMR (C₆D₆, 300 K) δ (ppm) = 49.44 [vbs, SiMe₃, Fe-HMDS or HMDS (4,6), 36H], -16.41 [vbs, SiMe₃, Fe-HMDS or HMDS (4,6), 36H], -104.24 [vbs, SiMe₃, HMDS (2), 18H]

Anal. Calcd for C₄₄H₉₅F₃Fe₂N₄Na₂O₄Si₈: C 43.04, H 9.03, N 6.97 Found: C 43.02, H 8.83, N 6.97

[1,3-bis(FeHMDS)-2,4,6-tris(HMDS)-C₆Br] (40)

A 1 mmol solution of **17a** was prepared in 20 mL of hexane before removing all solvent under vacuum. The green/white solid was redissolved in 5 mL of benzene to which 0.04 mL (0.33 mmol) of 1-bromo-2,4,6-trifluorobenzene was added. The solution was refluxed for one hour upon which it exhibited a distinct colour change from green to brown. Slow cooling facilitated the formation of thin yellow rod crystals. Solvent was removed via a syringe and the crystals were washed 2 x 2 mL of cold hexane and dried (0.1245 g, 37% yield with respect to 1-bromo-2,4,6-trifluorobenzene).

[1,3-diiodo-2,4,6-tris(HMDS)-C₆H] (41)

Crystals of [1,3-bis(FeHMDS)₂-2,4,6-tris(HMDS)-C₆H] (**38**) (1 mmol, 0.987 g) were subjected to addition of excess I₂ in THF and subsequent organic work-up (detailed *vide supra*). 0.525 g (65% yield) of colourless, block crystals were collected.

¹H NMR (CDCl₃, 300 K) δ (ppm) = 6.59 [s, aryl CH (C5), 1H], 0.27 [s, SiMe₃, HMDS (2), 18H], 0.14 [s, SiMe₃, HMDS (4,6), 36H]

¹³C{¹H} NMR (CDCl₃, 300 K) δ (ppm) = 151.45 [aryl CN (C2, C4, C6)], 125.93 [aryl CH (C5)], 113.18 [aryl CI (C1, C3)], 4.12 [SiMe₃, HMDS (2)], 2.41 [SiMe₃, HMDS (4,6)]

HR-MS for $C_{24}H_{55}I_2N_3Si_6$ (807.1101, $M+1 = 808.1174$) $M+1$ 808.1172

[1,3,5-tris(HMDS)-C₆H] (42)

Crystals of [1,3-bis(FeHMDS)₂-2,4,6-tris(HMDS)-C₆H] (**38**) (1 mmol, 0.987 g) were subjected to addition of excess H₂O and subsequent organic work-up (detailed *vide supra*). 0.395 g (71% yield) of large, colourless, block crystals were collected.

¹H NMR (CDCl₃, 300 K) δ (ppm) = 6.21 [s, aryl CH's, 3H], 0.06 [s, SiMe₃, 54H]

¹³C{¹H} NMR (CDCl₃, 300 K) δ (ppm) = 148.30 [aryl CN], 127.96 [aryl CH], 2.42 [SiMe₃, HMDS]

Anal. Calcd for C₂₄H₅₇N₃Si₆: C 51.82, H 10.33, N 7.55 Found: C 51.99, H 10.12, N 7.71

[dioxane·LiFe(HMDS)₂(1,3,5-C₆H₂F₃)] (43)

0.164 g (1 mmol) of LiHMDS and 0.377 g (1 mmol) of Fe(HMDS)₂ were added to Schlenk tube along with 20 mL of hexane. After stirring for 1 hour, 0.085 mL (1 mmol) of 1,4-dioxane was added producing an off-white precipitate. Hexane was removed under vacuum and the solid was redissolved in 5 mL of benzene to give a green solution and to which 0.11 mL (1 eq.) of 1,3,5-trifluorobenzene was added. No immediate reaction was apparent even after heating and thus the reaction was left to stir overnight. The solution had turned from green to yellow overnight. Large, flat yellow rod crystals were obtained by reduction of the solution volume and slow cooling from ~50°C (0.4666 g, 77.41% yield).

¹H NMR (C₆D₆, 300 K) δ (ppm) = 105.60 [s, aryl CH's, 2H], 9.79 [bs, CH₂, 1,4-dioxane, 8H], -3.70 [vbs, SiMe₃, 36H]

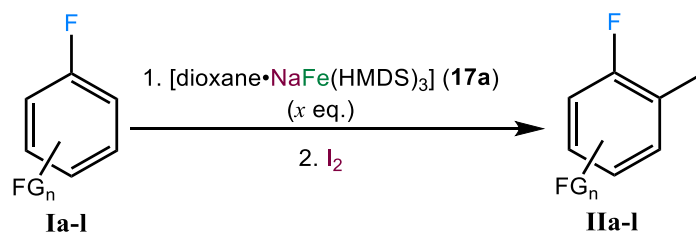
⁷Li NMR (C₆D₆, 300 K) δ (ppm) = No resonances observed

Anal. Calcd for C₂₂H₄₅F₃FeLiN₂O₂Si₄: C 43.84, H 7.69, N 4.65 Found: C 43.61, H 7.41, N 4.86

Solution Magnetic Moment (d₈-tol, 300 K) = 4.53 μ_B

III.III Synthesis and Characterisation of Numbered Organic Compounds

General Procedure for Electrophilic Quenching and Organic Work-Up



Scheme III-1 – General procedure for direct ferration and iodination of fluoroaromatic substrates.

To a Schlenk tube containing $\text{Fe}(\text{HMDS})_2$ (x eq.) and NaHMDS (x eq.) was added dry hexanes (20 mL per mmol). This was stirred for 1 hour then 1,4-dioxane (x eq.) was added. After stirring for a further hour all volatiles were removed *in vacuo*. The sodium ferrate species, $[\text{dioxane}\cdot\text{NaFe}(\text{HMDS})_3]$ (**17a**), formed was dissolved in dry benzene* (5 mL) and the substrate (1 mmol) was added at ambient temperature or the stated temperature. The reactions were allowed to proceed under the conditions given below. At ambient temperature, I_2 (5 eq. with respect to **17a**) was added. After stirring at ambient temperature for 1 hour the reaction was quenched with a saturated sodium thiosulfate solution. The organic compound was extracted with diethyl ether (3 x 50 mL). The combined organic fractions were washed with brine, dried over magnesium sulfate and solvents removed *in vacuo*.

N.B. Some reactions were run in neat substrate instead of benzene.

III.III.I Chapter 3

Table 3.1, Entry 1: 1-Fluoro-2-iodobenzene (**IIa**)³⁵⁴

$\text{Fe}(\text{HMDS})_2$ (1 eq., 1 mmol, 0.377 g) and NaHMDS (1 eq., 1 mmol, 0.184 g) and 1,4-dioxane (1 eq., 1 mmol, 0.085 mL) formed $[\text{dioxane}\cdot\text{NaFe}(\text{HMDS})_3]$, which was dissolved in fluorobenzene (**Ia**) (5 mL) and heated at 50°C for 16 hours. Upon vacuum distillation the title compound was obtained as a colourless liquid (0.1649 g, 74% yield).

^1H NMR (CDCl_3 , 300 K) δ (ppm) = 7.78-7.74 (m, 1H), 7.35-7.30 (m, 1H), 7.10-7.06 (m, 1H), 6.93-6.89 (m, 1H)

$^{13}\text{C}\{^1\text{H}\}$ NMR (CDCl_3 , 300 K) δ (ppm) = 169.94 and 160.49 (m), 139.44 (m), 130.07-130.00 (m), 125.78-125.71 (m), 115.73 (d, J = 23.1 Hz), 81.27 (d, J = 25.1 Hz)

$^{19}\text{F}\{^1\text{H}\}$ NMR (CDCl_3 , 300 K) δ (ppm) = -93.47

Table 3.1, Entry 2: 1,3-Difluoro-2-iodobenzene (IIb)³⁵⁵

$\text{Fe}(\text{HMDS})_2$ (2 eq., 2 mmol, 0.754 g) and NaHMDS (2 eq., 2 mmol, 0.368 g) and 1,4-dioxane (2 eq., 2 mmol, 0.17 mL). The [$\text{dioxane}\cdot\text{NaFe}(\text{HMDS})_3$] (**17a**) formed was dissolved in benzene and 1,3-difluorobenzene (**IIb**) (1 eq., 1mmol, 0.098 mL) was added. The reaction was heated at 50°C for 16 hours. The title compound was obtained as a colourless liquid upon column chromatography (petroleum ether) (0.2010 g, 84% yield).

^1H NMR (CDCl_3 , 300 K) δ (ppm) = 7.34-7.29 (m, 1H), 6.92-6.87 (m, 2H)

$^{13}\text{C}\{^1\text{H}\}$ NMR (CDCl_3 , 300 K) δ (ppm) = 162.76 (dd, J = 5.0, 246.4 Hz), 130.65-130.43 (m), 111.57-111.16 (m), 71.36-70.78 (m)

$^{19}\text{F}\{^1\text{H}\}$ NMR (CDCl_3 , 300 K) δ (ppm) = -92.08

Table 3.1, Entry 3: 1,2,4-Trifluoro-3-iodobenzene (IIc)³⁵⁶

$\text{Fe}(\text{HMDS})_2$ (1 eq., 1 mmol, 0.377 g) and NaHMDS (1 eq., 1 mmol, 0.184 g) and 1,4-dioxane (1 eq., 1 mmol, 0.085 mL). The [$\text{dioxane}\cdot\text{NaFe}(\text{HMDS})_3$] (**17a**) formed was dissolved in benzene and 1,2,4-trifluorobenzene (**IIc**) (1 eq., 1 mmol, 0.11 mL) was added. The reaction was stirred at RT for 16 hours. The title compound was obtained as a colourless liquid upon column chromatography (petroleum ether) (0.2061 g, 80% yield).

^1H NMR (CDCl_3 , 300 K) δ (ppm) = 7.22-7.14 (m, 1H), 6.91-6.85 (m, 1H)

$^{13}\text{C}\{^1\text{H}\}$ NMR (CDCl_3 , 300 K) δ (ppm) = 159.44 and 157.02 (m), 152.20 and 147.80 (m), 149.66 and 145.25 (m), 117.51-117.23 (m), 110.63-110.29 (m), 72.64-72.07 (m)

$^{19}\text{F}\{^1\text{H}\}$ NMR (CDCl_3 , 300 K) δ (ppm) = -98.22 (d, J = 11.3 Hz), -113.64 (d, J = 11.3 Hz), -139.40- -139.49 (m)

HR-MS (ESI): m/z calcd. for $[M]^+ C_6H_2F_3I = 257.9153$. Found 257.9156 (error = 1.2 ppm)

Table 3.1, Entry 4: 1,2,4,5-Tetrafluoro-3,6-diiodobenzene (II_d)³⁵⁷

Fe(HMDS)₂ (3 eq., 3 mmol, 1.131 g) and NaHMDS (3 eq., 3 mmol, 0.552 g) and 1,4-dioxane (3 eq., 3 mmol, 0.255 mL). The [dioxane·NaFe(HMDS)₃] (**17a**) formed was dissolved in benzene and 1,2,4,5-tetrafluorobenzene (**Id**) (1 eq., 1 mmol, 0.11 mL) was added. The reaction was stirred at RT for 16 hours. The title compound was obtained as a colourless solid upon column chromatography (petroleum ether) (0.3526 g, 88% yield).

¹³C{¹H} NMR (CDCl₃, 300 K) δ (ppm) = 148.01-147.73 and 145.51-145.23 (m), 73.20-72.64 (m)

¹⁹F{¹H} NMR (CDCl₃, 300 K) δ (ppm) = -118.04

Table 3.1, Entry 5: Pentafluoroiodobenzene (II_e)³⁵⁷⁻³⁶⁰

Fe(HMDS)₂ (1 eq., 1 mmol, 0.377 g) and NaHMDS (1 eq., 1 mmol, 0.184 g) and 1,4-dioxane (0.085 mL). The [dioxane·NaFe(HMDS)₃] (**17a**) formed was dissolved in benzene and pentafluorobenzene (**Ie**) (1 eq., 1 mmol, 0.11 mL) was stirred at ambient temperature for 16 hours. The title compound was obtained as a colourless liquid upon column chromatography (petroleum ether) (0.2673 g, 91% yield).

¹³C{¹H} NMR (CDCl₃, 300 K) δ (ppm) = 148.53-148.25 and 146.08-145.82 (m), 142.94-142.77 and 140.31-140.22 (m), 138.54-138.18 and 136.00-135.64 (m) and 66.29-65.70 (m)

¹⁹F{¹H} NMR (CDCl₃, 300 K) δ (ppm) = -118.90- -119.01 (m), -151.90- -152.02 (m), -159.10- -159.25 (m)

Table 3.1, Entry 6: 1-Bromo-3,5-difluoro-4-iodobenzene (II_f)³⁶¹

Fe(HMDS)₂ (1 eq., 1 mmol, 0.377 g) and NaHMDS (1 eq., 1 mmol, 0.184 g) and 1,4-dioxane (0.085 mL). The [dioxane·NaFe(HMDS)₃] (**17a**) formed was dissolved in benzene and 1-bromo-3,5-difluorobenzene (**If**) (1 eq., 1 mmol, 0.12 mL) was added at 0°C, stirred for 1 hour

then allowed to stand at ambient temperature for 16 hours. The title compound was obtained as a colourless solid upon column chromatography (petroleum ether) (0.2548 g, 80% yield).

^1H NMR (CDCl_3 , 300 K) δ (ppm) = 7.11-7.08 (m, 2H)

$^{13}\text{C}\{^1\text{H}\}$ NMR (CDCl_3 , 300 K) δ (ppm) = 162.64 (dd, J = 25.0, 7.0 Hz), 122.9-122.69 (m), 155.38 (dd, J = 30.2, 4.0 Hz), 70.29-69.70 (m)

$^{19}\text{F}\{^1\text{H}\}$ NMR (CDCl_3 , 300 K) δ (ppm) = -90.57

Table 3.1, Entry 7: 1,4-Dibromo-2,5-difluoro-3,6-diiodobenzene (IIg)

$\text{Fe}(\text{HMDS})_2$ (2 eq., 2 mmol, 0.754 g) and NaHMDS (2 eq., 2 mmol, 0.368 g) and 1,4-dioxane (0.17 mL). The $[\text{dioxane}\cdot\text{NaFe}(\text{HMDS})_3]$ (**17a**) formed was dissolved in benzene and 1,4-dibromo-2,5-difluorobenzene (**Ig**) (1 eq., 1 mmol, 0.2718 g) was stirred at ambient temperature for 16 hours. Upon crystallisation from chloroform the title compound was obtained as colourless needle crystals (0.4450 g, 85% yield).

$^{13}\text{C}\{^1\text{H}\}$ NMR (CDCl_3 , 300 K) δ (ppm) = 156.49-154.00 (m), 116.63-116.31 (m), 91.33-90.93 (m)

$^{19}\text{F}\{^1\text{H}\}$ NMR (CDCl_3 , 300 K) δ (ppm) = -70.38

HR-MS (ESI): m/z calcd. for $[\text{M}]^+ \text{C}_6\text{Br}_2\text{F}_3\text{I}_2$ = 521.6424. Found 521.6429 (error = 1.0 ppm)

Table 3.1, Entry 8: 4-Fluoro-3-iodobenzonitrile (IIh)³⁶²

$\text{Fe}(\text{HMDS})_2$ (1 eq., 1 mmol, 0.377 g) and NaHMDS (1 eq., 1 mmol, 0.184 g) and 1,4-dioxane (0.085 mL). The $[\text{dioxane}\cdot\text{NaFe}(\text{HMDS})_3]$ (**17a**) formed was dissolved in benzene and 4-fluorobenzonitrile (**Ih**) (1 eq., 1mmol, 0.121 g) was added. The reaction was heated at 50°C for 2 days. The title compound was obtained as a colourless solid upon column chromatography (petroleum ether:ethyl acetate, 95:5) (0.9770 g, 40% yield).

^1H NMR (CDCl_3 , 300 K) δ (ppm) = 8.08 (dd, J = 4 Hz, 1H), 7.68-7.64 (m, 1H), 7.18 (dd, J = 4 Hz, 1H)

$^{13}\text{C}\{^1\text{H}\}$ NMR (CDCl_3 , 300 K) δ (ppm) = 165.39 (d, J = 54.3 Hz, 1H), 143.35 (d, J = 3.0 Hz, 1H), 134.7 (d, J = 3.0 Hz, 1H), 116.73 (d, J = 8.0 Hz, 1H), 116.49 (d, J = 4.0 Hz, 1H), 110.32 (d, J = 4.0 Hz, 1H), 82..10(d, J = 25.1 Hz, 1H)

$^{19}\text{F}\{^1\text{H}\}$ NMR (CDCl_3 , 300 K) δ (ppm) = -83.20

HR-MS (ESI): m/z calcd. for $[\text{M}]^+$ $\text{C}_6\text{H}_3\text{FIN}$ = 246.9294. Found 246.9301 (error = 2.8 ppm)

Table 3.1, Entry 9: 1-Fluoro-2-iodo-3-methoxybenzene (III)³⁶³

$\text{Fe}(\text{HMDS})_2$ (2 eq., 2 mmol, 0.754 g) and NaHMDS (2 eq., 2 mmol, 0.368 g) and 1,4-dioxane (0.17 mL). The $[\text{dioxane}\cdot\text{NaFe}(\text{HMDS})_3]$ (**17a**) formed was dissolved in benzene and 3-fluoroanisole (**II**) (1 eq., 1mmol, 0.114 mL) was added. The reaction was heated at 50°C for 16 hours. The title compound was obtained as a colourless oil upon column chromatography (petroleum ether:ethyl acetate, 95:5) (0.1964 g, 78% yield).

^1H NMR (CDCl_3 , 300 K) δ (ppm) = 7.30-7.24 (m, 1H), 6.74-6.70 (m, 1H), 6.62 (d, J = 8.0 Hz, 1H), 3.91 (s, *OMe*, 3H)

$^{13}\text{C}\{^1\text{H}\}$ NMR (CDCl_3 , 300 K) δ (ppm) = 162.79 (d, J = 244.4 Hz), 159.86 (d, J = 6.0 Hz), 130.22 (d, J = 10.0 Hz), 108.25 (d, J = 20.0 Hz), 106.48 (d, J = 6.0 Hz), 74.14 (d, J = 27.0 Hz), 56.70 (s)

$^{19}\text{F}\{^1\text{H}\}$ NMR (CDCl_3 , 300 K) δ (ppm) = -91.43

Table 3.1, Entry 10: 1-Fluoro-2-iodo-4-methoxybenzene (IIj)³⁶⁴

$\text{Fe}(\text{HMDS})_2$ (2 eq., 2 mmol, 0.754 g) and NaHMDS (2 eq., 2 mmol, 0.368 g) and 1,4-dioxane (0.17 mL). The $[\text{dioxane}\cdot\text{NaFe}(\text{HMDS})_3]$ (**17a**) formed was dissolved in benzene and 4-fluoroanisole (**IIj**) (1 eq., 1mmol, 0.114 mL) was added. The reaction was heated at 50°C for 5 days. The title compound was obtained as a colourless oil combined with starting material. Analysis by NMR spectroscopy containing a ferrocene standard (10%) affords a conversion of 45%. Attempts to purify this compound were unsuccessful.

^1H NMR (CDCl_3 , 300 K) δ (ppm) = 7.26-7.24 (m, 1H), 6.99-6.95 (m, 1H), 6.86-6.82 (m, 1H), 3.78 (s, *OMe*, 3H)

$^{13}\text{C}\{^1\text{H}\}$ NMR (CDCl_3 , 300 K) δ (ppm) = 157.65-156.18 (m), 155.29 (m), 123.20 (s), 115.67-115.42 (m, 2C), 80.91 (d, $J = 27.0$ Hz), 55.95 (s)

$^{19}\text{F}\{^1\text{H}\}$ NMR (CDCl_3 , 300 K) δ (ppm) = -105.71

Table 3.1, Entry 11: 2-Fluoro-1-iodo-4-methylbenzene (IIk) and 1-Fluoro-2-iodo-3-methylbenzene (IIk')

$\text{Fe}(\text{HMDS})_2$ (1 eq., 1 mmol, 0.377 g) and NaHMDS (1 eq., 1 mmol, 0.184 g) and 1,4-dioxane (1 eq., 1 mmol, 0.085 mL) formed $[\text{dioxane}\cdot\text{NaFe}(\text{HMDS})_3]$ (**17a**), which was dissolved in 3-fluorotoluene (**Ik**) (2 mL) and heated at 50°C for 16 hours. The title compounds were obtained as isomer pairs of a colourless solid upon column chromatography (petroleum ether) (0.0577g, 24% yield). A 5:1 ratio for the isomers by ferrocene standard in the ^1H NMR spectrum was observed.

^1H NMR (CDCl_3 , 300 K) δ (ppm) Major = 7.62-7.58 (m, 1H), 6.89-6.87 (m, 1H), 6.75-6.72 (m, 1H), 2.33 (s, *Me*, 3H); ^1H NMR (CDCl_3 , 300 K) δ (ppm) Minor = 7.22-7.17 (m, 1H), 7.05-7.03 (m, 1H), 6.86-6.85 (m, 1H), 2.49 (s, *Me*, 3H)

$^{13}\text{C}\{^1\text{H}\}$ NMR (CDCl_3 , 300 K) δ (ppm) Major only = 162.77 (m), 166.35 (m), 140.87-140.80 (m), 138.83 (s), 126.71-126.79 (m), 116.56-116.33 (m), 20.95 (s)

$^{19}\text{F}\{^1\text{H}\}$ NMR (CDCl_3 , 300 K) δ (ppm) = -90.05 (minor), -95.13 (major)

GC-MS (ESI): m/z calcd. for $[\text{M}]^+$ $\text{C}_7\text{H}_6\text{FI} = 235.9498$. Found 235.9

III.III.II Chapter 4

Table 4.4, Entry 1: 1,3,5-Trifluoro-2-iodobenzene (III)³⁶⁵

$\text{Fe}(\text{HMDS})_2$ (1 eq., 1 mmol, 0.377 g) and NaHMDS (1 eq., 1 mmol, 0.184 g) and 1,4-dioxane (1 eq., 1 mmol, 0.085 mL). The formed $[\text{dioxane}\cdot\text{NaFe}(\text{HMDS})_3]$ (**17a**) was dissolved in benzene and after cooling 0°C to the 1,3,5-trifluorobenzene (**II**) (1 eq., 1 mmol, 0.103 mL) was added. After 1 hour the reaction was allowed to warm to ambient temperature and stirring was stopped. The reaction mixture was left to stand at ambient temperature for 16 hours. The

title compound was obtained as a colourless liquid; analysis by NMR containing a ferrocene standard affords a conversion of 58%. Attempts to purify this compound were unsuccessful.

^1H NMR (CDCl_3 , 300 K) δ (ppm) = 6.74 (m)

$^{19}\text{F}\{^1\text{H}\}$ NMR (CDCl_3 , 300 K) δ (ppm) = -89.28 (d, J = 7.5 Hz), -107.65 (dd, J = 7.5 Hz)

Table 4.4, Entry 2; 2,4,6-Trifluoro-1,3-diiodobenzene (III')³⁵⁸

$\text{Fe}(\text{HMDS})_2$ (2 eq., 2 mmol, 0.754 g) and NaHMDS (2 eq., 2 mmol, 0.368 g) and 1,4-dioxane (2 eq., 2 mmol, 0.17 mL). The formed [dioxane· $\text{NaFe}(\text{HMDS})_3$] (**17a**) was dissolved in benzene and after cooling 0°C to the 1,3,5-trifluorobenzene (**II**) (1 eq., 1mmol, 0.103 mL) was added. After 1 hour the reaction was allowed to warm to ambient temperature and stirring was stopped. The reaction mixture was left to stand at ambient temperature for 16 hours. The title compound was obtained as colourless needles after column chromatography (petroleum ether) (0.2158g, 56% yield).

^1H NMR (CDCl_3 , 300 K) δ (ppm) = 6.83-6.78 (m)

$^{13}\text{C}\{^1\text{H}\}$ NMR (CDCl_3 , 300 K) δ (ppm) = 164.51-163.02 (m), 162.03-160.60 (m), 100.55-99.95 (m)

$^{19}\text{F}\{^1\text{H}\}$ NMR (CDCl_3 , 300 K) δ (ppm) = -69.08 (dd, J = 3.8 Hz), -89.34 (d, J = 3.8 Hz)

Table 4.4, Entry 3, 1,3-Diiodo-2,4,6-tris(HMDS)- C_6H (41)

$\text{Fe}(\text{HMDS})_2$ (3 eq., 3 mmol, 1.131 g) and NaHMDS (3 eq., 3 mmol, 0.552 g) and 1,4-dioxane (0.255 mL). The [dioxane· $\text{NaFe}(\text{HMDS})_3$] (**17a**) formed was dissolved in benzene and 1,3,5-trifluorobenzene (**II**) (1 eq., 1mmol, 0.103 mL) was added. The reaction was heated for 5 mins before stirring at ambient temperature for 16 hours. The title compound was obtained as a colourless solid upon column chromatography (petroleum ether) (0.5898 g, 73%).

^1H NMR (CDCl_3 , 300 K) δ (ppm) = 6.66-6.77 (m)

$^{13}\text{C}\{^1\text{H}\}$ NMR (CDCl_3 , 300 K) δ (ppm) = 149.05 (s), 123.51 (s), 110.76 (s), 1.70 (s), 0.01 (s)

HR-MS (ESI): m/z calcd. for $[\text{M}+\text{H}]^+$ $\text{C}_{24}\text{H}_{55}\text{I}_2\text{N}_3\text{Si}_6$ = 808.1174. Found 808.1172 (error = -0.2 ppm)

III.IV X-Ray Crystallography

Single-crystal X-ray diffraction was performed on Oxford Diffraction Xcalibur and Gemini diffractometers at 123 K using Mo K α ($\lambda = 0.71073$) or Cu K α radiation ($\lambda = 1.54180$), respectively. The structures were solved by direct methods and refined on all unique F^2 values using the SHELXS³⁶⁶ package within either the WinGX³⁶⁷ or ShelXle³⁶⁸ GUIs.

Additionally, X-ray crystallographic data of complexes **39** and **40** were collected using synchrotron radiation on Beamline I19³⁶⁹ at the Diamond Light Source, Oxfordshire, U.K. This was carried out in collaboration with Professor Bill Clegg, Dr Mike Probert and Dr Paul Waddell at Newcastle University.

III.IV.I Chapter 1 Crystal Structures

After an initial examination it became apparent that the sample for **1** was a twin with the two components related by the matrix 1 0 0 0 -1 0 -1 0 -1. Refinement with a reprocessed hklf 5 formatted reflection file gave a much improved final model with the contribution of the minor crystal refined to 0.278. The crystal structure of compound **1** has been deposited into the Cambridge Crystallographic Data Centre (CCDC) and has been assigned the following number: **1** – 1412548. Selected crystallographic and refinement parameters are presented in Table III-1, Table III-2 and Table III-3.

Table III-1 - Selected crystal parameters and refinement data.

Compound Label	1	2	3	4
Chemical Identity	C ₁₈ H ₅₄ FeN ₃ NaSi ₆	C ₂₂ H ₆₂ FeN ₃ NaOSi ₆	C ₂₅ H ₇₁ FeN ₃ NaOSi ₆	C ₃₆ H ₆₉ FeN ₃ NaPSSi ₆
Formula weight	560.02	632.12	677.21	854.35
Crystal system	Monoclinic	Triclinic	Triclinic	Triclinic
Space Group	P2 ₁ /c	P-1	P-1	P-1
<i>a</i> Å	8.7352(4)	11.6122(4)	11.0525(5)	12.0375(8)
<i>b</i> Å	19.0049(7)	11.8144(4)	11.7597(5)	12.3483(6)
<i>c</i> Å	20.6750(9)	16.0033(5)	16.5751(6)	18.2344(11)
α °	90	73.075(3)	77.222(3)	70.547(5)
β °	105.660(4)	87.881(3)	84.935(3)	86.318(5)
γ °	90	62.358(4)	76.960(4)	70.498(5)
Volume Å ³	3304.9(2)	1848.18(13)	2045.13(15)	2405.7(3)
<i>Z</i>	4	2	2	2
λ Å	0.7107	0.71073	1.5418	1.5418
μ mm ⁻¹	0.698	0.633	4.897	4.956
Refls. Collected	9043 ^a	26363	23483	16616
Refls. Unique	9043 ^a	9236	8134	9222
Reflns. Observed	7480 ^a	7519	7262	7559
Rint	^a	0.0271	0.0712	0.0469
Goodness of Fit	0.887	1.029	1.065	1.039
R[I>2 σ (I)]	0.0456	0.0397	0.0603	0.0551
Rw2	0.1142	0.1007	0.1767	0.1514

^a Number of reflections in reprocessed hklf 5 formatted reflection file, see text for further details of twinning.

Table III-2 - Selected crystal parameters and refinement data.

Compound Label	5	7	8	9
Chemical Identity	C ₃₀ H ₈₆ FeN ₇ NaSi ₆	C ₃₆ H ₁₀₀ FeN ₉ NaSi ₆	C ₃₀ H ₈₄ FeN ₇ NaSi ₆	C ₃₂ H ₅₂ FeN ₈ NaSi ₄
Formula weight	792.43	906.62	790.42	772.87
Crystal system	Triclinic	Monoclinic	Monoclinic	Monoclinic
Space Group	P-1	P2 ₁ /c	P2 ₁ /n	P2 ₁ /c
<i>a</i> Å	11.7904(4)	22.8168(3)	11.1714(2)	9.3817(2)
<i>b</i> Å	11.8650(4)	22.2351(4)	30.1187(6)	20.4274(4)
<i>c</i> Å	18.4664(8)	22.4243(4)	14.7903(4)	10.5678(2)
α °	94.991(3)	90	90	90
β °	99.373(3)	96.718(2)	98.831(2)	104.402(2)
γ °	103.769(3)	90	90	90
Volume Å ³	2454.18(16)	3046.7(3)	4917.47(19)	1961.61(7)
Z	2	8	4	2
λ Å	0.71073	0.71073	0.71073	0.71073
μ mm ⁻¹	0.489	0.433	0.488	0.895
Refls. Collected	20802	48730	30603	11789
Refls. Unique	11173	24993	11233	4897
Reflns. Observed	8471	16626	8747	3951
Rint	0.0279	0.0376	0.0350	0.0279
Goodness of Fit	1.042	1.019	1.023	1.035
R[<i>I</i> >2 σ (<i>I</i>)]	0.0414	0.0501	0.0413	0.0335
Rw2	0.0916	0.1337	0.0938	0.0749

Table III-3 - Selected crystal parameters and refinement data.

Compound Label	10	11
Chemical Identity	$C_{30}H_{60}FeN_5NaO_2Si_4$	$C_{37.5}H_{36}FeN_9NaO$
Formula weight	714.03	707.59
Crystal system	Monoclinic	Monoclinic
Space Group	$P2_1/n$	$P2_1/c$
a Å	12.3817(2)	20.5102(10)
b Å	20.4492(4)	9.6402(4)
c Å	16.2656(3)	17.7307(7)
α °	90	90
β °	101.628(2)	99.067(4)
γ °	90	90
Volume Å ³	4033.86(13)	7180.4(5)
Z	4	4
λ Å	0.71073	1.54178
μ mm ⁻¹	0.535	3.974
Refls. Collected	33383	11902
Refls. Unique	9918	6609
Reflns. Observed	7690	3787
Rint	0.0399	0.0757
Goodness of Fit	1.031	0.990
R[$I > 2\sigma(I)$]	0.0384	0.0573
Rw2	0.0880	0.1339

III.IV.II Chapter 2 Crystal Structures

For compounds **13**, **14** and **16** disordered groups were refined over two sites with appropriate restraints imposed on atom to atom distances and on thermal displacement parameters. Such treatment was imposed on a SiMe₃ group for **14** and **16**, four isopropyl groups for **13** and one for **14** and two THF molecules in **14**. The crystal structures of compounds **12-16** have been deposited into the Cambridge Crystallographic Data Centre (CCDC) and have been assigned the following numbers: **12** - 1412549, **13** - 1412550, **14** - 1412551, **15** - 1412552, **16** - 1412553. Selected crystallographic and refinement parameters are presented in Table III-4 and Table III-5.

Table III-4 - Selected crystal parameters and refinement data.

Compound Label	12	13	14
Chemical Identity	$C_{16}H_{47}FeN_2NaSi_5$	$C_{72}H_{126}FeN_7NaSi_6$	$C_{55}H_{107}FeN_4NaO_3Si_5$
Formula weight	486.85	1337.17	1091.73
Crystal system	Triclinic	Monoclinic	Triclinic
Space Group	P-1	$P2_1/c$	P-1
a Å	10.1531(5)	20.763(3)	10.5144(5)
b Å	11.8733(5)	21.1154(19)	17.5343(9)
c Å	12.0556(5)	22.800(6)	18.5349(8)
α °	96.895(4)	90	90.401(4)
β °	100.584(4)	122.634(13)	96.397(4)
γ °	92.769(4)	90	100.632(4)
Volume Å ³	1414.56(11)	8418(3)	3336.2(3)
Z	2	4	2
λ Å	0.71073	0.7107	0.7107
μ mm ⁻¹	0.765	0.309	0.362
Refls. Collected	8652	59762	37201
Refls. Unique	5523	16510	14558
Reflns. Observed	4613	8756	9995
Rint	0.0249	0.1266	0.0431
Goodness of Fit	1.026	0.99	1.04
R[I>2 σ (I)]	0.0348	0.0761	0.0571
Rw2	0.0842	0.1748	0.1533

Table III-5 - Selected crystal parameters and refinement data.

Compound Label	15	16
Chemical Identity	C ₅₁ H ₉₅ FeN ₄ O ₃ Si ₄	C ₄₀ H ₇₄ FeN ₄ Si ₄
Formula weight	1003.5	779.24
Crystal system	Orthorhombic	Monoclinic
Space Group	P2 ₁ 2 ₁ 2 ₁	P2 ₁ /n
<i>a</i> Å	15.2296(3)	13.5831(3)
<i>b</i> Å	18.0203(4)	16.1634(4)
<i>c</i> Å	21.9241(6)	21.2440(6)
α °	90	90
β °	90	90.286(3)
γ °	90	90
Volume Å ³	6016.9(2)	4664.0(2)
Z	4	4
λ Å	0.7107	1.5418
μ mm ⁻¹	0.377	3.729
Refls. Collected	25202	20261
Refls. Unique	13981	8730
Reflns. Observed	10724	7148
Rint	0.0418	0.0451
Goodness of Fit	1.053	1.021
R[I>2 σ (I)]	0.0567	0.0476
Rw2	0.1093	0.1283

III.IV.III Chapter 3 Crystal Structures

Structures **18** and **33** were treated with the SQUEEZE routine within PLATON²⁸⁶ to remove the effects of disordered solvent from the model structures. For **18** approximately 107 electron equivalents were removed from 772 Å³ of unit cell space. For structure **33** approximately 47 electron equivalents were removed from 398 Å³ of unit cell space, this is believed to correspond to a third of a C₆H₅F molecule per K atom that was highly disordered about the -3 axis. The F atom of this group made a close approach to the K1 site. In structure **22**, one of the fluorobenzene molecules is disordered such that the major disorder component (74.7%) makes a Na---F contact but the minor disordered component does not (thus formally giving a co-crystal of two different metal complexes). Restraints were applied to both bond lengths and displacement parameters of this group to ensure an approximation to typical behaviour. Selected crystallographic and refinement parameters are presented in Table III-7, Table III-8, Table III-9, Table III-10 and Table III-11.

Table III-6 - Selected crystal parameters and refinement data.

Compound Label	17	18	19
Chemical Identity	$C_{23}H_{61}FeN_3NaOSi_6$	$C_{22}H_{48}FFeN_2NaO_2Si_4$	$C_{22}H_{47}F_2FeN_7NaO_2Si_4$
Formula weight	643.12	582.82	600.81
Crystal system	Triclinic	Monoclinic	Monoclinic
Space Group	P-1	$P2_1/c$	$P2_1/n$
a Å	8.8451(3)	11.5625(5)	9.4058(2)
b Å	11.1539(5)	15.6001(5)	17.9992(5)
c Å	21.0021(6)	21.6820(7)	19.5020(5)
α °	100.129(3)	90	90
β °	97.667(3)	103.665(4)	95.774(2)
γ °	109.543(4)	90	90
Volume Å ³	1880.48(13)	3800.2(2)	3284.88(14)
Z	2	4	4
λ Å	0.71073	1.54178	0.7107
μ mm ⁻¹	0.623	4.682	0.65
Refls. Collected	19279	26997	16649
Refls. Unique	7646	7499	6414
Reflns. Observed	6962	5476	5328
Rint	0.0157	0.0941	0.0218
Goodness of Fit	1.062	1.071	1.031
R[$I > 2\sigma(I)$]	0.025	0.0826	0.0305
Rw2	0.0666	0.231	0.0749

Table III-7 - Selected crystal parameters and refinement data.

Compound Label	20	21	22
Chemical Identity	$C_{44}H_{109}F_2Fe_2N_5Na_2O_4Si_{10}$	$C_{26}H_{47}F_4FeN_2NaOSi_4$	$C_{26}H_{47}F_4FeN_2NaOSi_4$
Formula weight	1248.94	670.85	670.85
Crystal system	Monoclinic	Monoclinic	Monoclinic
Space Group	$P2_1/c$	$P2_1/c$	$P2_1/n$
a Å	13.5915(2)	24.1748(7)	17.0380(2)
b Å	30.6303(4)	12.4609(3)	36.7640(5)
c Å	17.4637(3)	23.3126(8)	17.0348(2)
α °	90	90	90
β °	103.705(2)	92.272(3)	91.9630(10)
γ °	90	90	90
Volume Å ³	7063.34(19)	7017.2(4)	10664.1(2)
Z	4	8	12
λ Å	0.71073	0.71073	0.71073
μ mm ⁻¹	0.635	0.622	0.614
Refls. Collected	60487	32552	54981
Refls. Unique	15556	12544	24381
Reflns. Observed	12877	8416	18592
Rint	0.0306	0.0719	0.0269
Goodness of Fit	1.068	1.033	0.992
R[$I > 2\sigma(I)$]	0.0317	0.0497	0.0449
Rw2	0.0742	0.1323	0.1166

Table III-8 - Selected crystal parameters and refinement data.

Compound Label	23	24	25
Chemical Identity	$C_{19}H_{44}F_2FeN_2NaO_2Si_4$	$C_{26}H_{46}F_3FeN_2NaOSi_4$	$C_{26}H_{50}FFeN_2NaO_2Si_4$
Formula weight	561.76	688.85	632.88
Crystal system	Triclinic	Orthorhombic	Triclinic
Space Group	P-1	Pbca	P-1
a Å	12.6323(7)	12.0618(3)	11.0268(3)
b Å	15.4627(8)	23.5955(5)	12.2899(4)
c Å	16.6028(9)	25.4327(6)	14.4109(4)
α °	77.416(4)	90	104.165(2)
β °	74.423(5)	90	94.490(2)
γ °	84.634(4)	90	108.306(2)
Volume Å ³	3046.7(3)	7238.3(3)	1772.01(9)
Z	4	8	2
λ Å	0.71073	0.71073	0.7107
μ mm ⁻¹	0.696	0.608	0.602
Refls. Collected	23936	21158	17382
Refls. Unique	11506	7639	7784
Reflns. Observed	9348	4916	6055
Rint	0.0279	0.0619	0.0296
Goodness of Fit	1.108	0.944	1.056
R[$I > 2\sigma(I)$]	0.0452	0.0509	0.0376
Rw2	0.1181	0.1218	0.0895

Table III-9 - Selected crystal parameters and refinement data.

Compound Label	26	27	28
Chemical Identity	$C_{48}H_{100}Br_2F_4Fe_2N_4Na_2O_6Si_8$	$C_{48}H_{112}FFe_2N_5Na_2O_5Si_{10}$	$C_{82}H_{164}Fe_2N_6Na_2O_8Si_{12}$
Formula weight	1447.53	1260.97	1856.94
Crystal system	Monoclinic	Monoclinic	Orthorhombic
Space Group	$P2_1/n$	$P2_1/c$	Pbca
a Å	16.2918(4)	13.6708(6)	15.8340(8)
b Å	11.0502(3)	30.4612(13)	22.2719(10)
c Å	21.0172(5)	17.6993(5)	30.5970(12)
α °	90	90	90
β °	107.206(3)	103.040(4)	90
γ °	90	90	90
Volume Å ³	3614.35(17)	7180.4(5)	10790.1(8)
Z	2	4	4
λ Å	0.7107	0.71073	0.7107
μ mm ⁻¹	1.704	0.625	0.458
Refls. Collected	27083	44780	31282
Refls. Unique	8600	14600	10550
Reflns. Observed	6671	11366	7538
Rint	0.0335	0.0417	0.0362
Goodness of Fit	1.026	1.133	1.038
R[I>2 σ (I)]	0.0351	0.0490	0.0391
Rw2	0.0801	0.1042	0.0927

Table III-10 - Selected crystal parameters and refinement data.

Compound Label	29	30	31
Chemical Identity	C ₄₂ H ₉₀ F ₄ Fe ₂ N ₄ Na ₂ O ₄ Si ₈	C ₂₄ H ₇₂ Fe ₂ N ₄ O ₈ Si ₈	C ₂₈ H ₅₆ N ₂ Na ₂ O ₂ Si ₄
Formula weight	1173.57	815.25	611.08
Crystal system	Triclinic	Triclinic	Monoclinic
Space Group	P-1	P-1	C ₂
<i>a</i> Å	8.9433(5)	8.9460(6)	18.5766(12)
<i>b</i> Å	12.1304(6)	10.6305(7)	10.2593(6)
<i>c</i> Å	15.8452(8)	12.7643(6)	10.7149(9)
α °	79.360(4)	96.780(5)	90
β °	83.202(4)	109.279(5)	111.799(7)
γ °	69.189(5)	98.908(5)	90
Volume Å ³	1576.60(15)	1113.21(12)	1896.1(2)
Z	1	1	2
λ Å	0.7107	1.5418	0.71073
μ mm ⁻¹	0.675	7.657	0.204
Refls. Collected	23052	7869	12911
Refls. Unique	7499	4342	5054
Reflns. Observed	6207	4105	3920
Rint	0.0316	0.0284	0.0375
Goodness of Fit	1.036	1.055	1.147
R[<i>I</i> >2 σ (<i>I</i>)]	0.0334	0.0354	0.0484
Rw2	0.0840	0.0945	0.1347

Table III-11 - Selected crystal parameters and refinement data.

Compound Label	32	34	35
Chemical Identity	$C_{22}H_{62}FeLiN_3O_2Si_6$	$C_{22}H_{57.33}F_{0.67}FeKN_3Si_6$	$C_{36}H_{102}Fe_2N_4Na_2O_2Si_{10}$
Formula weight	632.07	640.20	1061.79
Crystal system	Triclinic	Trigonal	Monoclinic
Space Group	P-1	R-3c	P2 ₁ /n
<i>a</i> Å	11.4886(6)	17.9746(3)	11.1045(3)
<i>b</i> Å	11.8851(5)	17.9746(3)	17.4432(4)
<i>c</i> Å	15.5936(7)	17.9746(3)	17.0441(5)
α °	104.849(4)	97.773(3)	90
β °	90.192(4)	97.773(3)	106.453(3)
γ °	116.461(5)	97.773(3)	90
Volume Å ³	1825.41(17)	5631.0(3)	3166.22(15)
Z	2	6	2
λ Å	0.71073	0.7107	0.7107
μ mm ⁻¹	0.632	0.723	0.691
Refls. Collected	22556	21410	33154
Refls. Unique	8604	4803	7847
Reflns. Observed	6476	3788	6214
Rint	0.0527	0.0351	0.0478
Goodness of Fit	1.020	1.065	1.037
R[I>2 σ (I)]	0.0435	0.0442	0.0345
Rw2	0.1052	0.1474	0.0856

III.IV.IV Chapter 4 Crystal Structures

Structure **38** had a plate-like morphology and required an analytical absorption correction based upon face indexing to be applied. All other structures had absorption effects corrected by using multi-scan techniques. Selected crystallographic and refinement parameters are presented in Table III-12 and Table III-13.

Table III-12 - Selected crystal parameters and refinement data.

Compound Label	36	37	38	39
Chemical Identity	$C_{48}H_{100}F_6Fe_2N_4Na_2O_6Si_8$	$C_{50}H_{101}F_3Fe_2N_4Na_2O_4Si_{10}$	$C_{36}H_{91}Fe_2N_5Si_{10}$	$C_{36}H_{90}FFe_2N_5Si_{10}$
Formula weight	1325.71	1261.74	986.73	1004.72
Crystal system	Monoclinic	Triclinic	Monoclinic	Monoclinic
Space Group	C2/c	P-1	P2 ₁ /n	P2 ₁ /n
<i>a</i> Å	29.6087(16)	11.8043(7)	9.06940(10)	9.0520(11)
<i>b</i> Å	12.8261(6)	17.2228(6)	29.2209(3)	29.248(3)
<i>c</i> Å	20.4428(11)	18.2847(11)	65.2735(5)	21.767(3)
α °	90	86.444(4)	90	90
β °	112.430(6)	73.146(5)	91.9310(10)	91.359(2)
γ °	90	89.159(4)	90	90
Volume Å ³	7176.1(7)	3550.8(3)	17288.7(3)	5761.4(12)
Z	4	2	12	4
λ Å	0.71073	0.71073	1.54178	0.6889
μ mm ⁻¹	0.607	0.602	6.237	0.686
Refls. Collected	18637	38785	82217	80243
Refls. Unique	7261	15595	33731	14373
Reflns. Observed	5579	12350	26021	12889
Rint	0.0328	0.0351	0.0504	0.0599
Goodness of Fit	1.027	1.170	1.034	1.084
R[$I > 2\sigma(I)$]	0.0376	0.0510	0.0527	0.0362
Rw2	0.0871	0.1197	0.1335	0.1057

Table III-13 - Selected crystal parameters and refinement data.

Compound Label	40	42	43
Chemical Identity	C ₃₆ H ₉₀ BrFe ₂ N ₅ Si ₁₀	C ₂₄ H ₅₇ N ₃ Si ₆	C ₂₂ H ₄₆ F ₃ FeLiN ₂ O ₂ Si ₄
Formula weight	1065.63	556.27	602.76
Crystal system	Monoclinic	Trigonal	Orthorhombic
Space Group	P2 ₁ /n	R-3c	Pna2 ₁
<i>a</i> Å	9.1503(6)	11.1596(3)	18.1713(6)
<i>b</i> Å	29.340(2)	11.1596(3)	17.2228(6)
<i>c</i> Å	21.8190(14)	48.9347(9)	18.2847(11)
α °	90	90	90
β °	91.400(2)	90	90
γ °	90	120	90
Volume Å ³	5856.0(7)	5277.7(2)	3145.40(15)
Z	4	6	4
λ Å	0.6889	0.71073	0.7107
μ mm ⁻¹	1.298	0.254	0.671
Refls. Collected	87573	29802	12054
Refls. Unique	14410	1623	6913
Reflns. Observed	12889	1533	6222
Rint	0.0605	0.0276	0.0272
Goodness of Fit	1.073	1.120	1.064
R[I>2 σ (I)]	0.0538	0.0329	0.0399
Rw2	0.1633	0.0894	0.0907

III.V Supplementary Magnetic Data

Table III-14 details the parameters obtained from fitting the experimental data to the generalised Debye model³⁴³ for compound **38**, as shown in Figure 4.21 in Section 4.2.5.2.

Table III-14 - Fitted parameters for the AC susceptibility data of **38** in the Cole-Cole regime obtained under the applied magnetic field of 1000 Oe.

T (K)	χ_S (cm ³ mol ⁻¹)	χ_T (cm ³ mol ⁻¹)	τ (s)	α	Residual
1.80	0.13513	6.76363	0.00575	0.16856	0.01621
2.00	0.18843	6.1141	0.00338	0.13302	0.02864
2.25	0.23567	5.50473	0.00203	0.10532	0.03038
2.50	0.26864	4.99765	0.00132	0.08899	0.0228
2.75	0.27817	4.57885	9.23174×10^{-4}	0.08296	0.01444
3.00	0.29139	4.21863	6.84494×10^{-4}	0.08152	0.00855
3.25	0.29439	3.90993	5.27113×10^{-4}	0.08389	0.00626
3.50	0.29968	3.63089	4.1911×10^{-4}	0.08585	0.0047
3.75	0.30782	3.38677	3.42443×10^{-4}	0.08829	0.00351
4.00	0.30532	3.16581	2.83296×10^{-4}	0.09233	0.00459
4.25	0.29465	2.97621	2.40134×10^{-4}	0.09795	0.00366
4.50	0.31461	2.80036	2.09104×10^{-4}	0.09572	0.00252
4.75	0.33222	2.64555	1.84191×10^{-4}	0.09754	0.00325
5.00	0.35245	2.49821	1.65238×10^{-4}	0.09199	0.00226
5.25	0.38376	2.36902	1.50688×10^{-4}	0.08886	0.00173
5.50	0.35628	2.24863	1.34459×10^{-4}	0.08899	0.00125
5.75	0.39476	2.13976	1.24406×10^{-4}	0.08289	0.00117
6.00	0.38684	2.03971	1.13655×10^{-4}	0.08056	9.91824×10^{-4}

Table III-15 details the parameters obtained from fitting the experimental data to the generalised Debye model³⁴³ for compound **39**, as shown in Figure 4.22 in Section 4.2.5.2.

Table III-15 - Fitted parameters for the AC susceptibility data of **39** in the Cole-Cole regime obtained under the applied magnetic field of 1000 Oe.

<i>T</i> (K)	χ_S (cm ³ mol ⁻¹)	χ_T (cm ³ mol ⁻¹)	τ (s)	α	Residual
1.85	0.19561	7.64042	0.00151	0.01878	0.01059
2.00	0.20206	7.36881	0.00129	0.02278	0.01093
2.20	0.22925	6.86525	0.00102	0.01751	0.00984
2.40	0.23941	6.46735	8.4589 x 10 ⁻⁴	0.02185	0.01178
2.60	0.24487	6.16204	7.35572 x 10 ⁻⁴	0.02468	0.014
2.80	0.25326	5.93952	6.63236 x 10 ⁻⁴	0.02721	0.00935
3.00	0.25765	5.71126	6.02998 x 10 ⁻⁴	0.02664	0.01156
3.25	0.26858	5.4646	5.42649 x 10 ⁻⁴	0.02538	0.00927
3.50	0.27511	5.25195	4.92991 x 10 ⁻⁴	0.02866	0.00683
3.75	0.27653	4.97639	4.41366 x 10 ⁻⁴	0.02749	0.00735
4.00	0.28152	4.67893	3.88098 x 10 ⁻⁴	0.02863	0.00686
4.25	0.28347	4.40799	3.43673 x 10 ⁻⁴	0.02967	0.0049
4.50	0.29421	4.15393	3.06942 x 10 ⁻⁴	0.02874	0.00373
4.75	0.29526	3.91872	2.75997 x 10 ⁻⁴	0.02845	0.00277
5.00	0.29451	3.70068	2.48469 x 10 ⁻⁴	0.02944	0.00205
5.25	0.29083	3.50329	2.24893 x 10 ⁻⁴	0.029	0.00239
5.50	0.29769	3.32597	2.05021 x 10 ⁻⁴	0.02899	0.00179
5.75	0.29799	3.16157	1.88254 x 10 ⁻⁴	0.02663	0.00143
6.00	0.29787	3.00875	1.72321 x 10 ⁻⁴	0.02601	0.0013
6.50	0.30406	2.74171	1.47179 x 10 ⁻⁴	0.02355	6.37721 x 10 ⁻⁴
7.00	0.32038	2.51292	1.27211 x 10 ⁻⁴	0.01896	3.57077 x 10 ⁻⁴

References

- (1) Mulvey, R. E.; Mongin, F.; Uchiyama, M.; Kondo, Y. *Angew. Chem. Int. Ed. Engl.* **2007**, *46* (21), 3802.
- (2) Mongin, F.; Harrison-Marchand, A. *Chem. Rev.* **2013**, *113* (10), 7563.
- (3) Mulvey, R. E.; Armstrong, D. R.; Conway, B.; Crosbie, E.; Kennedy, A. R.; Robertson, S. D. *Inorg. Chem.* **2011**, *50* (24), 12241.
- (4) Krasovskiy, A.; Knochel, P. *Angew. Chem. Int. Ed. Engl.* **2004**, *43* (25), 3333.
- (5) Hevia, E.; Mulvey, R. E. *Angew. Chem. Int. Ed. Engl.* **2011**, *50* (29), 6448.
- (6) García-Alvarez, P.; Graham, D. V.; Hevia, E.; Kennedy, A. R.; Klett, J.; Mulvey, R. E.; O'Hara, C. T.; Weatherstone, S. *Angew. Chem. Int. Ed. Engl.* **2008**, *47* (42), 8079.
- (7) Klatt, T.; Markiewicz, J. T.; Sämann, C.; Knochel, P. *J. Org. Chem.* **2014**, *79* (10), 4253.
- (8) Mulvey, R. E. *Acc. Chem. Res.* **2009**, *42* (6), 743.
- (9) Armstrong, D. R.; Clegg, W.; Dale, S. H.; Hevia, E.; Hogg, L. M.; Honeyman, G. W.; Mulvey, R. E. *Angew. Chem. Int. Ed. Engl.* **2006**, *45* (23), 3775.
- (10) Armstrong, D. R.; Balloch, L.; Hevia, E.; Kennedy, A. R.; Mulvey, R. E.; O'Hara, C. T.; Robertson, S. D. *Beilstein J. Org. Chem.* **2011**, *7*, 1234.
- (11) Clayden, J. *Organolithiums: Selectivity for Synthesis.*; Elsevier, 2002; Vol. 23.
- (12) Mulvey, R. E.; Robertson, S. D. In *Organo-di-Metallic Compounds (or Reagents)*; 2014; pp 129–158.
- (13) Lochmann, L.; Pospíšil, J.; Lim, D. *Tetrahedron Lett.* **1966**, *2* (2), 257.
- (14) Schlosser, M. *J. Organomet. Chem.* **1967**, *8* (1), 9.
- (15) Lochmann, L. *Eur. J. Inorg. Chem.* **2000**, No. 6, 1115.
- (16) Mongin, F.; Maggi, R.; Schlosser, M. *Chimia* **1996**, *50* (12), 650.
- (17) Schlosser, M.; Jung, H. C.; Takagishi, S. *Tetrahedron* **1990**, *46* (16), 5633.

-
- (18) Caubere, P. *Chem. Rev.* **1993**, *93* (6), 2317.
- (19) Schlosser, M. *Angew. Chem. Int. Ed. Engl.* **2005**, *44* (3), 376.
- (20) Schlosser, M. *Pure Appl. Chem.* **1988**, *60* (11), 1627.
- (21) Schwindeman, J. a.; Woltermann, C. J.; Letchford, R. J. *Chem. Heal. Saf.* **2002**, *9* (3), 6.
- (22) Armstrong, D. R.; Kennedy, A. R.; Mulvey, R. E.; Parkinson, J. A.; Robertson, S. D. *Chem. Sci.* **2012**, *3* (9), 2700.
- (23) Andrikopoulos, P. C.; Armstrong, D. R.; Graham, D. V.; Hevia, E.; Kennedy, A. R.; Mulvey, R. E.; O'Hara, C. T.; Talmard, C. *Angew. Chem. Int. Ed. Engl.* **2005**, *44* (22), 3459.
- (24) Mulvey, R. E. *Organometallics* **2006**, *25* (5), 1060.
- (25) L'Helgoual'ch, J.-M.; Bentabed-Ababsa, G.; Chevallier, F.; Yonehara, M.; Uchiyama, M.; Derdour, A.; Mongin, F. *Chem. Comm.* **2008**, No. 42, 5375.
- (26) Armstrong, D. R.; Brammer, E.; Cadenbach, T.; Hevia, E.; Kennedy, A. R. *Organometallics* **2013**, *32* (2), 480.
- (27) Mulvey, R. E. *Organometallics* **2006**, *25* (5), 1060.
- (28) Martínez-Martínez, A. J.; Kennedy, A. R.; Mulvey, R. E.; O'Hara, C. T. *Science* **2014**, *346* (6211), 834.
- (29) Pedersen, C. J. *J. Am. Chem. Soc.* **1967**, No. I, 2495.
- (30) Kennedy, A. R.; Mulvey, R. E.; Rowlings, R. B. *J. Am. Chem. Soc.* **1998**, *120* (31), 7816.
- (31) Morgan, J.; Anders, E. *Proc. Natl. Acad. Sci. U. S. A.* **1980**, *77* (12), 6973.
- (32) Marjasvaara, A.; Torvinen, M.; Vainiotalo, P. *J. Mass Spectrom.* **2004**, *39* (10), 1139.
- (33) Egorova, K. S.; Ananikov, V. P. *Angew. Chem. Int. Ed. Engl.* **2016**, *2*.
- (34) World Steel Association. *Steel and Raw materials*; 2011.
- (35) Takami, T.; Sakaida, I. *J. Clin. Biochem. Nutr.* **2011**, *48* (2), 103.

-
- (36) Keiter, H. G.; Berman, H.; Jones, H.; Maclachlan, E. *Blood* **1955**, *10* (4), 370.
- (37) Wilson, M. T.; Reeder, B. J. *Exp. Physiol.* **2008**, *93* (1), 128.
- (38) Nam, W. *Acc. Chem. Res.* **2007**, *40* (7), 522.
- (39) Curatti, L.; Hernandez, J. a; Igarashi, R. Y.; Soboh, B.; Zhao, D.; Rubio, L. M. *Proc. Natl. Acad. Sci. U. S. A.* **2007**, *104* (45), 17626.
- (40) Fritsch, J.; Lenz, O.; Friedrich, B. *Nat. Rev. Microbiol.* **2013**, *11* (2), 106.
- (41) Groysman, S.; Holm, R. *Biochemistry* **2009**, No. Figure 2, 2310.
- (42) Schlögl, K. *Pure Appl. Chem.* **1970**, *23* (4), 413.
- (43) Cooke, M. P. *J. Am. Chem. Soc.* **1970**, *92* (20), 6080.
- (44) *Ammonia*; Nielsen, A., Ed.; Springer Berlin Heidelberg: Berlin, Heidelberg, 1995.
- (45) Chun, D. H.; Park, J. C.; Hong, S. Y.; Lim, J. T.; Kim, C. S.; Lee, H.-T.; Yang, J.-I.; Hong, S.; Jung, H. *J. Catal.* **2014**, *317*, 135.
- (46) Bolm, C. *Nat. Chem.* **2009**, *1* (August), 420.
- (47) Beller, M.; Zapf, A.; Mägerlein, W. *Chem. Eng. Technol.* **2001**, *24* (6), 575.
- (48) Corriu, R.; Masse, J. *J. Chem. Soc. Chem. Comm.* **1972**, No. 144, 7062.
- (49) Tamao, K.; Sumitani, K.; Kumada, M. *J. Am. Chem. Soc.* **1972**, *315* (1970), 4374.
- (50) Denmark, S. E.; Butler, C. R. *Chem. Comm.* **2009**, No. 1, 20.
- (51) Ferrer Flegeau, E.; Schneider, U.; Kobayashi, S. *Chem. - A Eur. J.* **2009**, *15* (45), 12247.
- (52) InfoMine. Palladium Price <http://www.infomine.com/investment/metal-prices/palladium/6-month/>.
- (53) InfoMine. Iron Ore (fine) Price <http://www.infomine.com/investment/metal-prices/iron-ore-fines/6-month/>.
- (54) Hajipour, A. R.; Azizi, G. *Green Chem.* **2013**, *15* (4), 1030.
- (55) Denkhaus, E.; Salnikow, K. *Crit. Rev. Oncol. Hematol.* **2002**, *42* (1), 35.
-

-
- (56) Tu, T.; Mao, H.; Herbert, C.; Xu, M.; Dötz, K. H. *Chem. Comm.* **2010**, 46 (41), 7796.
- (57) Bolm, C.; Legros, J.; Le Pailh, J.; Zani, L. *Chem. Rev.* **2004**, 104 (12), 6217.
- (58) Enthaler, S.; Junge, K.; Beller, M. *Angew. Chem. Int. Ed. Engl.* **2008**, 47 (18), 3317.
- (59) Miyaura, N.; Suzuki, A. *Chem. Rev.* **1995**, 95 (7), 2457.
- (60) Bedford, R. B. *Acc. Chem. Res.* **2015**, 48 (5), 1485.
- (61) Fürstner, A.; Martin, R.; Krause, H.; Seidel, G.; Goddard, R.; Lehmann, C. W. *J. Am. Chem. Soc.* **2008**, 130 (27), 8773.
- (62) Bedford, R. B.; Betham, M.; Bruce, D. W.; Davis, S. a; Frost, R. M.; Hird, M. *Chem. Comm.* **2006**, No. 13, 1398.
- (63) Aleandri, L. E.; Bogdanovic, B.; Diirr, C.; Gaidies, A.; Hartwig, T.; Hockett, S. C.; Lagarden, M.; Wilczok, U.; Brand, R. a. *Chem. Mater.* **1995**, 7 (6), 1153.
- (64) Kauffmann, T. *Angew. Chem. Int. Ed. Engl.* **1996**, 35 (4), 386.
- (65) Fürstner, A.; Leitner, A.; Méndez, M.; Krause, H. *J. Am. Chem. Soc.* **2002**, 124 (46), 13856.
- (66) Sherry, B. D.; Fürstner, A. *Acc. Chem. Res.* **2008**, 41 (11), 1500.
- (67) Fürstner, A. *Angew. Chem. Int. Ed. Engl.* **2014**, 53 (33), 8587.
- (68) Felkin, H.; Knowles, P. J.; Meunier, B. *J. Organomet. Chem.* **1978**, 146 (2), 151.
- (69) Bedford, R. B.; Brenner, P. B.; Carter, E.; Cogswell, P. M.; Haddow, M. F.; Harvey, J. N.; Murphy, D. M.; Nunn, J.; Woodall, C. H. *Angew. Chem. Int. Ed. Engl.* **2014**, 53 (7), 1804.
- (70) Al-Afyouni, M. H.; Fillman, K. L.; Brennessel, W. W.; Neidig, M. L. *J. Am. Chem. Soc.* **2014**, 136 (44), 15457.
- (71) Fürstner, A.; Krause, H.; Lehmann, C. W. *Angew. Chem. Int. Ed. Engl.* **2006**, 45 (3), 440.
- (72) Jonas, K.; Schieferstein, L.; Krüger, C.; Tsay, Y.-H. *Angew. Chem. Int. Ed. Engl.* **1979**, 18 (7), 550.

-
- (73) Martin, R.; Fürstner, A. *Angew. Chem. Int. Ed. Engl.* **2004**, *43* (30), 3955.
- (74) Sun, C.-L.; Li, B.-J.; Shi, Z.-J. *Chem. Rev.* **2011**, *111* (3), 1293.
- (75) Norinder, J.; Matsumoto, A.; Yoshikai, N.; Nakamura, E. *J. Am. Chem. Soc.* **2008**, *130* (18), 5858.
- (76) Wen, J.; Zhang, J.; Chen, S.-Y.; Li, J.; Yu, X.-Q. *Angew. Chem. Int. Ed. Engl.* **2008**, *47* (46), 8897.
- (77) Liu, W.; Cao, H.; Lei, A. *Angew. Chem. Int. Ed. Engl.* **2010**, *49* (11), 2004.
- (78) Cadenbach, T. *Final Report (Unpublished Results)*; 2012.
- (79) Vallée, F.; Mousseau, J. J.; Charette, A. B. *J. Am. Chem. Soc.* **2010**, *132* (5), 1514.
- (80) Bartlett, P. D.; Funahashi, T. *J. Am. Chem. Soc.* **1962**, *84* (13), 2596.
- (81) Nagaradja, E.; Chevallier, F.; Roisnel, T.; Jouikov, V.; Mongin, F. *Tetrahedron* **2012**, *68* (14), 3063.
- (82) Alborés, P.; Carrella, L. M.; Clegg, W.; García-Alvarez, P.; Kennedy, A. R.; Klett, J.; Mulvey, R. E.; Rentschler, E.; Russo, L. *Angew. Chem. Int. Ed. Engl.* **2009**, *48* (18), 3317.
- (83) Mulvey, R. E. *Chem. Comm.* **2001**, No. 12, 1049.
- (84) García Mancheño, O. *Angew. Chem. Int. Ed. Engl.* **2011**, *50* (10), 2216.
- (85) Sulway, S. A.; Collison, D.; McDouall, J. J. W.; Tuna, F.; Layfield, R. A. *Inorg. Chem.* **2011**, *50* (6), 2521.
- (86) Wunderlich, S. H.; Knochel, P. *Angew. Chem. Int. Ed. Engl.* **2009**, *48* (51), 9717.
- (87) Mulvey, R. E.; Robertson, S. D. *Angew. Chem. Int. Ed. Engl.* **2013**, *52* (44), 11470.
- (88) Grüning, R.; Atwood, J. L. *J. Organomet. Chem.* **1977**, *137* (1), 101.
- (89) Driess, M.; Pritzkow, H.; Skipinski, M.; Winkler, U. *Organometallics* **1997**, *16* (23), 5108.
- (90) Knizek, J.; Krossing, I.; Nöth, H.; Schwenk, H.; Seifert, T. *Chem. Ber.* **1997**, *130* (8), 1053.

-
- (91) Andersen, R. A.; Faegri, K.; Green, J. C.; Haaland, A.; Lappert, M. F.; Leung, W. P.; Rypdal, K. *Inorg. Chem.* **1988**, *27* (10), 1782.
- (92) Olmstead, M. M.; Power, P. P.; Shoner, S. C. *Inorg. Chem.* **1991**, *30* (11), 2547.
- (93) Schödel, H.; Näther, C.; Bock, H.; Butenschön, F. *Acta Crystallogr. Sect. B Struct. Sci.* **1996**, *52* (5), 842.
- (94) Cotton, F. A.; Daniels, L. M.; Jordan IV, G. T.; Murillo, C. A. *Polyhedron* **1998**, *17* (4), 589.
- (95) Baillie, S. E.; Clegg, W.; García-Álvarez, P.; Hevia, E.; Kennedy, A. R.; Klett, J.; Russo, L. *Organometallics* **2012**, *31* (14), 5131.
- (96) König, S. N.; Schneider, D.; Maichle-Mössmer, C.; Day, B. M.; Layfield, R. A.; Anwander, R. *Eur. J. Inorg. Chem.* **2014**, *2014* (26), 4302.
- (97) Armstrong, D. R.; Emerson, H. S.; Hernán-Gómez, A.; Kennedy, A. R.; Hevia, E. *Dalt. Trans.* **2014**, 1.
- (98) Uzelac, M.; Borilovic, I.; Amores, M.; Cadenbach, T.; Kennedy, A. R.; Aromí, G.; Hevia, E. *Chem. - A Eur. J.* **2016**, n/a.
- (99) Ming, L.-J. *Physical Methods in Bioinorganic Chemistry: Spectroscopy and Magnetism*; Que Jr., L., Ed.; University Science Books: Sausalito, CA, 2000.
- (100) Drago, R.; Zink, J. *J. Chem. Educ.* **1974**, *5* (6), 371.
- (101) Machonkin, T. E.; Westler, W. M.; Markley, J. L. *Inorg. Chem.* **2005**, *44* (4), 779.
- (102) Evans, D. F. *J. Chem. Soc.* **1959**, 2003.
- (103) Schubert, E. M. *J. Chem. Educ.* **1992**, *69*, 62.
- (104) Irwin, M.; Jenkins, R. K.; Denning, M. S.; Krämer, T.; Grandjean, F.; Long, G. J.; Herchel, R.; McGrady, J. E.; Goicoechea, J. M. *Inorg. Chem.* **2010**, *49* (13), 6160.
- (105) Pascualini, M. E.; Di Russo, N. V.; Thuijs, A. E.; Ozarowski, A.; Stoian, S. A.; Abboud, K. A.; Christou, G.; Veige, A. S. *Chem. Sci.* **2015**, *6* (1), 608.
- (106) Andres, H.; Bominaar, E. L.; Smith, J. M.; Eckert, N. a; Holland, P. L.; Münck, E. *J. Am. Chem. Soc.* **2002**, *124* (12), 3012.
-

-
- (107) Holland, P. L.; Cundari, T. R.; Perez, L. L.; Eckert, N. A.; Lachicotte, R. J. *J. Am. Chem. Soc.* **2002**, *124* (48), 14416.
- (108) Smith, J. M.; Lachicotte, R. J.; Holland, P. L. *Organometallics* **2002**, *21* (22), 4808.
- (109) Eckert, N. A.; Smith, J. M.; Lachicotte, R. J.; Holland, P. L. *Inorg. Chem.* **2004**, *43* (10), 3306.
- (110) Holland, P. L. *Acc. Chem. Res.* **2008**, *41* (8), 905.
- (111) Eichhöfer, A.; Lan, Y.; Mereacre, V.; Bodenstein, T.; Weigend, F. *Inorg. Chem.* **2014**, *53* (4), 1962.
- (112) Nichols, M. A.; Williard, P. G. *J. Am. Chem. Soc.* **1993**, *115* (4), 1568.
- (113) Reich, H. J.; Green, D. P.; Medina, M. A.; Goldenberg, W. S.; Gudmundsson, B. Ö.; Dykstra, R. R.; Phillips, N. H. *J. Am. Chem. Soc.* **1998**, *120* (29), 7201.
- (114) Clegg, W.; Dale, S. H.; Hevia, E.; Honeyman, G. W.; Mulvey, R. E. *Angew. Chem. Int. Ed. Engl.* **2006**, *45* (15), 2370.
- (115) Clegg, W.; Dale, S. H.; Harrington, R. W.; Hevia, E.; Honeyman, G. W.; Mulvey, R. E. *Angew. Chem. Int. Ed. Engl.* **2006**, *45* (15), 2374.
- (116) Margraf, G.; Schödel, F.; Sängler, I.; Bolte, M.; Wagner, M.; Lerner, H.-W. *Zeitschrift für Naturforsch. B* **2012**, *67b*, 549.
- (117) He, X.; Noll, B. C.; Beatty, A.; Mulvey, R. E.; Henderson, K. W. *J. Am. Chem. Soc.* **2004**, *126* (24), 7444.
- (118) Murray, B. D.; Power, P. P. *Inorg. Chem.* **1984**, *23* (26), 4584.
- (119) Davies, R. P. *Inorg. Chem. Comm.* **2000**, *3* (1), 13.
- (120) Forbes, G. C.; Kennedy, A. R.; Mulvey, R. E.; Rodger, P. J. a.; Rowlings, R. B. *J. Chem. Soc. Dalton Trans.* **2001**, No. 9, 1477.
- (121) Balanta-Díaz, J. a; Moya-Cabrera, M.; Jancik, V.; Pineda-Cedeño, L. W.; Toscano, R. a; Cea-Olivares, R. *Inorg. Chem.* **2009**, *48* (6), 2518.
- (122) Rodriguez, M. M.; Stubbert, B. D.; Scarborough, C. C.; Brennessel, W. W.; Bill, E.; Holland, P. L. *Angew. Chem. Int. Ed. Engl.* **2012**, *51* (33), 8247.

-
- (123) Coddling, P. W.; Kerr, K. a. *Acta Crystallogr. Sect. B Struct. Crystallogr. Cryst. Chem.* **1978**, *34* (12), 3785.
- (124) Fulmer, G. R.; Miller, A. J. M.; Sherden, N. H.; Gottlieb, H. E.; Nudelman, A.; Stoltz, B. M.; Bercaw, J. E.; Goldberg, K. I. *Organometallics* **2010**, *29* (9), 2176.
- (125) Hursthouse, M. B.; Rodesiler, P. F. *J. Chem. Soc. Dalt. Trans.* **1972**, No. 19, 2100.
- (126) Yousef, R. I.; Walfort, B.; Ruffer, T.; Wagner, C.; Schmidt, H.; Herzog, R.; Steinborn, D. *J. Organomet. Chem.* **2005**, *690* (5), 1178.
- (127) Robertson, G. M. *New Insights into Homo- and Heterometallic Alkali Metal Amide Chemistry*, Univeristy of Strathclyde, 2012.
- (128) Putzer, M. A.; Neumüller, B.; Dehnicke, K.; Magull, J. *Chem. Ber.* **1996**, *129* (6), 715.
- (129) Graham, D. V.; Hevia, E.; Kennedy, A. R.; Mulvey, R. E.; O'Hara, C. T.; Talmard, C. *Chem. Comm.* **2006**, No. 4, 417.
- (130) Blackman, A. G. *Polyhedron* **2005**, *24* (1), 1.
- (131) Cousins, D. M.; Davidson, M. G.; Frankis, C. J.; García-Vivó, D.; Mahon, M. F. *Dalt. Trans.* **2010**, *39* (35), 8278.
- (132) Davidson, M. G.; Garcia-Vivo, D.; Kennedy, A. R.; Mulvey, R. E.; Robertson, S. D. *Chem. - A Eur. J.* **2011**, *17* (12), 3364.
- (133) Armstrong, D. R.; Davidson, M. G.; Garcia-Vivo, D.; Kennedy, A. R.; Mulvey, R. E.; Robertson, S. D. *Inorg. Chem.* **2013**, *52* (20), 12023.
- (134) Kennedy, A. R.; Mulvey, R. E.; Urquhart, R. I.; Robertson, S. D. *Dalt. Trans.* **2014**, *43*, 14265.
- (135) Kennedy, A. R.; McLellan, R.; McNeil, G. J.; Mulvey, R. E.; Robertson, S. D. *Polyhedron* **2016**, *103*, 94.
- (136) Ojeda-Amador, A. I.; Martínez-Martínez, A. J.; Kennedy, A. R.; O'Hara, C. T. *Inorg. Chem.* **2015**, *54* (20), 9833.
- (137) Kim, J. J.; Yoon, J. *Inorganica Chim. Acta* **2013**, *394*, 506.
- (138) Madern, N.; Talbi, B.; Salmain, M. *Appl. Organomet. Chem.* **2013**, *27* (1), 6.

-
- (139) Burgos, M.; Crespo, O.; Gimeno, M. C.; Jones, P. G.; Laguna, A. *Eur. J. Inorg. Chem.* **2003**, 2170.
- (140) Armstrong, D. R.; Garden, J. A.; Kennedy, A. R.; Mulvey, R. E.; Robertson, S. D. *Angew. Chem. Int. Ed. Engl.* **2013**, 52 (28), 7190.
- (141) Cotton, F. A.; Daniels, L. M.; Jordan IV, G. T.; Murillo, C. A.; Pascual, I. *Inorganica Chim. Acta* **2000**, 297 (1–2), 6.
- (142) Sundberg, J.; Vad, M. S.; McGrady, J. E.; Björemark, P. M.; Håkansson, M.; McKenzie, C. J. *J. Organomet. Chem.* **2015**, 786, 40.
- (143) Nippe, M.; Berry, J. F. *J. Am. Chem. Soc.* **2007**, 129 (42), 12684.
- (144) Nippe, M.; Bill, E.; Berry, J. F. *Inorg. Chem.* **2011**, 50 (16), 7650.
- (145) Nippe, M.; Turov, Y.; Berry, J. F. *Inorg. Chem.* **2011**, 50 (21), 10592.
- (146) Turov, Y.; Berry, J. F. *Dalt. Trans.* **2012**, 41 (26), 8153.
- (147) Coronado, E.; Galán-Mascarós, J. R.; Martí-Gastaldo, C. *CrystEngComm* **2009**, 11 (10), 2143.
- (148) Chilton, N. F.; Anderson, R. P.; Turner, L. D.; Soncini, A.; Murray, K. S. *J. Comput. Chem.* **2013**, 34 (13), 1164.
- (149) Freedman, D. E.; Harman, W. H.; Harris, T. D.; Long, G. J.; Chang, C. J.; Long, J. R. *J. Am. Chem. Soc.* **2010**, 132 (4), 1224.
- (150) Harman, W. H.; Harris, T. D.; Freedman, D. E.; Fong, H.; Chang, A.; Rinehart, J. D.; Ozarowski, A.; Sougrati, M. T.; Grandjean, F.; Long, G. J.; Long, J. R.; Chang, C. J. *J. Am. Chem. Soc.* **2010**, 132 (51), 18115.
- (151) Hendrich, M. P.; Day, E. P.; Wang, C.-P.; Synder, B. S.; Holm, R. H.; Munck, E. *Inorg. Chem.* **1994**, 33 (13), 2848.
- (152) Holland, J. M.; McAllister, J. A.; Kilner, C. A.; Thornton-Pett, M.; Bridgeman, A. J.; Halcrow, M. A. *J. Chem. Soc. Dalt. Trans.* **2002**, 2 (4), 548.
- (153) McCusker, J. K.; Rheingold, A. L.; Hendrickson, D. N. *Inorg. Chem.* **1996**, 35 (7), 2100.

-
- (154) Marchivie, M.; Guionneau, P.; Létard, J.-F.; Chasseau, D. *Acta Crystallogr. Sect. B Struct. Sci.* **2003**, *59* (4), 479.
- (155) Halcrow, M. a. *Chem. Soc. Rev.* **2011**, *40* (7), 4119.
- (156) Craig, G. A.; Roubeau, O.; Aromí, G. *Coord. Chem. Rev.* **2014**, *269* (1), 13.
- (157) Jellema, E.; Sciarone, T. J. J.; Navarrete, N. M.; Hettinga, M. J.; Meetsma, A.; Hessen, B. *Eur. J. Inorg. Chem.* **2011**, *2011* (1), 91.
- (158) Glatz, G.; Demeshko, S.; Motz, G.; Kempe, R. *Eur. J. Inorg. Chem.* **2009**, *2009* (10), 1385.
- (159) Arduengo, A. J.; Harlow, R. L.; Kline, M. *J. Am. Chem. Soc.* **1991**, *113* (1), 361.
- (160) Díez-González, S.; Nolan, S. P. *Coord. Chem. Rev.* **2007**, *251* (5–6), 874.
- (161) Hopkinson, M. N.; Richter, C.; Schedler, M.; Glorius, F. *Nature* **2014**, *510* (7506), 485.
- (162) Bourissou, D.; Guerret, O.; Gabbai, F. P.; Bertrand, G. *Chem. Rev.* **2000**, *100* (1), 39.
- (163) Herrmann, W. A. *Angew. Chem. Int. Ed. Engl.* **2002**, *41* (8), 1290.
- (164) Bellemin-Laponnaz, S.; Dagorne, S. *Chem. Rev.* **2014**, *114* (18), 8747.
- (165) Díez-González, S.; Marion, N.; Nolan, S. P. *Chem. Rev.* **2009**, *109* (8), 3612.
- (166) Hahn, F. E.; Jahnke, M. C. *Angew. Chem. Int. Ed. Engl.* **2008**, *47* (17), 3122.
- (167) Arnold, P. L.; Pearson, S. *Coord. Chem. Rev.* **2007**, *251* (5–6), 596.
- (168) Albrecht, M. *Chem. Comm.* **2008**, No. 31, 3601.
- (169) Schuster, O.; Yang, L.; Raubenheimer, H. G.; Albrecht, M. *Chem. Rev.* **2009**, *109* (8), 3445.
- (170) Aldeco-Perez, E.; Rosenthal, A. J.; Donnadiou, B.; Parameswaran, P.; Frenking, G.; Bertrand, G. *Science* **2009**, *326* (5952), 556.
- (171) Gründemann, S.; Kovacevic, A.; Albrecht, M.; Faller, J. W.; Crabtree, R. H. *Chem. Comm.* **2001**, *4* (21), 2274.
- (172) Waters, J. B.; Goicoechea, J. M. *Coord. Chem. Rev.* **2015**, *293–294*, 80.

- (173) Prades, A.; Viciano, M.; Sanaú, M.; Peris, E. *Organometallics* **2008**, *27* (16), 4254.
- (174) John, A.; Shaikh, M. M.; Ghosh, P. *Dalt. Trans.* **2009**, No. 47, 10581.
- (175) Crabtree, R. H. *Coord. Chem. Rev.* **2013**, *257* (3–4), 755.
- (176) Heckenroth, M.; Neels, A.; Garnier, M. G.; Aebi, P.; Ehlers, A. W.; Albrecht, M. *Chem. - A Eur. J.* **2009**, *15* (37), 9375.
- (177) Melaimi, M.; Soleilhavoup, M.; Bertrand, G. *Angew. Chem. Int. Ed. Engl.* **2010**, *49* (47), 8810.
- (178) Chianese, A. R.; Kovacevic, A.; Zeglis, B. M.; Faller, J. W.; Crabtree, R. H. *Organometallics* **2004**, *23* (10), 2461.
- (179) Yang, L.; Krüger, A.; Neels, A.; Albrecht, M. *Organometallics* **2008**, *27* (13), 3161.
- (180) Day, B. M.; Pugh, T.; Hendriks, D.; Guerra, C. F.; Evans, D. J.; Bickelhaupt, F. M.; Layfield, R. A. *J. Am. Chem. Soc.* **2013**, *135* (36), 13338.
- (181) Day, B. M.; Pal, K.; Pugh, T.; Tuck, J.; Layfield, R. A. *Inorg. Chem.* **2014**, *53* (19), 10578.
- (182) Wang, Y.; Xie, Y.; Abraham, M. Y.; Wei, P.; Schaefer, H. F.; Schleyer, P. V. R.; Robinson, G. H. *J. Am. Chem. Soc.* **2010**, *132* (41), 14370.
- (183) Wang, Y.; Abraham, M. Y.; Gilliard, R. J.; Wei, P.; Smith, J. C.; Robinson, G. H. *Organometallics* **2012**, *31* (3), 791.
- (184) Wang, Y.; Xie, Y.; Abraham, M. Y.; Gilliard, R. J.; Wei, P.; Campana, C. F.; Schaefer, H. F.; Schleyer, P. V. R.; Robinson, G. H. *Angew. Chem. Int. Ed. Engl.* **2012**, *51* (40), 10173.
- (185) Armstrong, D. R.; Baillie, S. E.; Blair, V. L.; Chabloz, N. G.; Diez, J.; Garcia-Alvarez, J.; Kennedy, A. R.; Robertson, S. D.; Hevia, E. *Chem. Sci.* **2013**, *4* (11), 4259.
- (186) Ingleson, M. J.; Layfield, R. A. *Chem. Comm.* **2012**, *48* (30), 3579.
- (187) Riener, K.; Haslinger, S.; Raba, A.; Högerl, M. P.; Cokoja, M.; Herrmann, W. a; Kühn, F. E. *Chem. Rev.* **2014**, *114* (10), 5215.
- (188) Xiang, L.; Xiao, J.; Deng, L. *Organometallics* **2011**, *30* (7), 2018.

-
- (189) Layfield, R. A.; McDouall, J. J. W.; Scheer, M.; Schwarzmaier, C.; Tuna, F. *Chem. Comm.* **2011**, 47 (38), 10623.
- (190) Musgrave, R. A.; Turbervill, R. S. P.; Irwin, M.; Herchel, R.; Goicoechea, J. M. *Dalt. Trans.* **2014**, 43 (11), 4335.
- (191) Danopoulos, A. A.; Tsoureas, N.; Wright, J. A.; Light, M. E. *Organometallics* **2004**, 23 (2), 166.
- (192) Lavallo, V.; El-Batta, A.; Bertrand, G.; Grubbs, R. H. *Angew. Chem. Int. Ed. Engl.* **2011**, 50 (1), 268.
- (193) Maddock, L. C. H.; Cadenbach, T.; Kennedy, A. R.; Borilovic, I.; Aromí, G.; Hevia, E. *Inorg. Chem.* **2015**, 54 (18), 9201.
- (194) Kennedy, A. R.; Klett, J.; Mulvey, R. E.; Newton, S.; Wright, D. S. *Chem. Comm.* **2008**, No. 3, 308.
- (195) Francos, J.; Fleming, B. J.; García-Álvarez, P.; Kennedy, a R.; Reilly, K.; Robertson, G. M.; Robertson, S. D.; O'Hara, C. T. *Dalt. Trans.* **2014**, 14424.
- (196) Arduengo, A. J.; Krafczyk, R.; Schmutzler, R.; Craig, H. A.; Goerlich, J. R.; Marshall, W. J.; Unverzagt, M. *Tetrahedron* **1999**, 55 (51), 14523.
- (197) Hill, M. S.; Kociok-Köhn, G.; MacDougall, D. J. *Inorg. Chem.* **2011**, 50 (11), 5234.
- (198) Uzelac, M.; Hernán-Gómez, A.; Armstrong, D. R.; Kennedy, a R.; Hevia, E. *Chem. Sci.* **2015**, 5719.
- (199) Uchiyama, M.; Wang, C. In *Organo-di-Metallic Compounds (or Reagents)*; 2014; pp 159–202.
- (200) Martínez-Martínez, A. J.; Fuentes, M. Á.; Hernán-Gómez, A.; Hevia, E.; Kennedy, A. R.; Mulvey, R. E.; O'Hara, C. T. *Angew. Chem. Int. Ed. Engl.* **2015**, n/a.
- (201) Danopoulos, A. A.; Braunstein, P.; Frison, G. *Chem. Comm.* **2015**, 51 (15), 3049.
- (202) El-Hellani, A.; Lavallo, V. *Angew. Chem. Int. Ed. Engl.* **2014**, 53 (17), 4489.
- (203) Arnold, P. L.; Liddle, S. T. *Organometallics* **2006**, 25 (6), 1485.
- (204) Pugh, T.; Layfield, R. a. *Dalt. Trans.* **2014**, 43 (11), 4251.

-
- (205) Boča, R. *Coord. Chem. Rev.* **2004**, *248* (9–10), 757.
- (206) Bendix, J.; Brorson, M.; J, C. E. S. *Inorg. Chem.* **1993**, No. 8, 2838.
- (207) Goswami, T.; Misra, A. *J. Phys. Chem. A* **2012**, *116* (21), 5207.
- (208) Lin, P.-H.; Smythe, N. C.; Gorelsky, S. I.; Maguire, S.; Henson, N. J.; Korobkov, I.; Scott, B. L.; Gordon, J. C.; Baker, R. T.; Murugesu, M. *J. Am. Chem. Soc.* **2011**, *133* (40), 15806.
- (209) Shilov, A. E.; Shul'pin, G. B. *Chem. Rev.* **1997**, *97* (8), 2879.
- (210) O'Hagan, D. *Chem. Soc. Rev.* **2008**, *37* (2), 308.
- (211) Amii, H.; Uneyama, K. *Chem. Rev.* **2009**, *109*, 2119.
- (212) Weaver, J.; Senaweera, S. *Tetrahedron* **2014**, *70* (41), 7413.
- (213) Purser, S.; Moore, P. R.; Swallow, S.; Gouverneur, V. *Chem. Soc. Rev.* **2008**, *37* (2), 320.
- (214) O'Hagan, D. *J. Fluor. Chem.* **2010**, *131* (11), 1071.
- (215) Wang, J.; Sánchez-Roselló, M.; Aceña, J. L.; del Pozo, C.; Sorochinsky, A. E.; Fustero, S.; Soloshonok, V. A.; Liu, H. *Chem. Rev.* **2014**, *114* (4), 2432.
- (216) Sun, A. D.; Love, J. A. *Dalt. Trans.* **2010**, *39* (43), 10362.
- (217) (CHMP), C. for M. P. for H. U. *Guideline on the Specification Limits for Residues of Metal Catalysts or Metal Reagents*; London, 2008.
- (218) Pauling, L. *J. Am. Chem. Soc.* **1932**, *54* (9), 3570.
- (219) Slocum, D. W.; Jennings, C. A. *J. Org. Chem.* **1976**, *41* (23), 3653.
- (220) Alessi, M. *Synthetic Methods and Application Based on Directed ortho Metalation and Suzuki Cross Coupling Strategies*, Queen's University, 2008.
- (221) Maggi, R.; Schlosser, M. *J. Org. Chem.* **1996**, *61* (16), 5430.
- (222) van Eikema Hommes, N. J. R.; von Ragué Schleyer, P. *Angew. Chem. Int. Ed. Engl.* **1992**, *31* (6), 755.

-
- (223) Schlosser, M. *Angew. Chem. Int. Ed. Engl.* **1998**, *37* (11), 1496.
- (224) J. Bridges, A.; Lee, A.; Maduakor, E. C.; Schwartz, C. E. *Tetrahedron Lett.* **1992**, *33* (49), 7495.
- (225) Mongin, F.; Schlosser, M. *Tetrahedron Lett.* **1996**, *37* (36), 6551.
- (226) Schlosser, M.; Katsoulos, G.; Takagishi, S. *Synlett* **1990**, *1990* (12), 747.
- (227) Katsoulos, G.; Takagishi, S.; Schlosser, M. *Synlett* **1991**, *1991* (10), 731.
- (228) Wittig, G.; Pieper, G.; Fuhrmann, G. *Berichte der Dtsch. Chem. Gesellschaft (A B Ser.)* **1940**, *73* (11), 1193.
- (229) Wittig, G. *Naturwissenschaften* **1942**, *30* (46–47), 696.
- (230) Roberts, J. D.; Simmons, H. E.; Carlsmith, L. A.; Vaughan, C. W. *J. Am. Chem. Soc.* **1953**, *75* (13), 3290.
- (231) Wittig, G.; Pohmer, L. *Chem. Ber.* **1956**, *89* (5), 1334.
- (232) Wittig, G. *Acc. Chem. Res.* **1974**, *7* (1), 6.
- (233) Gilman, H.; Gorsich, R. *J. Am. Chem. Soc.* **1956**, 1258 (4).
- (234) Gilman, H.; Soddy, T. *J. Org. Chem.* **1957**, *22* (12), 1715.
- (235) Zhu, Y.; Smith, D. a; Herbert, D. E.; Gatard, S.; Ozerov, O. V. *Chem. Comm.* **2012**, *48* (2), 218.
- (236) Esteruelas, M. a.; Oliván, M.; Vélez, A. *Organometallics* **2015**, 150501125054002.
- (237) DeMott, J. C.; Bhuvanesh, N.; Ozerov, O. V. *Chem. Sci.* **2013**, *4* (2), 642.
- (238) Tsang, J. Y. K.; Buschhaus, M. S. a.; Legzdins, P.; Patrick, B. O. *Organometallics* **2006**, *25* (17), 4215.
- (239) Bailey, B. C.; Fan, H.; Huffman, J. C.; Baik, M.-H.; Mindiola, D. J. *J. Am. Chem. Soc.* **2007**, *129* (28), 8781.
- (240) Hauser, S. a.; Prokes, I.; Chaplin, A. B. *Chem. Commun.* **2015**, *51* (21), 4425.
- (241) Fossatelli, M.; Verkruijsse, H. D.; Brandsma, L. *Synth. Comm.* **1990**, *20* (11), 1701.

- (242) Armstrong, D. R.; Balloch, L.; Clegg, W.; Dale, S. H.; García-Alvarez, P.; Hevia, E.; Hogg, L. M.; Kennedy, A. R.; Mulvey, R. E.; O'Hara, C. T. *Angew. Chem. Int. Ed. Engl.* **2009**, *48* (46), 8675.
- (243) Armstrong, D. R.; Blair, V. L.; Clegg, W.; Dale, S. H.; Garcia-Alvarez, J.; Honeyman, G. W.; Hevia, E.; Mulvey, R. E.; Russo, L. *J. Am. Chem. Soc.* **2010**, *132* (27), 9480.
- (244) Garden, J. A.; Armstrong, D. R.; Clegg, W.; García-Alvarez, J.; Hevia, E.; Kennedy, A. R.; Mulvey, R. E.; Robertson, S. D.; Russo, L. *Organometallics* **2013**, *32* (19), 5481.
- (245) Andrews, P. C.; Armstrong, D. R.; Baker, D. R.; Mulvey, R. E.; Clegg, W.; Horsburgh, L.; O'Neil, P. A.; Reed, D. *Organometallics* **1995**, *14* (1), 427.
- (246) Langer, J.; Krieck, S.; Fischer, R.; Görls, H.; Walther, D.; Westerhausen, M. *Organometallics* **2009**, *28* (19), 5814.
- (247) Shen, K.; Fu, Y.; Li, J.-N.; Liu, L.; Guo, Q.-X. *Tetrahedron* **2007**, *63* (7), 1568.
- (248) Kim, B.; Woo, H.; Kim, W. *Bull. Korean Chem. Soc.* **2000**, *21* (2), 211.
- (249) Lee, Y. R. *Bull. Korean Chem. Soc.* **2006**, *27* (4), 503.
- (250) Vela, J.; Smith, J. M.; Yu, Y.; Ketterer, N. A.; Flaschenriem, C. J.; Lachicotte, R. J.; Holland, P. L. *J. Am. Chem. Soc.* **2005**, *127* (21), 7857.
- (251) Schaub, T.; Fischer, P.; Meins, T.; Radius, U. *Eur. J. Inorg. Chem.* **2011**, *2011* (20), 3122.
- (252) Chukwu, R.; Hunter, A. D.; Santarsiero, B. D.; Bott, S. G.; Atwood, J. L.; Chassignac, J. *Organometallics* **1992**, *11* (2), 589.
- (253) Hunter, A. D.; Szigety, A. B. *Organometallics* **1989**, *8* (11), 2670.
- (254) Romanov, A. S.; Bochmann, M. *Organometallics* **2015**, *34* (11), 2439.
- (255) Hatnean, J. A.; Beck, R.; Borrelli, J. D.; Johnson, S. A. *Organometallics* **2010**, *29* (22), 6077.
- (256) Rivada-Wheelaghan, O.; Ortuño, M. A.; Díez, J.; Lledós, A.; Conejero, S. *Angew. Chem. Int. Ed. Engl.* **2012**, *51* (16), 3936.

- (257) Godoy, F.; Higgitt, C. L.; Klahn, A. H.; Oelckers, B.; Parsons, S.; Perutz, R. N. *J. Chem. Soc. Dalton Trans.* **1999**, No. 12, 2039.
- (258) Tanabe, T.; Brennessel, W. W.; Clot, E.; Eisenstein, O.; Jones, W. D. *Dalt. Trans.* **2010**, 39 (43), 10495.
- (259) Slocum, D. W. In *Encyclopedia of Reagents for Organic Synthesis*; John Wiley & Sons, Ltd: Chichester, UK, 2001.
- (260) Fraser, R. R.; Bresse, M.; Mansour, T. S. *J. Chem. Soc. Chem. Comm.* **1983**, No. 11, 620.
- (261) Fraser, R. R.; Bresse, M.; Mansour, T. S. *J. Am. Chem. Soc.* **1983**, 105 (26), 7790.
- (262) Volbeda, J.; Meetsma, A.; Bouwkamp, M. W. *Organometallics* **2009**, 28 (1), 209.
- (263) Wang, L.; Sun, H.; Li, X. *Eur. J. Inorg. Chem.* **2015**, 2015 (16), 2732.
- (264) Chernega, A. N.; Graham, A. J.; Green, M. L. H.; Haggitt, J.; Lloyd, J.; Mehnert, C. P.; Metzler, N.; Souter, J. *J. Chem. Soc. Dalton Trans.* **1997**, No. 13, 2293.
- (265) Bondi, A. *J. Phys. Chem.* **1964**, 68 (3), 441.
- (266) Lide, D. R. *CRC Handbook of Chemistry and Physics, 89th Edition*, 89th ed.; CRC Press: Boca Raton, FL, 2008.
- (267) Qian, H.-F.; Liu, Y.; Tao, T.; Gu, K.-H.; Yin, G.; Huang, W. *Inorganica Chim. Acta* **2013**, 405, 1.
- (268) Kashima, A.; Sakate, M.; Ota, H.; Fuyuhiko, A.; Sunatsuki, Y.; Suzuki, T. *Chem. Commun.* **2015**, 51 (10), 1889.
- (269) Hänninen, M. M.; Pal, K.; Day, B. M.; Pugh, T.; Layfield, R. A. *Dalt. Trans.* **2016**, 45 (28), 11301.
- (270) Ishida, T.; Kawakami, T.; Mitsubori, S.; Nogami, T.; Yamaguchi, K.; Iwamura, H. *J. Chem. Soc. Dalton Trans.* **2002**, No. 16, 3177.
- (271) Lloret, F.; De Munno, G.; Julve, M.; Cano, J.; Ruiz, R.; Caneschi, A. *Angew. Chem. Int. Ed. Engl.* **1998**, 37 (1–2), 135.
- (272) Holmes, S. a.; Thomas, T. D. *J. Am. Chem. Soc.* **1975**, 97 (9), 2337.

- (273) Beak, P.; Brown, R. A. *J. Org. Chem.* **1982**, *47* (1), 34.
- (274) Kennedy, A. R.; Mulvey, R. E.; Rowlings, R. B. *Angew. Chem. Int. Ed. Engl.* **1998**, *37* (22), 3180.
- (275) Forbes, G. C.; Kennedy, A. R.; Mulvey, R. E.; Rowlings, R. B.; Clegg, W.; Liddle, S. T.; Wilson, C. C. *Chem. Comm.* **2000**, *2* (18), 1759.
- (276) Bradley, D. C.; Hursthouse, M. B.; Rodesiler, P. F. *J. Chem. Soc. D Chem. Comm.* **1969**, No. 1, 14.
- (277) Duncan, J. S.; Nazif, T. M.; Verma, A. K.; Lee, S. C. *Inorg. Chem.* **2003**, *42* (4), 1211.
- (278) Shriver, D. A.; Drezden, M. A. *The manipulation of air-sensitive compounds*; 1986.
- (279) Reger, D. L.; Pascui, A. E.; Smith, M. D.; Jezierska, J.; Ozarowski, A. *Inorg. Chem.* **2012**, *51* (21), 11820.
- (280) Eckert, N. A.; Stoian, S.; Smith, J. M.; Bominaar, E. L.; Münck, E.; Holland, P. L. *J. Am. Chem. Soc.* **2005**, *127* (26), 9344.
- (281) Gorun, S. M.; Lippard, S. J. *Inorg. Chem.* **1991**, *30* (7), 1625.
- (282) Weihe, H.; Güdel, H. U. *J. Am. Chem. Soc.* **1997**, *119* (28), 6539.
- (283) Sarazin, Y.; Coles, S. J.; Hughes, D. L.; Hursthouse, M. B.; Bochmann, M. *Eur. J. Inorg. Chem.* **2006**, *2006* (16), 3211.
- (284) Karl, M.; Seybert, G.; Massa, W.; Harms, K.; Agarwal, S.; Maleika, R.; Stelter, W.; Greiner, A.; Neumüller, W. Heitz, B.; Dehnicke, K. *Zeitschrift für Anorg. und Allg. Chemie* **1999**, *625* (8), 1301.
- (285) Edelmann, F. T.; Pauer, F.; Wedler, M.; Stalke, D. *Inorg. Chem.* **1992**, *31* (20), 4143.
- (286) Spek, A. L. *Acta Crystallogr. Sect. D Biol. Crystallogr.* **2009**, *65* (2), 148.
- (287) Carlson, D. P.; Schmiegel, W. In *Ullmann's Encyclopedia of Industrial Chemistry*; Wiley-VCH Verlag GmbH & Co. KGaA: Weinheim, Germany, 2000; Vol. 15, pp 735–768.
- (288) Kiplinger, J. L.; Richmond, T. G.; Osterberg, C. E. *Chem. Rev.* **1994**, *94* (2), 373.

-
- (289) Ahrens, T.; Kohlmann, J.; Ahrens, M.; Braun, T. *Chem. Rev.* **2015**, *115*, 931.
- (290) Burdeniuc, J.; Jedicka, B.; Crabtree, R. H. *Chem. Ber.* **1997**, *130* (2), 145.
- (291) Hughes, R. P. *Eur. J. Inorg. Chem.* **2009**, No. 31, 4591.
- (292) Saeki, T.; Takashima, Y.; Tamao, K. *Synlett* **2005**, No. 11, 1771.
- (293) Clot, E.; Eisenstein, O.; Jasim, N.; MacGregor, S. a.; McGrady, J. E.; Perutz, R. N. *Acc. Chem. Res.* **2011**, *44* (5), 333.
- (294) Kowalczyk, B. A. *Synthesis* **1997**, *1997* (12), 1411.
- (295) Grecian, S. A.; Hadida, S.; Warren, S. D. *Tetrahedron Lett.* **2005**, *46* (27), 4683.
- (296) Vaganova, T. A.; Kusov, S. Z.; Rodionov, V. I.; Shundrina, I. K.; Malykhin, E. V. *Russ. Chem. Bull.* **2007**, *56* (11), 2239.
- (297) Sun, Y.; Sun, H.; Jia, J.; Du, A.; Li, X. *Organometallics* **2014**, *33* (4), 1079.
- (298) Robson, P.; Stacey, M.; Stephens, R.; Tatlow, J. C. *J. Chem. Soc.* **1960**, No. 4754, 4754.
- (299) Goryunov, L. I.; Shteingarts, V. D.; Grobe, J.; Krebs, B.; Triller, M. U. *Zeitschrift für Anorg. und Allg. Chemie* **2002**, *628* (8), 1770.
- (300) Lu, P.; Boorman, T. C.; Slawin, A. M. Z.; Larrosa, I. *J. Am. Chem. Soc.* **2010**, *132* (16), 5580.
- (301) Selmecky, A. D.; Jones, W. D.; Partridge, M. G.; Perutz, R. N. *Organometallics* **1994**, *13* (2), 522.
- (302) Källäne, S. I.; Teltewskoi, M.; Braun, T.; Braun, B. *Organometallics* **2015**, No. I, 150121145048004.
- (303) Wagner, G.; Wuthrich, K. *J. Magn. Reson.* **1979**, *33* (3), 675.
- (304) Dua, S. S.; Gilman, H. *J. Organomet. Chem.* **1974**, *64* (1), C1.
- (305) Howells, R. D.; Gilman, H. *Tetrahedron Lett.* **1974**, *15* (14), 1319.
- (306) Schlosser, M.; Guio, L.; Leroux, F. *J. Am. Chem. Soc.* **2001**, *123* (16), 3822.

-
- (307) Gupton, J. T.; Idoux, J. P.; Baker, G.; Colon, C.; Crews, a. D.; Jurss, C. D.; Rampi, R. *C. J. Org. Chem.* **1983**, *48* (17), 2933.
- (308) Deck, P. A.; Konaté, M. M.; Kelly, B. V.; Slobodnick, C. *Organometallics* **2004**, *23* (5), 1089.
- (309) Cochran, F. V.; Bonitatebus, P. J.; Schrock, R. R. *Organometallics* **2000**, *19* (13), 2414.
- (310) Hoyt, H. M.; Michael, F. E.; Bergman, R. G. *J. Am. Chem. Soc.* **2004**, *126* (4), 1018.
- (311) Schrock, R. R.; Adamchuk, J.; Ruhland, K.; Lopez, L. P. H. *Organometallics* **2003**, *22* (24), 5079.
- (312) Rumin, R.; Pétilion, F. Y.; Manojlović-Muir, L.; Muir, K. W.; Yufit, D. S. *J. Chem. Soc., Chem. Comm.* **1995**, No. 14, 1431.
- (313) Rumin, R.; Guennou, K.; Pétilion, F. Y.; Muir, K. W. *J. Chem. Soc. Dalt. Trans.* **1997**, No. 8, 1381.
- (314) Xu, X.; Jia, J.; Sun, H.; Liu, Y.; Xu, W.; Shi, Y.; Zhang, D.; Li, X. *Dalt. Trans.* **2013**, *42* (10), 3417.
- (315) Xu, X.; Sun, H.; Shi, Y.; Jia, J.; Li, X. *Dalt. Trans.* **2011**, *40* (31), 7866.
- (316) Power, P. P. *Chem. Rev.* **2012**, *112* (6), 3482.
- (317) Reiff, W. M.; LaPointe, A. M.; Witten, E. H. *J. Am. Chem. Soc.* **2004**, *126* (33), 10206.
- (318) Reiff, W. M.; Schulz, C. E.; Whangbo, M.; Seo, J. I.; Lee, Y. S.; Potratz, G. R.; Spicer, C. W.; Girolami, G. S. *J. Am. Chem. Soc.* **2009**, *131* (2), 404.
- (319) Alexander Merrill, W.; Stich, T. A.; Brynda, M.; Yeagle, G. J.; Fettinger, J. C.; Hont, R. De; Reiff, W. M.; Schulz, C. E.; Britt, R. D.; Power, P. P. *J. Am. Chem. Soc.* **2009**, *131* (35), 12693.
- (320) LaPointe, A. M. *Inorganica Chim. Acta* **2003**, *345*, 359.
- (321) Viehhaus, T.; Schwarz, W.; Hübler, K.; Locke, K.; Weidlein, J. *Zeitschrift für Anorg. und Allg. Chemie* **2001**, *627* (4), 715.
- (322) Ni, C.; Power, P. P. *Chem. Comm.* **2009**, No. 37, 5543.

- (323) Ellison, J. J.; Ruhlandt-Senge, K.; Power, P. P. *Angew. Chem. Int. Ed. Engl.* **1994**, *33* (11), 1178.
- (324) Evans, D. J.; Hughes, D. L.; Silver, J. *Inorg. Chem.* **1997**, *36* (4), 747.
- (325) Ohta, S.; Ohki, Y.; Ikagawa, Y.; Suizu, R.; Tatsumi, K. *J. Organomet. Chem.* **2007**, *692* (21), 4792.
- (326) Müller, H.; Seidel, W.; Görls, H. *J. Organomet. Chem.* **1994**, *472* (1–2), 215.
- (327) Werncke, C. G.; Bunting, P. C.; Duhayon, C.; Long, J. R.; Bontemps, S.; Sabo-Etienne, S. *Angew. Chem. Int. Ed. Engl.* **2015**, *54* (1), 245.
- (328) Murray-Rust, P.; Stallings, W. C.; Monti, C. T.; Preston, R. K.; Glusker, J. P. *J. Am. Chem. Soc.* **1983**, *105* (10), 3206.
- (329) Kulawiec, R. J.; Crabtree, R. H. *Coord. Chem. Rev.* **1990**, *99* (C), 89.
- (330) Samuels, J. A.; Lobkovsky, E. B.; Streib, W. E.; Folting, K.; Huffman, J. C.; Zwanziger, J. W.; Caulton, K. G. *J. Am. Chem. Soc.* **1993**, *115* (12), 5093.
- (331) Janjetovic, M.; Träff, A. M.; Hilmersson, G. *Chem. - A Eur. J.* **2015**, *21* (9), 3772.
- (332) Chilton, N. F.; Lei, H.; Bryan, A. M.; Grandjean, F.; Long, G. J.; Power, P. P. *Dalt. Trans.* **2015**, *44* (24), 11202.
- (333) Zadrozny, J. M.; Atanasov, M.; Bryan, A. M.; Lin, C.-Y.; Rekker, B. D.; Power, P. P.; Neese, F.; Long, J. R. *Chem. Sci.* **2013**, *4* (1), 125.
- (334) Ishida, T.; Mitsubori, S.; Nogami, T.; Takeda, N.; Ishikawa, M.; Iwamura, H. *Inorg. Chem.* **2001**, *40* (27), 7059.
- (335) Fernández, I.; Ruiz, R.; Faus, J.; Julve, M.; Lloret, F.; Cano, J.; Ottenwaelder, X.; Journaux, Y.; Muñoz, M. C. *Angew. Chem. Int. Ed. Engl.* **2001**, *40* (16), 3039.
- (336) Paital, A. R.; Mitra, T.; Ray, D.; Wong, W. T.; Ribas-Ariño, J.; Novoa, J. J.; Ribas, J.; Aromí, G. *Chem. Comm.* **2005**, No. 41, 5172.
- (337) Palacios, M. a; Rodríguez-Diéguez, A.; Sironi, A.; Herrera, J. M.; Mota, A. J.; Cano, J.; Colacio, E. *Dalt. Trans.* **2009**, *2* (40), 8538.
- (338) Quesada, M.; de Hoog, P.; Gamez, P.; Roubeau, O.; Aromí, G.; Donnadieu, B.;

- Massera, C.; Lutz, M.; Spek, A. L.; Reedijk, J. *Eur. J. Inorg. Chem.* **2006**, 2006 (7), 1353.
- (339) Gatteschi, D.; Sessoli, R. *Angew. Chem. Int. Ed. Engl.* **2003**, 42 (3), 268.
- (340) Gatteschi, D.; Sessoli, R.; Villain, J. *Molecular Nanomagnets*; Oxford University Press, 2006.
- (341) Goda, S.; Nikai, M.; Ito, M.; Hashizume, D.; Tamao, K.; Okazawa, A.; Kojima, N.; Fueno, H.; Tanaka, K.; Kobayashi, Y.; Matsuo, T. *Chem. Lett.* **2016**, 45 (6), 634.
- (342) Mathonière, C.; Lin, H.-J.; Siretanu, D.; Clérac, R.; Smith, J. M. *J. Am. Chem. Soc.* **2013**, 135 (51), 19083.
- (343) Cole, K. S.; Cole, R. H. *J. Chem. Phys.* **1941**, 9 (4), 341.
- (344) Benelli, C.; Gatteschi, D. *Introduction to Molecular Magnetism. From Transition Metals to Lanthanides*; Wiley-VCH Verlag GmbH & Co. KGaA: Weinheim, Germany, 2015.
- (345) Craig, G. A.; Murrie, M. *Chem. Soc. Rev.* **2015**, 44 (8), 2135.
- (346) Frost, J. M.; Harriman, K. L. M.; Murugesu, M. *Chem. Sci.* **2016**, 7 (4), 2470.
- (347) Schenker, R.; Leuenberger, M. N.; Chaboussant, G.; Loss, D.; Güdel, H. U. *Phys. Rev. B* **2005**, 72 (18), 184403.
- (348) Zadrozny, J. M.; Xiao, D. J.; Atanasov, M.; Long, G. J.; Grandjean, F.; Neese, F.; Long, J. R. *Nat. Chem.* **2013**, 5 (7), 577.
- (349) Hurley, M. D.; Wallington, T. J.; Javadi, M. S.; Nielsen, O. J. *Chem. Phys. Lett.* **2008**, 450 (4–6), 263.
- (350) Tovar, C. M.; Blanco, M. B.; Barnes, I.; Wiesen, P.; Teruel, M. A. *Atmos. Environ.* **2014**, 88, 107.
- (351) Simas, A. B. C.; Pereira, V. L. P.; Barreto Jr., C. B.; Sales, D. L. de; Carvalho, L. L. de. *Quim. Nova* **2009**, 32 (9), 2473.
- (352) Pangborn, A. B.; Giardello, M. a.; Grubbs, R. H.; Rosen, R. K.; Timmers, F. J. *Organometallics* **1996**, 15 (5), 1518.

- (353) Clegg, W.; Conway, B.; Kennedy, A. R.; Klett, J.; Mulvey, R. E.; Russo, L. *Eur. J. Inorg. Chem.* **2011**, No. 5, 721.
- (354) Logulu, E.; Katircioglu, H.; Tilki, T.; Öktemer, A. *Asian J. Chem.* **2007**, *19* (3), 2029.
- (355) Bennetau, B.; Rajarison, F.; Dunoguès, J.; Babin, P. *Tetrahedron* **1993**, *49* (47), 10843.
- (356) Itadani, S.; Yashiro, K.; Aratani, Y.; Sekiguchi, T.; Kinoshita, A.; Moriguchi, H.; Ohta, N.; Takahashi, S.; Ishida, A.; Tajima, Y.; Hisaichi, K.; Ima, M.; Ueda, J.; Egashira, H.; Sekioka, T.; Kadode, M.; Yonetomi, Y.; Nakao, T.; Inoue, A.; Nomura, H.; Kitamine, T.; Fujita, M.; Nabe, T.; Yamaura, Y.; Matsumura, N.; Imagawa, A.; Nakayama, Y.; Takeuchi, J.; Ohmoto, K. *J. Med. Chem.* **2015**, *58* (15), 6093.
- (357) Do, H. Q.; Daugulis, O. *Org. Lett.* **2009**, *11* (2), 421.
- (358) Deacon, G.; Smith, R. *Aust. J. Chem.* **1982**, *35* (8), 1587.
- (359) Abate, A.; Saliba, M.; Hollman, D. J.; Stranks, S. D.; Avolio, R.; Petrozza, A.; Snaith, J. *Nano Lett.* **2014**, *14* (6), 3247.
- (360) Popov, I.; Do, H. Q.; Daugulis, O. *J. Org. Chem.* **2009**, *74* (21), 8309.
- (361) Unsinn, A.; Rohbogner, C. J.; Knochel, P. *Adv. Synth. Catal.* **2013**, *355* (8), 1553.
- (362) Chambers, R. D.; Skinner, C. J.; Atherton, M. J.; Moilliet, J. S. *J. Chem. Soc. Perkin Trans. 1* **1996**, *1* (14), 1659.
- (363) Grunewald, G. L.; Arrington, H. S.; Bartlett, W. J.; Reitz, T. J.; Sall, D. J. *J. Med. Chem.* **1986**, *29* (10), 1972.
- (364) Weiss, M.; Dimauro, E. F.; Dineen, T.; Graceffa, R.; Guzman-Perez, A.; Huang, H.; Kreiman, C.; Marx, I. E.; Nguyen, H. N.; Peterson, E.; Deak, H. L. Bicyclic sulfonamide compounds as sodium channel inhibitors. WO 2014201173 A1, 2014.
- (365) Leroux, F.; Simon, R.; Nicod, N. *Lett. Org. Chem.* **2006**, *3* (12), 948.
- (366) Sheldrick, G. M. *Acta Crystallogr. Sect. A Found. Crystallogr.* **2008**, *64* (Pt 1), 112.
- (367) Farrugia, L. J. *J. Appl. Crystallogr.* **1999**, *32* (4), 837.
- (368) Hübschle, C. B.; Sheldrick, G. M.; Dittrich, B. *J. Appl. Crystallogr.* **2011**, *44* (Pt 6), 1281.

- (369) Nowell, H.; Barnett, S. A.; Christensen, K. E.; Teat, S. J.; Allan, D. R. *J. Synchrotron Radiat.* **2012**, *19* (3), 435.